Development of an integrated process flowsheet for the recovery of valuable metals from waste cathode ray tubes and printed circuit boards

By
Sello Tsebe

A dissertation submitted in partial fulfilment of the degree of
Master of Science in Engineering
in the School of Chemical and Metallurgical Engineering
University of the Witwatersrand
Johannesburg

February 2023

DECLARATION

I, Sello Peter Tsebe, declare that the research reported in this dissertation, except where otherwise stated, is my own original work. This dissertation does not contain other persons' writing or material, unless specifically acknowledged as being sourced from other researchers. This dissertation has not been submitted for any degree or examination at any other university or academic institution.

Signature : 

Surname & initials : Tsebe, S.P

Student number : 0307527A

Date : 06 February 2023

SUMMARY

Electrical and electronic waste (e-waste) is currently the fastest growing waste stream in the world. Generation of e-waste is driven mainly by rapid technological advancements and frequent innovations which in turn result in shorter lifespan of electronic devices and high rate of obsolescence of digital products. E-waste is considered a valuable stream of secondary metal resources because it contains valuable metals such as copper (Cu) and gold (Au). However, it is also classified as hazardous waste as it contains toxic heavy metals such as lead (Pb) and cadmium (Cd). If e-waste is not managed properly, the toxic metals may pose serious risks to the environment and human health.

In 2018, South Africa produced an estimated 360,000 t e-waste with reports of only about 10% recycled. The lack of processing technology was cited as an explanation for the low levels of recycling, especially for complex fractions such as printed circuit boards (PCBs) and cathode ray tubes (CRTs). Partially beneficiated PCBs are exported to Europe for processing, and stripped CRTs are either landfilled or stockpiled. Landfilling of CRTs has been banned effective August 2021. Exporting of partially beneficiated PCBs deprives the South African economy the opportunity to take full advantage of the value contained in PCBs. There is a need for a technology that will provide capacity for local processing of CRTs and PCBs for metal recovery.

The current study investigated a new process flowsheet for the thermal treatment of CRTs and PCBs in the same integrated flowsheet for metal recovery. The aim was to recover a crude Cu alloy from the PCBs and a crude Pb alloy from the CRTs. The two processes were integrated by flow of material from one process to the other. That is, slag from the CRTs furnace was recycled to the PCBs furnace to be utilised as a fluxing agent, and fume from the PCBs furnace was recycled to the CRTs furnace to be utilised as a source of lead oxide (PbO). The study aimed to answer this primary question:

Is it technically feasible to integrate the smelting of waste CRT funnel glass into the same flowsheet as the smelting of waste PCB concentrate?

In order to answer the above question, the study explored the following two questions:

1. Can oxidative smelting of PCB concentrate and CRT slag produce a crude Cu alloy with a grade of more than 95% Cu?

2. Can reductive smelting of CRT funnel glass and PCB fume produce a crude Pb alloy with a grade of more than 95% Pb?

The investigation was undertaken in a pilot-scale top blown rotary converter (TBRC). The furnace facility consisted of an oxy-propane burner supported by a gas supply train; a cylindrical refractory-lined reactor with a working volume of 20 L; and off-gas handling system featuring a two-stage filtration system, whereby primary filtration occurs through a bank of cartridge filters and secondary filtration occurs in a baghouse.

The PCBs smelting condition that achieved the required alloy grade was an average oxidation temperature of 1350°C, flame stoichiometry of 100 mol% O_2, and an oxidation time of 1 h. The amount of material recycled to integrate to the PCBs process was 45% CRT slag, per unit mass of PCB concentrate, to the PCBs smelting furnace. The grade of the Cu alloy obtained was 95.1% Cu.

The CRTs smelting condition that achieved the required alloy grade was an average reduction temperature of 1200°C, flame stoichiometry of 95 mol% O_2, and reduction time of 2 h. The amount of material recycled to integrate to the CRTs process was 10% PCB fume, per unit mass of CRT funnel glass, to the CRTs smelting furnace. The grade of the Pb alloy obtained was 96.1% Pb.

The test work provided experimental evidence that the integrated process can produce crude alloys of Cu and Pb at the required grade specification. Therefore, the study has shown that it is technically feasible to integrate the smelting of waste CRT funnel glass into the same flowsheet as the smelting of waste PCB concentrate. This process flowsheet can be optimised and developed into a technology that can provide technical capacity to locally process low-grade PCBs and CRTs for metal recovery.

TABLE OF CONTENTS

LIST OF FIGURES

LIST OF TABLES

LIST OF ACRONYMS

AAS	Atomic absorption spectrometry
ACD	Analytical Chemistry Division
BFRs	Brominated flame retardants
BSE	Backscattered electron
CRTs	Cathode ray tubes
DC	Direct current
DEA	Department of Environmental Affairs
EDS	Energy dispersive spectroscopy
EEE	Electrical and electronic equipment
ERA	E-waste recycling authority
eWASA	E-waste Association of South Africa
e-Waste	Electrical and electronic waste
FA	Fire assay
FEG	Field emission gun
FR-2, FR-4	Flame retardant-2, -4
ICER	Industry Council for Electronic Equipment Recycling
ICP-MS	Inductively coupled plasma - mass spectrometry
ICP-OES	Inductively coupled plasma - optical emission spectrometry
ISO	International Organisation of Standardization
LCDs	Liquid crystal displays
MNL	Mineralogy Division
NEMWA	National Environmental Management: Waste Act No. 59 of 2008
PCBs	Printed circuit boards
PDPs	Plasma display panels
PE	Polyethylene
PGMs	Platinum group metals
PP	Polypropylene
PTFE	Polytetrafluoroethylene
PVC	Polyvinyl-chloride
QEMSCAN	Quantitative evaluation of materials by scanning electron microscopy
SA	South Africa
SAEWA	Southern African e-waste Alliance
SANAS	South African National Accreditation System
SEM	Scanning electron microscopy
SIP	Species identification protocol
StEP	Solving the e-waste problem
TBRC	Top blown rotary converter
TV	Television
UNEP	United Nations Environment Programme
UNU	United Nations University
WEEE	Waste electrical and electronic equipment
XRF	X-ray fluorescence

LIST OF SYMBOLS

Symbols and units	
$[i]_{\text{metal}}$	Species *i* dissolved in liquid metal phase
$(i)_{\text{slag/solid}}$	Species *i* dissolved in liquid slag phase or present as pure solid
$\{i\}_{\text{gas}}$	Species *i* in gas phase
$\Delta G^{o}_{react[i]}$	Change in the standard Gibbs free energy of reaction *i* in kJ/mol
ΔG^{o}_{f}	Change in the standard Gibbs free energy of formation in kJ/mol
a*(i)*	Activity of element or compound *i*
kJ	Kilojoule
k	Oxidation rate constant, in m/s
$K_{\text{react}[i]}$	Equilibrium constant of reaction [*i*]
$L^{g/m}$	Distribution ratio between gas and metal phase
$L^{s/m}$	Distribution ratio between slag and metal phase
m/s	Metre per second
m^3/h	Cubic metre per hour
mol	Mole (amount of substance)
mol%	Mole per cent (mole/mole) x 100
N	Normal temperature and pressure, 20°C and 1 atm, respectively
p(i)	Partial pressure of gas species "*i*"
Pa.s	Pascal second, equivalent to 10 poise
ppm	Parts per million (mass/mass)
R	Ideal gas constant in J/(K·mol)
s	Second
t	Metric ton, equivalent to 1000 kg
vol%	Volume percent (vol/vol × 100)
wt%	Weight percent (mass/mass × 100)
Chemical species	
$3Al_2O_3{\cdot}2SiO_2$	Mullite
Al_2O_3	Alumina or aluminium (III) oxide
Al_2SiO_5	Aluminium silicate
As_2O_3	Arsenic (III) oxide
BaO	Barium oxide
C_3H_8	Propane gas
$CaCO_3$	Limestone or calcium carbonate
CaO	Lime or calcium (II) oxide, alkaline earth oxide
CH_4N_2S	Thiourea
Cl^-	Chloride, belongs to halide group
CN^-	Cyanide
CO	Carbon monoxide
CO_2	Carbon dioxide
Cu_2O	Cuprous oxide or copper (I) oxide
CuO	Cupric oxide or copper (II) oxide
Cu-Zn	Brass

$FeCr_2O_4$	Chromite
Fe_2O_3	Ferric oxide or iron(III) oxide
Fe_2SiO_4	Fayalite
FeO	Iron (II) oxide
H_2O_2	Hydrogen peroxide
H_2SO_4	Sulfuric acid
HCl	Hydrochloric acid
HNO_3	Nitric acid
HNO_3 + HCl	Aqua Regia
K_2CO_3	Potassium carbonate
K_2O	Potassium oxide
MgO	Magnesia or magnesium (II) oxide, alkaline earth oxide
$Na_2B_4O_7$	Anhydrous borax
Na_2CO_3	Soda ash or sodium carbonate
Na_2O	Sodium oxide
Na_2O_2	Sodium peroxide
NaOH	Sodium hydroxide
Na_2SiO_3	Sodium silicate
O_2	Oxygen gas
PbO	Lead oxide
$S_2O_3^{2-}$	Thiosulfate
Sb_2O_3	Antimony (III) oxide
SiC	Silicon carbide
SiO_2	Silica, quartz, silicon dioxide or silicon (IV) oxide
Sn-Pb	Solder
SrO	Strontium oxide
TiN	Titanium nitride
ZnO	Zinc (II) oxide

ACKNOWLEDGEMENTS

I would like to extend my deepest gratitude to the following persons:

- Mintek for providing the funding and resources to complete the research work;
- The Pyrometallurgy Division's project support team and team of engineers (Metcons) for the hard work and dedication in executing the pilot-smelting campaigns;
- My supervisors, Dr Joalet Steenkamp and Mr Paul den Hoed, for their passion in academic research and providing technical guidance and critical review of the proposal and dissertation; and
- My former line-manager, Glen Denton, for sharing his wealth of technical knowledge and operational experience to finding solutions to some of the technical challenges encountered throughout this research project.

This MSc is dedicated to my wife,

Mahlodi Christina Tsebe

(OLO)

Thank you for the inspiration, encouragement, and unwavering support.

1 INTRODUCTION

The purpose of this study is to investigate the feasibility of a new process flowsheet to recover valuable metals from waste printed circuit boards (PCBs) and cathode ray tubes (CRTs). The process flowsheet involves integration of the smelting of waste PCBs and CRTs to recover alloys of copper (Cu) and lead (Pb), respectively. The study aims to develop a processing technology that is appropriate for implementation in the South African e-waste recycling industry.

1.1 Background

Waste electrical and electronic equipment (WEEE) or simply e-waste is a broad term that encompasses all discarded end-of-life electrical equipment (*e.g.,* refrigerators, washing machines, and microwave ovens) and electronic devices (*e.g.,* computers, monitors, cell phones, and printers). It is considered a valuable stream of secondary metal resources especially because it comprises precious metals in concentrations higher than their respective primary resources (Bizzo *et al*., 2014).

E-waste contains valuable metals such as Cu, tin (Sn), palladium (Pd), silver (Ag) and gold (Au) (Ogunniyi *et al*., 2009). It also contains toxic metals such as Pb, barium (Ba), arsenic (As), antimony (Sb) and cadmium (Cd) (Korf *et al*., 2019). If not managed properly, the toxic metals may pose serious risks to the environment and human health (Robinson, 2009).

Balde *et al*. (2017) estimated that about 44.7 Mt of e-waste was generated globally in 2016, and projected that this number could reach 120 Mt by 2050. E-waste is now the fastest-growing waste stream in the world and only about 20 wt% is dealt with appropriately (Balde *et al*., 2017). The same applies in South Africa, but recycling rates are much lower: South Africa had an e-waste average growth rate of 4 wt% during the period 2007 to 2013 (UNEP, 2013), and currently produces an estimated 360,000 t e-waste with reports of about 10 wt% recycled (DEA, 2018).

A study conducted by Lydall *et al*. (2017) reported that the absence of processing technology is often cited as explanation for the low levels of e-waste recycling in South Africa, particularly for complex fractions such as PCBs and CRTs. The absence of processing technology is attributed to the lack of investment and low volumes of e-waste to make up sufficient economies of scale for conventional technologies.

There are several streams of e-waste produced in South Africa, and these include ferrous and non-ferrous fractions, plastics, lamp glass, and complex fractions such as PCBs, CRTs, lithium (Li) ion batteries, and mercury (Hg) and phosphor dust (Finlay and Liechti, 2008). Whereas there are local markets and well-established technologies for processing of the other fractions, there is none (or limited) for complex fractions (ERA, 2018). The current study focussed on developing a process for PCBs and CRTs largely because of the similar chemical nature of these two fractions and the relatively larger annual volumes produced in contrast to the other complex fractions.

PCBs are sheets of non-conductive substrate that provide mechanical support for the electrical circuit and electronic components embedded in the board. They are found in every piece of electrical and electronic equipment. The generation of waste PCBs is generally driven by, among other factors, rapid technological advancements and frequent innovations, which in turn resulted in shorter life-span of electronic devices and high rate of obsolescence of digital products (Nair, 2021).

In 2013 South Africa generated more than 7,500 t PCBs, and in 2018 collections were estimated to be as high as 10,000 t PCBs (ERA, 2018). These volumes are expected to increase each year due to increase in demand of electronic devices (Nair, 2021).

The South African e-waste recycling industry has become more integrated, formalised and diversified over the past decade, but there is still limited participation in the processing stage of the value chain (Lydall *et al.*, 2017). There are only two companies in South Africa that can process e-waste to value-added products, namely, Rand Refinery and SA Precious Metals. The processing capacity in these facilities is limited, and only specific high-grade PCBs fractions with high value are accepted (ERA, 2018).

Currently, only about 20 wt% of PCBs are fully beneficiated locally (Lydall *et al.*, 2017). In other words, about 80 wt% of PCBs are exported overseas for metal recovery. The absence of a commercial operation in South Africa with the appropriate technology and enough capacity to process low-grade PCBs compels local e-waste recyclers to export PCBs to integrated smelting and refining facilities in Europe and Asia (Lydall *et al.*, 2017). The development of local processing capacity will enable the South African economy to benefit fully from the value contained in PCBs.

CRTs can be defined as the video display components of old generation television (TV) screens and computer monitors making use of electron-beam technology. CRT technology for manufacture of TVs and monitors went obsolete due to the introduction

of plasma display panels (PDPs) and liquid crystal displays (LCDs). Since the advent of new technologies for TVs and monitors, an increasing amount of CRTs is discarded each year (Xu *et al*., 2012).

In 2007 South Africa generated an estimated 43,100 t CRTs (Finlay and Liechti, 2008), and in 2015 the volumes almost doubled to about 80,000 t CRTs (DEA, 2018). These volumes are projected to increase each year with increasing investment in public education and awareness, and establishment of sustainable collection systems as prescribed in the industry waste management plan (ERA, 2018).

Local recyclers generally either stockpile or landfill CRTs after dismantling the TVs and monitors to salvage any components of value that can be recycled such as metals, wiring, circuit boards and plastics. The inherent low value of the remaining CRT does not allow for export to overseas markets (Lydall *et al.,* 2017). Landfilling of e-waste is now no longer an option since it was banned effective August 2021 (DEA, 2013). Leaving stockpiling as the only available option. However, recyclers are also running out of storage space to stockpile waste CRTs (ERA, 2018), as illustrated in Figure 1.

Figure 1. Stockpiling of waste CRTs at an e-waste recycling centre (source: https://blog.idrenvironmental.com/; visited:20/11/2021)

Pyrometallurgy is the traditional method of recovering valuable metals from recycled PCBs (Cui and Zhang, 2008). Currently, more than 70 wt% of waste PCBs is treated in Cu smelters, Pb blast furnaces, and plasma arc furnaces (Kaya, 2016). These large integrated smelter-refinery facilities such as the Umicore plant in Hoboken, Belgium (Hageluken, 2006), and the Aurubis plant in Lunen, Germany (Alvear Flores *et al*., 2014), require significant capital investment and large volumes of PCBs to achieve economies of scale. Establishing such facilities is not considered a viable option in South Africa (Lydall *et al.,* 2017). A much more viable option is to establish smaller plants, focused on the recovery of Cu, Au and Ag, with potential for future scale up (Lydall *et al.,* 2017).

Over the recent past, CRTs collected for recycling were recycled into new CRTs through glass-to-glass recycling, or co-processed in secondary Pb smelters to recover Pb through glass-to-Pb recycling (ICER, 2004). Glass-to-glass recycling has been the most common management method but at present there are none or few options for glass-to-glass recycling especially since CRTs have been replaced by new technologies (Shaw, 2013). Glass-to-Pb recycling in Pb smelters is also not ideal, as the low Pb content in the CRT glass results in generation of large volumes of slag that increases treatment and disposal fees (ICER, 2004). As such, only small volumes are treated through this recycling option.

The capacity limitations with existing recycling options encouraged research into processing of CRT funnel glass as the primary feedstock. Several researchers in the last decade investigated reductive smelting of CRT funnel glass to recover Pb using different reducing agents, and thermal reduction methods under a vacuum (Hu and Hui, 2017; Lu *et al*., 2013; Meng *et al*., 2016; Veit *et al*., 2015). However, none of these technologies has been commercially implemented (Xu *et al.,* 2012).

The problem that this study aims to address is that there is currently no publications in the open literature discussing the recovery of valuable metals from smelting of waste CRTs and PCBs in an integrated flowsheet. There is also nothing published in relation to the use of CRT slag as a flux during smelting of waste PCBs, nor is there any literature reporting on recycling of PCB fumes to a CRT smelting process for use as a source of lead oxide (PbO).

Therefore, the research aim of this study is to investigate the development of a flowsheet that integrates the smelting of CRT funnel glass with that of a low-grade PCB concentrate to evaluate the technical feasibility for metal recovery.

The novel concept was conceived through the observation that the two materials, while significantly different in their phase compositions, largely comprise the same major elements; which means that a by-product from one process could be compatible with or even conducive to, the chemical thermodynamics of the other process. For example, slag produced in the CRT smelting process can be used to improve properties of slag produced in the PCB smelting process. This presented an opportunity to integrate the two processes, and to explore any potential technical benefits that would otherwise not be realized if the processes were operated independently.

The specific waste PCBs and CRTs materials studied for this investigation were:

(i) Low-grade PCB concentrate, which comprises a coarse fraction of metallic granules obtained after physical beneficiation of PCBs and containing less than 100 ppm Au; and
(ii) CRT funnel glass, which is the Pb-rich conical glass section at the rear end of a CRT.

The study focused on recovering high-grade Cu alloy from PCB concentrate and high-grade Pb alloy from CRT funnel glass. The two processes were integrated by recycling of one of their by-product streams from one process to the other. This can be elaborated as follows: in the first interconnection, CRT slag from the CRT smelting process was recycled to the PCB smelting furnace to be utilised as a fluxing agent; in the second interconnection, PCB fume from the PCB smelting process was recycled to the CRT smelting furnace to be utilised as a source of PbO (see Figure 2).

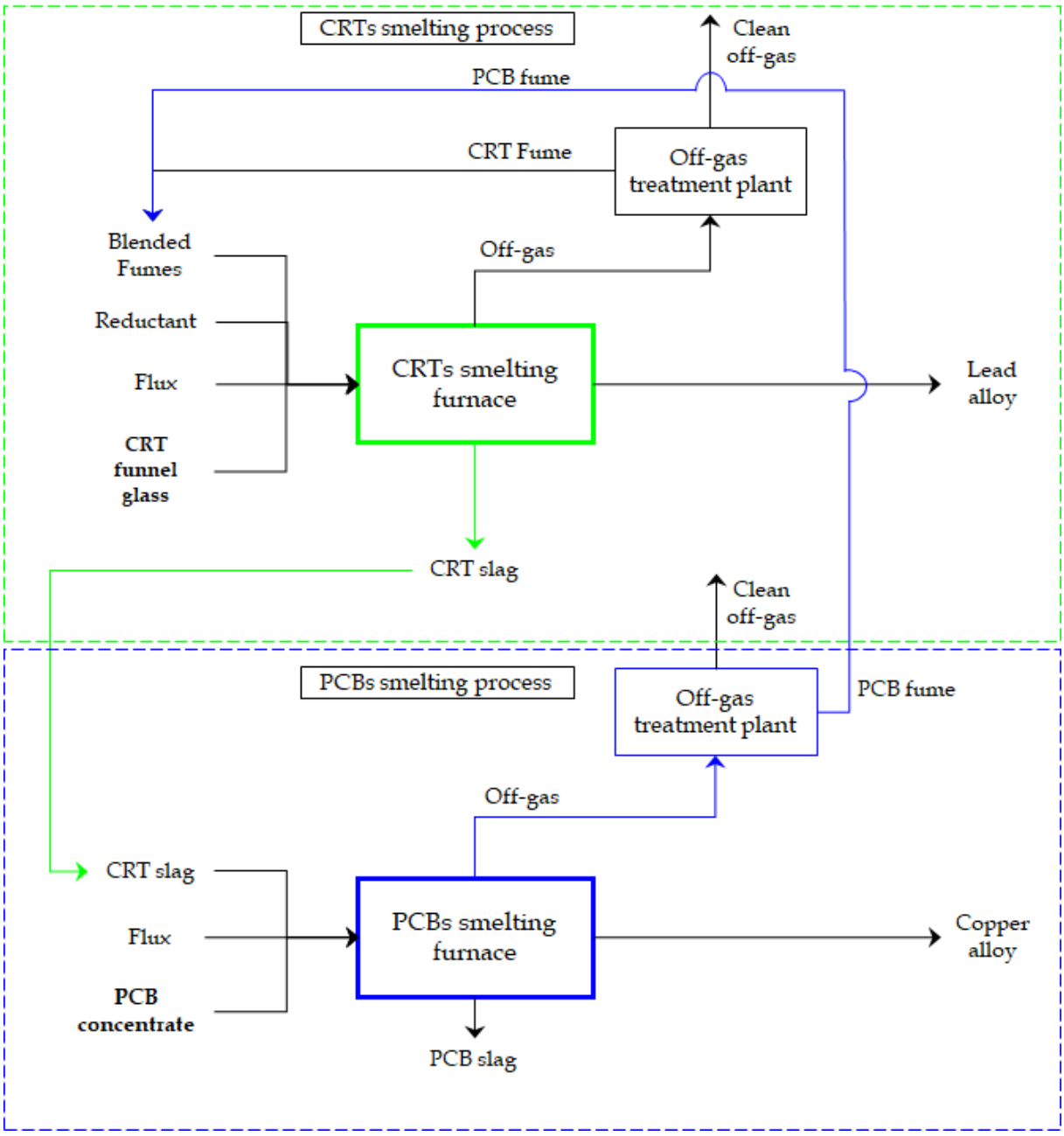

Figure 2. Simplified conceptual integrated flowsheet for the processing of CRTs and PCBs

2 LITERATURE REVIEW

A review of publications in the open literature relevant to the recycling and processing of PCBs and CRTs was undertaken. Firstly, the structure and composition of each material is presented, followed by an overview of e-waste pre-processing techniques as well as existing and alternative processing technologies. The last section of the literature study discusses physicochemical principles of impurity removal from Cu metal and reduction smelting of metal oxides.

2.1 Material structure and composition

E-waste streams such as PCBs and CRTs are considered complex fractions not only due to their intricate structures and large number of components but also due to the presence of numerous metallic elements that requires a very complex recovery process (Kaya, 2016). To select an appropriate recycling technique and processing route to recover the contained metal values, it is essential to characterise e-waste in terms of structure, components, and chemical composition (Kaya, 2016).

2.1.1 Printed circuit boards

PCBs consist of three basic parts: (i) non-conducting substrate; (ii) conductive circuit printed on or inside the substrate; and (iii) mounted components. There are generally two types of PCB substrates, namely, flame retardant-2 (FR-2) and flame retardant-4 (FR-4). Both PCB types make use of brominated flame retardants (BFRs) to reduce flammability (Tsydenova and Bengtsson, 2011).

The FR-4 type is composed of multilayers of fiberglass reinforced epoxy resin coated with a Cu layer. The FR-2 type is a single layer of cellulose phenolic paper coated with a Cu layer (Murugan *et al*., 2008; William and Williams, 2007). The FR-4 epoxy resins are generally green in colour and have high value while the FR-2 phenolic resins are yellow/brown in colour and have low value (Ladou, 2006). The value of the PCBs is based on the monetary value of the contained recoverable metals. Pictures of examples of the two PCB types are shown in Figure 3.

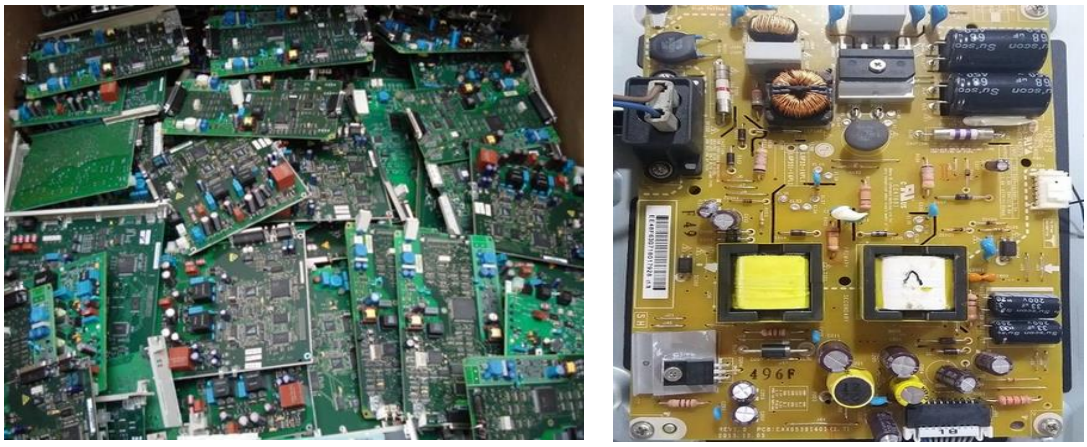

(a) (b)

Figure 3. Picture of (a) Type FR-4 PCBs (high value), and (b) Type FR-2 PCB (low value) (source: (a) https://www.copperwirerecyclingmachinery.com/news/pcb_disposal_methods650.html, and (b) https://www.aliexpress.com/item/32821985190.html)

According to Hageluken (2006), PCBs can also be classified by Au content as shown in Table 1. For example, low-grade PCBs contain less than 100 ppm Au and they are typically sourced from large household appliances such as fridges, washing machines and microwaves ovens.

Table 1. Classification of waste PCBs and their respective sources (adapted from Hageluken(2006))

Classification	**Au content**	**Source of waste PCBs**
High grade	>400 ppm Au	Circuit boards from main-frames, some mobile phones, integrated circuits, hard drives
Medium grade	100–400 ppm Au	PC-boards, laptops, handheld computers, mobile phones, digital cameras
Low grade	<100 ppm Au	Old TV-boards, monitor boards, calculators, microwave oven, fridges, washing machine

The heterogeneous nature of PCBs is widely acknowledged by researchers, especially challenges associated with proper sampling, appropriate sample preparation, and accurate analysis of PCBs (Hubau *et al*., 2019; Korf *et al*., 2019; Laubertova *et al*., 2019; Ogunniyi *et al*., 2009). Ogunnyi *et al*. (2009) noted that the high heterogeneity of PCBs can make determinations of accurate quantitative analysis difficult because any source of error (*e.g*., sampling, digestion, dilution, calibration, and interference) may have a detrimental effect on the results. Laubertova *et al*. (2019) commented that the success of treatment of e-waste depends mostly on the quality of sampling and assaying.

However, sampling is difficult for e-waste composition analysis due to the highly inhomogeneous nature of these materials.

There is no standard theory applied for e-waste sampling nor is there a standard reference method for determining the chemical composition of PCBs (Hubau *et al*., 2019; Korf *et al*., 2019; Ogunniyi *et al*., 2009). Literature reviews and investigations on PCBs have mentioned techniques such as atomic absorption spectrometry (AAS), inductively coupled plasma-optical emission spectrometry (ICP-OES), inductively coupled plasma-mass spectrometry (ICP-MS), fire assay (FA), and X-ray fluorescence (XRF) as applicable (Legarth *et al*., 1995; Li *et al*., 2004; Zhang and Forssberg, 1997).

Previously published chemical compositions of PCBs cover a wide range of elements and were produced with numerous methods for sampling, digestion, and measurement (Korf *et al*., 2019). Sampling of PCBs invariably occurs after some form of comminution for size reduction of the bulky boards. A study by Laubertova *et al*. (2019) revealed that the particle size distribution of the representative sample had the most significant impact on the accuracy of the sampling procedure to determine Au content in PCBs. The smaller the particle size of a representative sample, the higher the accuracy in determining the precious metal content in the sample. The coarser the representative sample, the larger the mass of sample required.

Generally, PCBs constitute 30 wt% ceramics, 30 wt% plastics and 40 wt% metals (Shuey *et al*., 2006). The typical compositions of PCBs reported in literature are given in Table 62 in APPENDIX A. There is a wide range in the concentration of each species in PCBs reported in literature. This signifies the heterogeneous nature of PCBs sourced from different appliances and devices, geographical location, and year produced (Korf *et al*., 2019).

The ceramic component comprises mainly silica (SiO_2), alumina (Al_2O_3) and alkaline earth oxides (such as calcium oxide (CaO) and magnesium oxide (MgO)) while the plastic component comprises polyethylene (PE), polypropylene (PP), polyvinyl-chloride (PVC), polytetra-fluoroethane (PTFE), polyesters, epoxy, and nylon (Shuey *et al*., 2006). Ceramics are used to create bridges and slots on the board, and plastics are used primarily as the base structure of the substrate and can also be used as covers and supports for other electronic components on the board (Li *et al*., 2004).

The concentration of metallic species can range considerably, with Cu reported between 10.0 and 26.8 wt%, and Au between 80 and 1000 ppm. Other major metallic

elements include Pb, zinc (Zn), Sn, aluminium (Al), nickel (Ni) and iron (Fe). Metallic elements present in trace amounts include precious metals such as Ag and Pd; scarce metals such as gallium (Ga) and germanium (Ge); and hazardous metals such as Cd and Sb.

The heterogeneous mixture of metals in PCBs is attributed to the many electronic components attached to the board. These include capacitors, integrated circuits, relays, resistors and transistors (Li *et al*., 2004). A brief description of the components and the metals they contain is provided in APPENDIX A.

Kamberovic *et al.* (2018) conducted smelting tests on a PCB sample that was mechanically and physically beneficiated to remove the ceramic and plastic components from the board. The chemical composition was determined by XRF and was performed using a sample cut from the middle of a cylindrical ingot, obtained by melting 1.0 kg of granules in a medium-induction furnace under reducing conditions (at 1250°C for 1 h). The mass difference, prior and after melting (0.17%), represented the content of organic materials. The concentrate sample was significantly upgraded in metal content to 80.4 wt% Cu, 5.58 wt% Pb and 10.0 wt% Sn (see Table 2), relative to compositions presented in Table 62 in APPENDIX A.

Table 2. Chemical composition of mechanically beneficiated PCBs, wt%
(adapted from Kamberovic et al. [2018])

								Mass, ppm			
Cu	**Zn**	**Fe**	**Sn**	**Pb**	**Ni**	**Ti**	**Non-metallics**	**Bi**	**Ag**	**Au**	**Total**
80.4	3.0	0.17	10.0	5.58	0.31	0.13	0.17	95	405	22	**99.7**

2.1.2 Cathode ray tubes

A CRT monitor or TV is a complete assembly involving different materials and several components including plastic housing, metallic components, circuit boards and wiring (Menad, 1999). The CRT is the main glass component enclosed inside the casing. There are two types of CRT screens: monochrome (black and white) and colour screen. Both types of CRTs are composed of three glass sections, namely (Andreola *et al*., 2005; Lee *et al*., 2000):

1. Panel glass – the video display section of the CRT. It features a thick glass rich in barium oxide (BaO) and strontium oxide (SrO) and accounts for 66 wt% of the CRT. Panel glass has been free of Pb since 1995.

2. Funnel glass – the conical glass section attached to the back of the panel section. It is composed of a thinner glass rich in PbO and accounts for 33 wt% of the CRT.
3. Neck glass – this glass section encloses the electron gun at the rear end of the CRT. It accounts for less than 1 wt% of the CRT and commonly features a clear thin glass rich in PbO.

An image of a typical CRT is shown in Figure 4 and a schematic is provided in Figure 79 in APPENDIX A.

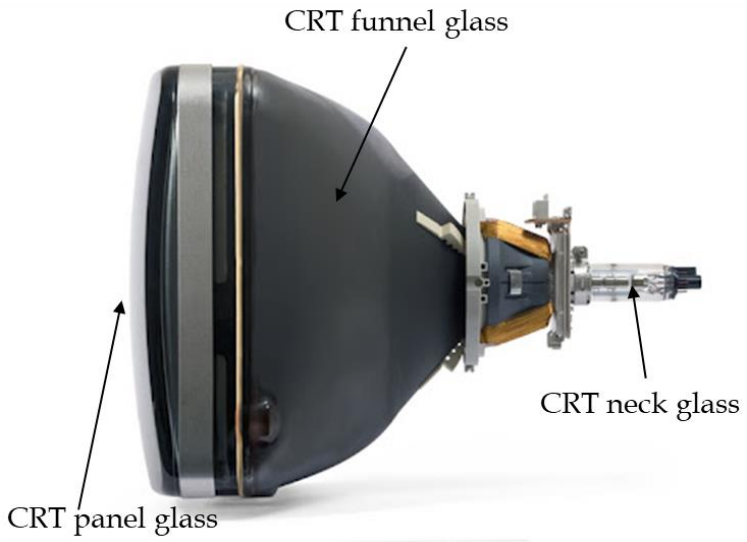

Figure 4. An image of a typical CRT showing different glass sections (source: http://www.electronicstakeback.com/2012/11/15/recyclers-stockpiling-millions-of-pounds-of-toxic-glass-from-crt-tvs-and-monitors/)

The inside of the panel glass is coated with a conductive material and three layers of phosphor powder (Menad, 1999). A phosphor is a substance that emits visible light when exposed to radiation such as an electron beam. It is used to produce coloured images on the display panel. The inside of the funnel glass is coated with a layer of iron oxide (FeO) while a graphite monolayer coats the outside to prevent users from exposure to radiation (Mear *et al.*, 2006).

The rear end of the CRT is equipped with an electron gun assembly that produces a beam of electrons from a heated metal cathode surrounded by a metal anode (Meek, 1993). The beam is accelerated and focused by a Cu yoke and a series of Ni alloy plates are used to deflect the beam across the inside surface of the panel glass. A shadow mask is a thin metal plate (Ni-Fe alloy) punched with tiny holes positioned behind the panel glass to assist with producing clear and focused colour images (Meek, 1993). The

panel and funnel glass are wholly composed of silicate glass and their interface, welded with frit, is clamped with a tensioned metal band to protect against implosion (Meek, 1993).

CRT glass is a silicate glass with a complex formulation including several oxide components incorporated into the glassy network. The oxides can be classified into three groups as follows (Mear *et al.*, 2006):

1. Network formers – oxides that intrinsically form a glassy network structure (*e.g.*, SiO_2, antimony oxide [Sb_2O_3] and arsenic oxide [As_2O_3]);
2. Network modifiers – oxides that break glassy network structure (*e.g.*, sodium oxide [Na_2O], potassium oxide [K_2O], CaO, MgO, *etc.*); and
3. Network intermediates – oxides that join in glassy networks but cannot themselves form glass (*e.g.*, Al_2O_3, PbO, zinc oxide [ZnO], *etc.*).

A study by Mear (2006) investigated the chemical composition of CRT glass from discarded TVs and monitors from different manufacturers (*viz.*, Hitashi, Matsushita, Samsung, Sony Toshiba, and Clinton corp.). The glass compositions (see Table 4 in APPENDIX A) were in good agreement with values in the literature (Andreola *et al.*, 2005; Bernardo *et al.*, 2003; Hedemalm *et al.*, 1995; Menad, 1999; Musson *et al.*, 2000; Valache *et al.*, 1997).

The funnel glass of colour screens contained on average 49.8 wt% SiO_2, 22.9 wt% PbO, 0.36 wt% BaO and 0.62 wt% SrO. Other major oxide species included K_2O and Na_2O, with minor and trace presence of Sb_2O_3 and As_2O_3, respectively. PbO is used in funnel and neck glass to absorb X-ray radiation from the electron gun (Meek, 1993). In the panel glass of colour screens, BaO and SrO are used instead of PbO because panel glass needs to be colourless, and Ba–Sr silicate glass is transparent under X-ray radiation (Meek, 1993). PbO is only used in the panel glass of black and white screens because Pb is less expensive than Ba, and the panel glass of black and white screens need not be colourless (Meek, 1993).

2.2 Overview of pre-processing techniques

The e-waste recycling value chain generally consists of four stages (see Figure 5): collection, dismantling, pre-processing and processing. This section discusses techniques applied in the pre-processing stage of PCBs and CRTs.

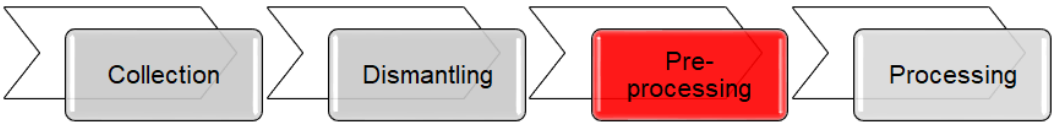

Figure 5. The four stages of the e-waste recycling value chain highlighting the pre-processing stage

2.2.1 PCBs pre-processing techniques

Pre-processing of PCBs is accomplished through three main processes, that is, mechanical, physical, and chemical processes. But before the PCBs are pre-processed, they are first dismantled. The PCB is dismantled for removal of reusable parts or toxic electronic components such as batteries and mercury containing lamps and switches (X. Chi *et al.*, 2011).

The dismantled board is then put through mechanical processes such as comminution for size reduction, size classification, and sampling for chemical analysis (Zhang and Forssberg, 1997). Physical processes such as gravity, magnetic, and electrostatic separation are commonly applied to separate the metallics from the non-metallic fractions (Lu *et al.*, 2008; Sarvar *et al.*, 2015; Yamane *et al.*, 2011). Chemical processes that are typically applied to decompose the polymers of the plastics include pyrolysis, gasification, and depolymerization (Guo *et al.*, 2009).

A generic flowsheet depicting the steps involved in the pre-processing stage of PCBs is illustrated in Figure 83 in APPENDIX B, and additional details of each process step are also discussed in APPENDIX B.

2.2.2 CRTs pre-processing techniques

Pre-processing of CRTs can be divided into three groups of techniques: manual, semi-automatic, and automatic techniques. All three techniques are designed around primarily separating the panel glass from the funnel glass because the composition, hazardous characteristics, and therefore, downstream processing of these two glass sections are different (Lee *et al.*, 2004).

The CRT, however, comes assembled with several other components that must be removed to free the CRT. Thus, waste CRT TVs and monitors go through the dismantling stage for disassembly. Besides the release of the CRT from the assembly, recyclable components such as plastics, metals, internal wirings and circuit boards are recovered and sent to their respective secondary industries (see Figure 84 in APPENDIX C).

The stripped CRT can then be treated through one of the three separation techniques. Manual techniques involve the use of tools such a hammer, chisel, and screw driver to separate the components (Liu *et al*., 2006). There are three semi-automatic techniques applied in industry and these are:

1. Acid bath method (chemical separation) (Yan *et al*., 2008);
2. Electric wire heating and laser cutter (thermal separation) (Lee *et al*., 2004; Yin *et al*., 2008); and
3. Diamond saw cutter (mechanical separation) (Herat, 2008).

The last separation technique is the fully automatic technique which normally employs sensor guided optical sorting (Xu *et al*., 2012) to separate panel from funnel glass. Further details of the above techniques are provided in APPENDIX C.

2.3 Existing processing technologies

The last stage of the value chain in e-waste recycling is processing. This section discusses existing processing technologies for PCBs and CRTs in respect of pyrometallurgical methods, with a focus on smelting processes. Other processing methods based in hydrometallurgy and biometallurgy will be discussed in the next section as alternative processing technologies. It is important to note that industrial processes for recovery of metals from e-waste are based on combined pyrometallurgical, hydrometallurgical, and electrometallurgical routes (Kaya, 2019; Khaliq *et al*., 2014).

2.3.1 PCBs smelting technologies

The final extraction and purification of metals from PCBs is achieved through metallurgical processes (see Figure 6). The fraction of non-ferrous metals generated after the electrostatic separation step can be processed via (i) pyrometallurgy, by smelting; (ii) hydrometallurgy, by leaching; or (iii) biometallurgy, by leaching through bacterial action (Brandl *et al*., 2001; Cui and Zhang, 2008; Gosh *et al*., 2015). Technologies applied in industry, and those under development, for the pyrometallurgical process route are discussed in this section.

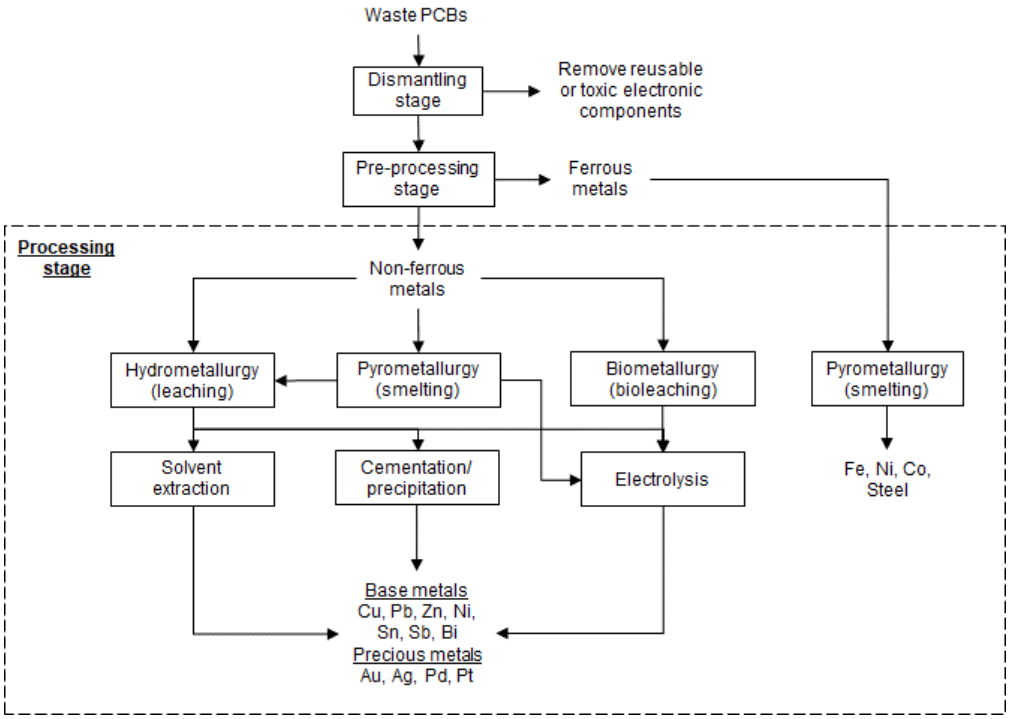

Figure 6. Flow sheet showing the processing stage of PCBs (adapted from Kaya [2016])

2.3.1.1 Co-smelting in secondary smelters

Well-established technologies in the processing of PCBs include the ISASMELT™ and Ausmelt top submerged-lance (TSL) smelters. Leading examples of the Ausmetl TSL application include DOWA mining plant in Japan and GRM plant in Korea (Wood *et al.*, 2011). Leading examples of ISASMELT TSL application include the Aurubis plant in Germany and the Umicore plant in Belgium (Alvear Flores *et al.*, 2014). The PCBs are co-smelted with Cu scrap, slimes and residues. A schematic flowsheet of the Umicore ISASMELT plant is depicted in Figure 80 in APPENDIX A. This plant features pyrometallurgical and hydrometallurgical circuits, where Cu and Pb are used as base metal collectors to recover the precious metals (Ag, Au & platinum group metals [PGMs]) and other valuable metals (Cu, Pb, Sn, Sb, indium [In], selenium [Se], tellurium [Te] & bismuth [Bi]) (Alvear Flores *et al.*, 2014). The disadvantages of these plants are the significant capital cost and the requirement for large volumes of PCBs feedstock (Lydall *et al.*, 2017).

2.3.1.2 Smelting in plasma arc furnaces

Another developed technology is the application of plasma arc furnaces to smelt shredded and calcined PCBs by Tetronics International (Tetronics, 2019). Unlike the ISASMELT technology, the Tetronics technology uses PCBs as primary feedstock. A

schematic of the process flowsheet of the Tetronics electronics waste treatment process is given in Figure 81 in APPENDIX A. Similarly to the previous technology, i.e. ISASMELT™, Tetronics plasma arc furnaces require significant capital investment, which necessitates large volumes of PCBs feedstock for commercialisation.

Szalatkiewics (2013) investigated the smelting of PCBs in a plasma arc furnace without shredding the PCBs, and without addition of any fluxing agents and reductant. The tests were carried out at 1375–1560°C under an oxidising furnace atmosphere. As much as 76 wt% of the metals in the feed PCBs were recovered with the rest of the metals oxidized to the slag. The alloy formed was heterogeneous. On re-melting, two distinct alloy phases were obtained with Fe-rich phase floating on top of a Cu-rich phase. This investigation did not analyse the Fe- and Cu-rich phases for precious metals to evaluate the partitioning of the precious metals between the two phases.

Byung *et al*. (2013) patented a method for the thermal recovery of metals from PCBs and automotive catalysts by making use of Cu, Fe, Sn and Ni contained in the PCBs as collector metals for noble metals. The method includes the use of a nonferrous slag fluxed with CaO. The materials are mixed and reacted in a plasma arc furnace at 1300–1450°C for periods of up to 40 min. The method claimed to achieve 98 wt% recovery of the precious metals (Ag, Au, PGMs) in a Cu alloy containing Fe, Sn and Ni.

The work by Kamberovic (2018) investigated smelting of a PCB concentrate obtained after physical beneficiation to remove the ceramic and plastic components. The concentrate comprised 80 wt% Cu with 10 wt% Sn, 5.6 wt% Pb and 3.0 wt% Zn as the main impurities. The PCB concentrate was first oxidised at 680°C to convert some of the Cu into Cu_2O to act as a solid oxidant. This process step added up to 9.4 wt% O_2 to the concentrate. The pre-oxidised concentrate was smelted in a 100 kW DC arc furnace at 1350°C along with charges of FeO, CaO and SiO_2 as flux (at 10 wt% of charge with Fe/SiO_2=1 and CaO at 12.5 wt% of flux). The test produced an alloy with a Cu grade of 98 wt%. However, this process obtained a significantly low Cu recovery of 25 wt% to the metal.

2.3.1.3 Smelting in top blown rotary converter

Bernardes *et al*. (1997) investigated the melting of PCBs in a TBRC that involved first an oxidising step followed by a reducing step. The process was able to achieve an environmentally friendly slag and a Cu-Ni-Sn alloy containing the precious metals. The slag composition approximated that of mullite ($3Al_2O_3{\cdot}2SiO_2$), deficient in Fe, and

the alloy contained up to 0.3 wt% Au. The dust captured in the flue gas was rich in the oxides of Pb and Zn that contained Ag. Although this study failed to remove most of the Sn (8.0 wt%), Pb (1.72 wt%) and Fe (1.52 wt%) from the alloy with a grade of 74 wt% Cu and 7.4% Ni, it confirmed the loss of Ag to the off-gas dust when smelting PCBs in a gas-fired rotary furnace.

Boliden's Ronnskar smelter in Sweden is one of the world's largest recyclers of e-waste employing the Ausmelt Kaldo technology (Reuter, 2014). The smelter's annual capacity for electrical material is 120,000 t which includes PCBs from computers and mobile phones (Tesfaye *et al.*, 2017). The Kaldo furnace produces a crude copper alloy known as black copper, and this alloy joins the facility's main smelter flow for further refining to extract copper and precious metals.

The SMS group (2017) announced that they will be building an UrbanGold compact plant for a Russian company named Aurus. The UrbanGold compact plant is a new commercial processing technology for the smelting of PCBs, as primary feedstock, in a TBRC. The TBRC smelting step produces a slag, Cu alloy, and Pb-Sn alloy stream. The latter alloy is refined in a rotary furnace to produce pure Pb-Sn alloy while the Cu alloy is refined in a Polyrefine™ furnace to produce Cu-anode alloy (see Figure 7).

It was claimed that the UrbanGold compact plant can recover more than 98 wt% of the precious metals (SMS group, 2018). This technology is ideal for the South African e-waste industry because the smelter furnaces are not completely dependent on electricity, and a commercial-scale plant can be built with a capacity to process 6000 t/a PCBs (SMS group, 2018). The UrbanGold compact plant is evidence that PCBs can be economically treated in gas-fired rotary furnaces, as the primary feedstock.

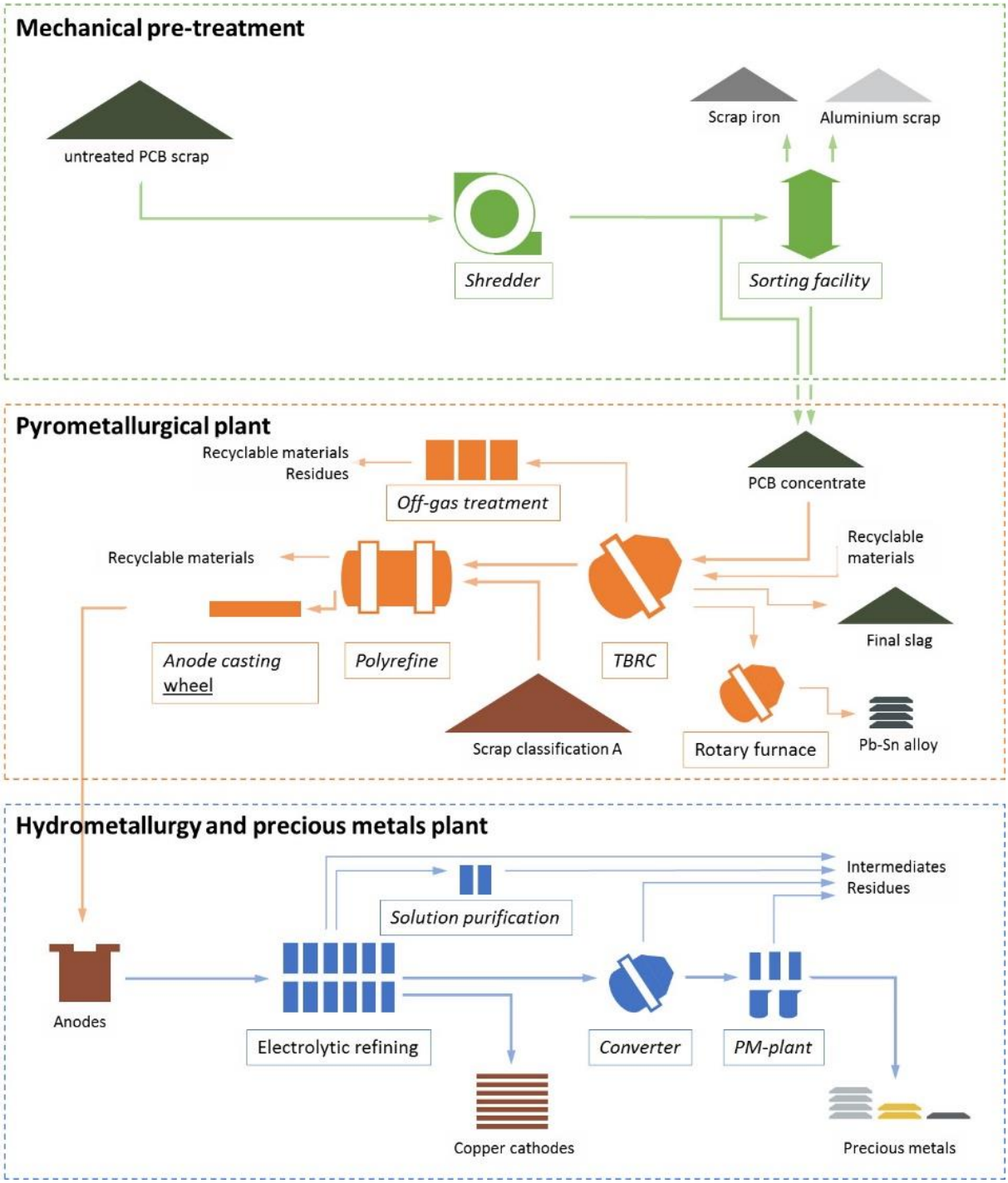

Figure 7. Process flow sheet of UrbanGold compact plant (source: SMS group [2017])

2.3.2 CRTs smelting technologies

The pre-processing stage produces separate streams of panel and funnel glass as illustrated in Figure 8. Closed-loop recycling of both glass types went obsolete due to obsolescence of CRT TVs and monitors (Xu *et al*., 2012). Each glass type follows a different processing route largely due to the presence or absence of Pb. This section discusses the processing of CRT funnel glass by pyrometallurgical methods to recover Pb metal.

2.3.2.1 Co-smelting in secondary smelters

The traditional recycling option for CRT funnel glass has been as a fluxing agent in secondary Pb smelters (Shaw, 2013; Xu *et al*., 2012). However, not all secondary Pb smelters can process CRT glass. The primary raw material of a secondary Pb smelter is recycled Pb-acid batteries. In an effort to minimize sulfur emissions, most secondary Pb smelters applied a soda-based slag (Siegmund, 2001). The need to produce more environmentally stable slags resulted in some of the smelters changing their operating slag composition to SiO_2- or fayalite (Fe_2SiO_4)-based slag systems (Siegmund, 2001). It is mostly such smelters that can accept CRT funnel glass. A typical flow sheet of a secondary Pb smelter in North America given in Figure 82 in APPENDIX A. Details of smelters that accept CRT funnel glass in North America are shown in Table 3.

Co-smelting of CRT funnel glass in secondary Pb smelters has the disadvantage of producing significant volumes of slag, which is associated with increased loss of valuable metals and higher treatment costs (Meng *et al*., 2016; Xu *et al*., 2012). Thus, only small amounts can be tolerated in these smelters as indicated by the annual plant capacities presented in Table 3. This limitation encouraged studies to focus on processing methods that can treat CRT funnel glass as the primary feedstock (Xu *et al*., 2012).

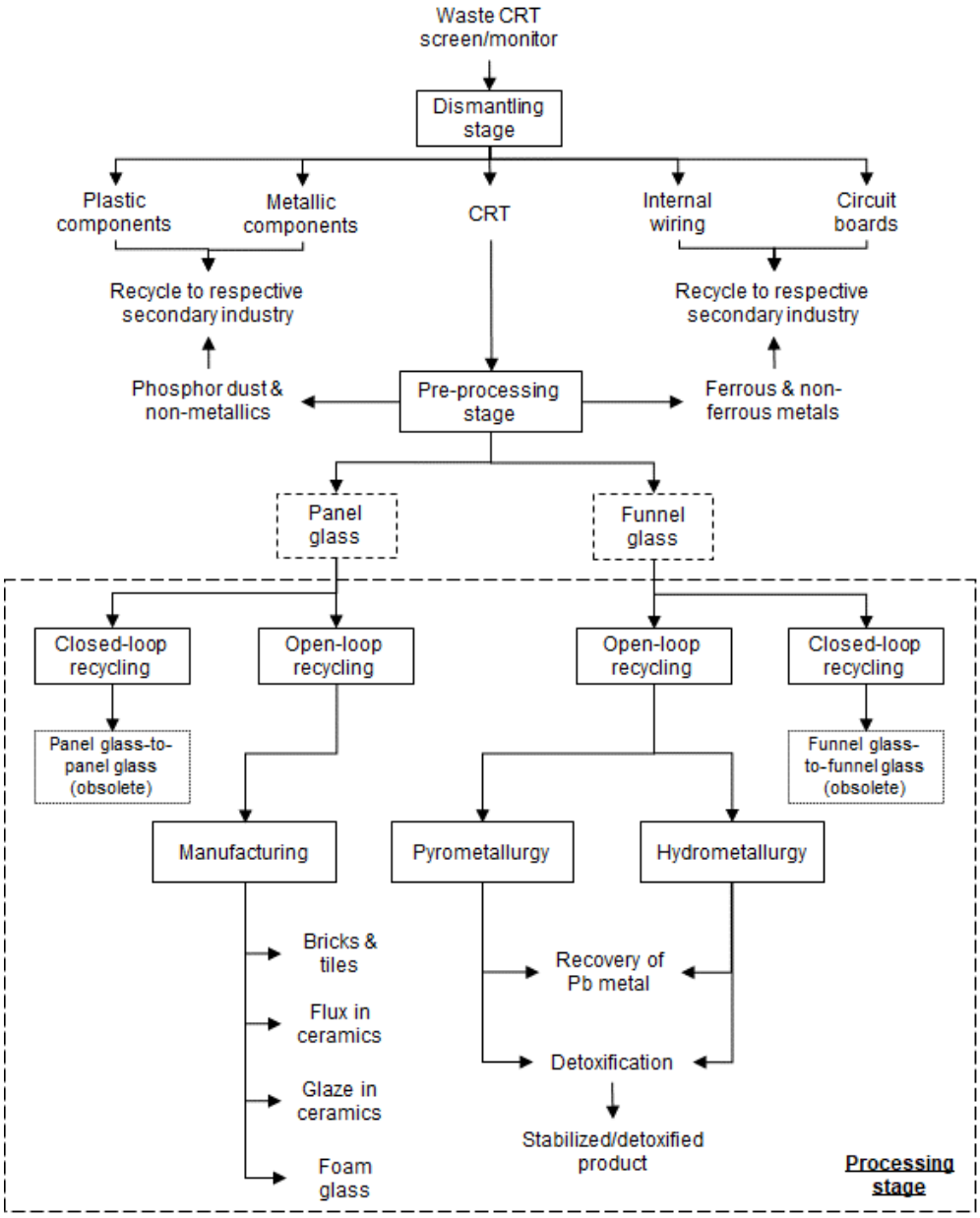

Figure 8. Flow sheet showing the processing stage of CRTs (adapted from Xu et al. *[2012])*

Table 3. Facilities in North America that can process CRT funnel glass (adapted from Shaw [2013])

Facility	**Location**	**Technology**	**Materials accepted**	**Capacity, t/a**
Doe Run Co.	Boss, Missouri, United States	Secondary Pb smelter	Stripped CRTs	8,000
Xstrata Zn	Bellendune, New Brunswick, Canada	Secondary Pb smelter	CRT funnel glass cullet	3,000
Teck Resources	Trail, British Columbia, Canada	Secondary Pb smelter	CRT funnel glass cullet or stripped CRTs	15,000
Total				**26,000**

2.3.2.2 Smelting at high temperatures and under vacuum

Wang and Zhu (2012) studied the extraction of Pb from CRT funnel glass by reacting the glass with magnesium (Mg) metal and ferric oxide (Fe_2O_3) at temperatures above 1745°C under atmospheric pressure. The method achieved Pb recoveries of over 90 wt%. The Pb was recovered as superfine PbO nanoparticles in a collecting chamber. A study by Veit *et al*. (2015) obtained 92 wt% Pb recovery from waste CRT funnel glass at 800°C under 1.3 kPa vacuum. These studies showed that Pb recoveries in excess of 90 wt% are achievable, but the high temperatures and vacuum conditions require expensive high-quality equipment, and such processes are typically complex to operate and to implement on an industrial scale (Meng *et al*., 2016).

2.3.2.3 Smelting with different reductants

Yot and Mear (2009) studied the use of silicon carbide (SiC) and titanium nitride (TiN) as reducing agents. Their studies showed that 5 wt% (of the mass of CRT funnel glass in a test) SiC and 5 wt% TiN mixed with CRT funnel glass, and reacted at 950°C for 60 min resulted in only 20 wt% and 40 wt% Pb recovery from the glass, respectively. In each case, metallic prills of Pb were obtained on the surface of the porous sintered residue.

Inano *et al*. (2019) developed a process that treats CRT glass and PCBs together in the same unit to simultaneously recover metals from each material. The process involved reduction melting of CRT glass with PCBs added as a source of reductant and precious metals. The study claims that 100 wt% Cu and Ni, 81 wt% Ag, and 73 wt% Au were recovered to the Pb alloy in the process. The process suggested by Inano *et al*. (2019) produces an alloy of Pb and Cu. Such an alloy is not ideal for downstream processing as it will require additional intermediate steps to separate the Pb from the Cu.

Lu *et al*. (2013) investigated the use of Fe powder as a reducing agent. Fe powder and CRT funnel glass powder were mixed at a mass ratio of 1:1 and pressed into blocks. The pressed blocks were reacted at 700°C for 30 min to achieve a Pb recovery of 58 wt%. The Pb was recovered as metallic prills disseminated throughout the sintered block of residue. Use of Fe as a reducing agent improved the Pb recovery but it was still relatively low. The advantage of this process was the application of an operation temperature as low as 700°C.

Further work by Lu *et al*. (2018a) culminated in a patent that provided a method for the thermal reduction of PbO in CRT funnel glass making use of C powder as a reductant and soda ash (Na_2CO_3) or potassium carbonate (K_2CO_3) as fluxing agents. The preferred feed mass ratio of C–to–glass was 1–3:10 and the preferred mass ratio of C–to–flux was 1:1–4. High recoveries of Pb were obtained when these mass ratios were applied. The patent claimed that the highest Pb recovery of 87.3 wt% was achieved at a temperature of 1100°C and a reaction time of 2 h under normal pressure.

2.3.3 Disadvantages of pyrometallurgical technologies

Pyrometallurgical routes are generally more economical, eco-efficient and maximize the recovery of precious metals, however, they have certain limitations that are summarized here (Cui and Zhang, 2008; Hageluken, 2006; Khaliq *et al*., 2014):

- Hazardous emissions such as dioxins are generated during smelting of feed materials containing halogenated flame retardants. Therefore special installations are required to minimize environmental pollution;
- A large investment is required for installing integrated e-waste recycling plants that maximize the recovery of valuable metals and also protect the environment by controlling hazardous gas emissions;
- Ceramic components in feed material can increase the volume of slag generated in the blast furnaces, which thereby increases the risk of losing precious metals from base metals; and
- Partial recovery and purity of precious metals are achieved by pyrometallurgical routes. Therefore, subsequent hydrometallurgical and electrochemical techniques are necessary to extract pure metals from base metals.

2.4 Alternative processing technologies

This section discusses hydrometallurgical and biometallurgical processes for recovering metals from PCBs and CRTs. Conventional or bio-leaching of the target metals is usually followed by purification processes such as solvent extraction, precipitation, and electrowinning (Silvas *et al*., 2015).

2.4.1 Alternative processing of PCBs

Leaching of PCBs to extract valuable metals is the most important step and the focus of most research (Gu *et al*., 2019). A detailed literature review completed by Gu *et al*.

(2019) indicated that leaching of PCBs can be carried out with acids, thiourea (CH_4N_2S), thiosulfate ($S_2O_3^{2-}$), halides (*e.g.*, chloride [Cl^-]), and by bacterial action. Acid leaching is discussed here and the other leachates are discussed in APPENDIX D.

Acid leaching is feasible with acids such as Aqua Regia ($HCl+HNO_3$), hydrochloric acid (HCl), nitric acid (HNO_3) and sulfuric acid (H_2SO_4) (Gu *et al.*, 2019). Kasper *et al.* (2011) reported a leaching efficiency of 92.8 wt% Cu under optimum conditions utilizing Aqua Regia but noted that this reagent cannot dissolve all the metals found in PCBs. Higher acid concentration and elevated temperatures generally enhance metal leaching rate (Gu *et al.*, 2019). However, Kim *et al.* (2011) achieved 97 wt% Cu and 93 wt% Au leaching efficiency utilising HCl at room temperature (25°C). Xiu *et al.* (2013) reported that a wide range of metals, including Pb, Sn, Zn, manganese (Mn), chromium (Cr), etc., can be leached out using HCl, but leaching rates of different metals heavily depended on acid concentration. Calgaro *et al.* (2015) demonstrated improved Cu leaching (90 wt% Cu) by H_2SO_4 and hydrogen peroxide (H_2O_2) with the aid of supercritical carbon dioxide (CO_2).

Kim *et al.* (2011) stated that smaller particle size and lower pulp density are also generally required for efficient metal leaching, which could require prolonged processing time, increased energy consumption and operating costs, ultimately compromising the practicability of the process.

2.4.2 Alternative processing of CRTs

CRT panel and funnel glass follow different processing routes due to their differences in the composition of Pb. The absence of Pb in panel glass makes it eligible to several secondary applications (ICER, 2004). Panel glass can be used in the following applications (Xu *et al.*, 2012):

- Use in manufacture of decorative bricks and cladding tiles. This application consumes about 300,000 t/a panel glass by factories in China.
- Use as a flux in manufacture of clay bricks and ceramic ware. This application consumes around 100,000 t/a panel glass in China.
- Use in ceramic glaze. This application consumes about 80,000 t/a panel glass in China.

The presence of Pb in funnel glass considerably limits its applications in secondary markets (ICER, 2004). The one application of funnel glass is its use in the manufacture

of X-ray shields which consumes about 25,000 t/a funnel glass in China (Xu *et al*., 2012).

The low consumption of funnel glass by secondary markets does not provide sufficient capacity for the volumes arising (Xu *et al*., 2012). Apart from the research in thermal methods, researchers have been looking into the possibility to recover Pb from funnel glass through hydrometallurgical methods (Xu *et al*., 2012). Preliminary results found that the strong bonds of the silicate glass network structure make it difficult to dissolve Pb-ions into solution at room temperature (Xu *et al*., 2012). As a result, most leaching-based processes occur at temperatures much higher than room temperature.

Okada *et al*. (2013) studied alkaline leaching of funnel glass in sulfur-containing medium. The highest Pb leaching rate (75 wt%) was achieved after 8 h at 180°C with an alkaline concentration of 6 mol/kg. Zhang *et al*. (2013) reported that more than 97 wt% Pb can be extracted from funnel glass with a stirring ball mill leaching process in 5 mol/kg sodium hydroxide (NaOH) at 70°C. They further noted that the combination of mechanical activation and a chemical leaching process in a single operation is more effective than the mechanical activation and subsequent chemical leaching. Additional studies are discussed in APPENDIX D.

The presented studies illustrate that it is feasible to remove Pb from the funnel glass by hydrometallurgical processes. However, none of these processes has been demonstrated to be commercially viable because some of them are quite problematic to industrialise or less attractive from a socio-economic and environmental point of view (Xu *et al*., 2012).

2.4.3 Disadvantages of hydrometallurgical technologies

Hydrometallurgical routes have been successfully used to recover precious metals from e-waste. However, these processes are associated with certain disadvantages that limit their application on the industrial scale. Some common limitations are (Arshadi *et al*., 2016; Cui and Zhang, 2008; Hilson and Monhemius, 2006; Khaliq *et al*., 2014; La Brooy *et al*., 1994):

- Overall, hydrometallurgical routes are slow and time consuming and negatively impact recycling economy.

- Cyanide (CN^-) is a dangerous leachant and should therefore be used with high safety standards. It can cause contamination of rivers and seawater, especially near Au mines, which poses serious health risks to the inhabitants.
- Halide leaching is difficult to implement due to strong corrosive acids and oxidizing conditions. Specialized equipment made of stainless steel and rubbers is required for leaching of Au using halide agents from e-waste.
- The use of thiourea leachants is limited in Au extraction due to its high cost and consumption. Moreover, further developments are required to improve the current technology of thiourea-based Au leaching.
- Bioleaching process generally have low leaching efficiencies and those that achieve high leaching efficiencies are still associated with extended leaching durations that make bioleaching processes challenging to industrialize.

2.5 Physicochemical principles

The application of high temperatures in pyrometallurgical processes generally results in rapid kinetics of the chemical reactions involved. Under such conditions, most steps in the overall process tend to proceed near equilibrium conditions (Seetharaman *et al*., 2014). As such, important principles involved in the pyrometallurgical removal of impurities from re-melted metal, by evaporation or oxidation, are related to several thermodynamic parameters, such as the Gibbs free energy change of the oxidation reaction, total pressure, activity coefficients of the impurity in the metal and its oxide in slag, oxygen (O_2) partial pressure, and temperature (Nakajima *et al*., 2011).

The same principles apply for reduction smelting except in this case instead of oxidation, the metals of interest are reduced from their metal oxides. In addition to the above thermodynamic parameters, the ratio of the equilibrium partial pressure of carbon monoxide (CO) to CO_2 gas becomes important in reduction reactions, especially those involving the use of carbon (C) and CO as reductants (Shamsuddin, 2016). This section looks into the physicochemical principles involved in the removal of impurities from Cu metal and reduction smelting of metal oxides, and by extension, the reduction of PbO in CRT funnel glass.

2.5.1 Removal of impurities

Impurities can be removed from molten metal by mass transfer to other phases in contact with the metal as shown in Figure 9. Possible routes for the removal of

impurities include (a) removal to the slag phase; (b) removal to the gas phase; (c) formation of inclusions; (d) absorption of inclusions; and (e) reaction with refractory (Seetharaman *et al.*, 2014). Impurity removal to the gas and slag phase are considered the most important routes in industrial pyrometallurgical processes, and are discussed further in this section.

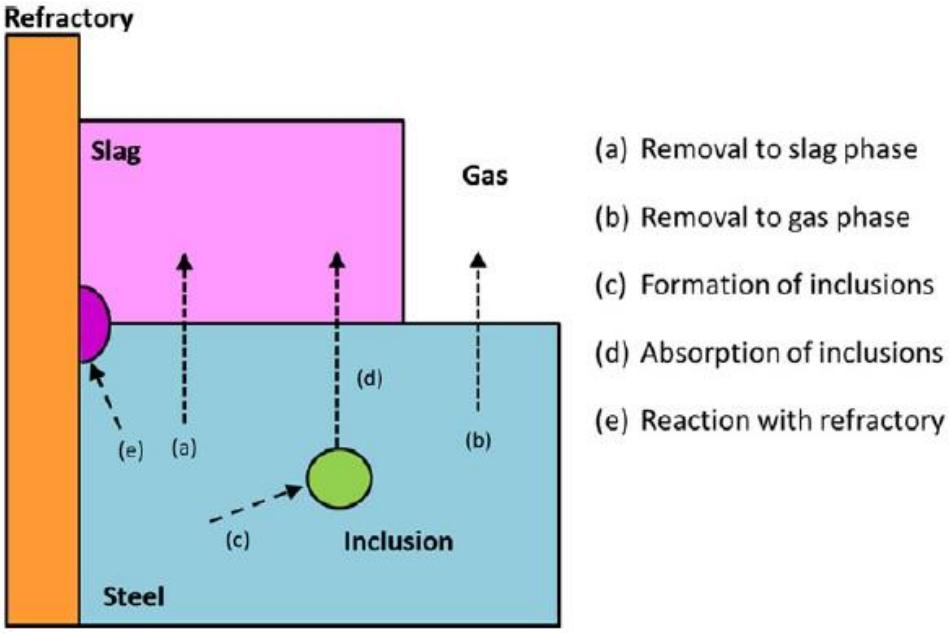

Figure 9. An example of possible routes for removal of impurities from steel (source: Seetharaman et al. *[2014])*

A measure of an element's tendency to be removed in the gas phase is the vapour pressure of the pure element at any particular temperature (Seetharaman *et al.*, 2014). Elements with high vapour pressure are relatively easy to remove in the gas phase, while those with lower vapour pressure are more difficult to remove by evaporation (Seetharaman *et al.*, 2014). It can be noted from Figure 10 that elements such as Pb and Zn have higher vapour pressures than Cu at the selected temperature. Thus, these two elements should be easier to remove in the gas phase.

An important indicator of the oxidation behaviour of an element is the O_2 partial pressure in equilibrium with the pure element and the corresponding oxide at any particular temperature (Seetharaman *et al.*, 2014). Elements that are oxidized at relatively low O_2 partial pressure tend to be easily oxidized and are then removed by the slag phase (Seetharaman *et al.*, 2014). In Figure 10, an element such as Al has an exceedingly lower O_2 partial pressure relative to Cu, implying it will be much easier to oxidize and remove by slag phase.

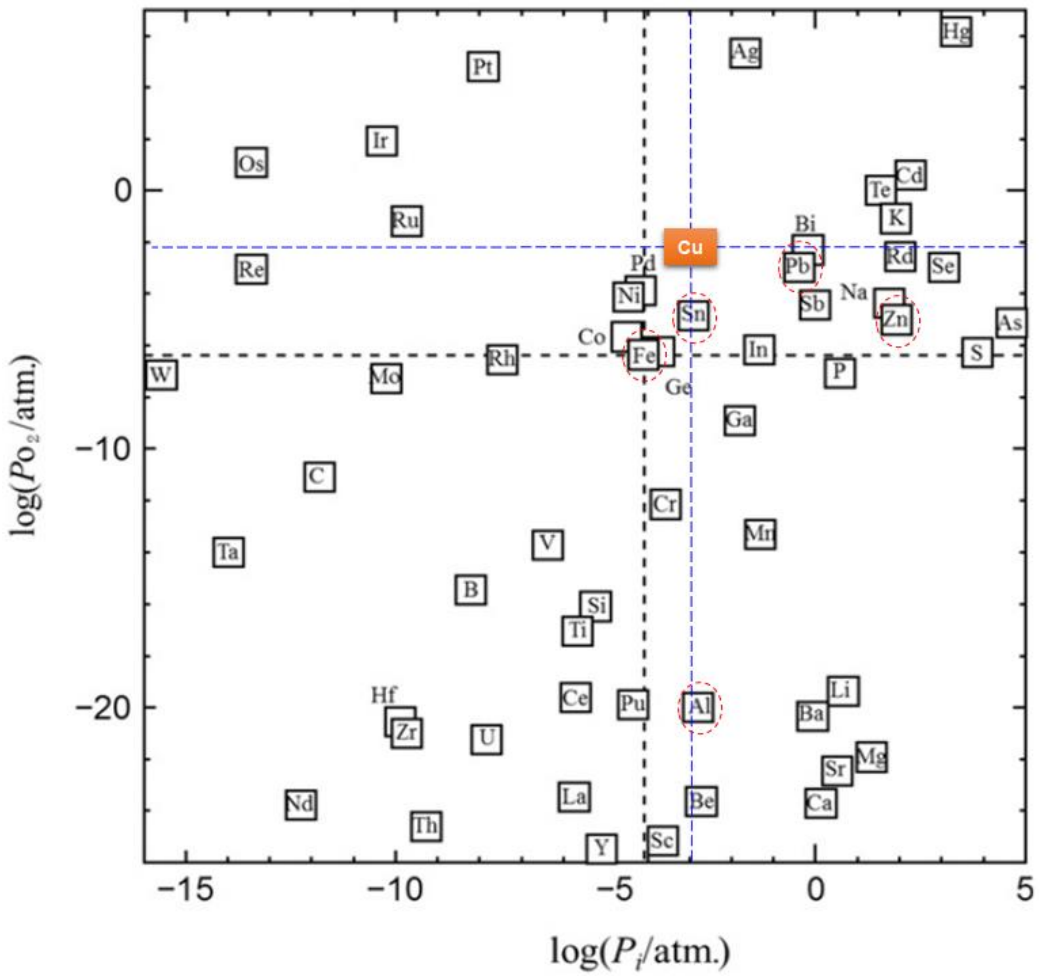

Figure 10. Relationship between vapour pressure of pure element and O_2 partial pressure for metal/oxide equilibrium at 1600°C. Note: P_i *is vapour pressure of element* i *(source: Seetharaman* et al. *[2014])*

In fire refining of Cu, as studied by Zhukov *et al*. (2016), the principle discussed in the previous section, in relation to the relative ease of oxidation of elements with low O_2 partial pressures at equilibrium, is applied for the removal of impurities by the slag. During fire refining the metal is oxidized by blowing air or O_2 to the molten bath of metal. Since Cu is present in high concentration, it is oxidized first according to reaction [1]:

$$4[Cu]_{metal} + \{O_2\}_{gas} \rightarrow 2(Cu_2O)_{slag/solid} \qquad [1]$$

Where $[i]_{metal}$ is species i dissolved in metal phase, $\{i\}_{gas}$ is species i in the gas phase, and $(i)_{slag/solid}$ is species i dissolved in the slag or separate solid phase. The cuprous oxide (Cu_2O) formed, reacts with other impurity metals (indicated as M) with higher affinity for O_2 compared to Cu, according to reaction [2]:

$$(Cu_2O)_{slag/solid} + [M]_{metal} \rightarrow 2[Cu]_{metal} + (MO)_{slag/solid} \quad [2]$$

The oxides of impurity metals collectively form slag and float over the metal bath surface. Removal of the slag further enhances refining as this lowers the chemical potential of species *MO* in slag. The impurity metals may be oxidized not only by Cu_2O but also by other metal oxides present in the molten Cu as shown by reaction [3]:

$$[M_1]_{metal} + (M_2O)_{slag/solid} \rightarrow [M_2]_{metal} + (M_1O)_{slag/solid} \quad [3]$$

In reaction [3], impurity metal M_1 has a higher affinity for O_2 than impurity metal M_2. Any metal present in the system, having higher affinity for O_2, is preferentially oxidized and removed to the slag at a higher rate than those with lower O_2 affinity. Thus, the sequence of removal will follow the order Al, Si, Mn, Fe, Zn, As, Sn, Sb, Ni, and Pb.

According to Azakami and Yazawa (1976) the distribution of impurity metals in fire refining can be divided into three groups using the equilibrium constant (*K*) of reaction [2], as shown in equation [4]:

$$K_{react\,[2]} = \frac{(a_{Cu})^2 \times a_{MO}}{a_{Cu2O} \times a_M} \quad [4]$$

Where, a_i is the activity of species *i*. Impurity metals with *K* values of less than 10^{-2}, such as Au, Hg, Ag, platinum (Pt), Pd, Se, thallium (Tl), and Te, will not oxidize. Impurity metals with *K* values higher than 10^3, like Fe, Zn, Na, Cr, Mn, Si, titanium (Ti), Al, Ba, Mg, Be, and Ca, will oxidize easily and will not remain in the refined Cu. Impurity metals with intermediate *K* values present difficulties and are not easily removed from Cu, and they include Bi, Pb, Ga, Ni, Cd, Sb, As, cobalt (Co), Ge, Sn, and In.

Nakajima *et al*. (2011) theoretically evaluated the distribution of elements to the gas, slag, and metal phase in a simulated Cu converter (see Figure 11). The results confirmed that precious metals (Au, Ag, Pd and Pt) completely distribute to the metal phase while metals such as Al and Fe completely distribute to the slag. It was further noted that Zn partially distributed to the gas and slag phase while Sn partially distributed to the metal and slag phase. Pb, on the other hand, partially distributed to all three phases.

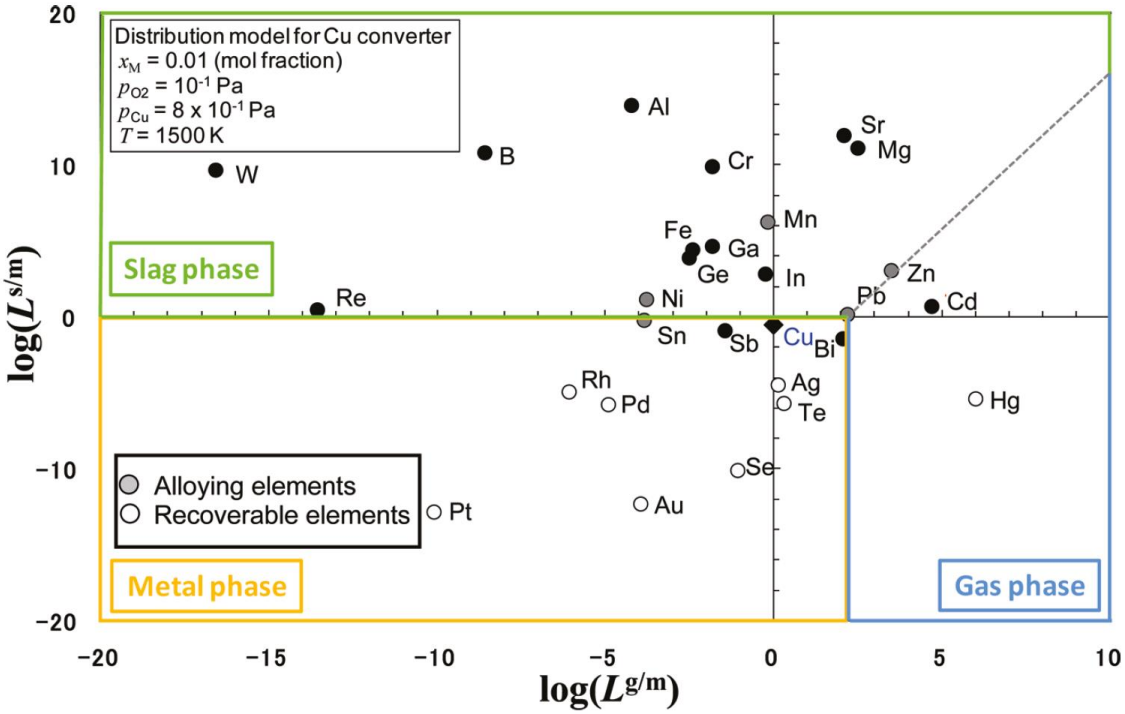

Figure 11. Elemental distribution among gas, slag and metal phases under simulated atmosphere of a Cu converter. Note: $L^{s/m}$ is distribution ratio between slag and metal phase, $L^{g/m}$ is distribution ratio between gas and metal phase (source: Nakajima et al. *[2011])*

The study by Chen *et al.* (2021) and Sukhomlinov *et al.* (2020, 2019) showed that the distribution of Ag and Sn between copper alloy and FeO-saturated slag is highly dependent on temperature and O_2 partial pressure (see Figure 12). It was shown that the removal of Ag and Sn from copper alloy was favoured at higher temperatures and O_2 partial pressures.

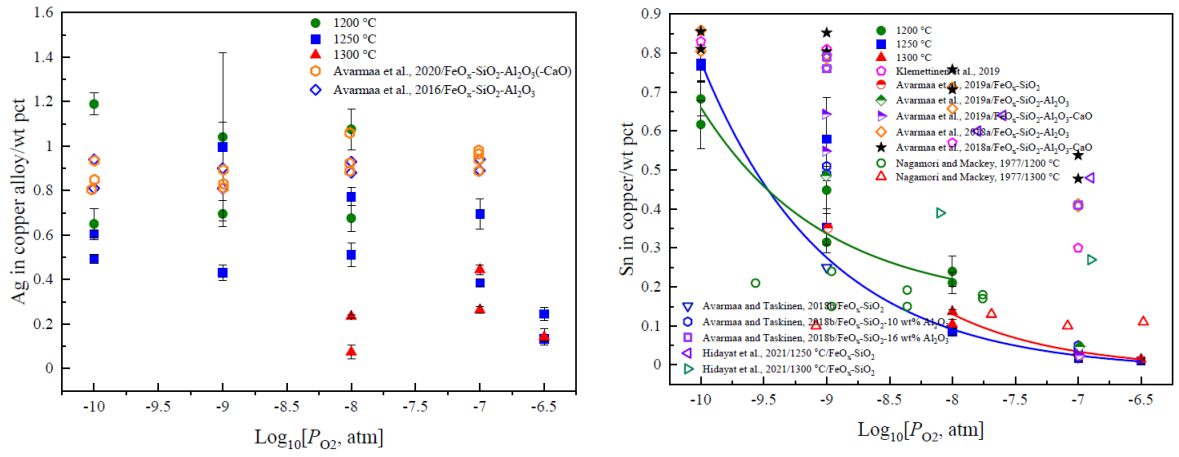

(a) (b)

Figure 12. Concentrations of (a) Ag and (b) Sn in copper alloy as function of P_{O2} *at 1200–1300°C (source: Chen* et al. *[2021])*

The rate of O_2 absorption into liquid Cu plays an important role in the removal of impurities from Cu during fire refining (Marin and Utigard, 2005). The effect of three process parameters on the rate of O_2 absorption into liquid Cu by top blowing of O_2 is discussed in APPENDIX E. In this section, the effect of O_2 partial pressure on the oxidation rate constant (k) is presented. The studies by Marin (2006) and Wastawino (2005) showed that the rate of oxidation of impurities from a Cu alloy during fire refining is directly proportional to the O_2 partial pressure (see Figure 13).

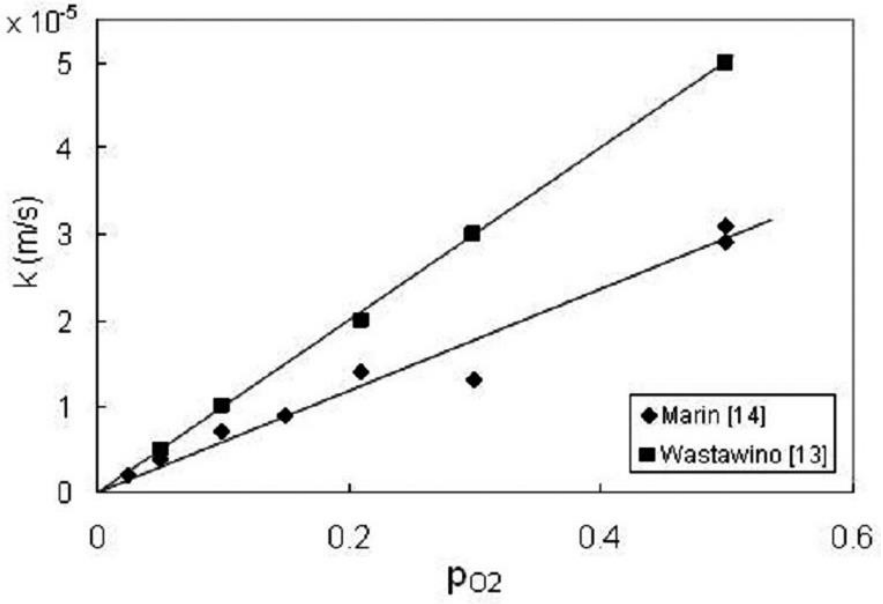

*Figure 13. Plot showing relationship of oxidation rate constant (*k*) vs. O_2 partial pressure (source: Marin [2006])*

2.5.2 Reduction smelting

Metals extracted from their oxides by pyrometallurgical processes are generally reduced by means of a suitable reducing agent. Physical characteristics such as melting and boiling points, and vapour pressure of the metal as well as the relative stability of its oxide as compared to the oxides of impurity metals and gangue mineral oxides are major factors in the selection of reducing agents (Shamsuddin, 2016). The most common reducing agents of commercial and industrial importance include C , CO, and H_2 (Rosenqvist, 1974). This section discusses reduction smelting by C and CO.

The change in the standard Gibbs free energy of formation of a compound, ΔG_f^o, is a measure of the thermodynamic driving force or chemical potential of a reaction (Shamsuddin, 2016). The ΔG_f^o vs T relations for oxidation reactions involving one mole of gaseous O_2 are known as Ellingham diagrams. These diagrams are based on

pure metals and their oxides whose activities equal one. Typical pyrometallurgical processes involve production of solutions such as alloys and slags that are not necessarily saturated in specific component. Thus, it is important to use Elligham diagrams with caution since the activities of such components are generally less than one. Alternatively, thermochemical software that features databases with solution phases can be used to estimate realistic activities. Nonetheless, useful qualitative pyrometallurgical information can be extracted from the Ellingham diagrams and the three main uses are (Seetharaman *et al*., 2014):

- To determine the relative ease of reducing a given metal oxide to metal;
- To determine the partial pressure of O_2 that is in equilibrium with a metal and its oxide at a given temperature; and
- To determine the ratio of the partial pressure of CO to CO_2 that is required to reduce the metal oxide to metal at a given temperature.

Now consider reduction reaction [5] making use of CO as a reducing agent (Shamsuddin, 2016):

$$(MO)_{slag/solid} + \{CO\}_{gas} = [M]_{metal} + \{CO\}_{gas} \quad [5]$$

If *M* and *MO* are present as pure condensed phases that are mutually immiscible (activity = 1), then the equilibrium constant *K* of reaction [5] is dependent on the ratio of the partial pressure of CO to CO_2 as shown by equation [6]:

$$K_{react\,[7]} = \frac{P_{CO2} \times a_M}{P_{CO} \times a_{MO}} = \left(\frac{P_{CO2}}{P_{CO}}\right) \quad [6]$$

At equilibrium, the change in Gibbs free energy for reaction [5] can be calculated from equation [7]:

$$\Delta G^o_{react\,[7]} = -RTln(K) = -RTln\left(\frac{P_{CO2}}{P_{CO}}\right) = 4.606RTlog\left(\frac{P_{CO}}{P_{CO2}}\right) \quad [7]$$

Thus, to drive reaction [5] to the right, in other words, to promote reduction of *MO* to *M*, the ratio of the partial pressure of CO to CO_2 must be higher than the ratio at equilibrium, which can be estimated from the Ellingham chart.

When the reduction reaction is occurring in the presence of a pure solid C (activity = 1), the Boudouard reaction, given by reaction [8], will also occur:

$$(C)_{solid} + \{CO_2\}_{gas} = \{2CO\}_{gas} \quad [8]$$

The equilibrium constant of reaction [8] is also highly dependent on the ratio of the partial pressure of CO to CO_2 as follows:

$$K_{react\,[10]} = \frac{P_{CO}}{P_{CO2} \times a_C} = \left(\frac{P_{CO}^2}{P_{CO2}}\right) \qquad [9]$$

According to the Boudouard reaction, CO is the dominant oxide of C at temperatures above 700°C, and the higher the temperature the more effective a reductant C is (Shamsuddin, 2016).

The effect of four process parameters on the extraction and recovery of Pb from CRT funnel glass is discussed. The studies by Lu *et al*. (2018b) are presented for the following parameters: (i) reductant addition, (ii) reaction temperature, (iii) flux addition, and (iv) reaction time. Lu *et al*. (2018b) investigated reduction smelting of CRT funnel glass in air, with pure C used as a reductant and Na_2CO_3 as a flux.

The effect of increasing reductant addition on Pb recovery is presented in Figure 14. The results show a trend of increasing Pb recovery with increasing reductant addition, until a point above which no further increase in Pb recovery is observed (*i.e.,* C/Pb glass = 0.2 in Figure 14).

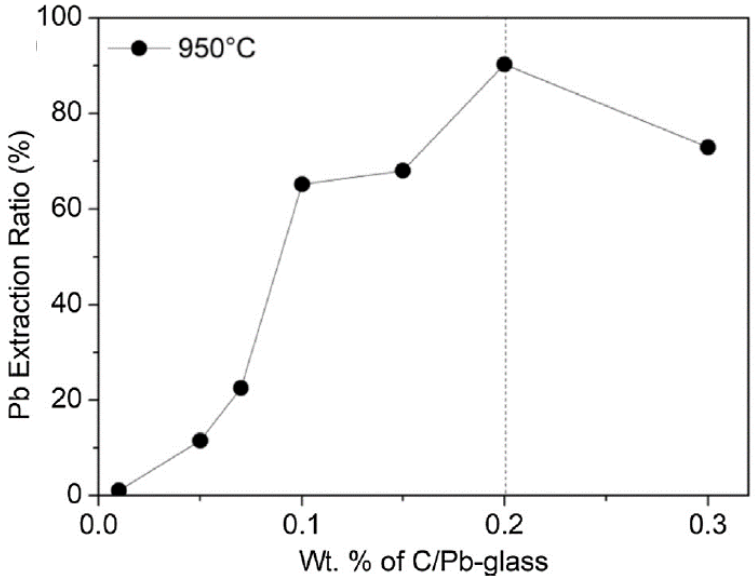

Figure 14. Effect of increasing reductant addition on Pb recovery/extraction (source: (a) Lv et al. *[2016]; (b) Lu* et al. *[2018b])*

Figure 15 presents the effect of increasing reaction temperature. Reaction temperature has a similar effect on Pb recovery as reductant addition. The higher the temperature

the higher the Pb recovery, until a point above which no further increase in Pb recovery is observed (*i.e.*, 950°C).

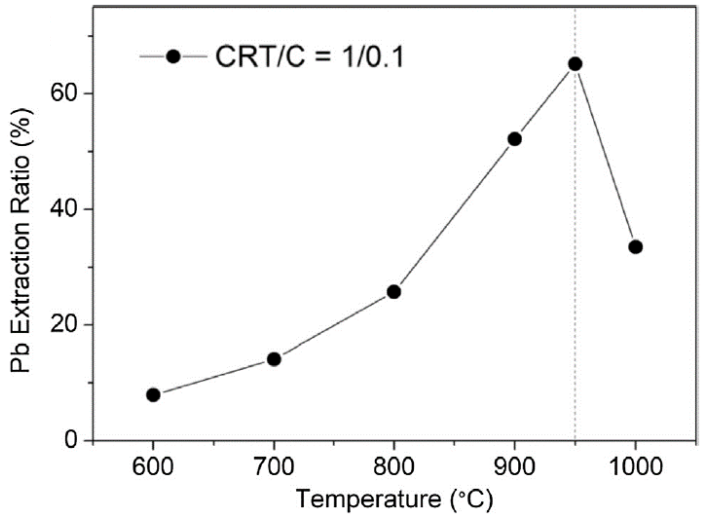

Figure 15. Effect of increasing temperature on Pb recovery/extraction (source: (a) Lv et al*. [2016]; (b) Lu* et al.*[2018b])*

The effect of increasing flux addition is presented in Figure 16. Lead recovery initially increases with increasing addition of flux until it reaches a maximum (*i.e.*, $C/Na_2CO_3 = 1/3$). Further increase in flux addition beyond this maximum resulted in a decrease in the Pb recovery.

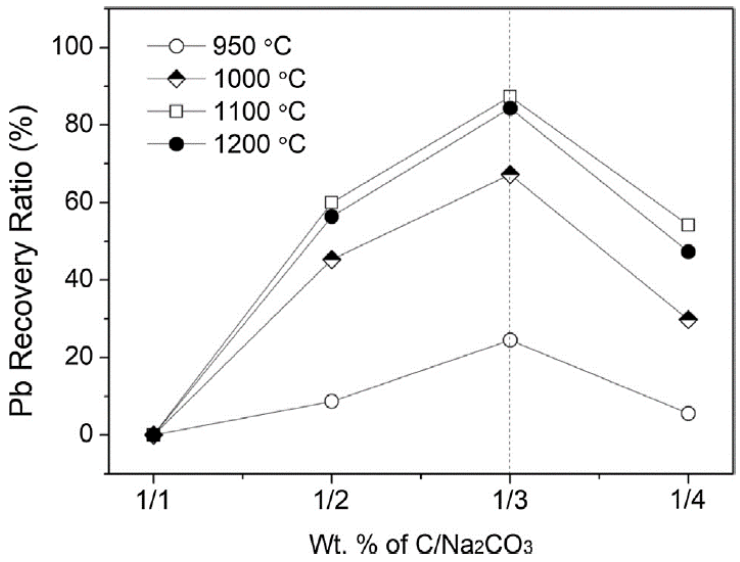

Figure 16. Effect of increasing flux addition on Pb recovery/extraction (source: (a) Lv et al. *[2016]; (b) Lu* et al.*[2018b])*

Figure 17 depicts the effect of reaction time on Pb recovery. A trend of decreasing Pb recovery with increasing reaction time was obtained. This indicates that extended reaction time negatively impacts recovery of Pb to the metal phase.

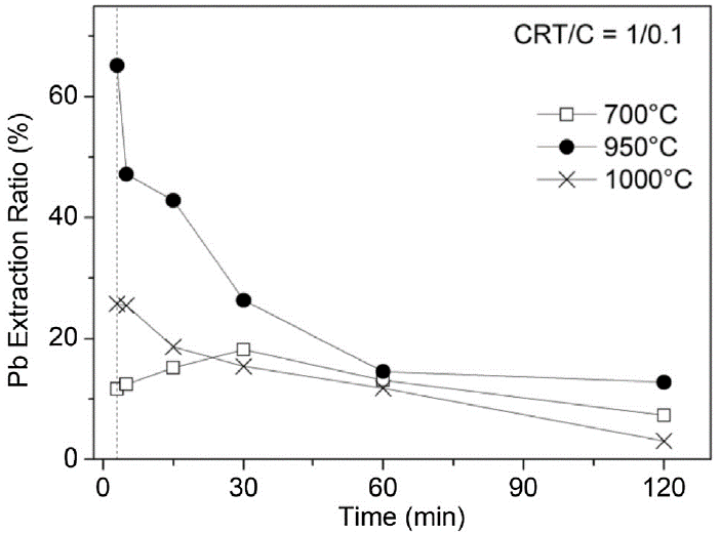

Figure 17. Effect of increasing reaction time on Pb recovery/extraction (source: (a) Lv et al. *[2016]; (b) Lu* et al. *[2018b])*

2.6 Thermochemical software

There is limited data for the exact system under study where all the aspects of the processes investigated are addressed. Theoretical calculations can be undertaken to assess the system at equilibrium under different process conditions, and the model output obtained therefrom can be compared with the experimental results. Such calculations require an extensive database of reliable thermodynamic data. Thermochemical software packages such as Factsage™ (Bale *et al.*, 2009) can be applied to assess systems where limited empirical data exist.

Factsage is a fully integrated thermochemical software and database package. It consists of a series of information, database, calculation and manipulation modules that enable one to access and manipulate pure substances and solution databases. With the various modules one can perform a wide variety of thermochemical calculations and generate tables, graphs, and figures to describe the properties of a thermodynamic system under study (Bale *et al.*, 2009).

The solution databases contain optimized model parameters for the Gibbs free energy of solution phases as functions of composition and temperature. The compound databases contain properties of stoichiometric compounds (pure substances), either obtained from published experimental data and phase diagram optimizations or referenced from standard compilations (Bale *et al.,* 2016).

In the past decade, most of the databases have been revised and updated, and some new ones have been added (Bale *et al.,* 2016). The current study made use of version 8.0 of the software (Fastsage 8.0) and databases used are FactPS, FToxid, and SGTE. FactPS contains thermodynamic data for pure substances, and now contains data for 4777 compounds. FToxid is the oxide database for slags, glasses, minerals, ceramics, refractories, etc. It has been extensively updated and now contains data for 374 stoichiometric oxides and 87 oxide solutions. SGTE is the alloy database for a wide range of alloys. It contains data for 78 elements, and now incorporates about 317 different solution phases and 1166 stoichiometric intermetallic compound phases (Bale *et al.,* 2016). The selected databases in Factsage 8.0 contain data for all elements of interest (*i.e.*, Al, Ag, Au, Ba, Ca, Cr, Cu, Fe, K, Mg, Mn, Na, Pb, Pd, Pt, Si, Sn, and Zn) within the temperature range (200–1500°C) of systems considered in the current study.

2.7 Research questions

The primary goal of the current study is to experimentally answer the following question:

Is it technically feasible to integrate the smelting of waste CRT funnel glass into the same flowsheet as the smelting of waste PCB concentrate?

In order to answer the above question, the study explored the following two technical questions:

1. Can oxidative smelting of PCB concentrate and CRT slag (recycled from the CRT process) produce a crude Cu alloy with a grade of more than 95 wt% Cu?
2. Can reductive smelting of CRT funnel glass and PCB fumes (recycled from the PCB process) produce a crude Pb alloy with a grade of more than 95 wt% Pb?

The above questions set out a criteria against which the feasibility of the integrated process will be measured. The experimental results of the tests that meet the alloy grade requirement will be ranked by recovery to determine the process conditions that provide the highest recovery of Cu (for PCBs) and Pb (for CRTs) to the metal.

2.8 Research objectives

This section presents the main research activities which outline the technical scope of the research work. The objectives of the research are:

1. To characterize the raw materials and products by determining the bulk chemical and phase-chemical composition.
2. To perform chemical thermodynamic calculations with the Factsage™ software package (Bale *et al.,* 2009) to estimate the highest achievable theoretical recovery of Cu and Pb to the metal stream to produce a crude alloy with a grade of more than 95 wt% Cu and 95 wt% Pb, respectively.
3. To conduct a series of tests in a pilot-scale TBRC furnace to (i) smelt PCB concentrate under oxidizing conditions to confirm the highest achievable recovery of Cu at the required alloy grade; and (ii) smelt CRT funnel glass under reducing conditions to confirm the highest achievable recovery of Pb at the required alloy grade.

3 EXPERIMENTAL PROCEDURES

The description of equipment, materials, and operating procedures adopted during the test work is presented in this chapter. The main equipment in the pilot facility, including gas supply train and rotary furnace, are described first, followed by description of methods and techniques applied to sample and analyse the raw materials. Before the experimental procedure of the smelting tests is described, an overview of the experimental plan for each smelting campaign is presented. Lastly, sampling and analytical methods applied to characterise the products are described along with mass balance techniques.

3.1 Equipment description

This section focuses on describing the key features of equipment utilised in the pilot smelting tests. The overview of the pilot facility is presented. This is followed by descriptions of pertinent equipment and instruments in the three main sections of the facility.

3.1.1 Facility overview

The pilot facility consists of three main sections, namely: (i) gas supply train; (ii) TBRC furnace; and (iii) off-gas handling system. A schematic and an image showing the relative arrangement of the major equipment in the facility is given in Figure 18 and Figure 19, respectively. The facility is completely manually controlled, attesting to its simple design. The TBRC is a versatile unit with capability to handle a wide variety of pyrometallurgical processes including refining, reductive and oxidative smelting, roasting, and fuming processes.

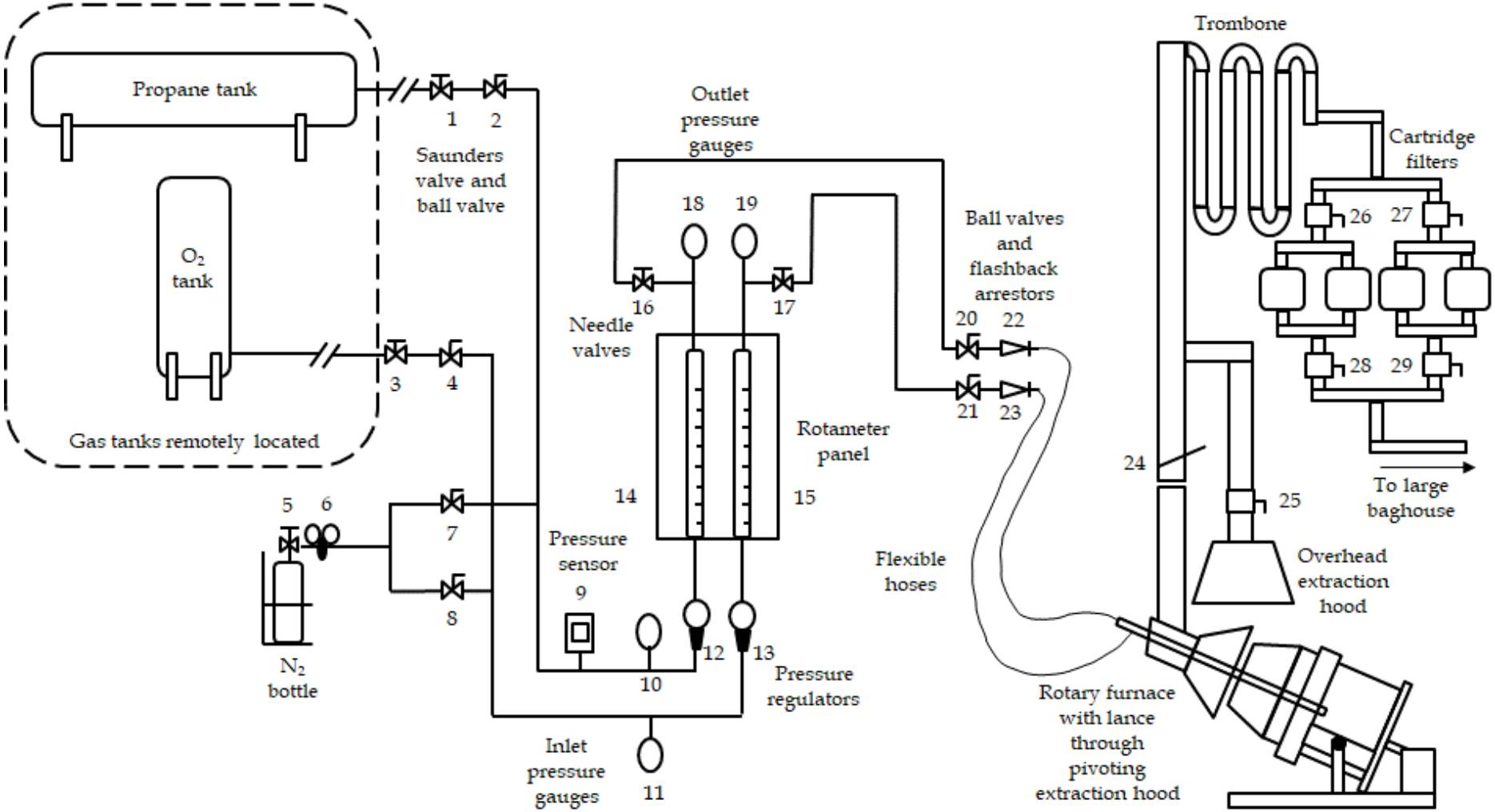

Figure 18. Schematic overview of the TBRC facility

Figure 19. Photograph of the TBRC facility showing furnace tapping operation

3.1.2 Gas supply train

The facility uses an oxy-propane burner to continuously supply O_2 and propane (C_3H_8) gas for combustion to heat the furnace. O_2 was supplied from a 3 t bulk O_2 tank located remotely from the facility. O_2 was supplied at a maximum line pressure of 650 kPa (gauge). C_3H_8 was supplied from a 4.5 t bulk C_3H_8 tank also located a distance away from the facility. C_3H_8 was supplied at a maximum line pressure of 160 kPa (gauge).

An infrastructure of gas pipelines from the bulk storage tanks supplies gas to the various take-off points in the pilot facilities. The pipeline delivering gas from the bulk storage tank to the rotary furnace is called a gas supply train. The C_3H_8 line has steam piping and is fitted with a Tecfluid variable area flowmeter (No. 14, Figure 18) model PS31-0400. This flowmeter makes use of a Teflon float to deliver a maximum flow of 5.6 Nm^3/h at 50 kPa (gauge). The letter *N* in Nm^3/h stands for normal temperature and pressure, which is defined as 20°C and 1 atm, respectively. The O_2 line has steam piping and is also fitted with a Tecfluid variable area flow meter (no. 15) model PS31-0630. The O_2 flow meter uses a stainless steel float to give a maximum flow of 30 Nm^3/h at 200 kPa (gauge).

Pressure regulators (no. 12 and 13) and needle valves (no. 16 and 17) were used to regulate the inlet line pressure and the flow rate of the gases, respectively. The pressure through the flow meters were kept constant at 200 kPa (gauge) for O_2 and 50 kPa

(gauge) for C_3H_8. Each solid gas line was terminated with a ball valve (No. 20 and 21) and a flashback arrestor (No. 22 and 23) installed before a stainless steel flexible hose that is connected to the burner.

The burner is a metal pipe with several concentric pipes welded together. The burner was designed to a flame power rating of 120 kW. It was mounted in the pivotal extraction hood to ensure easy access to the furnace. The burner was 1.2 m long with 4 × concentric pipes that were made of stainless steel. Figure 20 shows a technical drawing of the burner. The inner most pipe had a 10 mm diameter pipe and carried the C_3H_8 gas, while the 20 mm diameter annulus surrounding it carried O_2 gas. The gas ensemble was surrounded with a 30 and 50 mm diameter pipes for cooling water.

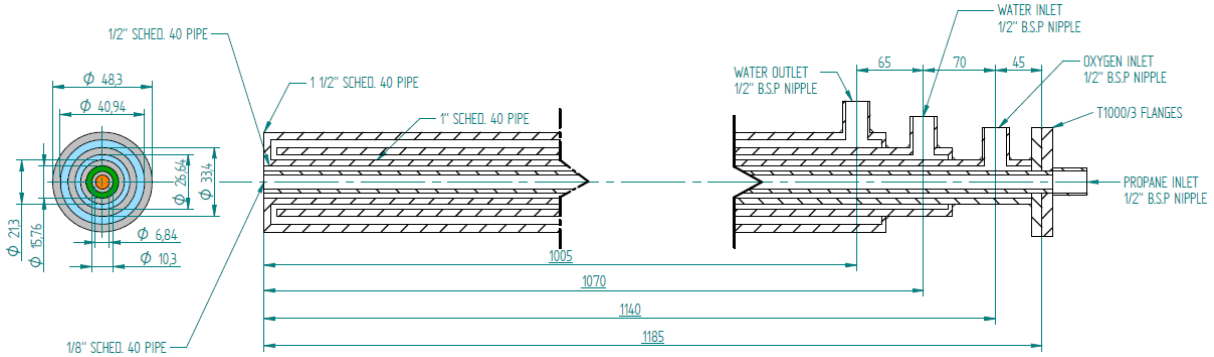

Figure 20. Technical drawing of burner

3.1.3 Furnace

The rotary furnace vessel was made of a cylindrical mild steel shell with a diameter of 600 mm and height of 585 mm. It had a conical shape that tapered from 600 mm in diameter to 400 mm as shown in Figure 21. The shell was lined with a monolithic refractory with 138 mm thickness on the side walls and 150 mm thickness on the base. The vessel was mounted on a steel frame inclined at 30° to the floor, and the frame was tilted by hydraulic pistons operated from a portable hydraulic pressure pack. A 0.37 kW variable speed motor enabled the vessel to be rotated at 2–10 rpm. Images showing the front and rear view of the furnace are presented in Figure 22.

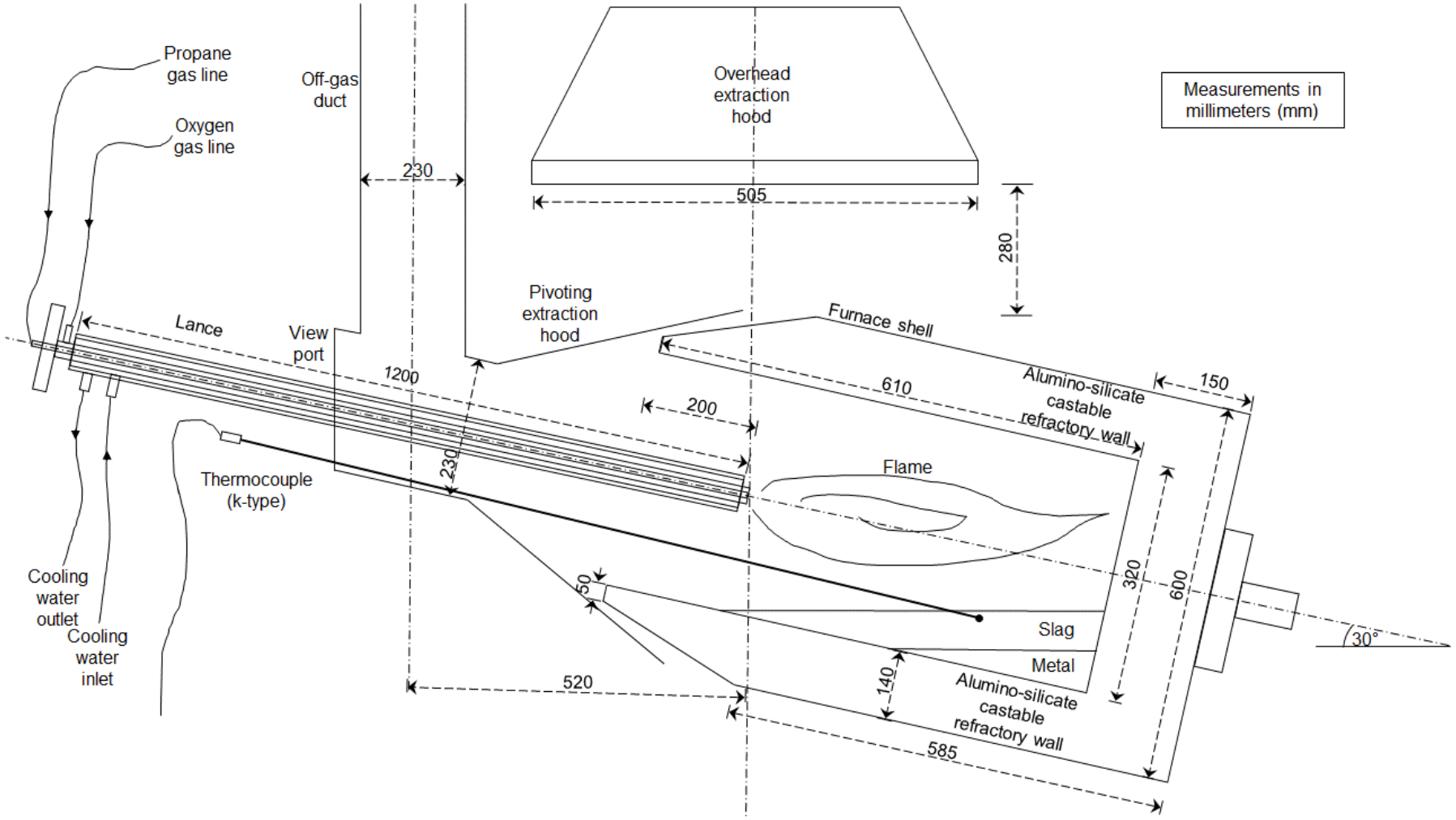

Figure 21. Section view of TBRC furnace, with dimensions in mm

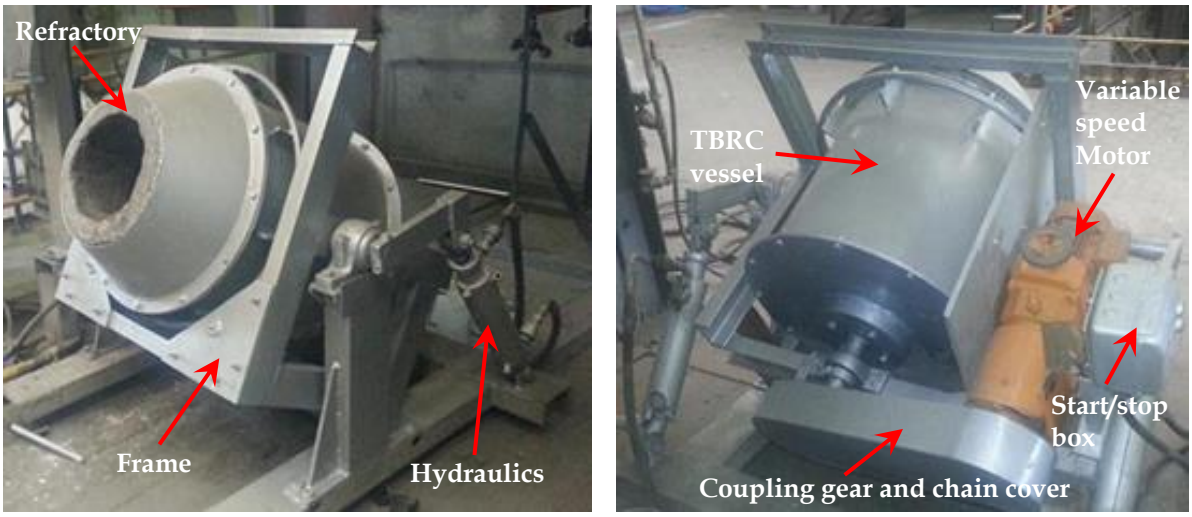

Figure 22: Pictures of front and rear view of the TBRC furnace

The monolithic refractory was a conventional castable composed of high-grade Al_2O_3. The refractory lining provided a protective and insulating layer to withstand the prevailing corrosive environment and high temperatures inside the furnace. The type and grade of refractory applied to the furnace was specified for a maximum operating temperature of 1650°C with chemical compatibility to acidic slags (see composition in Table 4).

Table 4: Chemical Composition of high-grade Al_2O_3 refractory

Component	Mass, wt%
Al_2O_3	93
SiO_2	0.5
Fe_2O_3	0.1
TiO_2	0.1
CaO+MgO	5.5
K_2O+Na_2O	0.3

3.1.4 Off-gas handling system

The facility employed a two-stage filtration system. Primary filtration occurred through a bank of cartridge filters and secondary filtration in a baghouse downstream of the cartridge filters. Fumes, dust and gases produced during feeding and smelting operations were captured by the pivoting and overhead extraction hoods. The overhead extraction hood captured fugitive gases that escaped the pivoting extraction hood or fumes coming off during feeding operation when the pivoting extraction hood was pulled away from the mouth of the furnace. The off-gas captured by the extraction

hoods was transferred through a mild steel duct to the cartridge filters before it was transferred to the baghouse for secondary filtration. The suction intensity for both extraction hoods was controlled with butterfly valves located directly above each respective hood.

Ducting is the piping section of the off-gas handling system that was responsible for channelling the off-gas from the furnace, through the cartridge filters, and all the way to the baghouse. The ducting included a trombone section that was utilised to provide an extended surface area for cooling the off-gas before it reached the cartridge filters. The trombone was fitted with a fan to improve cooling of the off-gas. The cartridge filters were cylindrical with a length and diameter of 406 and 282 mm, respectively. The filtration medium of the filters was specified to retain solid particles greater than 1 μm, and withstand operating temperatures up to 80°C.

The baghouse was equipped with a high capacity fan that provided suction for extraction of off-gas from the furnace. The extraction fan had a nominal suction capacity of 3500 m^3/h with a power rating of 22 kW. Enclosed inside the baghouse was a bank of 80 filter bags made of polyester. The filter bags could withstand temperatures up to 135°C with a solid particle retention size of 1 μm. The baghouse featured a pulsating mechanism that facilitated release of dust and prevent premature clogging of the filter bags. The filtered dust was discharged at the bottom and collected in a bulk bag placed underneath the baghouse as shown in Figure 23.

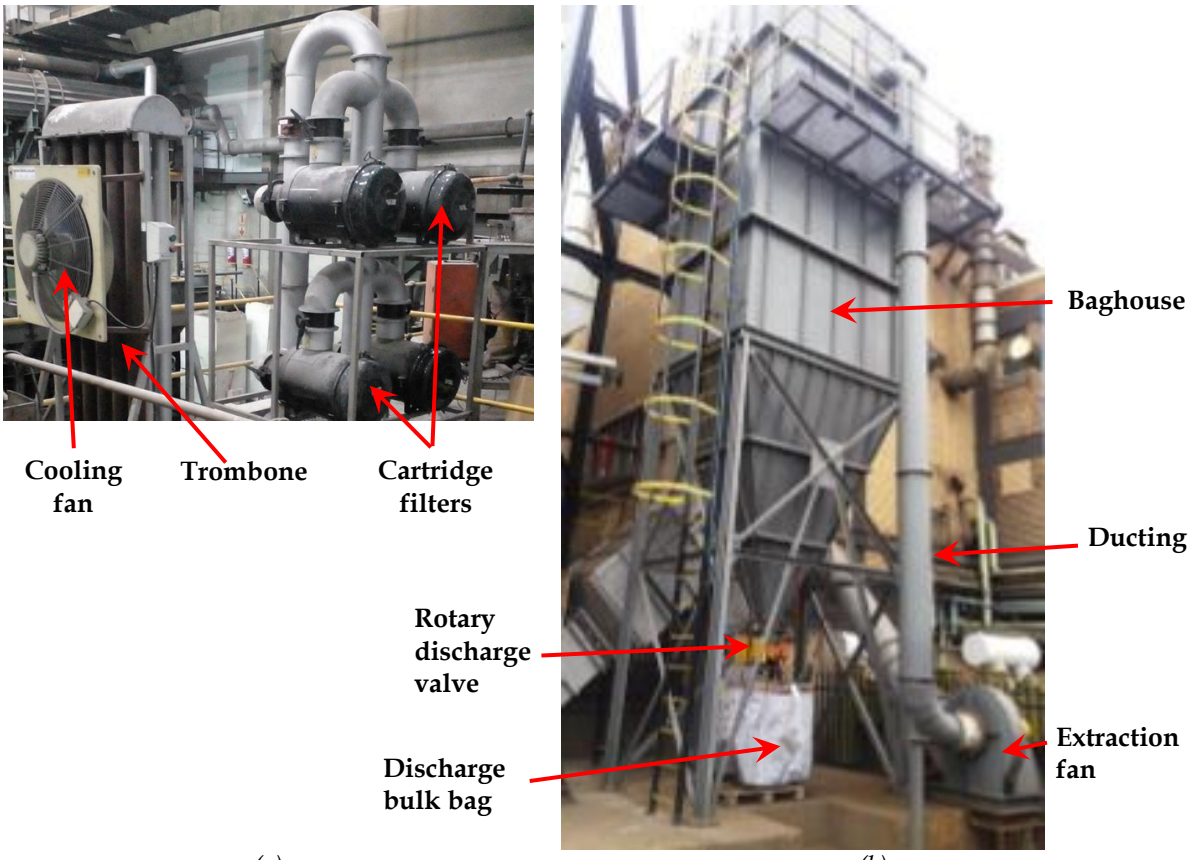

Figure 23. Picture of (a) bank of cartridge filters utilised as primary filtration unit, and (b) baghouse utilised as secondary filtration unit

3.2 Raw materials

The raw materials investigated can be grouped into main and other raw materials. The main raw materials included PCB concentrate and CRT funnel glass while the other raw materials comprised recycled fumes and CRT slag, fluxing agents, reductant, and industrial gases (see Table 5).

Table 5. List of raw materials

Main	Other
PCB concentrate	Recycled CRT slag Fluxing agents Industrial gases
CRT funnel glass	Reductant Fluxing agents Recycled fumes Industrial gases

3.2.1 PCB concentrate

The PCBs were sourced from a local e-waste recycler. A total of 382 kg PCB concentrate was received in four batches with quantities shown in Table 6. The concentrate was prepared by mechanical and physical beneficiation of waste PCBs as per pre-processing flowsheet depicted in Figure 83 in APPENDIX B. That is, comminution by shredding, gravity and magnetic separation followed by electrostatic separation to produce a concentrate of coarse metallic granules free of the plastic and ceramic components as shown in Figure 24.

Table 6. Delivered batches of PCB concentrate

PCB concentrate	Mass, kg	Delivered
Batch 1	82	04 Oct 2020
Batch 2	100	19 Jul 2021
Batch 3	100	26 Jul 2021
Batch 4	100	10 Aug 2021
Total	**382**	

Figure 24. As-received PCB concentrates

3.2.2 CRT funnel glass

The CRTs were sourced from another local e-waste recycler and were delivered completely or partially stripped. More than 1200 units were received with a total mass of about 10,431 kg (see Figure 25). Each CRT unit was manually dismantled to separate the different components. A step-wise procedure to safely dismantle the CRTs and manually separate the metallic, plastic, and rubber components is presented in APPENDIX F.

Figure 25. As-received CRT units

The masses of the respective components recovered after the manual separation of CRTs are presented in Table 7. Pictures of metallic, plastic, and rubber components can be seen in APPENDIX G, and those for panel and funnel glass are shown Figure 26. The CRT glass (panel + funnel) constitute majority of the mass at 87 wt% of the total CRT mass. Only the CRT funnel glass was investigated in the current study. All other components were either recycled or disposed of.

Table 7. Masses of different components separated from CRTs

Item	Component	Mass, kg	Mass, wt%	Item	Component	Mass, kg	Mass, wt%
(a)	Shadow mask	797	7.64	(e)	Rubber inserts	16	0.15
(b)	Metal bands	392	3.76	(f)	Phosphor dust	4	0.04
(c)	Plastic casings	121	1.16	(g)	Panel glass	5329	51.1
(d)	Electron gun	27	0.26	(h)	Funnel glass	3745	35.9
Total					**10431 kg**		

(g) (h)

Figure 26. CRT glass manually separated into (g) panel glass, and (h) funnel glass

3.2.3 *Other raw materials*

Anthracite was used in the CRTs smelting test work as a carbonaceous reductant, and Na_2CO_3 and limestone ($CaCO_3$) were added as fluxing agents. These chemical reagents were selected and used in the test work because they were identified in literature (Lu *et al.*, 2018a) as suitable reagents for reduction smelting of CRT funnel glass and they were available at Mintek in sufficient quantities and suitable particle size to be used in the pilot TBRC furnace.

CRT and PCB fumes were recycled to the CRT smelting process as sources of PbO. Recycling of CRT fumes to the CRT smelting process is standard best practice in pyrometallurgical plants to improve recovery of the metal product. Recycling of PCB fumes to the CRT smelting process forms part of the key aspect of the new integrated flow sheet investigated in the current study.

The PCBs smelting test work added recycled CRT slag and Fe_2O_3 as the main fluxing agents. The recycled CRT slag was sourced from products of a previous CRTs smelting campaign completed at Mintek in 2019. Fe_2O_3 was selected to serve a dual purpose as a fluxing agent to modify the properties of the ensuing slag and as a solid oxidant to oxidize some of the metallic impurities. The quantities shown in Table 8 were made available for the test work.

Table 8. Quantities of secondary raw materials available for test work

Material	**Mass, kg**
Anthracite	150
Na_2CO_3	300
$CaCO_3$	100
CRT fume	23
PCB fume	29
CRT slag	130
Fe_2O_3	100

Industrial-grade bulk O_2 and C_3H_8 gases were utilised in the burner to provide combustion heat to the furnace throughout the test work. These utilities were ordered from and delivered by Afrox in bulk quantities as and when needed.

3.2.4 *Sampling*

All the raw materials, with the exception of PCB concentrate, were either crushed to 100 wt% passing 2 mm (i.e., funnel glass, CRT slag, $CaCO_3$, Fe_2O_3, and anthracite) or

they were available in a fine particle size (*i.e.*, Na_2CO_3, CRT and PCB fumes). These materials were generally uniform throughout as such they were sampled with the five-point grab sampling technique. For each sample, the grab samples were combined in a plastic bag and weighed to a final mass of 100 g. A subsample with an approximate mass of 50 g was prepared from each 100 g sample with a rotary riffler. Before the samples were submitted for chemical analysis, they were pulverised to 100 wt% passing 75 μm in a micronizing mill using a stainless steel bowl.

Owing to the coarse particle size and heterogeneous nature of the PCB concentrate, each bulk batch delivered was split into 10 x 10 kg subsamples with a rotary riffler. One of the 10 kg subsamples was randomly selected and further split into smaller subsamples to generate 100 g samples for chemical and phase-chemical analysis.

3.2.5 Characterization

Bulk chemical and phase-chemical analysis of the raw materials was undertaken by Mintek's Analytical Chemistry Division (ACD) and Mineralogy Division (MNL), respectively. ACD and MNL are ISO 9001 (quality management) certified laboratories, and ACD is also ISO 17025 (testing and calibration) certified and SANAS accredited for specific analytical techniques.

While the analysis of all other raw materials was amenable to conventional analytical methods, the characterization of PCB concentrate proved challenging. To increase confidence in the chemical composition of PCB concentrate, a mineralogical technique was adopted to validate the composition. In addition, triplicate samples were sent out to external SANAS accredited laboratories for verification. For this purpose, several local laboratories were contacted including SGS South Africa (Pty) Ltd and UIS Analytical Services (Pty) Ltd. Most of these laboratories declined to analyse the PCBs samples. Only Scrooby's Laboratory Services cc offered the service and managed to successfully analyse the samples.

3.2.5.1 Bulk chemical analysis

The techniques selected for analysis of the raw materials are listed in Table 9. Brief descriptions of the main analytical techniques are provided thereafter.

Table 9. List of analytical techniques applied to raw materials by Mintek's ACD

	Analytical technique	Analytes	Lower Detection limit	Sample Analysed
1	ICP-OES	Al, Ca, Co, Cr, Cu, Fe, Mg, Mn, Ni, Pb, Si, Ti, V, Zn	0.05 wt%	PCB conc, CRT glass, CRT slag, anthracite, Fe_2O_3, $CaCO_3$, Na_2CO_3
2	ICP-OES (ICP1_CONC)	Ca, Cu, Fe	Above 20 wt%	PCB conc, $CaCO_3$, Fe_2O_3
3	ICP-OES (ICP10)	Sn	0.05 wt%	PCB conc
4	ICP-OES (ICP12)	Ag, Au, Pd, Pt	5 ppm	PCB conc
5	ICP-OES (ICP52)	Ba, Sr	100 ppm	CRT glass, CRT slag
6	Atomic Absorption	K, Na	2 ppm	CRT glass, CRT slag
7	Carrier-gas hot extraction	Total C	0.01 wt%	Na_2CO_3
8	Proximate analysis	Fixed C, ash, moisture, volatiles	0.05 wt%	Anthracite

Base metals were analysed with ICP-OES. In this method, a powdered sample of 0.2 g is mixed with 3 g sodium peroxide (Na_2O_2), as a flux. The mixture is fused, cooled, and digested in a beaker with 40 ml of HCl (1 mol/kg) acid solution. The digestion liquor is transferred into a volumetric flask containing 10 ml internal standard solution and filled to the 200 ml mark with distilled water. The resultant solution is then measured with ICP-OES.

Other elements such as Ba, Sr, Sn, and precious metals were analysed by variants of the ICP-OES method. The main difference among the variants lie with the use of a different fluxing agent and/or digestion acid. For example, the ICP1_CONC variant, for analysing Ca, Cu, and Fe present in concentrations above 20 wt%, made use of Aqua Regia for complete dissolution of the fused sample.

Alkali metals such as K and Na were analysed by AAS. A sample of 0.2 g was fused with a strong alkali flux followed by acid digestion to convert mixture into a solution. The solution was measured by AAS.

Total C was analysed by carrier-gas hot extraction technique. In this method, a sample of 0.5–1 g is heated in air in a combustion furnace. C is oxidized and detected as CO_2 with an infrared detector. Anthracite was characterised with the proximate analysis technique. This method involves heating a sample of anthracite under various conditions of temperature and atmosphere for variable amounts of time to determine moisture, volatiles, ash, and fixed C.

For the analysis of PCB concentrate, a different approach was adopted. The PCBs were first hand sorted into four fractions comprising Cu-rich, brass-rich (Cu-Zn), solder-rich (Sn-Pb), and mixed fraction (see Figure 27). Two subsamples were prepared for each fraction. One was submitted for chemical analysis and the other for phase-chemical examination. The masses of samples available for chemical analysis were 24.9 g Cu-rich fraction, 38.1 g Cu-Zn-rich fraction, 14.9 g Sn-Pb-rich fraction, and 44.9 g mixed-fines fraction. Each fraction was dissolved whole in a solution of Aqua Regia. Once the reaction was complete, the solution was filtered, and the insoluble fraction was washed, dried, and milled. The filtrate solution, wash solution, and insoluble fraction were analysed by ICP-OES.

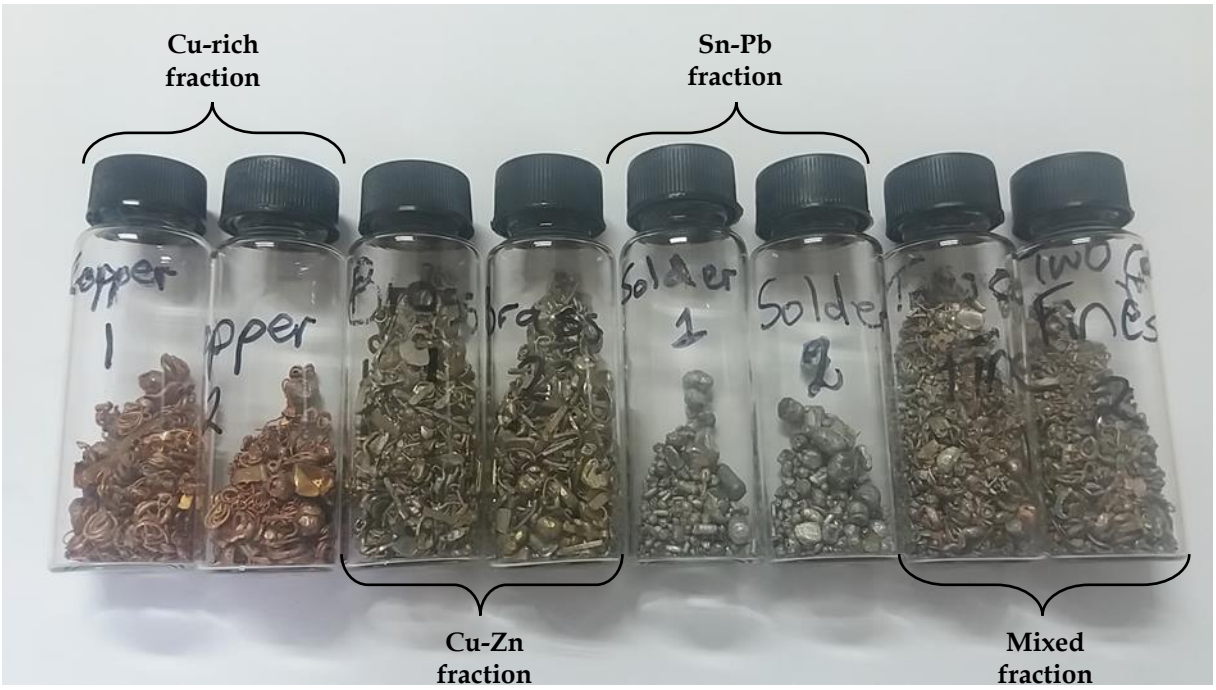

Figure 27. PCB concentrate hand sorted into (a) Cu-rich fraction, (b) Cu-Zn fraction, (c) Sn-Pb fraction, and (d) mixed fractions

For the verification exercise by Scrooby's Laboratory, the following method was adopted. Triplicate subsamples of the mixed or normal batch of PCB concentrate were digested in Aqua Regia. Once the reaction was complete, the solution was filtered, filled to a known volume with deionised water, and analysed with ICP-OES. The acid insoluble fraction was dried at 110°C and weighed. The insoluble fraction was further fused in sodium peroxide and digested in HCl acid. The resultant solution was filtered, filled to a known volume with deionised water, and analysed with ICP-OES. The residues captured on the filter paper were dried and weighed.

3.2.5.2 Phase-chemical analysis

The phases present in PCB concentrate and CRT funnel glass were examined with a scanning electron microscope (SEM). Prior to the examination, PCBs subsamples were extracted from each hand sorted fraction (shown in Figure 27) and mounted in resin to create slabs of 80 × 80 × 20 mm. For the CRTs, several funnel glass pieces were randomly selected and also mounted in resin to create slabs. The slabs were ground, polished, and coated with C under a vacuum.

The examination was undertaken with a Carl Zeiss Evo MA15 SEM coupled with a Bruker energy dispersive spectroscopy (EDS) system. The SEM was used to optically scan and map areas of interest by capturing back-scattered electron (BSE) images. The EDS system was applied to determine the elemental composition of phases mapped.

In order to validate the bulk chemical composition of the PCB concentrate, and thus increase the confidence in the chemical analysis, the PCBs were analysed with quantitative evaluation of materials by scanning electron microscopy (QEMSCAN) through auto-SEM. A representative sample of PCBs was screened into four size classes, viz., −6.75+3.35 mm; −3.35+2.36 mm; −2.36+1.7 mm; and −1.7 mm. A subsample was collected from each size class, prepared, and run on a field emission gun (FEG) QEMSCAN using a species identification protocol (SIP). A SIP is a table of entries each with a set of user criteria that are used to match scanned elemental compositional data and BSE brightness to different phases in a material. The SIP was used with other phase composition database software (*e.g.*, Esprit) to quantitatively evaluate the composition of the different size classes and consolidate the composition into a bulk chemical composition.

3.2.6 PCBs raw materials

The chemical composition of the raw materials processed in the PCBs smelting tests are presented in this section. The phase-chemical composition of the PCB concentrate are also presented.

3.2.6.1 Chemical composition

The compositions of PCB concentrate as analysed by Mintek's ACD and MNL as well as Scrooby's are compared in Table 10. The detailed analytical results of the PCBs from each laboratory can be viewed in APPENDIX H. The results of the three different methods were reasonably comparable, given the heterogeneous nature of the PCBs. This increased the confidence in the base metal composition of the PCB concentrate. All laboratories reported Cu as the predominant element (61.2–64.3 wt% Cu) with Sn (13.5–14.3 wt%), Zn (8.10–10.6 wt%) and Pb (6.68–7.0 wt%) reported as the major elements. ACD reported Pb at 2.4% which was much lower than values reported by MNL and Scrooby's. Such a discrepancy is not surprising for such a heterogeneous material. Minor elements detected include Al, Fe, Ni and Si. Elements such as Cr, Mg, Mn and Ca were present in concentrations less than 0.1 wt%.

A significant discrepancy with the analytical results was apparent with the reported content of precious metals. Mintek's ACD results reported 1239 ppm Ag, 260 ppm Pd and 10 ppm Pt but Au was not detected. Scrooby's results reported 648 ppm Ag and 12 ppm Au while Pd and Pt were not detected. Mintek's MNL method could only detect Ag at 2000 ppm.

Table 10. Comparison of chemical composition of PCB concentrate as analysed by Mintek's ACD and MNL, and Scrooby's

Element	MINTEK		EXTERNAL	Average	Units
	ACD	MNL	Scrooby's		
Al	1.90	2.0	2.84	2.25	wt%
Ca	0.02	-	0.07	0.03	wt%
Cu	64.3	62.2	61.2	62.6	wt%
Fe	1.96	1.1	0.93	1.33	wt%
Mg	0.04	0.01	0.10	0.05	wt%
Mn	0.05	0.1	0.06	0.07	wt%
Ni	0.46	0.3	0.26	0.34	wt%
Pb	2.44^	6.8	6.68	6.74	wt%
Si	0.38	0.3	0.52	0.4	wt%
Sn	13.8	13.5	14.3	13.9	wt%
Zn	8.82	10.6	8.10	9.17	wt%
Ag	1239	2000	648	1296	ppm
Au	<0.1	-	12	12	ppm
Pd	260	-	<0.1	260	ppm
Pt	10	-	<0.1	10	ppm
Total	**94.4**	**97.1**	**95.0**	**96.4**	

^ - *ACD Pb value not included in calculation of average*

This significant discrepancy warranted further investigation into the analysis of the precious metals. Additional PCB concentrate samples were submitted to Mintek's ACD to investigate different preparation methods. The e-waste recycler, from which the PCBs were sourced, was also contacted to provide the precious metals content of the batch of PCBs sold to Mintek. The results of the additional analysis and the analysis provided by the e-waste recycler are presented in Table 11.

Three different preparation methods were investigated. The results obtained were still of poor quality with significant variations among the replicate samples. The averaged results were also significantly different to the results provided by the supplier.

Table 11. Additional analysis of precious metals in PCB concentrate as analysed by Mintek's ACD, mass in ppm

Sample	Au	Pd	Pt	Ag
Prep A 1	23.1	1.74	0.13	-
Prep A 2	30.0	2.02	0.37	-
Prep A 3	11.1	1.13	0.06	-
Prep B 1	9.51	0.45	0.16	-
Prep B 2	69.0	0.51	<0.1	-
Prep B 3	26.8	0.27	0.11	-
Prep C 1	49.8	4.01	0.06	-
Prep C 2	25.7	0.42	<0.1	-
Prep C 3	46.2	0.55	<0.1	-
Prep C 4	11.0	1.22	<0.1	-
Average	**30.2**	**1.23**	**0.1**	**-**
e-waste recycler	43.1	9.40	<0.1	1760

There is no confidence in the precious metals content of the PCB concentrate. The technical difficulty with analysing for precious metals present in trace amounts in the PCB concentrate is associated with the coarse particle size distribution, as described by Laubertova *et al*. (2019), and the difficulty of grinding the sample into a fine powder due to the malleability of the metallics component of the PCBs.

The lack of confidence with the current results of precious metals in PCB concentrate will present challenges with the mass balance calculations. In this instance, only a mass balance formulation (*i.e.,* elemental distribution) that is independent of the concentration of the element in the feed stream will be considered.

The chemical composition of the other raw materials is presented in Table 12. The CRT slag was rich in SiO_2 (51.2 wt%) and contained up to 14.9 wt% Na_2O. The Fe_2O_3 had a grade of 74 wt% Fe_2O_3 and a SiO_2 content of 13.9 wt%. The Na_2CO_3 and $CaCO_3$ had a grade of 99.1 wt% Na_2CO_3 and 91.3 wt% $CaCO_3$, respectively.

Table 12. Chemical composition of other raw materials

CRT slag		Ferric oxide		Soda ash		Limestone	
Species	**Mass, wt%**	**Species**	**Mass, wt%**	**Species**	**Mass, wt%**	**Species**	**Mass, wt %**
Al_2O_3	4.81	Al_2O_3	4.7	Al_2O_3	<0.05	Al_2O_3	0.75
BaO	1.97	CaO	0.10	CaO	<0.05	$CaCO_3$	91.3
CaO	7.37	Fe_2O_3	74.0	Fe_2O_3	<0.05	Fe_2O_3	0.46
FeO	0.40	MgO	0.20	MgO	<0.05	$MgCO_3$	0.91
K_2O	2.38	MnO	2.98	Na_2CO_3	99.1	SiO_2	6.46
MgO	1.85	PbO	0.46	SiO_2	0.14		
Na_2O	14.9	SiO_2	13.9				
PbO	4.14						
SiO_2	51.2						
SrO	1.67						
Total	**91**	**Total**	**96**	**Total**	**99**	**Total**	**100**

3.2.6.2 Phase-chemical composition

The results of the phase-chemical composition of the Sn-Pb-rich fraction is presented here. Results for other fractions are presented in APPENDIX H. In the Sn-Pb-rich fraction, Cu metal occurs as inclusions and as rims in or around the predominant Sn-Pb alloy particles as shown in Figure 28. The EDS point analysis of the Sn-Pb fraction is given in Table 13.

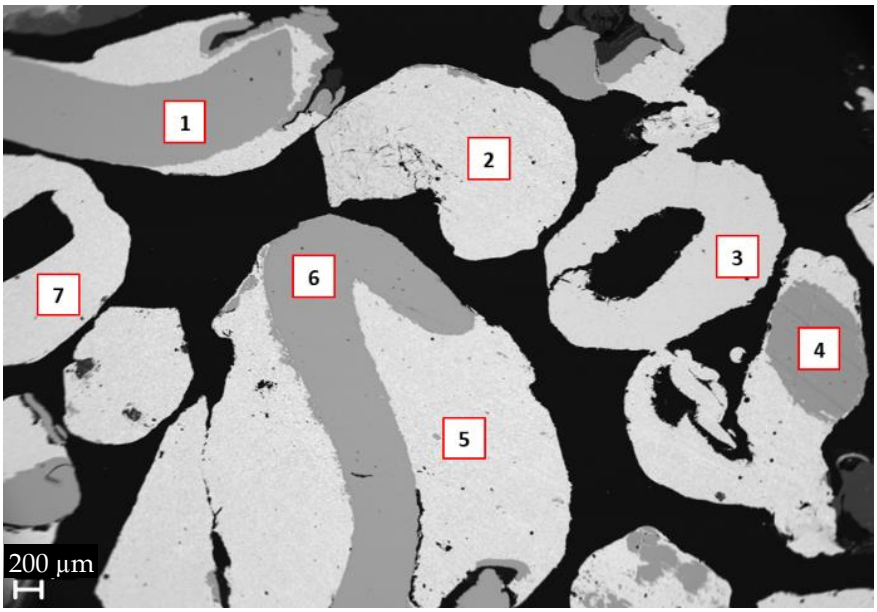

Figure 28. (a) SEM BSE micrograph of SnPb-rich fraction of PCB concentrate, with scale-bar indicating 200 µm

Table 13. EDS point analysis of SnPb-rich fraction of PCB concentrate shown in Figure 28, mass in wt%

No.	Cu	Zn	Sn	Pb	Phase
1	72.9	27.1	–	–	CuZn alloy
2	–	–	57.5	42.5	SnPb alloy
3	–	–	100	–	Sn metal
4	100	–	–	–	Cu metal
5	–	–	46.7	53.3	SnPb alloy
6	67.4	32.6	–	–	CuZn alloy
7	–	–	55.0	45.0	SnPb alloy

3.2.7 CRTs raw materials

The solid raw materials investigated were characterized for bulk chemical composition and only the CRT funnel glass was further characterized for phase-chemical composition.

3.2.7.1 Chemical composition

The chemical composition of CRT funnel glass and PCB fume is presented in Table 14. The composition of anthracite and fluxing agents is given in Table 15.

Table 14. Chemical composition of CRT funnel glass and recycled fumes

CRT funnel glass	
Species	**Mass, wt%**
Al_2O_3	3.27
BaO	2.04
CaO	3.20
FeO	0.71
K_2O	4.06
MgO	2.16
Na_2O	4.87
PbO	18.7
SiO_2	54.1
SrO	1.88
ZnO	0.24
Total	**95.2**

CRT fume	
Species	**Mass, wt%**
C	1.07
CaO	0.42
CuO	0.12
FeO	0.24
K_2O	1.69
MgO	0.09
Na_2O	1.47
NiO	0.09
PbO	82.4
SiO_2	0.62
SnO	0.92
ZnO	10.9
Total	**100.0**

PCB fume	
Species	**Mass, wt%**
CuO	1.65
K_2O	0.72
Na_2O	0.78
PbO	27.5
SnO	14.9
ZnO	47.9
Ag	0.34
Total	**93.8**

Table 15. Chemical composition of anthracite and fluxing agents

Anthracite	
Species	**Mass, wt%**
Al_2O_3	2.16
CaO	0.35
Fe_2O_3	1.47
MgO	0.10
SiO_2	4.05
C	81.8
P	0.04
S	0.58
Moisture	3.16
Volatile	4.42
Total	**98.1**

Soda ash	
Species	**Mass, wt%**
Al_2O_3	<0.05
CaO	<0.05
Fe_2O_3	<0.05
MgO	<0.05
Na_2CO_3	99.1
SiO_2	0.14
Total	**99.2**

Limestone	
Species	**Mass, wt%**
Al_2O_3	0.75
$CaCO_3$	91.3
Fe_2O_3	0.46
$MgCO_3$	0.91
SiO_2	6.46
Total	**99.8**

3.2.7.2 Phase-chemical composition

The BSE images of the CRT funnel glass captured with the SEM and point analysis measured with EDS are presented in Figure 29 and Table 16, respectively. The CRT funnel glass is amorphous and the Pb is uniformly distributed throughout the silicate glass matrix.

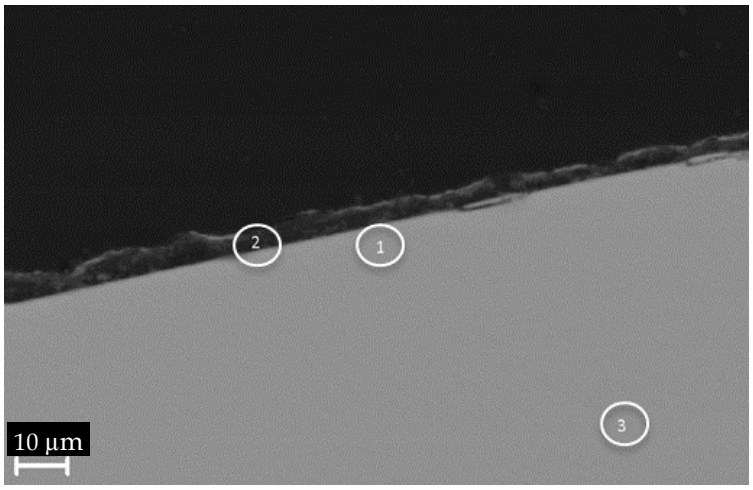

Figure 29. SEM BSE micrograph of CRT funnel glass, with scale-bar indicating 10 µm

Table 16. EDS point analysis of CRT funnel glass samples shown in Figure 29, mass in wt%

No.	O	Si	Pb	K	Na	Ca	Al	Mg	Ti	Ba	Total
1	37	26	19	8	4	3	2	1	-	-	100
2	48	35	-	8	-	-	-	-	9	-	100
3	36	25	23	6	4	3	2	1	-	1	100

3.3 Chemical thermodynamic calculations

Before the smelting tests were conducted, chemical thermodynamic calculations were carried out to evaluate the process variables that provided the necessary conditions to produce a crude alloy at the required grade with the highest recovery of Cu or Pb to the metal stream. The results from the theoretical calculations were used as input to the design of the experimental plan. The calculations were carried out with the software package Factsage™ (Bale *et al.*, 2009).

3.3.1 Calculations in Factsage

All chemical equilibria calculations were carried out with the Equilib module. The PCBs and CRTs smelting systems comprise the same elements as such both systems were simulated with the same databases. The database FactPS was selected for pure gas and solid compounds. All possible gas and solid species were selected for the calculations. The FToxid and SGTE databases were selected for oxide and alloy solutions, respectively. The solution phases FToxid-SLAGA and SGTE-LIQUID were respectively selected for the possible liquid slag and alloy streams.

The viscosity module was used to calculate slag viscosities making use of the melts database. The calculations were based on the composition of the major components of the slag (*i.e.*, Al_2O_3, CaO, FeO, Fe_2O_3, K_2O, MgO, Na_2O and SiO_2). Oxide species such as BaO, SrO, SnO and Cu_2O were not included in the viscosity estimates.

The stoichiometric amount of O_2 was based on combustion reaction [10] with 3.36 kg or 0.076 kmol C_3H_8, for PCBs, and 2.94 kg or 0.067 kmol C_3H_8, for CRTs.

$$\{C_3H_8\}_{gas} + \{5O_2\}_{gas} \rightarrow \{4H_2O\}_{gas} + \{3CO_2\}_{gas} \quad [10]$$

The process variables that were evaluated theoretically for each smelting process are presented in Table 17. The calculations sought to determine the process conditions that result in the highest theoretical recovery of Cu and Pb to the metal at the required alloy grade.

Table 17. Process variables that were evaluated in the theoretical calculations

PCBs smelting process		
Process variable	**Fixed**	**Changing**
Reaction temperature	X	
Flame stoichiometry		X
Flux addition		X
Amount of burner gas		X

CRTs smelting process		
Process variable	**Fixed**	**Changing**
Reaction temperature		X
Flame stoichiometry	X	
Flux addition		X
Reductant addition		X
Recycled fume addition		X

3.3.2 PCBs smelting system

The PCBs smelting process is an oxidative refining process involving three stages, namely: (i) melting and volatilisation; (ii) oxidation; and (iii) slag formation. The thermodynamic system illustrated schematically in Figure 30 was used as the basis of the calculations.

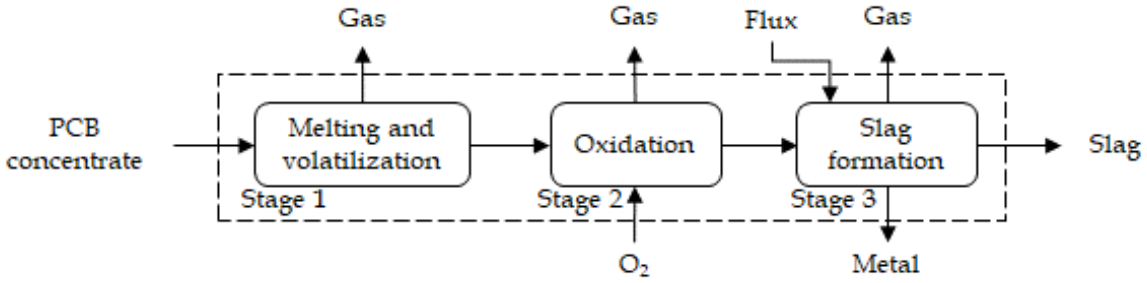

Figure 30. Schematic representation of the thermodynamic system of the PCBs smelting process

The normalised chemical compositions of the three components of the PCB concentrate are presented in Table 18. The compositions were adapted from the analytical results reported by Scrooby's. The metallics account for 95.1% of the PCB concentrate mass, and the ceramics and plastics account for 4.0 and 0.9%, respectively. The normalized chemical compositions of the fluxing agents are presented in Table 19.

Table 18. Normalized chemical compositions of the three components of PCB concentrate used in the chemical thermodynamic calculations

PCB metallics	
Element	**Mass, wt%**
Al	1.66
Cu	62.6
Fe	0.93
Mn	0.05
Ni	0.25
Pb	6.79
Sn	14.6
Zn	8.28
Total	**95.1**

PCB ceramics	
Species	**Mass, wt%**
Al_2O_3	2.38
BaO	0.04
CaO	0.10
CuO	0.01
Fe_2O_3	0.03
K_2O	0.03
MgO	0.18
MnO	0.01
NiO	0.02
PbO	0.05
SiO_2	1.15
SrO	0.002
Total	**4.0**

PCB plastics	
Species	**Mass, wt%**
Plastics	0.90
Total	**0.9**

Table 19. Normalized chemical compositions of fluxing agents used in the chemical thermodynamic calculations of PCBs smelting process

Ferric oxide	
Species	**Mass, wt%**
Al_2O_3	4.80
CaO	0.10
Fe_2O_3	76.8
MgO	0.21
MnO	3.09
PbO	0.48
SiO_2	14.4
Total	**100**

CRT slag	
Species	**Mass, wt%**
Al_2O_3	5.30
BaO	2.17
CaO	8.13
FeO	0.44
K_2O	2.62
MgO	2.04
Na_2O	16.4
PbO	4.57
SiO_2	56.5
SrO	1.84
Total	**100**

The first stage of the process removes volatile species such as Zn, some of the Pb, and the plastics fraction by volatilization. The calculations were undertaken to determine the process conditions that promoted the highest recovery of Zn to the gas stream and minimized recovery of Pb and Sn to the slag stream. Recovery of Pb and Sn to the slag is unfavourable as it will prevent recycling of these elements to the CRT smelting furnace for recovery to the metal stream.

A flame stoichiometry of 90 mol% O_2 and an operating temperature of 1500°C resulted in the highest theoretical recovery of Zn and Pb to the gas stream and minimized

recovery of Zn, Pb and Sn to the slag stream, as illustrated in Figure 31 and Figure 32, respectively.

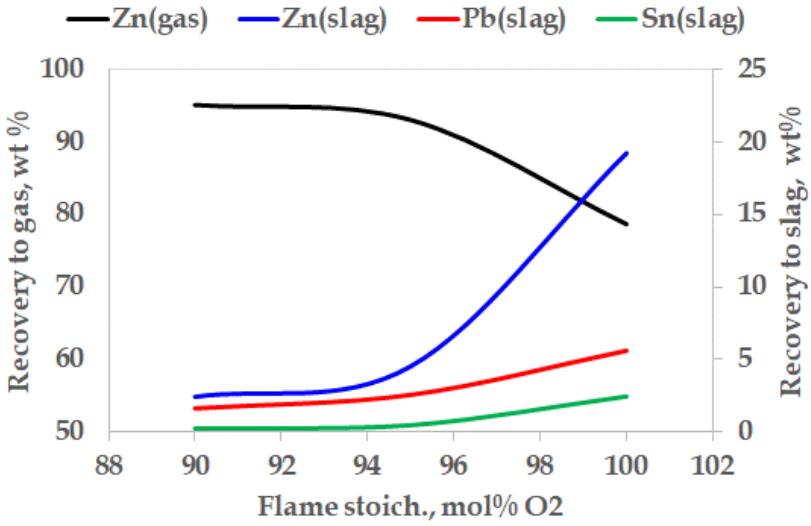

Figure 31. Plot showing relationship of recovery to gas and slag vs. flame stoichiometry at 1350°C, with a flame stoichiometry of 90 mol% O_2

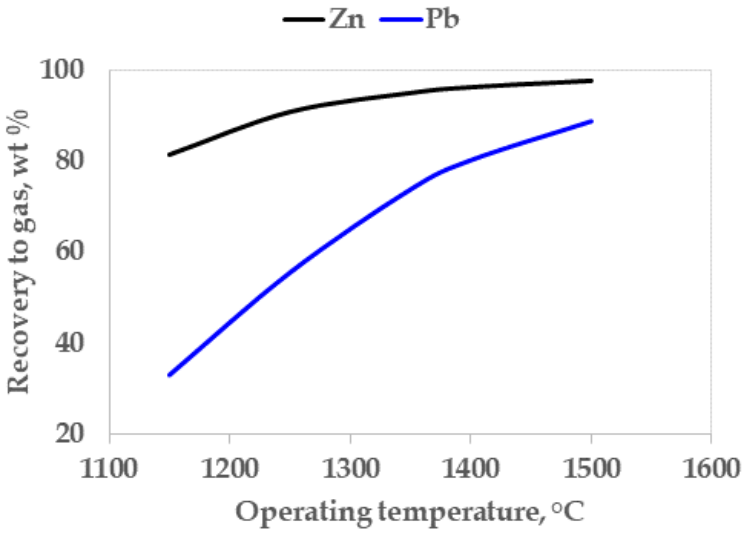

Figure 32. Plot showing relationship of recovery to gas vs. operating temperature, with a flame stoichiometry of 90 mol% O_2

The theoretical compositions of the product streams from the volatilisation stage are presented in Table 20. Although an operating temperature of 1500°C resulted in the highest recovery of Zn to the gas stream, a temperature of 1350°C was selected to generate products from Stage 1 because this temperature can be practically obtained in the pilot TBRC furnace.

Table 20. Theoretical chemical compositions of product streams after volatilisation PCB concentrate at 1350°C with a flame stoichiometry of 90 mol% O_2

Stage 1 Gas		Stage 1 Metal		Stage 1 Slag		Stage 1 Slag	
Species	**Mass, wt%**	**Species**	**Mass, wt%**	**Species**	**Mass, wt%**	**Species**	**Mass, wt%**
H_2O	32.0	Cu	79.1	Al_2O_3	25.0	MnO	1.73
CO_2	48.9	Fe	0.08	SiO_2	27.5	SnO	0.89
CO	10.2	Ni	0.33	CaO	2.43	Cu_2O	1.26
H_2	0.38	Pb	2.12	FeO	26.0	BaO	0.02
Zn	5.09	Sn	18.1	Fe_2O_3	0.99	SrO	0.04
Pb	3.14	Zn	0.26	MgO	3.72	$KAlO_2$	1.36
SnO	0.19			PbO	2.83	$BaAl_2O_4$	0.33
				ZnO	5.90	$SrAl_2O_4$	0.02
Total	**100**	**Total**	**100**			**Total**	**100**
Mass, kg	**15.5**	**Mass, kg**	**7.90**			**Mass, kg**	**0.42**

Note: This system has a precipitate of a pure solid Al_2O_3 of 0.43 kg

In the next process stage (oxidation stage), free O_2 is required to remove the remaining metallic impurities from Stage 1 metal. The stoichiometric amount of O_2 required to completely oxidise Fe, Pb, Sn and Zn was calculated from reaction [11] to [14].

$$[2Fe]_{metal} + \{O_2\}_{gas} \rightarrow (2FeO)_{slag/solid} \quad [11]$$
$$[2Pb]_{metal} + \{O_2\}_{gas} \rightarrow (2PbO)_{slag/solid} \quad [12]$$
$$[2Sn]_{metal} + \{O_2\}_{gas} \rightarrow (2SnO)_{slag/solid} \quad [13]$$
$$[2Zn]_{metal} + \{O_2\}_{gas} \rightarrow (2ZnO)_{slag/solid} \quad [14]$$

For a mass of 7.9 kg Stage 1 metal, an amount of 0.212 kg O_2 (or 0.159 Nm^3) is required to react completely with the impurities as shown in Table 21. Calculations were undertaken to determine the process conditions that result in complete removal of impurities from Stage 1 metal and promote the highest recovery of Cu to Stage 2 metal.

Table 21. Calculation of stoichiometric amount of O_2 required to oxidise remaining impurities from Stage 1 metal

Parameter	Cu	Fe	Ni	Pb	Sn	Zn	Total
Mass of element, kg	6.25	0.01	0.03	0.17	1.43	0.02	**7.900**
Moles of element, kmol	0.098	0.0001	0.0004	0.0008	0.0120	0.0003	**0.112**
Stoich. ratio to O_2	-	0.5	-	0.5	0.5	0.5	-
Stoich. amount O_2, kmol	-	0.0001	-	0.0004	0.0060	0.0002	**0.007**
Stoich. amount O_2, kg	-	0.002	-	0.013	0.192	0.005	**0.212**
Reaction no.	-	[13]	-	[14]	[15]	[16]	-

In these calculations, reactions occurring in Stage 2 and 3 were evaluated in one step under the same equilibria. The lowest impurity level was obtained with a flame stoichiometry of 110 mol% O_2 at 1350°C but this condition was associated with the

lowest recovery of Cu to the metal stream (see Figure 33 and Figure 34). None of the conditions evaluated provided a Cu recovery greater than 90 wt%. The best achievable theoretical Cu recovery was 87 wt% with a Cu grade of 90 wt% and was obtained with a flame stoichiometry of 100 mol% O_2 at 1350°C after oxidising for a period of 1 h. At this grade, the composition of residual impurities in the metal was 9.4 wt% Sn and 0.5 wt% Pb.

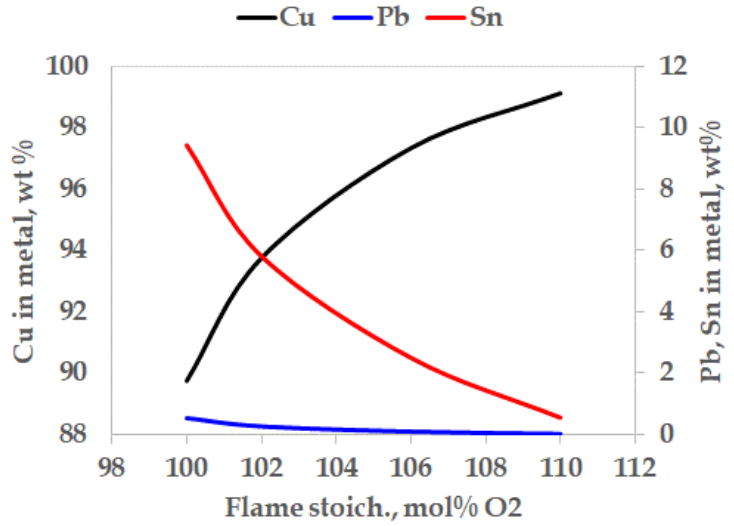

Figure 33. Plot showing relationship of (a) Cu, Pb and Sn in metal vs. flame stoichiometry at 1350°C

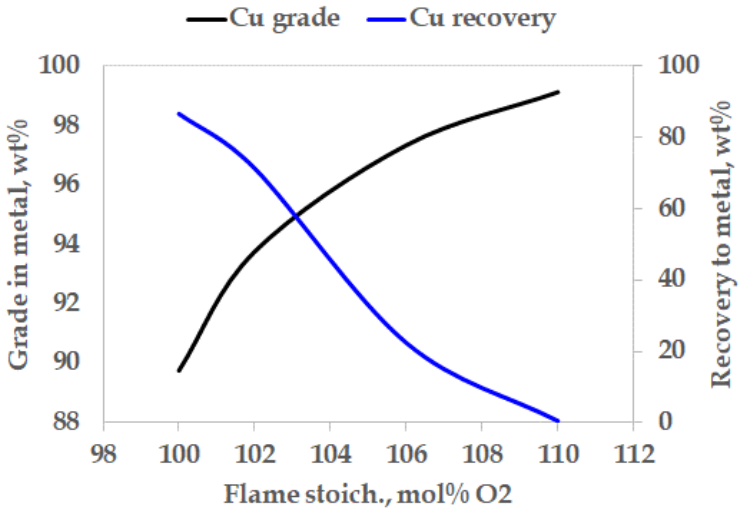

Figure 34. Plot showing relationship of Cu grade and recovery to metal vs. flame stoichiometry at 1350°C

The amount of burner gas was evaluated to determine how much of it is required to completely oxidize the Sn and Pb from the metal. The calculations estimated that more than 1000 kg is required to oxidize Sn and Pb to below 1 wt% with a flame stoichiometry of 100 mol% O_2 (see Figure 35).

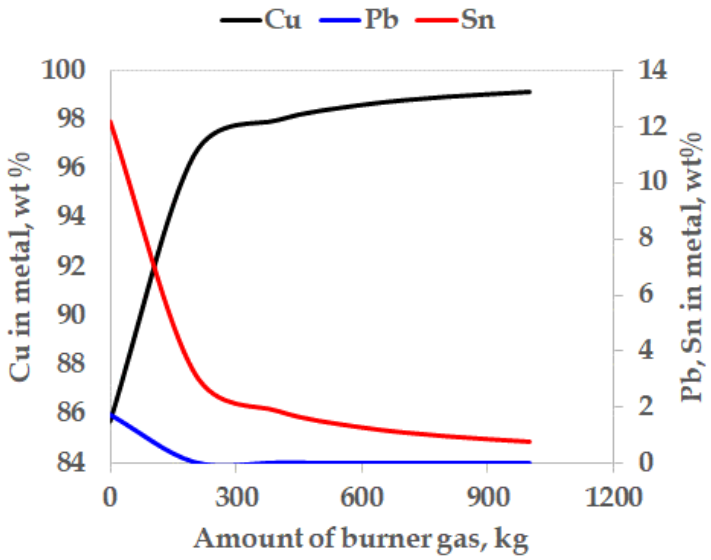

Figure 35. Plot showing relationship of Cu, Pb and Sn in metal vs. amount of burner gas at 1350°C with a flame stoichiometry of 100 mol% O_2

The calculations further showed that such an enormous amount of gas was also associated with excessive loss of Cu to the slag (more than 50 wt%), as depicted in Figure 36. However, the requirement is to obtain an alloy grade of 95 wt% Cu and this was achieved after 200 kg of burner gas was delivered. An alloy grade of 97 wt% Cu was obtained at 69 wt% Cu recovery to the metal.

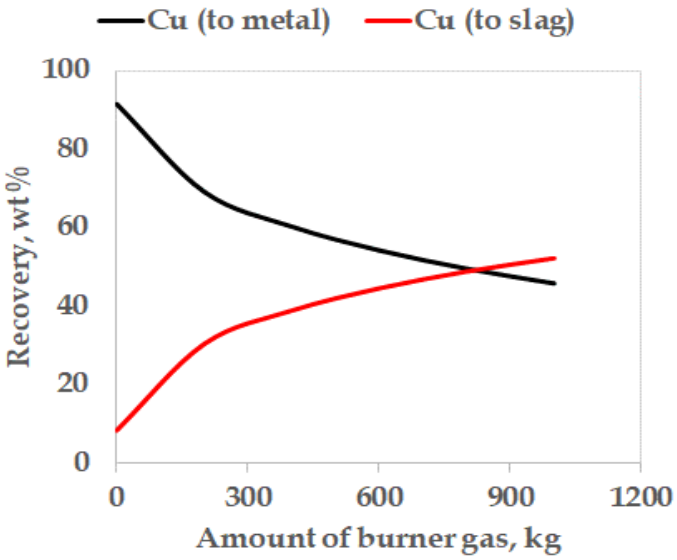

Figure 36. Plot showing relationship of recovery of Cu to metal and slag vs. amount of burner gas at 1350°C with a flame stoichiometry of 100 mol% O_2

An oxidation temperature of 1000°C provided the highest theoretical recovery of 98% Cu to the metal with a flame stoichiometry of 100 mol% O_2 (see Figure 37). However, this temperature resulted in poor slag properties such as viscosities in excess of 600 Pa.s and occurrence of precipitates of pure solid compounds (see Figure 38). Slag viscosities below 1 Pa.s were obtained at temperatures above 1300°C and there were no solid precipitates above this temperature.

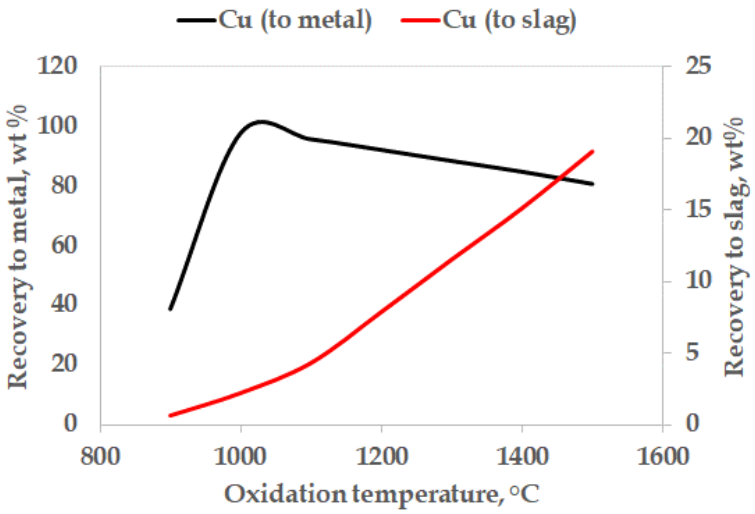

Figure 37. Plot showing relationship of recovery of Cu to metal and slag vs. oxidation temperature, with a flame stoichiometry of 100 mol% O_2

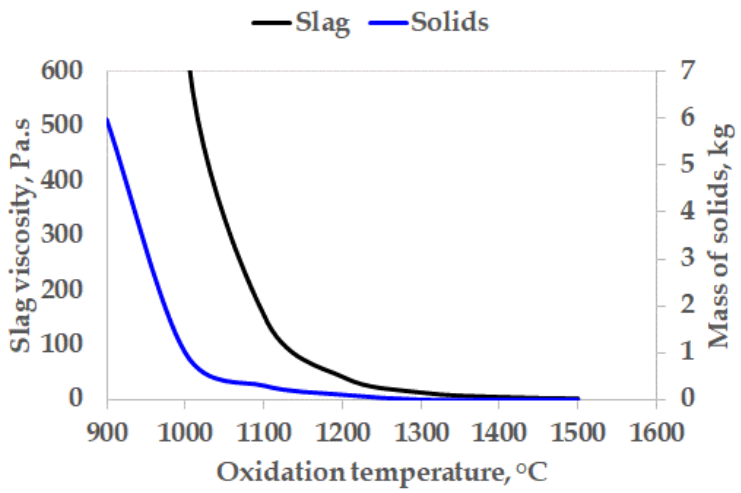

Figure 38. Plot showing relationship of slag viscosity and mass of solids vs. oxidation temperature, with a flame stoichiometry of 100 mol% O_2

Slag viscosity can also be lowered by increased flux addition. In the PCBs smelting process, CRT slag and Fe_2O_3 are added as fluxing agents. A ratio of 0.6:1 Fe_2O_3:CRT slag was selected for the calculations to ensure sufficient FeO is introduced to the slag to dilute the high SiO_2 content of the CRT slag. A flux addition (CRT slag + Fe_2O_3) of 120 wt% (per kg PCB concentrate) resulted in the lowest theoretical slag viscosity of 0.57 Pa.s, as shown in Figure 39. This amount of flux was associated with more than 20 wt% Cu recovery to the slag (see Figure 40) due to the increased oxidising potential of the slag resulting from a higher Fe_2O_3 content.

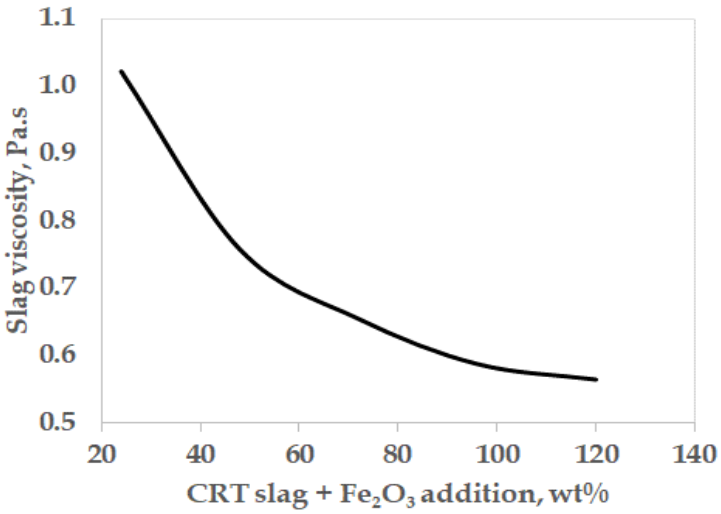

Figure 39. Plot showing relationship of slag viscosity vs. flux addition, at 1350°C with a flame stoichiometry of 100 mol% O_2

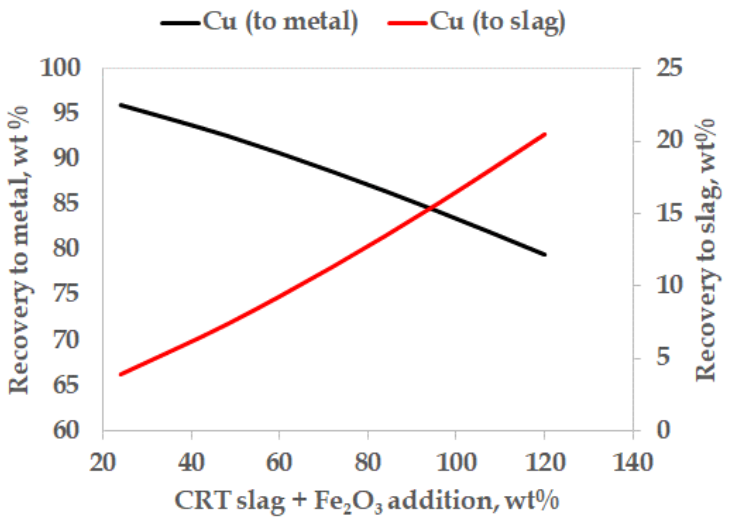

Figure 40. Plot showing relationship of recovery of Cu to metal and slag vs. flux addition, at 1350°C with a flame stoichiometry of 100 mol% O_2

The ideal process condition that provided the highest achievable theoretical recovery of Cu to the metal at the required alloy grade is summarized in Table 22.

Table 22. Theoretically determined ideal process conditions for the PCBs smelting process

Ideal process conditions	**Values**
Highest Cu recovery	69 wt% Cu to metal
Alloy grade	97 wt% Cu, 3.3 wt% Sn, 0.05 wt% Pb
Flame stoichiometry	100 mol% O_2
Oxidation temperature	1350°C
Amount of burner gas	200 kg
Flux addition	45 wt% CRT slag + 27 wt% Fe_2O_3

3.3.3 CRTs smelting system

The CRTs smelting process is a reductive process involving two stages, namely: (i) melting, and (ii) reduction. The thermodynamic system illustrated schematically in Figure 41 was used as the basis of the calculations.

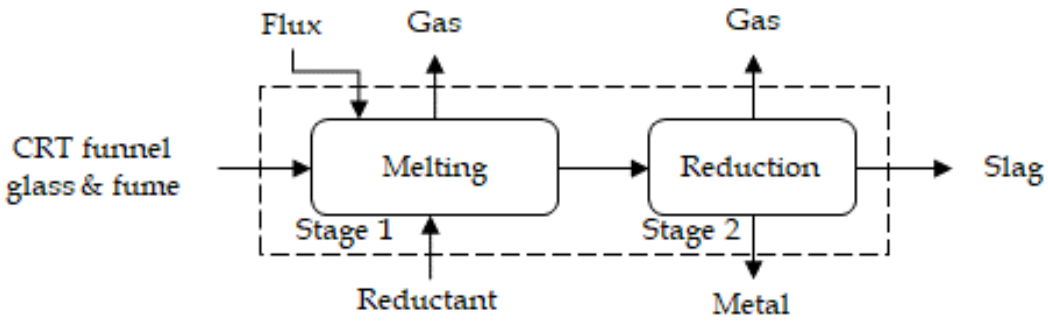

Figure 41. Schematic representation of the two stages of the CRTs smelting system

The normalised compositions of the raw materials evaluated in the theoretical calculations are presented in Table 23. The normalised compositions of Na_2CO_3 and $CaCO_3$ flux added in the CRT smelting system are given in Table 24.

Table 23. Normalized chemical compositions of raw materials of CRTs smelting system used in the chemical thermodynamic calculations

CRT funnel glass	
Species	**Mass, wt%**
Al_2O_3	3.43
BaO	2.14
CaO	3.36
FeO	0.75
K_2O	4.26
MgO	2.27
Na_2O	5.11
PbO	19.6
SiO_2	56.8
SrO	1.97
ZnO	0.25
Total	**100**

CRT fume	
Species	**Mass, wt%**
C	1.07
CaO	0.42
CuO	0.12
FeO	0.24
K_2O	1.69
MgO	0.09
Na_2O	1.47
NiO	0.09
PbO	82.4
SiO_2	0.62
SnO_2	0.92
ZnO	10.9
Total	**100**

PCB fume	
Species	**Mass, wt%**
CuO	1.77
K_2O	0.77
Na_2O	0.83
PbO	29.4
SnO	15.9
ZnO	51.3
Total	**100.0**

Anthracite	
Species	**Mass, wt%**
Al_2O_3	2.21
CaO	0.36
Fe_2O_3	1.49
MgO	0.11
SiO_2	4.13
C	83.4
P	0.04
S	0.59
Moisture	3.22
Volatile	4.51
Total	**100**

Table 24. Normalized chemical compositions of fluxing agents used in the chemical thermodynamic calculations of CRTs smelting process

Soda ash	
Species	**Mass, wt%**
Al_2O_3	<0.05
CaO	<0.05
Fe_2O_3	<0.05
MgO	<0.05
Na_2CO_3	99.9
SiO_2	0.14
Total	**100**

Limestone	
Species	**Mass, wt%**
Al_2O_3	0.75
$CaCO_3$	91.3
Fe_2O_3	0.46
$MgCO_3$	0.91
SiO_2	6.46
Total	**100**

In the calculations of the CRTs smelting system, the flame stoichiometry was fixed at 95 mol% O_2 to provide for a mildly reducing burner gas. Flame stoichiometry values much lower than 95 mol% O_2 will introduce higher concentrations of CO gas into the system, which will influence the reduction reactions.

The reduction temperature that resulted in the highest theoretical recovery of Pb and Sn to the metal is 900°C (see Figure 42). At this temperature, however, the system forms precipitates of pure solid species as shown in Figure 43. These solids disappear at temperatures above 1100°C. The calculations also indicate that the recovery of Pb and Sn to the metal decreases with increasing temperature with a reduction temperature of 1300°C resulting in the lowest recovery.

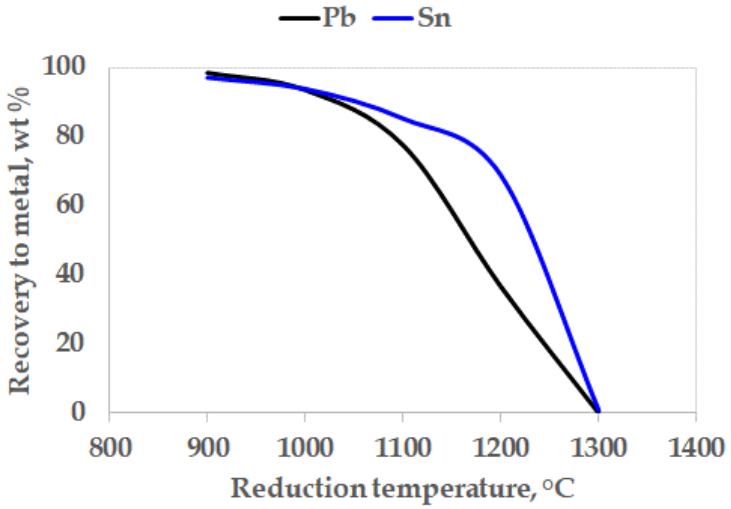

Figure 42. Plot showing relationship of recovery to metal vs. reduction temperature, with flame stoichiometry of 95 mol% O_2

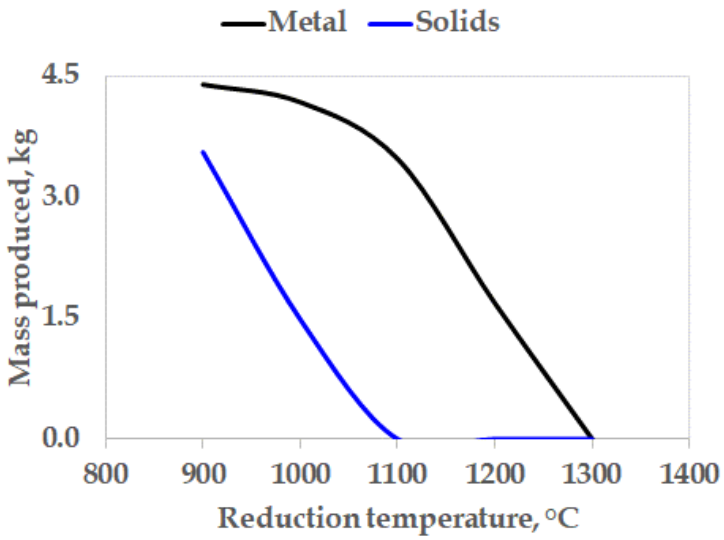

Figure 43. Plot showing relationship of mass produced and reduction temperature, with flame stoichiometry of 95 mol% O_2

Higher reduction temperatures promote recovery of Pb and Sn to the gas stream (see Figure 44). Unlike with PCBs smelting, recovery of Pb and Sn to the gas stream is unfavourable with CRTs smelting. In this process, ideal conditions are those that promote recovery of Pb and Sn to the metal. The best theoretical recovery of Pb (78 wt%) and Sn (85 wt%) to the metal was obtained at 1100°C with a C addition of 12.5 wt% (per kg CRT funnel glass), as depicted in Figure 42.

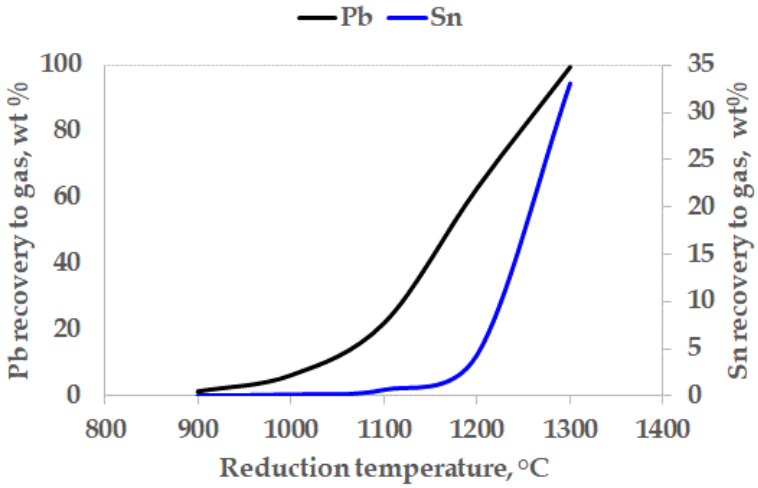

Figure 44. Plot showing relationship of recovery to gas vs. reduction temperature, with flame stoichiometry of 95 mol% O_2

Increasing reductant addition promote the recovery of Sn to the metal. The highest theoretical recovery of 97 wt% Sn to the metal was obtained with a C addition of 25 wt% at 1150°C, as illustrated in Figure 45. In contrast, increasing C additions result in a decrease in the recovery of Pb to the metal in favour of Pb recovery to the gas stream (see Figure 46). The highest theoretical recovery of 80 wt% Pb to the metal was obtained with a C addition of 4 wt% at 1150°C.

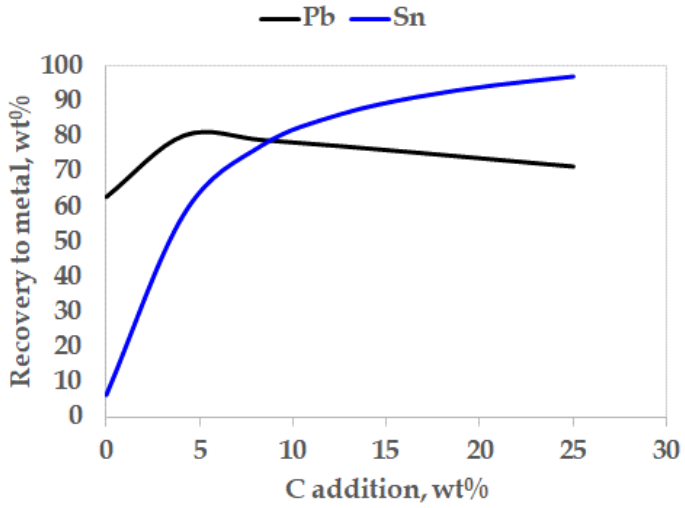

Figure 45. Plot showing relationship of recovery to metal vs. C addition, at 1150°C with flame stoichiometry of 95 mol% O_2

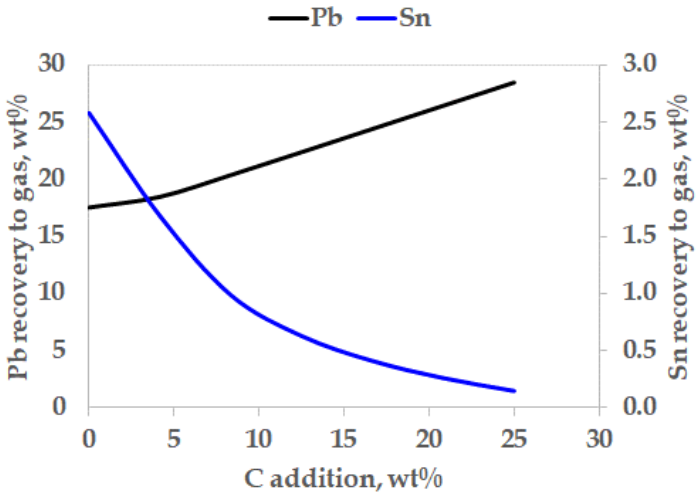

Figure 46. Plot showing relationship of recovery to gas vs. C addition, at 1150°C with flame stoichiometry of 95 mol% O_2

Figure 47 further demonstrates that no Pb is recovered to the slag at C additions as low as 5 wt% however much higher C additions are necessary to decrease the recovery of Sn to the slag to less than 3 wt%. The theoretical recovery of Pb to the metal, at the C addition where the highest recovery of Sn to the metal is obtained, is 72 wt% giving a metal with a grade slightly above 95 wt% Pb, as shown in Figure 48.

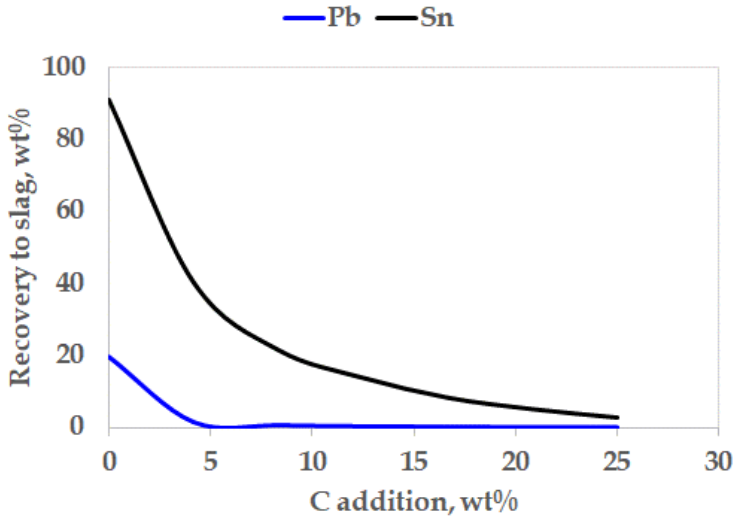

Figure 47. Plot showing relationship of recovery to slag vs. C addition, at 1150°C with flame stoichiometry of 95 mol% O_2

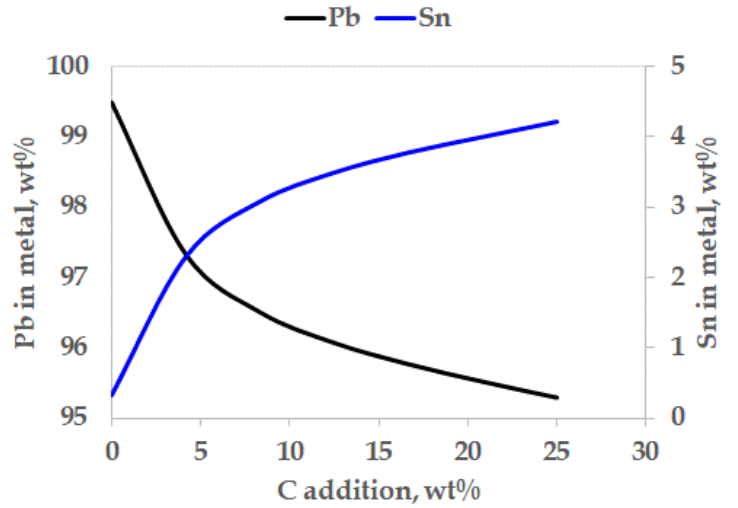

Figure 48. Plot showing relationship of mass in metal vs. C addition, at 1150°C with flame stoichiometry of 95 mol% O_2

The viscosity of slags produced during CRTs smelting was evaluated at different temperatures and at increasing flux additions. Two fluxing agents are added during CRTs smelting (*i.e.*, Na_2CO_3 and $CaCO_3$). In these calculations, the addition of $CaCO_3$ was fixed at 10 wt% (per kg CRT funnel glass) and only Na_2CO_3 addition was varied. The lowest theoretical viscosity of 3 Pa.s was obtained with a Na_2CO_3 addition of 50 wt% at a temperature of 1200°C (see Figure 49).

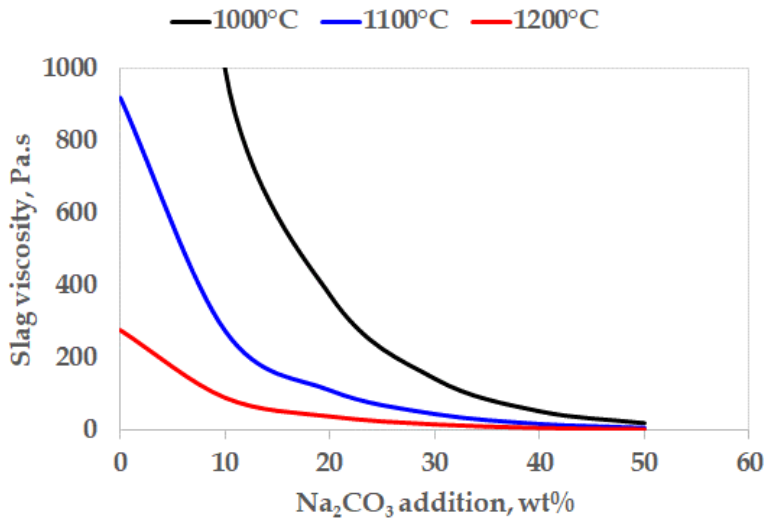

Figure 49. Plot showing relationship of slag viscosity vs. Na_2CO_3 addition under different temperatures

The ideal process condition that provided the highest achievable theoretical recovery of Pb and Sn to the metal is summarised in Table 25.

Table 25. Theoretically determined ideal process condition for CRTs smelting process

Ideal process conditions	**Values**
Highest Pb recovery	78 wt% Pb, 85 wt% Sn to metal
Alloy grade	96 wt% Pb, 3.44 wt% Sn
Flame stoichiometry	95 mol% O_2
Reduction temperature	1100°C
Reductant addition	12.5 wt% C
Flux addition	40 wt% Na_2CO_3 + 10 wt% $CaCO_3$

3.4 Experimental plan

The experimental plan for PCBs and CRTs smelting tests is presented in Table 26 and Table 27, respectively. A total of 36 tests was completed for each material. The tests were designed around the theoretically determined ideal process conditions summarised in Table 22 (for PCBs smelting) and Table 25 (for CRTs smelting).

3.4.1 PCBs smelting tests

The process variables that were changed during these tests were oxidation time, flame stoichiometry, and additions of CRT slag, Fe_2O_3, Na_2CO_3, and $CaCO_3$. The reaction temperature was kept constant throughout the test work at 1350°C, as well as a constant batch feed mass of 10 kg PCB concentrate. The test work evaluated oxidation time of 30, 60, and 70 min, and flame stoichiometry of 100, 102, 106, and 110 mol% O_2. CRT slag additions of 5, 25, and 45 wt%, and Fe_2O_3 additions of 3, 14, 15, 27, and 45 wt% were tested. For Na_2CO_3 and $CaCO_3$, only 42 and 43 wt% additions were tested respectively.

3.4.2 CRTs smelting tests

The process variables that were changed during these tests were reaction time and temperature, CRT and PCB fume additions, and additions of anthracite, Na_2CO_3, and $CaCO_3$. A batch feed mass of 20 kg CRT funnel glass was kept constant throughout the test work. The test work evaluated reaction temperature of 1100, 1150, and 1200°C, and reaction time of 2, 2.5, and 3 h. CRT fume additions of 2.5, 5, and 65%, and PCB fume additions of 2.5, 5, 10, and 60 wt% were tested. Anthracite additions of 5, 10, and 15 wt% were evaluated along with Na_2CO_3 additions of 20, 30, and 40 wt%, and $CaCO_3$ additions of 5, 10, and 15 wt%.

Table 26. Experimental plan of PCBs smelting tests

Test no.	Temp, °C	Oxidation Time, min			Flame Stoichiometry, mol%				CRT Slag, wt%			Fe_2O_3, wt%					Na_2CO_3, wt%	$CaCO_3$, wt%
	1350	30	60	90	100%	102%	106%	110%	5%	25%	45%	3%	14%	15%	27%	45%	42%	43%
1	X	X				X			X			X						
2	X		X			X			X			X						
3	X			X		X			X			X						
4	X	X				X				X				X				
5	X		X			X				X				X				
6	X			X		X				X				X				
7	X	X				X					X				X			
8	X		X			X					X				X			
9	X			X		X					X				X			
10	X	X				X					X				X			
11	X	X					X				X				X			
12	X	X						X			X				X			
13	X		X			X					X							
14	X		X			X					X							X
15	X		X			X					X						X	
16	X	X				X			X			X						
17	X		X			X			X			X						
18	X			X		X			X			X						
19	X	X				X				X				X				
20	X		X			X				X				X				
21	X			X		X				X				X				
22	X	X				X					X				X			
23	X	X					X				X				X			
24	X	X						X			X				X			

Test no.	Temp, °C	Oxidation Time, min			Flame Stoichiometry, mol%				CRT Slag, wt%			Fe_2O_3, wt%					Na_2CO_3, wt%	$CaCO_3$, wt%
	1350	30	60	90	100%	102%	106%	110%	5%	25%	45%	3%	14%	15%	27%	45%	42%	43%
25	X		X			X					X							
26	X		X			X					X							X
27	X		X			X					X						X	
28	X	X				X					X				X			
29	X		X			X					X				X			
30	X			X		X					X				X			
31	X	X			X						X				X			
32	X		X		X						X				X			
33	X			X	X						X				X			
34	X		X			X					X		X					
35	X		X			X					X					X		
36	X		X			X										X		

Note: This table is a continuation of Table 26

Table 27. Experimental plan of CRTs smelting tests

Test no.	Flame stoich.	Reduction temp, °C			Reduction time, h			CRT Fumes, wt%			PCB Fumes, wt%				Anthracite, wt%			Na_2CO_3, wt%			$CaCO_3$, wt%		
	95 mol% O_2	1100-1150	1150-1200	1200-1250	2	2.5	3	2.5	5	65	2.5	5	10	60	5	10	15	20	30	40	5	10	15
1	X			X	X										X				X			X	
2	X			X	X											X			X			X	
3	X			X	X												X		X			X	
4	X			X	X												X	X				X	
5	X			X	X												X			X		X	
6	X			X	X												X		X		X		
7	X			X	X												X		X				X
8	X			X	X			X									X		X			X	
9	X			X	X			X				X					X		X			X	
10	X			X		X		X				X					X		X			X	
11	X			X			X	X				X					X		X			X	
12	X	X			X			X				X					X		X			X	
13	X		X		X			X				X					X		X			X	
14	X	X			X			X				X					X			X		X	
15	X		X		X			X				X					X			X		X	
16	X			X	X			X				X					X			X		X	
17	X			X	X			X				X					X			X		X	
18	X		X		X			X				X					X			X		X	
19	X		X		X			X				X					X		X			X	
20	X	X			X			X				X					X			X		X	
21	X	X			X			X				X					X		X			X	
22	X			X	X			X				X					X		X			X	

Test no.	Flame stoich.	Reduction temp, °C			Reduction time, h			CRT Fumes, wt%			PCB Fumes, wt%				Anthracite, wt%			Na_2CO_3, wt%			$CaCO_3$, wt%		
	95 mol% O_2	1100-1150	1150-1200	1200-1250	2	2.5	3	2.5	5	65	2.5	5	10	60	5	10	15	20	30	40	5	10	15
23	X			X		X		X				X					X		X			X	
24	X			X			X	X				X					X		X			X	
25	X			X	X										X				X			X	
26	X			X	X											X			X			X	
27	X			X	X												X		X			X	
28	X			X	X												X	X				X	
29	X			X	X												X			X		X	
30	X			X	X												X		X		X		
31	X			X	X												X		X				X
32	X			X	X				X				X				X			X		X	
33	X			X	X				X		X						X			X		X	
34	X			X	X				X				X				X			X		X	
35	X			X	X				X		X						X			X		X	
36	X			X	X					X				X			X			X		X	

Note: This table is a continuation of Table 27

3.5 Experimental procedures

The procedures adopted to undertake the pilot smelting tests are described. Firstly, the steps undertaken to operate the furnace are discussed. Secondly, the process stages and furnace operating data of PCBs and CRTs smelting tests is presented.

3.5.1 Furnace operation

The main activities involved in executing the pilot smelting tests include gas flow control, furnace warm-up, smelting process, furnace tapping, and product handling.

3.5.1.1 Gas control and flame stoichiometry

The gas control system was an integral component of the furnace facility as it was used to control the power output of the flame from the burner. During operation, the flame power was controlled by increasing or decreasing the C_3H_8 and O_2 gas flow rates. The gas flow rates were adjusted by gently throttling the needle valves.

The rotameter set-points for the required gas flow rates were calculated with a Microsoft Excel spreadsheet. The spreadsheet required input of C_3H_8 gas flow rate set-point and the flame stoichiometry required. The spreadsheet then calculated an appropriate rotameter set-point for the required O_2 flow rate. A flame stoichiometry of less than 100 mol% O_2 was selected when reducing conditions were required in the furnace; more than 100 mol% O_2 for oxidising and 100 mol% for neutral furnace conditions. Figure 50 illustrates an example of the calculated corresponding O_2 gas flow rate set-point for 32 vol% C_3H_8 at a flame stoichiometry of 100 mol% O_2.

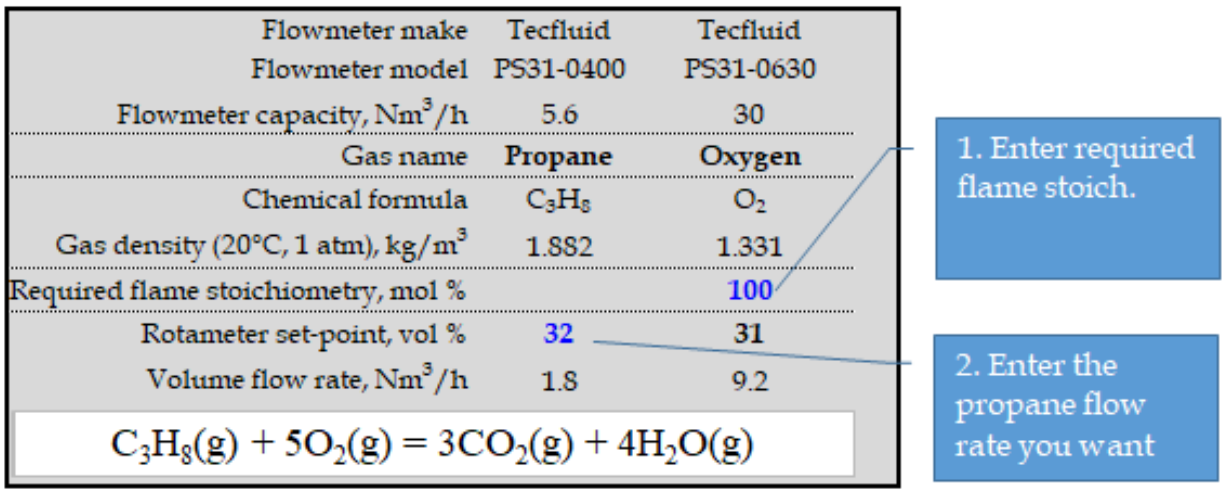

Figure 50. Example of spreadsheet showing calculated rotameter set points.

3.5.1.2 Furnace warm-up

During furnace warm-up, the gas lines were initially purged with nitrogen gas for approximately 30 seconds. Purging of the pipelines ensured displacement of any flammable mixture of gas in the lines. The gas lines were then pressurised with nitrogen gas and checked for leaks. Gas leaks were checked by spraying soapy water at all fitting connections, valves, and gauges as well as welded connections. Before the flame was ignited, cooling water flow was opened to allow cooling water to circulate through the burner. The fan from the baghouse was also switched on for extraction.

To ignite the flame, the C_3H_8 gas needle valve was slightly opened to allow a low flow of C_3H_8 through the burner. A paper, attached to the tip of a broom, was set alight with a lighter and used to ignite the C_3H_8 from the burner. Once the burner was ignited, both the O_2 and C_3H_8 flow were slowly increased until a compact flame was obtained. The burner was pivoted into the furnace and the furnace rotation was started to initiate warm up of the furnace refractory. The warm-up programme involved 1 vol% increments of gases every 15 min over a period of 120 min. This duration ensured that the inside walls of the vessel were pre-heated to about 900–1000 °C before charging of feed material could commence. The temperature of the walls of the refractory was measured with an optical pyrometer.

3.5.1.3 Furnace charging and smelting

In the CRT smelting tests, the recipe amounts of the feed materials were individually weighed and then blended together into a homogenous batch. The total batch was then divided into 4 equal sub-batches to facilitate charging to the furnace. For the first charging operation, two sub-batches were charged to the furnace and allowed to melt with a flame stoichiometry of 95 mol% O_2. Subsequent sub-batches were charged one at a time. For the PCBs smelting, the whole 10 kg batch was charged to the furnace and melted with a flame stoichiometry of 90 mol% O_2.

Charging and melting of the CRTs feed materials took about 15–20 min per charge and a total of 1.5–2 h for the whole batch. The PCBs batch was melted and allowed to fume off volatile metallic species such as Zn for a period of 1 h. Once the whole batch was fed to the furnace, the flame power was adjusted to increase the furnace contents to the reaction temperature. The furnace bath temperature was measured with an optical pyrometer. The pyrometer was a Minolta/Land Cyclops 52 infrared thermometer and can measure temperatures between 300–3000°C with a range of emissivity melting.

The emissivity setting of each slag type was established by validating the pyrometer readings with a K-type thermocouple. The thermocouple was dipped into the slag bath and the pyrometer emissivity was adjusted until the pyrometer reading was similar to the temperature reading of the thermocouple.

The residence time commenced after the furnace bath temperature reached the target reaction temperature. The bath temperature was measured every 30 min. The gas flow rate were adjusted up or down in order to maintain the temperature within 50°C of the target operating temperature. For example, for a target operating temperature of 1200°C, the slag bath temperature was maintained at 1200–1250°C. However, during smelting of PCBs temperatures ranged at 1350–1450°C especially in tests were oxidising conditions were applied for an extended period.

Once the reaction time elapsed, the flame was extinguished and the furnace rotation was stopped. The bath temperature was measured before the products were tapped into a refractory-lined ladle by tilting the furnace vessel. At the end of the tap, the vessel was tilted back to its original position. The vessel rotation was started again and the feed batch for the next test was introduced into the furnace.

3.5.2 PCBs smelting tests

This section describes the different process stages involved in the smelting of PCB concentrate, along with furnace operating data, verified operating temperatures, and the masses of raw materials fed in each test.

3.5.2.1 Process stages

PCBs smelting was undertaken in three stages. The activities of Stage 1, 2, and 3 are shown in Table 28, Table 29, and Table 30, respectively. Stage 1, melting and volatilisation, was carried out with a reducing flame stoichiometry of 90 mol% O_2. The PCBs charge was heated to temperatures above 1300°C to ensure the metallics component of the PCBs was completely molten and to promote rapid volatilisation of metallic impurities such as Zn. The melting and volatilisation period was constant at 60 min. This stage achieved the first refining action of the Cu alloy.

Table 28. Activities of Stage 1 of PCBs smelting test

	TEST NO.		
PROCESS STAGE ACTIVITIES	**4**	**5**	**6**
Stage 1: Melting & volatilisation			
Add PCBs only and melt, kg	10	10	10
Flame stoich., mol%	90	90	90
C_3H_8/ O_2, vol%	36/31	36/31	36/31
Time at gas flow set points, min	30	30	30
Take temperature, °C	1247	1258	1271
C_3H_8/ O_2, vol%	32/28	32/28	32/28
Time at gas flow set points, min	30	30	30
Take temperature, °C	1294	1308	1335
Total melting period, min	60	60	60

Oxidation of the rest of the metallic impurities such as Al, Fe, Si, Pb and Sn was undertaken in Stage 2 of the process. During this stage and for the specific tests used as an example, an oxidising flame stoichiometry of 102 mol% O_2 was applied. The operating temperature was maintained between 1300–1350°C. The oxidation period was 30, 60, or 90 min.

Table 29. Activities of Stage 2 of PCBs smelting test

	TEST NO.		
PROCESS STAGE ACTIVITIES	**4**	**5**	**6**
Stage 2: Oxidation			
Flame stoich., mol%	102	102	102
C_3H_8/ O_2, vol%	36/35	36/35	36/35
Oxidising period, min	30	30	30
Take temperature, °C	1328	1310	1342
Oxidising period, min	-	30	30
Take temperature, °C	-	1336	1354
Oxidising period, min	-	-	30
Take temperature, °C	-	-	1361
Total oxidation period, min	30	60	90

The last stage of the smelting process was Stage 3, slag formation. In this stage, metal oxides formed during the oxidation stage were fluxed to form a molten and fluid slag phase. The flame stoichiometry was maintained at 100 mol% O_2 to induce neutral conditions during the slag formation stage. The operating temperature of this stage was also maintained between 1300–1350°C, for a period of 60 min.

Table 30. Activities of Stage 3 of PCBs smelting test

	TEST NO.		
PROCESS STAGE ACTIVITIES	**4**	**5**	**6**
Stage 3: Slag formation			
Add CRT slag, kg	1.5	1.5	1.5
Add Fe_2O_3, kg	1.0	1.0	1.0
Flame stoich., mol%	100	100	100
C_3H_8/ O_2, vol%	34/32	34/32	34/32
Time at gas flow set points, min	30	30	30
Take temperature, °C	1352	1321	1333
Add CRT slag, kg	1	1	1
Add Fe_2O_3, kg	0.5	0.5	0.5
C_3H_8/ O_2, vol%	32/30	32/30	32/30
Time at gas flow set points, min	30	30	30
Take temperature, °C	1379	1339	1349
Total slag forming period, min	60	60	60
Total test duration, h	2.5	3	3.5

3.5.2.2 Furnace operating data

The typical furnace operating data showing rotameter melting, and gas volumes delivered during smelting of PCBs are given in Table 31 and Table 32, respectively. It can be noted that for this particular test a flame stoichiometry of 110 mol% O_2 was applied for a period of 30 min in the oxidation stage (Stage 2).

Table 31. Typical furnace operating data of PCBs smelting test

	Time			Rotameter setting, vol%		Flame stoich. mol%	Operating temp °C	Comment
Process step	**Start time**	**Finish time**	**Duration min**	**C_3H_8 50 kPa(g)**	**O_2 200 kPa(g)**			
1	21:40	21:45	5	26	24	95	-	Keep furnace warm
2	21:45	22:15	30	34	29	90	1325	Stage 1
3	22:15	22:45	30	32	28	90	1331	
4	22:45	23:16	30	32	34	110	1435	Stage 2
5	23:16	23:45	30	30	28	100	1312	Stage 3
6	23:45	00:16	31	30	28	100	1362	
7	00:16	00:18	2	-	-	-	-	Tapping furnace

To achieve the operating temperatures, gas flow rates of 1.7–1.9 Nm^3/h C_3H_8 and 8.4–10.2 Nm^3/h O_2 were applied. For this particular test, a total of 8.6 and 30.3 kg of C_3H_8 and O_2 gas was delivered, respectively. The densities of the gases used to calculate the masses delivered are given in Table 33.

Table 32. Typical gas flow rate, volume and mass delivered

	Time			Flow rates		Volume delivered		Mass delivered	
Process Step	**Start Time**	**Finish time**	**Duration min**	**C_3H_8 Nm^3/h**	**O_2 Nm^3/h**	**C_3H_8 Nm^3**	**O_2 Nm^3**	**C_3H_8 kg**	**O_2 kg**
1	21:40	21:45	5	1.4	7.2	0.12	0.60	0.23	0.80
2	21:45	22:15	30	1.9	8.7	0.95	4.35	1.78	5.79
3	22:15	22:45	30	1.8	8.4	0.89	4.20	1.68	5.59
4	22:45	23:15	30	1.8	10.2	0.89	5.10	1.68	6.79
5	23:15	23:45	30	1.7	8.4	0.84	4.20	1.57	5.59
6	23:45	00:16	31	1.7	8.4	0.86	4.34	1.63	5.78
Total			**156**			**4.55**	**22.8**	**8.6**	**30.3**

Table 33. Gas densities under normal temperature and pressure

Gas	Temp, K	Pressure, kPa	Density, kg/m3
C_3H_8	293	101.325	1.882
O_2	293	101.325	1.331

The typical operating temperature profiles of PCBs smelting tests are illustrated in Figure 51. Temperature verification of slag bath performed during Stage 3 of Test 24, and that of off-gas and flame performed during Stage 3 of Test 25 are depicted in Figure 52 and Figure 53, respectively. Temperature verification profiles of several other tests are provided in APPENDIX I. For the slag bath temperature verification, a K-type thermocouple was dipped briefly into the slag (see Figure 54) and withdrawn. This was repeated twice to obtain curves observed in Figure 52.

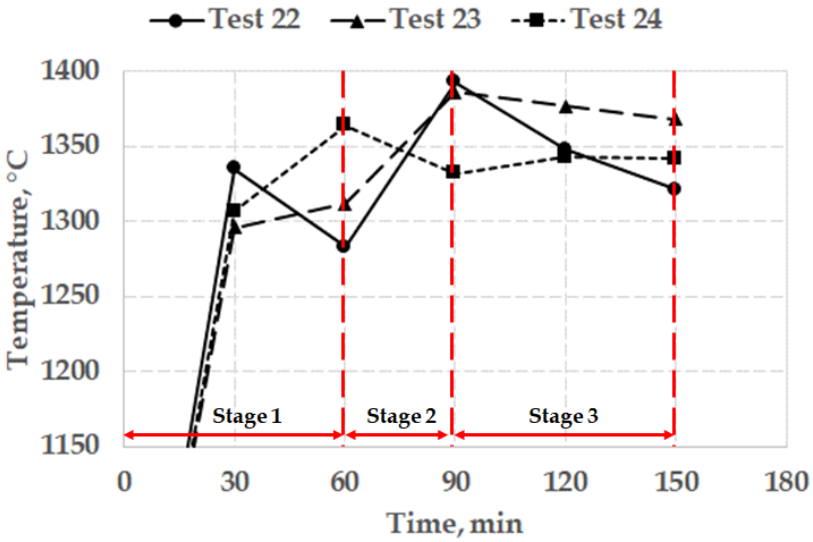

Figure 51. Typical temperature profile of PCBs smelting tests

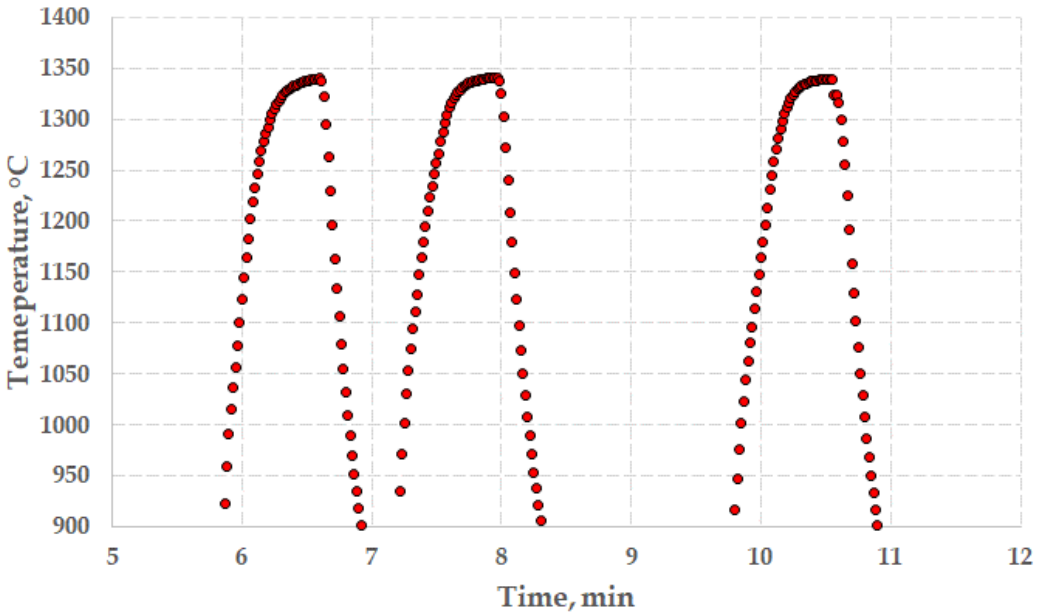

Figure 52. Temperature verification of slag bath from PCBs smelting Test 24 during Stage 3

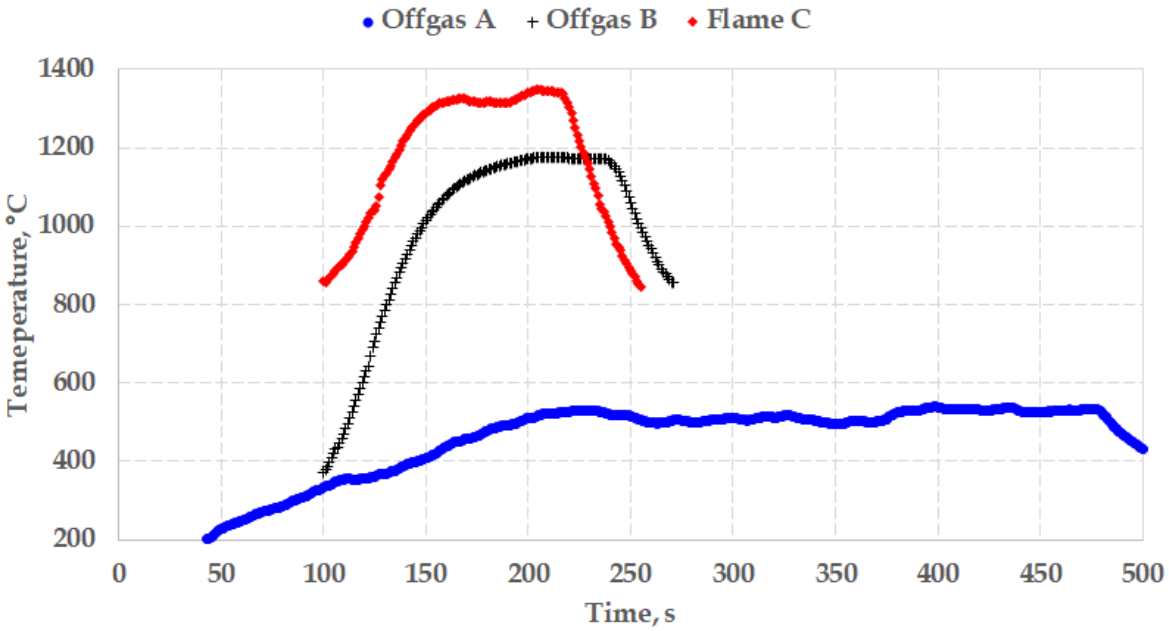

Figure 53. Temperature verification of off-gas inside and outside furnace, and flame from PCBs smelting Test 25 during Stage 3

For verification of off-gas temperature at point A (see Figure 54), a K-type thermocouple was used. For verification of off-gas temperature at point B and flame temperature at point C (see Figure 54), a B-type thermocouple was employed.

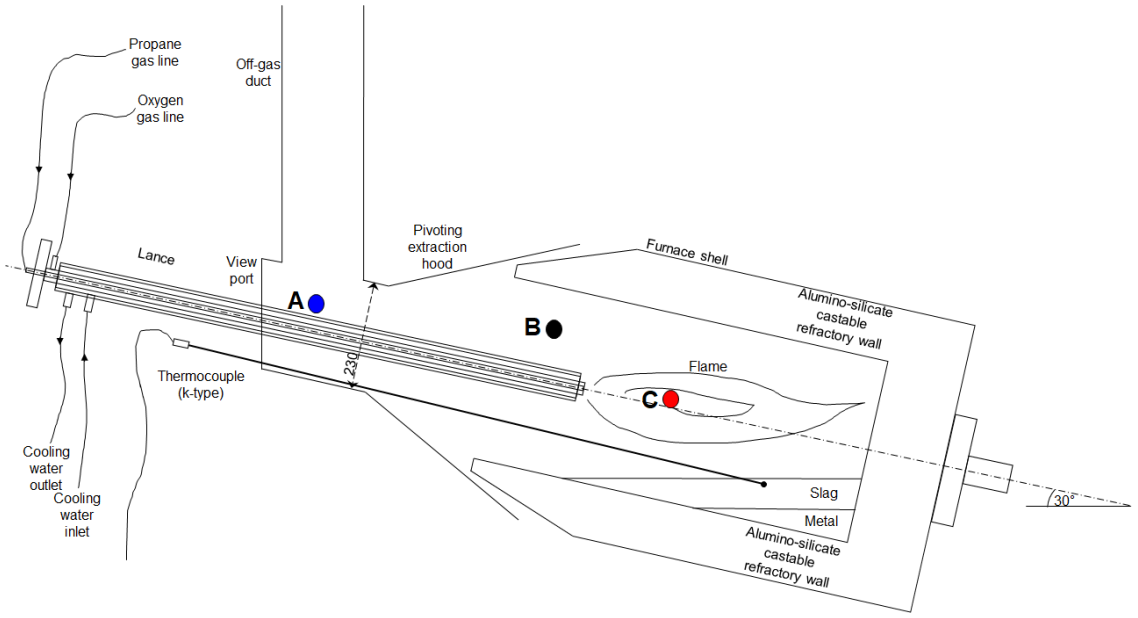

Figure 54. Schematic of TBRC vessel highlighting points where off-gas and flame temperature verification measurements were taken

Figure 55 provides the operating temperatures measured during the different stages of each smelting test. The operating temperatures predominantly ranged between 1300–1400°C. Temperatures measured in excess of 1400°C were observed mainly in Stage 2 (oxidation stage), and temperatures below 1300°C were observed mainly in Stage 1 (melting stage).

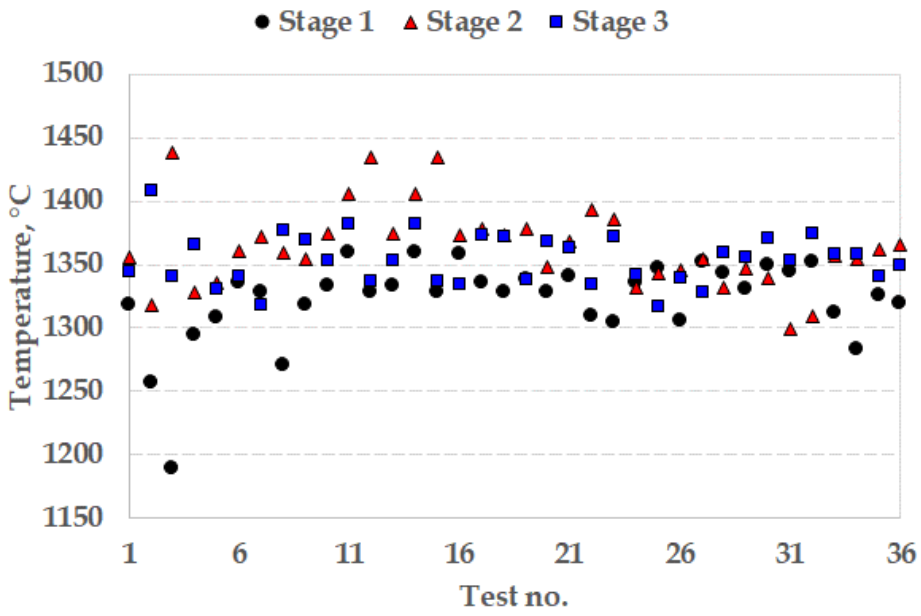

Figure 55. Operating temperatures as measured during the different stages of PCBs smelting tests

3.5.2.3 Raw material masses

The masses of raw materials fed in the PCBs smelting tests are presented in Table 34. Table 34 also presents the mass of excess O_2 delivered during the oxidation stage.

Table 34. Masses of raw materials fed during PCBs smelting tests

Test No.	Total C_3H_8, kg	Total O_2, kg	Flame stoich., mol% O_2	Excess O_2, kg	PCBs, kg	CRT slag, kg	Fe_2O_3, kg	Na_2CO_3, kg	$CaCO_3$, kg	Total solids fed, kg
1	12.8	44.6	102	0.137	10	0.5	0.3	-	-	10.8
2	9.8	34.4	102	0.269	10	0.5	0.3	-	-	10.8
3	11.3	39.9	102	0.367	10	0.5	0.3	-	-	10.8
4	8.7	29.9	102	0.121	10	2.5	1.5	-	-	14.0
5	10.4	37.5	102	0.246	10	2.5	1.5	-	-	14.0
6	10.8	38.3	102	0.485	10	2.5	1.5	-	-	14.0
7	9.8	34.0	102	0.121	10	4.5	2.7	-	-	17.2
8	11.3	39.8	102	0.243	10	4.5	2.7	-	-	17.2
9	12.2	43.1	102	0.360	10	4.5	2.7	-	-	17.2
10	10.7	35.8	102	0.110	10	4.5	2.7	-	-	17.2
11	8.3	28.9	106	0.362	10	4.5	2.7	-	-	17.2
12	8.6	30.3	110	0.617	10	4.5	2.7	-	-	17.2
13	10.2	36.3	102	0.243	10	4.5	-	-	-	14.5
14	10.5	36.8	102	0.243	10	4.5	-	-	4.3	18.8
15	10.2	35.9	102	0.247	10	4.5	-	4.2	-	18.7
16	8.9	30.8	102	0.121	10	0.5	0.3	-	-	10.8
17	9.9	34.7	102	0.243	10	0.5	0.3	-	-	10.8
18	11.8	41.5	102	0.364	10	0.5	0.3	-	-	10.8
19	8.3	28.7	102	0.121	10	2.5	1.5	-	-	14.0
20	10.1	35.3	102	0.243	10	2.5	1.5	-	-	14.0
21	12.0	42.5	102	0.364	10	2.5	1.5	-	-	14.0
22	8.5	29.5	102	0.121	10	4.5	2.7	-	-	17.2
23	8.5	29.7	106	0.362	10	4.5	2.7	-	-	17.2
24	8.9	32.1	110	0.617	10	4.5	2.7	-	-	17.2
25	10.7	37.6	102	0.243	10	4.5	-	-	-	14.5
26	10.0	34.9	102	0.243	10	4.5	-	-	4.3	18.8
27	10.0	34.9	102	0.243	10	4.5	-	4.2	-	18.7
28	8.6	29.1	102	0.110	10	4.5	2.7	-	-	17.2
29	10.1	35.3	102	0.243	10	4.5	2.7	-	-	17.2
30	11.8	41.7	102	0.364	10	4.5	2.7	-	-	17.2
31	8.5	29.3	100	-	10	4.5	2.7	-	-	17.2
32	10.4	36.1	100	-	10	4.5	2.7	-	-	17.2
33	11.6	40.3	100	-	10	4.5	2.7	-	-	17.2
34	10.1	35.1	102	0.243	10	4.5	1.35	-	-	15.9
35	10.0	34.9	102	0.243	10	4.5	4.5	-	-	19.0
36	10.4	36.8	102	0.243	10	-	4.5	-	-	14.5
Total	**365**	**1277**	**-**	**8.90**	**360**	**122**	**61.7**	**8.4**	**8.6**	**560**

3.5.3 CRTs smelting tests

This section describes the process stages involved in the reductive smelting of CRT funnel glass. The furnace operating data, verified operating temperatures, and the raw material masses fed in each test are presented.

3.5.3.1 Process stages

The smelting of CRTs was carried out over two stages. Melting of the raw materials was undertaking in Stage 1 over a period of 60 min. Reductive smelting of the CRTs was undertaken in Stage 2 over a period of 2, 2.5, or 3 h. The activities of the process stages from Test 7, 8 and 9 are shown in Table 35. The flame stoichiometry for the CRTs smelting tests was kept constant at 95 mol% O_2 in all stages. This was to ensure that mildly reducing conditions are maintained inside the furnace throughout the test.

Table 35. Activities of Stage 1 and 2 of CRTs smelting tests

	TEST NO		
PROCESS STAGE ACTIVITIES	**7**	**8**	**9**
STAGE 1: Melting			
Flame stoich., mol%	95	95	95
C_3H_8/ O_2, vol%	34/31	34/31	34/31
Add batch 1 (after 15 min add batch 2)	Batch 1	Batch 1	Batch 1
Add batch 2 (after 15 min add batch 3)	Batch 2	Batch 2	Batch 2
Add batch 3 (after 15 min add batch 4)	Batch 3	Batch 3	Batch 3
Add batch 4 (after 15 min move to Stage 2)	Batch 4	Batch 4	Batch 4
Time at gas flow set points, min	60	60	60
Take temperature, °C	1161	1116	1126
Total melting period, min	60	60	60
STAGE 2: Reduction			
Flame stoich., mol%	95	95	95
C_3H_8/ O_2, vol%	34/31	34/31	34/31
Reduction period, min	30	30	30
Take temperature, °C (1st 30min)	1236	1219	1243
Flame stoich., mol%	95	95	95
C_3H_8/ O_2, vol%	34/31	34/31	34/31
Reduction period, min	30	30	30
Take temperature, °C (2nd 30min)	1282	1263	1258
Flame stoich., mol%	95	95	95
C_3H_8/ O_2, vol%	32/29	30/27	30/27
Reduction period, min	30	30	30
Take temperature, °C (3rd 30min)	1299	1283	1238
Flame stoich., mol%	95	95	95
C_3H_8/ O_2, vol%	30/27	28/25	30/27

Table 35—Continued

Reduction period, min	30	30	30
Take temperature, °C (4th 30min)	1271	1250	1263
Total reduction period, min	120	120	120
Total test duration, h	3	3	3

3.5.3.2 Furnace operating data

The typical furnace operating data showing rotameter setting, and volumes and masses of gases delivered during smelting of CRTs are given in Table 36 and Table 37, respectively. For this particular test, a total amount of 9.3 kg C_3H_8 and 32.1 kg O_2 gas was delivered to the furnace over a period of 3 h.

Table 36. Typical furnace operating data of CRTs smelting test

	Time			**Rotameter setting, vol%**		**Flame**	
Process Step	**Start Time**	**Finish time**	**Duration min**	**C_3H_8 50 kPa(g)**	**O_2 200 kPa(g)**	**Stoich mol%**	**Comment**
1	07:30	07:45	15	34	31	95	Stage 1
2	07:45	08:00	15	34	31	95	
3	08:00	08:15	15	34	31	95	
4	08:15	08:30	15	34	31	95	
5	08:30	08:45	15	32	29	95	Stage 2
6	08:45	09:00	15	32	29	95	
7	09:00	09:15	15	28	25	95	
8	09:15	09:30	15	28	25	95	
9	09:30	09:45	15	26	24	95	
10	09:45	10:00	15	24	22	95	
11	10:00	10:15	15	24	22	95	
12	10:15	10:30	15	24	22	95	
13	10:30						Furnace tapping
Total			**3.00**				

Table 37. Typical gas flow rate, volume and mass delivered

	Time			Flowrates		Volume delivered		Mass delivered	
Process Step	**Start Time**	**Finish time**	**Duration min**	**C_3H_8 Nm^3/h**	**O_2 Nm^3/h**	**C_3H_8 Nm^3**	**O_2 Nm^3**	**C_3H_8 kg**	**O_2 kg**
1	07:30	07:45	15	1.9	9.3	0.47	2.33	0.89	3.09
2	07:45	08:00	15	1.9	9.3	0.47	2.32	0.89	3.09
3	08:00	08:15	15	1.9	9.3	0.47	2.33	0.89	3.09
4	08:15	08:30	15	1.9	9.3	0.47	2.33	0.89	3.09
5	08:30	08:45	15	1.8	8.7	0.45	2.17	0.84	2.89
6	08:45	09:00	15	1.8	8.7	0.45	2.18	0.84	2.89
7	09:00	09:15	15	1.6	7.5	0.39	1.88	0.73	2.50
8	09:15	09:30	15	1.6	7.5	0.39	1.87	0.73	2.50
9	09:30	09:45	15	1.4	7.2	0.36	1.80	0.68	2.40
10	09:45	10:00	15	1.3	6.6	0.33	1.65	0.63	2.20
11	10:00	10:15	15	1.3	6.6	0.33	1.65	0.63	2.20
12	10:15	10:30	15	1.3	6.6	0.33	1.65	0.63	2.20
13	10:30								
Total			**3.00**			**4.93**	**24.2**	**9.3**	**32.1**

The typical operating temperatures applied during CRTs smelting tests are depicted in Figure 56. Temperature verification of slag bath from Test 8 is given in Figure 57 and that of off-gas temperature inside and outside of furnace is given in Figure 58. The points at which the slag bath and off-gas temperature measurements were verified are shown in Figure 59. Profiles of temperature verifications obtained for other tests are provided in APPENDIX I. The operating temperatures measured during the different stages of the CRTs smelting tests are plotted in Figure 60.

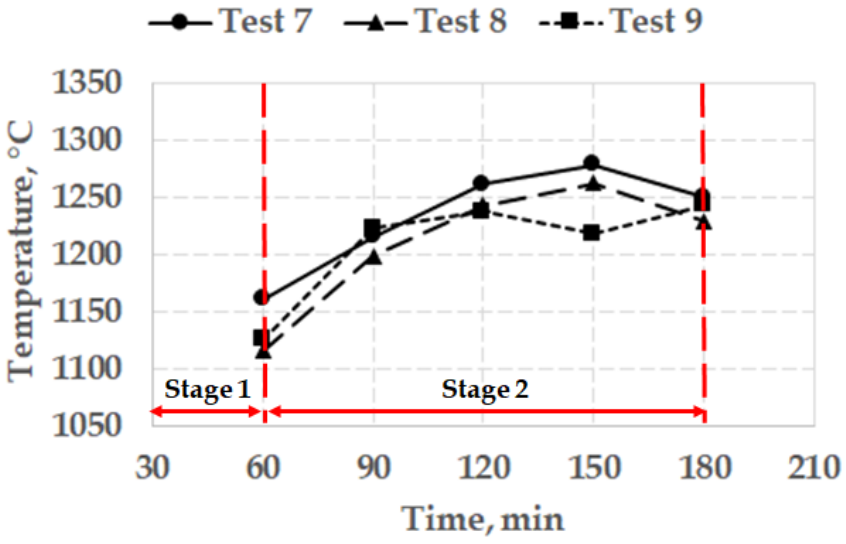

Figure 56. Typical operating temperature profile of CRTs smelting tests

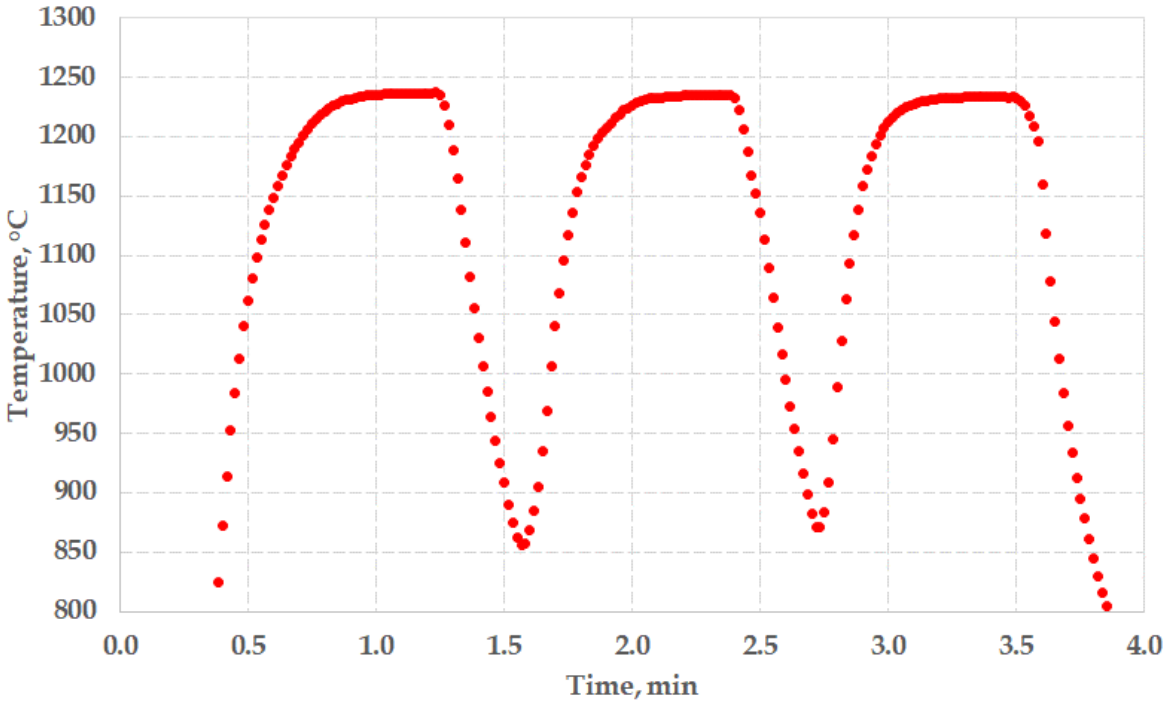

Figure 57. Temperature verification of slag bath from CRTs smelting Test 8 during Stage 2.

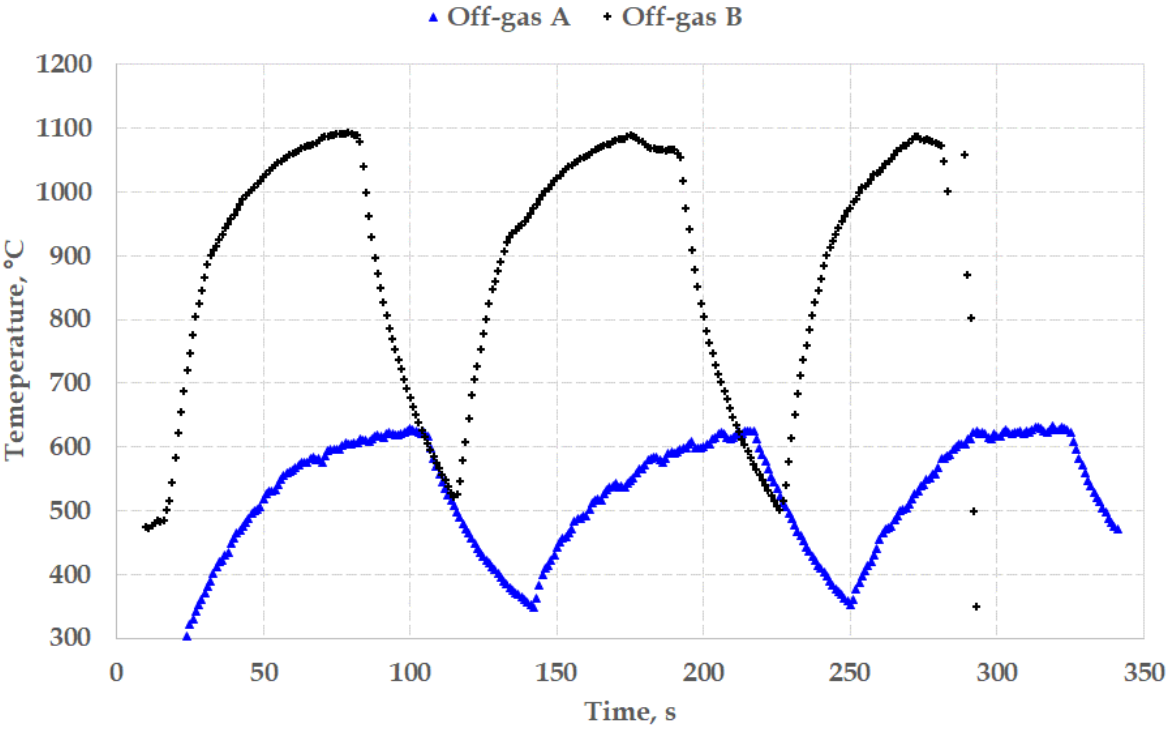

Figure 58. Temperature verification of off-gas inside and outside furnace from CRTs smelting Test 31 during Stage 3

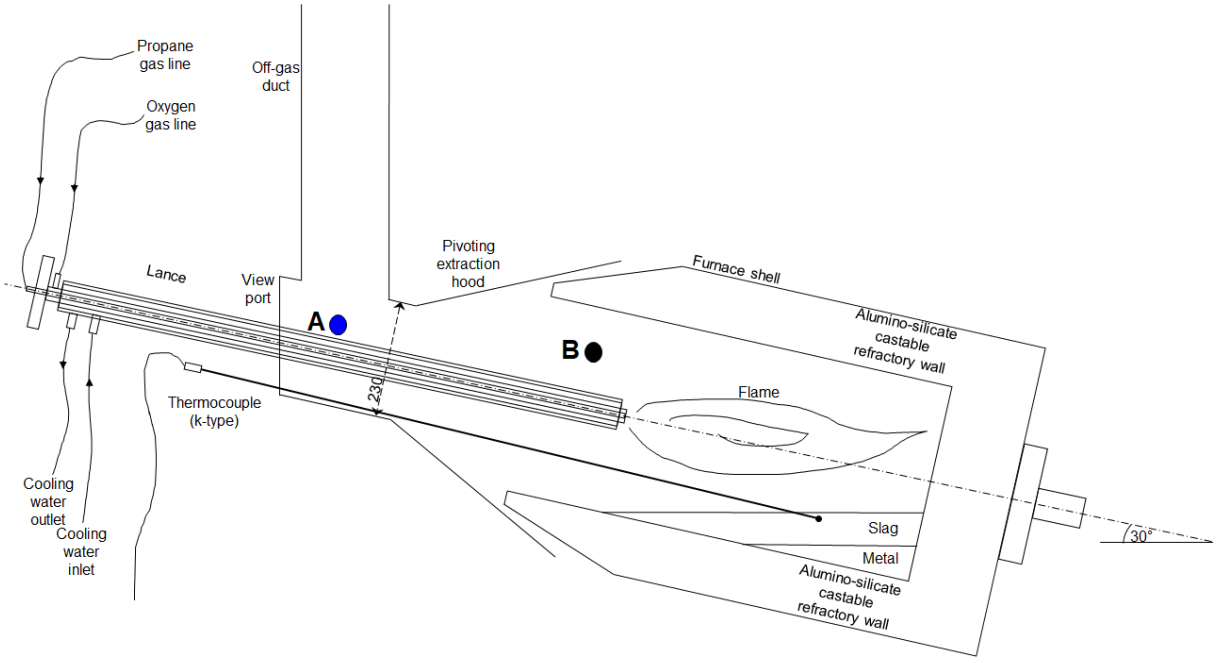

Figure 59. Schematic of TBRC vessel highlighting points where off-gas temperature verification measurements were taken

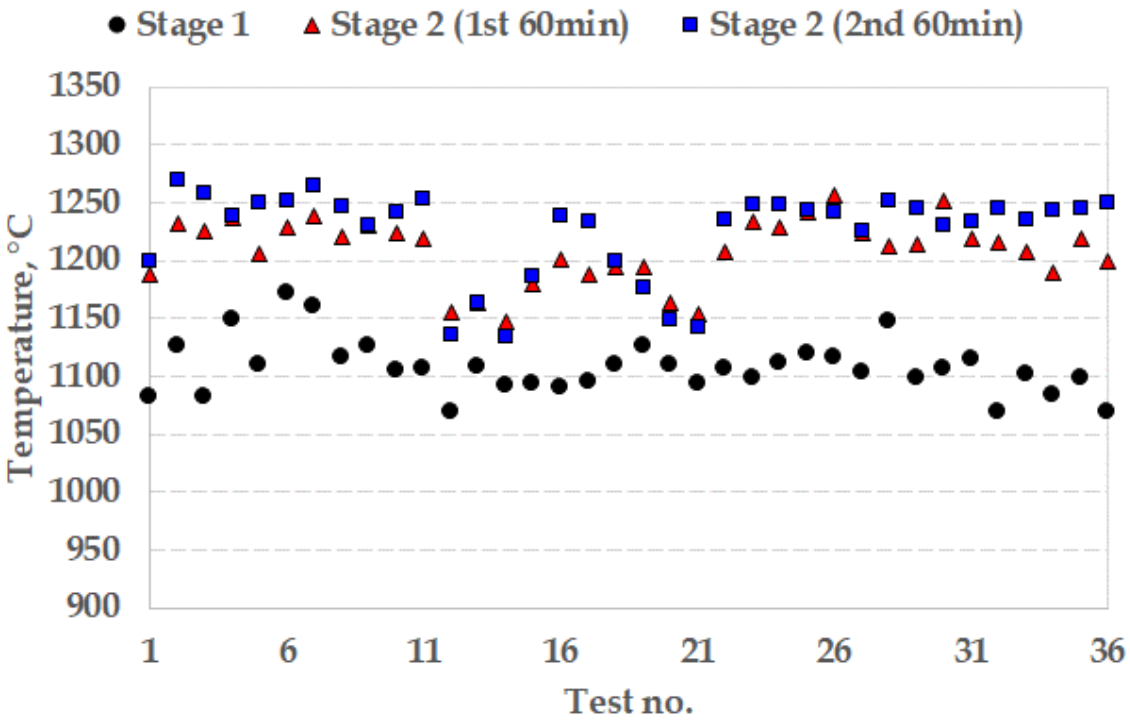

Figure 60. Operating temperatures as measured during the different stages of CRTs smelting tests

3.5.3.3 Raw material masses

The masses of raw materials fed in the CRTs smelting tests are given Table 38.

Table 38. Masses of raw materials fed during CRTs smelting tests

Test No.	C_3H_8, kg	O_2, kg	CRTs glass, kg	CRT fume, kg	PCB fume, kg	Anthracite, kg	Na_2CO_3, kg	CaCO3, kg	Total solids fed, kg
1	16.6	57.9	20	-	-	1	6	2	29.0
2	10.6	36.8	20	-	-	2	6	2	30.0
3	10.5	36.2	20	-	-	3	6	2	31.0
4	9.9	33.9	20	-	-	3	4	2	29.0
5	10.6	36.5	20	-	-	3	8	2	33.0
6	8.8	30.4	20	-	-	3	6	1	30.0
7	12.1	42.0	20	-	-	3	6	3	32.0
8	11.0	37.1	20	1.0	-	3	6	3	33.0
9	8.9	30.7	20	0.5	1.0	3	6	2	32.5
10	12.9	44.4	20	0.5	1.0	3	6	2	32.5
11	13.4	46.4	20	0.5	1.0	3	6	2	32.5
12	8.9	30.8	20	0.5	1.0	3	6	2	32.5
13	8.6	29.9	20	0.5	1.0	3	6	2	32.5
14	8.3	28.7	20	0.5	1.0	3	8	2	34.5
15	9.3	32.1	20	0.5	1.0	3	8	2	34.5
16	9.9	34.2	20	0.5	1.0	3	8	2	34.5
17	10.5	36.1	20	0.5	1.0	3	8	2	34.5
18	9.2	31.9	20	0.5	1.0	3	8	2	34.5
19	9.0	31.1	20	0.5	1.0	3	6	2	32.5
20	8.5	29.5	20	0.5	1.0	3	8	2	34.5
21	8.0	27.6	20	0.5	1.0	3	6	2	32.5
22	10.2	35.4	20	0.5	1.0	3	6	2	32.5
23	11.8	40.9	20	0.5	1.0	3	6	2	32.5
24	13.8	47.7	20	0.5	1.0	3	6	2	32.5
25	10.0	34.4	20	-	-	1	6	2	29.0
26	10.0	34.6	20	-	-	2	6	2	30.0
27	10.1	34.7	20	-	-	3	6	2	31.0
28	10.2	35.3	20	-	-	3	4	2	29.0
29	10.3	35.5	20	-	-	3	8	2	33.0
30	9.9	34.3	20	-	-	6	6	1	33.0
31	10.1	34.7	20	-	-	3	6	3	32.0
32	10.4	35.7	20	1.0	2.0	3	8	2	36.0
33	10.1	34.7	20	1.0	0.5	3	8	2	34.5
34	10.2	35.3	20	1.0	2.0	3	8	2	36.0
35	10.2	35.2	20	1.0	0.5	3	8	2	34.5
36	10.1	34.7	10	6.5	6.0	3	8	2	35.5
Total	**372**	**1288**	**710**	**19.5**	**27**	**105**	**238**	**73**	**1172**

3.6 Products

There were four types of product generated in the test work, *viz*., metal, slag, fume, and gas. All the products, except for gas, were collected, sampled, and analysed.

3.6.1 Product handling

The fumes generated from the furnace were primarily captured in a bank of cartridge filters. These fumes were collected and recycled to the furnace during the CRTs smelting tests. This was done on a test-to-test basis. It involved switching from one set of cartridge filters to the other. The valves for the new set of cartridges were opened 10 min before the furnace was tapped. The valves for the set of cartridge filters used in the previous test were then closed and the filters were removed for collection of fumes. Compressed air was blown through the sides of the filter to release the fume from the filter. After cleaning, the cartridge filters were reinstalled in the filter drums.

The molten products (metal and slag) were tapped into refractory-lined ladle and the remaining material was scraped out using a metallic spoon. The products were allowed to cool and solidify in the ladle. After the products were tipped out of the ladle, the ladle refractory was re-coated with mould wash to ensure that products from the next test do not stick to the refractory. The metal was separated from the slag (see Figure 61) and cleaned before being weighed.

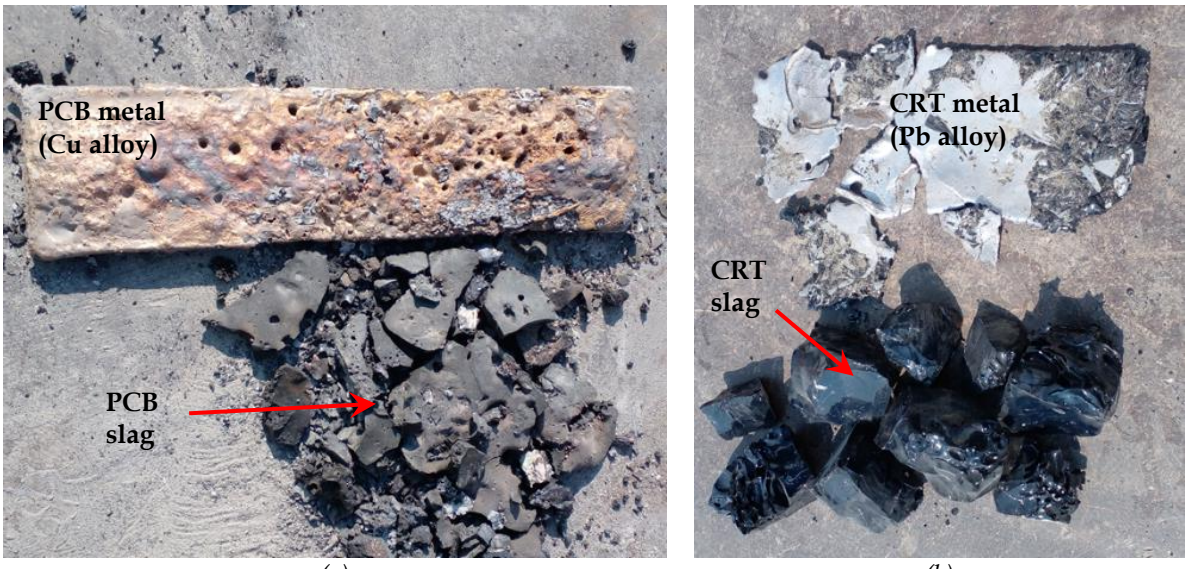

(a) (b)

Figure 61. Product metal and slag from (a) PCBs smelting test, and (b) CRTs smelting test

3.6.2 *Sampling*

The fume product occurred in a uniform fine particle size. This material was blended and sampled with the grab sampling technique to prepare a 50 g subsample. The metal and slag products were allowed to solidify and cool before being sampled. The slag was firstly separated from the metal before being broken into smaller pieces (<50 mm). Clean slag pieces, free of metal entrainment, were carefully selected for analysis. In some cases it was necessary to break the slag pieces even smaller (<5 mm) to ensure the samples were completely free of any metal prills. A mass of 100 g slag was collected for each test. Before the samples were submitted for chemical analysis, they were pulverised to 100 wt% passing 75 µm in a micronizing mill using a stainless steel bowl.

The metal slabs were sampled by drilling holes into the slab on clean surfaces as shown in Figure 62. Multiple holes were drilled into the metal to generate metal chips weighing 50 g. The slabs were not drilled all the way through (see Figure 62(c)) to avoid contamination with slag adhering to the bottom side of the metal slab. The metal chips were submitted for analysis as is.

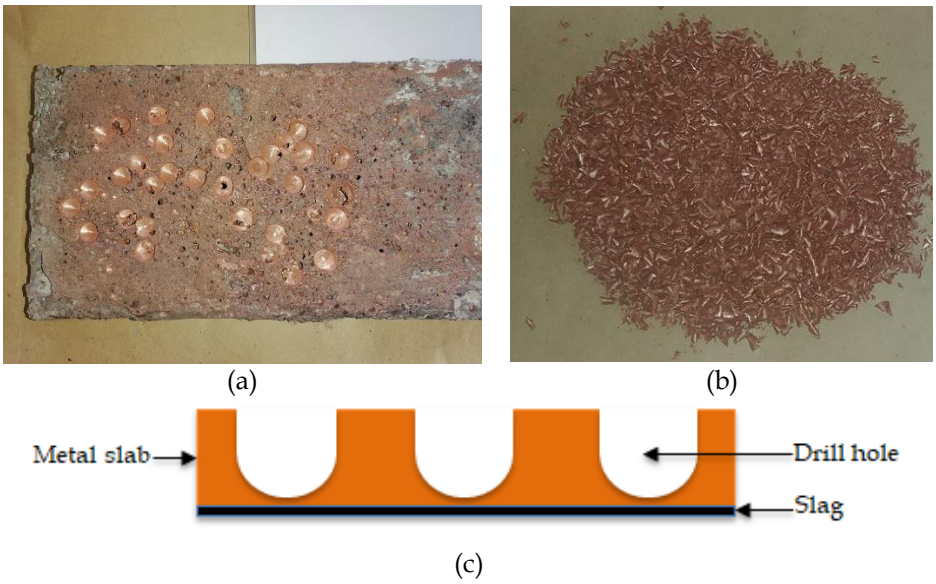

Figure 62. Image of (a) PCB metal slag with drill holes, (b) metal chips generated from drilling of metal slab, and (c) schematic showing how deep the metal slabs were drilled

3.6.3 *Characterization*

The bulk chemical analysis of the products was undertaken by Mintek's ACD (see Table 39), and Scrooby's Laboratory verified the analysis of selected samples. The phase-chemical analysis of selected samples was carried out by Mintek's MNL.

Table 39. List of analytical techniques applied to products by Mintek's ACD

	Analytical technique	Analytes	Lower Detection limit	Sample Analysed
1	ICP-OES	Al, Ca, Co, Cr, Cu, Fe, Mg, Mn, Ni, Pb, Si, Ti, V, Zn	0.05 wt%	PCB slag & fume, CRT slag & fume
2	ICP-OES (ICP1)	Al, Ca, Co, Cr, Cu, Fe, Mg, Mn, Ni, Pb, Si, Ti, V, Zn	0.05 wt%	PCB & CRT metal
3	ICP-OES (ICP8)	Au, Pd, Pt	0.02 ppm	PCB Metal
4	ICP-OES (ICP8)	Ag	0.2 wt%	PCB Metal & fume
5	ICP-OES (ICP10)	Sn	0.01 wt%	All
6	ICP-OES (ICP52)	Ba, Sr	<100 ppm	CRT slag
7	ICP-MS	Ag	0.02 ppm	PCB Slag, CRT metal & CRT fume
8	Atomic Absorption (AA)	K, Na	<2 ppm	PCB & CRT slag, PCB & CRT fume
9	Fire Assay (FA)	Au, Pd, Pt	0.02 ppm	PCB & CRT slag, PCB & CRT fume
10	Carrier-gas hot extraction	Total C	0.01 wt%	CRT fume

The same ICP-OES, atomic absorption, and carrier-gas hot extraction method described in section 3.2.5.1 was applied for the analysis of product samples.

The fire assay method, with Pb collection, was used to determine low levels of Au, Pd, and Pt in slag and fume samples. The samples were mixed with a flux consisting of fused borax ($Na_2B_4O_7$), Na_2CO_3, SiO_2, PbO and reducing agent. Silver nitrate solution was added to the mixtures before placing the samples in the furnace. Borax and Na_2CO_3 fused with the sample and released the noble metals from the matrix which was collected by metallic Pb and settled to the bottom of the crucible. The Pb was then separated from the slag and placed in a cupel in a muffle furnace where the Pb was oxidized and absorbed by the cupel material. A remaining prill containing the noble metals was then subjected to a pressure dissolution technique before being measured by ICP-OES.

The same analytical verification method and phase-chemical analysis technique described for raw materials in section 3.2.5.2, was applied for the analysis of selected product samples. In addition, two different analytical techniques were applied to evaluate compositional variation across the surface and depth of the PCB metal slab.

The two techniques applied were micro-XRF spectrometry and spark emission spectrometry.

Spark emission spectrometry was used to analyse the sample using a Cu/Sn/Pb-alloys program. This technique is a surface analysis and can only penetrate up to 400 µm per spark. As such, the PCB metal slab was sectioned into 14 pieces and each piece was ground to remove any scale and to reveal the metallic surface to achieve a better representation of the alloy. A Cu/Sn/Pb standard reference alloy was used to verify the accuracy of the instrument.

Analysis with the micro-XRF used a Bruker M4 Tornado instrument. This instrument was fitted with a rhodium tube as a source of X-rays and two Si drift detectors for maximum count throughput. The PCB metal slab was sectioned into 14 pieces and each piece was analysed on the surface and along the cross-section. The samples were analysed at 100 µm pixel spacing and counting time of 5 ms. Imaging was conducted via the M4 micro-XRF software and EDS was used to determine elemental composition. The images provide an overall element map of the surface analysed and the difference in intensities provide an indication of the difference in composition.

3.7 Mass Balance Techniques

This section describes the principle and techniques used to calculate the elemental mass balance of each test and the overall elemental mass balance of each campaign.

3.7.1 Principle

The mass balance calculation used to evaluate the test work data was based on the law of conservation of elemental mass, which states that the sum of masses of an element entering a system is equal to the sum of masses of the element leaving the system and the accumulation of the element in the system as defined in equation 15.

$$\sum m_{i,in} = \sum m_{i,out} + \sum m_{i,acc} \qquad [15]$$

Where,

$m_{i,in}$ = *mass of element i in stream entering system*

$m_{i,out}$ = *mass of element i in stream leaving system*

$m_{i,acc}$ = *mass of element accumulated in system*

For illustrative purposes, the equations governing the Fe mass balance are described in equations 16 to 18. Note that the accumulation term falls out because the tests were batch process.

$$m_{Fe,in} = M_{Fe}\left(\frac{x_{Fe,PCBs} \times m_{PCBs}}{M_{Fe}} + 2\frac{x_{Fe2O3,Ferric\ oxide} \times m_{Ferric\ oxide}}{M_{Fe2O3}} + \frac{x_{FeO,CRT\ slag} \times m_{CRT\ slag}}{M_{FeO}}\right) \quad [16]$$

$$m_{Fe,out} = M_{Fe}\left(\frac{x_{FeO,Slag} \times m_{slag}}{M_{FeO}} + \frac{x_{FeO,Fume} \times m_{Fume}}{M_{FeO}}\right) + x_{Fe,Metal} \times m_{Metal} \quad [17]$$

$$m_{Fe,in} - m_{Fe,out} = 0 \quad [18]$$

Where,
M_i = *molar mass of i*
$x_{i,j}$ = *mass fraction of element i in stream j*
m_j = *mass of stream j*

The mass balance can be closed ideally if the difference between the mass in and out for each element converges perfectly to zero. This is however an improbable goal. Inaccuracies in weighing of materials, sampling, and analytical errors all contribute to the inability to perfectly close a mass balance. A variety of techniques can be used to characterise the elemental mass balance.

3.7.2 Techniques and definitions

Several formulations of the mass balance can be used to describe the process. The mass balance techniques used in this report are briefly summarized and defined in this section as references are made to these formulations throughout the report.

Overall elemental accountability: The overall accountability is based on elements present in the feed, slag, metal and fume, and denotes the percentage of the elements in the feed material that are recovered as products. It is a useful tool for assessing the quality of the test work and the resulting elemental mass balance. The overall accountability is generally affected by uncertainties in the analyses or masses of both the raw materials and the products.

$$Accountability = \frac{\sum m_{i,out}}{\sum m_{i,in}} \times 100 \quad [19]$$

Where,
$m_{i,out}$ = *mass of element i from all materials coming out of the process*
$m_{i,in}$ = *mass of element i from all materials coming in to the process*

Elemental recovery: Elemental recovery differs from accountability in that it quantifies the percentage of elements in the feed material that reports to, or is recovered to, a particular product (*i.e.* slag, metal or fume). References in this the report to recovery of an individual element (unless stated otherwise) will be defined as in equation 20.

$$Recovery_{i,slag} = \left(\frac{m_{i,slag}}{m_{i,feed}}\right) \times 100 \quad [20]$$

Where,
$Recovery_{i,slag}$ = *recovery of element i to slag stream*
$m_{i,slag}$ = *mass of element i in slag stream*
$m_{i,feed}$ = *mass of element i in feed stream*

Elemental distribution: This establishes the partitioning of an element to a particular product stream in respect of the total mass of that element reporting to all the solid product streams (metal, slag and dust). The expression for distribution is given in equation 21. This mass balance formulation is especially useful when the accountabilities are generally poor as it only considers and accounts for masses of elements recovered to the solid product streams.

$$Distribution_{i,metal} = \frac{M_{i,metal}}{M_{i,products}} \times 100 \quad [21]$$

Where,

$Distribution_{i,metal}$ = *partitioning of element i to metal stream*
$m_{i,metal}$ = *mass of element i in metal stream*
$m_{i,products}$ = *Total mass of element i in product streams= (metal+slag+fume)*

4 EXPERIMENTAL RESULTS

The results from the PCBs smelting tests are presented first and those from CRTs smelting tests are presented thereafter.

4.1 PCBs smelting tests

The material masses, elemental mass balance, and chemical compositions of products from the PCBs smelting tests are presented in this section. The results presented are only from tests that achieved Cu recoveries above 90 wt%. The complete set of results can be found in APPENDIX J.

4.1.1 Product masses

The feed and product masses from the selected tests are presented in Table 40. Of the tests presented, Test 4 had a lowest flux addition which corresponds with the lowest slag generated. Test 32 applied a flame stoichiometry of 100 mol% O_2, thus theoretically it had no excess O_2. Test 11 applied the highest flame stoichiometry of 106 mol% O_2 which corresponds with the highest excess O_2 introduced to the metal, and consequently, highest slag generated. The total masses fed for the tests are consistent and correspond well with the total masses recovered after the tests.

Table 40. Feed and product masses of PCBs smelting tests that obtained Cu recoveries above 90 wt%

FEED MASSES						
Test No.	**Flame stoich., mol% O_2**	**Excess O_2, kg**	**Mass PCBs, kg**	**Mass CRT slag, kg**	**Mass Fe_2O_3, kg**	**Total mass fed, kg**
4	102	0.121	10	2.5	1.5	14.1
8	102	0.243	10	4.5	2.7	17.4
11	106	0.362	10	4.5	2.7	17.6
32	100	–	10	4.5	2.7	17.2

PRODUCT MASSES						
Test No.	**Changing process variable**	**Oxidation Time, min**	**Mass PCB Metal, kg**	**Mass PCB Slag, kg**	**Mass Cartridge Fumes, kg**	**Total mass recovered, kg**
4	Oxid. time	30	6.11	7.34	0.39	13.8
8	Oxid. time	60	6.50	8.50	0.67	15.7
11	Flame stoich.	30	6.05	9.12	0.68	15.9
32	Oxid. time	60	6.21	8.77	0.57	15.6

Table 41 presents the overall material mass balance of the PCBs smelting campaign. A total of 360 kg PCB concentrate was processed during the test work along with flux

additions of 122 kg recycled CRT slag, 62 kg Fe_2O_3, 8 kg Na_2CO_3, and 9 kg $CaCO_3$. The campaign produced a total of 243 kg Cu alloy and 231 kg PCB slag, and a total of 79 kg fumes was collected. An overall material mass accountability of 97% was obtained in this campaign. An estimated total of 365 kg C_3H_8 and 1277 kg O_2 gas was consumed during the campaign.

Table 41. Overall material mass balance of the PCBs smelting campaign

Feed	**Mass, kg**	**Products**	**Mass, kg**
PCB concentrate	360	Metal	243
CRT slag	122	Slag	231
Fe_2O_3	62	Cartridge fumes	24
Na_2CO_3	8.4	Extraction hood fumes	7
$CaCO_3$	8.6	Baghouse fumes	48
Excess O_2	8.9		
Total IN	**569**	**Total OUT**	**552**
Overall material mass accountability, mass %			**97%**

Only 30 wt% of the fume collected was captured in the cartridge filters. This amount is low given that the fume is a valuable source of PbO. Only fume collected in the cartridge filters was recycled to the CRT smelting tests as it was not contaminated, in contrast to fume collected in the baghouse. This meant that a small amount of fume was available to recycle to each CRT smelting test.

4.1.2 Elemental mass balance

The overall elemental accountability of PCBs smelting tests is presented in Table 42. Elemental accountabilities are a good measure of the quality of the test work and they are generally considered good and satisfactory when they are within ±10% of 100%. This is especially the case for elements that are not present in high concentrations in the refractory material and do not predominantly report to the off-gas stream (e.g., Cu, Fe, Si and Na). With that measure, good accountabilities were obtained for many of the elements in the system such as Ca, Cu, Fe, Mg, Mn, Si, Na, and Sr. This signifies that the quality of the test work, in respect of mass measurements, sampling procedure and analytical measurements, was adequate and satisfactory to assess the results with high confidence.

Table 42. Overall elemental accountability of PCBs smelting tests

Element	Mass IN, kg	Mass OUT, kg	Accountability, wt%
Al	12.7	16.5	130
Ca	9.75	9.45	97
Cu	225	225	100
Fe	37.1	34.4	93
Mg	1.43	1.56	109
Mn	1.67	1.61	96
Ni	1.22	1.05	85
Pb	28.7	23.3	81
Si	33.1	32.8	99
Zn	33.1	27.2	82
Sn	50.0	39.1	78
K	2.41	5.13	213
Na	17.0	16.1	95
Ba	2.13	2.76	130
Sr	1.72	1.82	106
Total	458	440	96

The furnace refractory comprised 93 wt% Al_2O_3. It is reasonable to expect a certain degree of dissolution of Al_2O_3 into the slag especially at high operating temperatures applied in the PCBs smelting tests (>1300°C). As such, the over accountability of Al (130 wt%) can be attributed to the Al from the furnace refractory wall. The under accountability of Ni is not surprising since it is present in the raw materials in low concentrations, thus it is susceptible to minor errors in sampling and chemical analysis. The over accountability of K and Ba was not expected as both elements were present in the raw materials in concentrations above 1 wt%.

The under accountability of Pb (80 wt%), Zn (82 wt%), and Sn (78 wt%) can be attributed to the material mass that is lost through or in the off-gas handling system since these elements predominantly reported to the off-gas stream during the test work. Mass can be lost through the off-gas handling system due to inefficient extraction leading to off-gas or smoke escaping the system. The off-gas handling system consists of ducting of extensive length which provides surface area for some of the fumes to deposit on the internal walls as accretions. These accretions accumulate in the ducting and are generally not recovered after a campaign resulting in poor accountabilities of the elements concerned.

Take note that the accountabilities of the precious metals Ag, Au, Pd and Pt were not calculated owing to the lack of confidence in the accuracy and consistency of the results obtained from the analysis of precious metals in PCB concentrate. The results of the

analysis of precious metals from the product samples were of a better quality than those obtained with the PCB concentrate. The mass balance of the precious metals will be described with the distribution formulation.

The elemental recoveries of selected elements to the product streams are given in Table 43. A reference to the colour scale applied is given in Table 44. There is a consistent pattern in the recovery of elements to the respective product streams in all the tests. Cu was predominantly recovered to the metal with Test 8 and 32 recording the highest recovery of 94 wt%. Fe predominantly reported to the slag stream, and Pb and Zn predominantly reported to the fume. There is no clear preferential product stream to which Sn and Ni were recovered.

Table 43. Elemental recovery of selected elements to the product streams from PCBs smelting tests that achieved a Cu recovery of more than 90 wt%, mass in wt %

	Test 4			Test 11			Test 8			Test 32		
	Metal	**Slag**	**Fume**	**Metal**	**Slag**	**Fume**	**Metal**	**Slag**	**Fume**	**Metal**	**Slag**	**Fume**
Cu	91	10	0	92	12	0	94	5	0	94	7	0
Fe	0	107	7	0	95	4	0	86	4	0	97	4
Ni	70	47	0	37	43	3	63	16	0	49	34	5
Pb	8	8	53	6	20	59	9	4	59	5	10	55
Sn	21	34	14	14	51	17	38	25	14	17	31	14
Zn	0	11	64	0	10	75	0	5	79	0	6	75

Table 44. Reference to the colour scale

1-9	10-19	20-29	30-39	40-49	50-59	60-69	70-79	80-89	90-99

The distribution formulation allows for a better analysis of the preferential partitioning of elements to the respective product streams. The distributions of elements (including precious metals) to the product streams are presented in Table 45. The distribution patterns of all the elements are the same in all tests. Aluminium, Ca, Fe, Si, K and Na preferentially distributed to the slag stream. Elements such as Cu, Ni and the precious metals (Au, Pd, Pt and Ag) preferentially distributed to the metal stream.

The low melting point metals, Pb and Zn, preferentially distributed to the fume however Sn, also a low melting point metal, distributed to all three product streams with no clear pattern in the stream of preference.

Table 45. Elemental distribution to the product streams from PCBs smelting tests that achieved a Cu recovery of more than 90 wt%, mass in wt %

	Test 4			Test 11			Test 8			Test 32		
	Metal	**Slag**	**Fume**	**Metal**	**Slag**	**Fume**	**Metal**	**Slag**	**Fume**	**Metal**	**Slag**	**Fume**
Al	0	100	0	0	99	1	0	100	0	0	100	0
Ca	0	99	1	0	100	0	0	100	0	0	100	0
Cu	90	10	0	88	11	1	95	5	0	93	7	0
Fe	0	94	6	0	96	4	0	95	5	0	96	4
Ni	59	40	1	46	53	1	80	20	0	59	40	1
Pb	12	11	77	6	24	70	12	6	82	7	15	78
Si	0	100	0	0	100	0	0	100	0	0	100	0
Zn	0	15	85	0	12	88	0	6	94	0	7	93
Sn	31	49	20	18	62	20	49	32	19	28	49	23
K	0	99	1	0	99	1	0	98	2	0	98	2
Na	0	97	3	0	98	2	0	98	2	0	98	2
Au	97	2	1	98	1	1	98	2	1	98	1	1
Pd	100	0	0	100	0	0	100	0	0	100	0	0
Pt	93	3	4	95	2	3	100	0	0	99	1	0
Ag	80	9	11	74	4	22	80	3	17	62	4	34

4.1.3 Chemical composition

The chemical composition of metals is presented in Table 46. From the four tests, only Test 4 and 32 produced alloys with a Cu grade that was above 95 wt%. Between the two tests, Test 32 had a higher Cu recovery to the metal. Therefore, Test 32 achieved the best results in terms of Cu grade and recovery to the metal. The metal from Test 32 had a composition of 95.1 wt% Cu, 0.27 wt% Ni and residual impurities of 3.9 wt% Sn and 0.65 wt% Pb. The metal had a precious metal content of 53.9 ppm Au, 178 ppm Pd, 38.5 ppm Pt and 1100 ppm Ag.

Table 46. Chemical composition of metals from PCBs smelting tests that achieved a Cu recovery of more than 90 wt%, mass in wt %

									Mass, ppm				
Test	**Cu**	**Fe**	**Mn**	**Ni**	**Pb**	**Si**	**Zn**	**Sn**	**Au**	**Pd**	**Pt**	**Ag**	**Total**
4	93.6	<0.05	<0.05	0.39	1.02	<0.05	<0.05	4.83	47.1	187	<2	1500	100
11	95.5	<0.05	<0.05	0.21	0.77	<0.05	<0.05	3.31	72.6	197	<2	1700	100
8	90.3	<0.05	<0.05	0.33	1.16	<0.05	<0.05	8.08	54.8	54.8	54.8	1400	100
32	95.1	<0.05	<0.05	0.27	0.65	<0.05	<0.05	3.89	53.9	178	38.5	1100	100

Note: Al, Ca, Cr, Mg, Ti, V <0.05 wt%

Compositional variation across the surface of the metals produced from the PCBs tests was assessed with spark spectrometry. The results showed that the composition of the metals does not vary across the surface of the metal (see Table 79 in APPENDIX J).

The chemical composition of slags and fumes is presented in Table 47 and Table 48, respectively. The slags from the four tests had similar compositions except Test 4 and 11 had higher CuO content, and Test 8 and 32 had higher SiO_2 content. The precious metals content of the slags was generally low (<1.5 ppm Au+Pd+Pt and <150 ppm Ag). The slag from Test 32 had 31.9 wt% SiO_2, 21.9 wt% FeO and 11.2 wt% Al_2O_3 as the major slag components, and 0.86 ppm Au+Pd+Pt and 46.3 ppm Ag as precious metal losses to the slag. The fumes were also quite similar in composition, and as expected, they were rich in ZnO, PbO, SnO_2 and Ag. The fumes from Test 32 had a composition of 52.3 wt% ZnO, 29.1 wt% PbO, 18.2 wt% SnO_2 and 5000 ppm Ag.

The elemental map of Cu and EDS spectrum of Test 32 metal is shown in Figure 63 and Figure 64, respectively. The elemental map shows that Cu is present in high concentration and is uniformly distributed throughout the metal. The EDS spectrum detected peaks of Cu, Ni and Sn in the metal, corroborating the analytical results that most of the impurities have been removed from the metal.

A BSE image and EDS point analysis of slag from Test 32 is shown in Figure 65 and Table 49, respectively. The results indicate that the primary slag phase comprised a mixture of Fe and Al silicates. This correlates well with the chemical composition of Test 32 slag. There is evidence of entrainment of microscopic pure Cu metal prills and formation of a pure solid Al_2O_3 phase. Some of the Sn is present in the slag as entrained metal prills of pure Sn and CuSn alloy and the rest as inclusions of FeSn oxide.

Table 47. Chemical composition of slags from PCBs smelting tests that achieved a Cu recovery of more than 90 wt%, mass in wt %

															Mass, ppm				
Test	**Al_2O_3**	**CaO**	**CuO**	**FeO**	**MgO**	**MnO**	**NiO**	**PbO**	**SiO_2**	**ZnO**	**SnO_2**	**K_2O**	**Na_2O**	**BaO**	**SrO**	**Au**	**Pd**	**Pt**	**Ag**	**Total**
4	18.2	3.43	10.6	17.2	0.95	0.83	0.28	0.86	22.0	1.75	8.24	2.81	5.59	1.21	0.69	1.05	0.29	0.06	147	94.7
11	9.07	3.85	10.1	20.7	0.99	0.76	0.20	1.99	24.2	1.23	9.79	3.20	6.17	1.29	0.90	0.55	0.12	0.02	56.4	94.5
8	14.2	4.08	4.16	20.1	1.12	0.99	0.08	0.44	32.9	0.63	5.22	2.83	7.37	1.60	0.98	0.66	0.16	0.03	44.8	96.7
32	11.2	3.88	5.96	21.9	0.98	1.11	0.17	1.08	31.9	0.75	6.22	2.03	7.01	1.29	0.93	0.56	0.12	0.18	46.3	96.4

Table 48. Chemical composition of fume from PCBs smelting tests that achieved a Cu recovery of more than 90 wt%, mass in wt %

															Mass, ppm				
Test	**Al_2O_3**	**CaO**	**CuO**	**FeO**	**MgO**	**MnO**	**NiO**	**PbO**	**SiO_2**	**ZnO**	**SnO_2**	**K_2O**	**Na_2O**	**BaO**	**SrO**	**Au**	**Pd**	**Pt**	**Ag**	**Total**
4	0.15	0.36	1.46	0.40	0.22	<0.05	0.07	25.0	<0.05	46.8	24.4	0.43	0.22	<0.05	<0.05	1.16	0.19	0.15	750	99.6
11	0.20	<0.05	1.48	0.09	<0.05	<0.05	<0.05	30.1	<0.05	44.7	21.5	0.38	0.16	<0.05	<0.05	1.53	0.12	0.03	3050	98.8
8	<0.05	0.11	1.70	0.15	0.10	<0.05	<0.05	29.7	<0.05	52.4	15.9	0.40	0.20	<0.05	<0.05	1.20	0.19	0.03	1400	101
32	<0.05	<0.05	1.34	<0.05	<0.05	<0.05	<0.05	29.1	<0.05	52.3	18.2	0.56	0.43	<0.05	<0.05	1.16	0.17	<0.02	5000	103

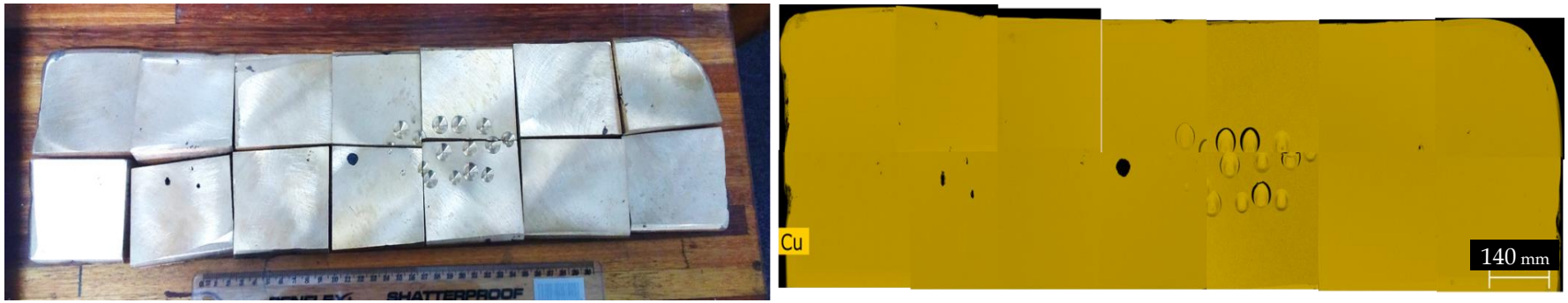

Figure 63. Elemental map of Cu generated by micro-XRF analysis of metal from PCBs smelting Test 32, with scale bar indicating 140 mm

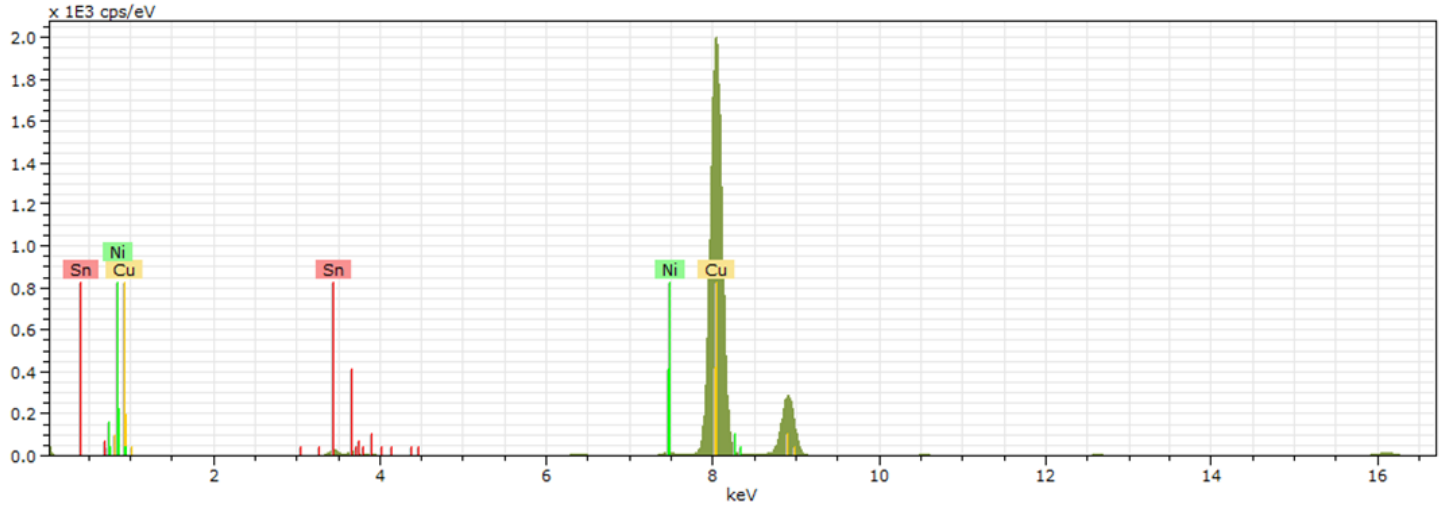

Figure 64. EDS spectrum indicating the peaks of Cu, Ni and Sn detected by micro-XRF from PCBs smelting Test 32 metal

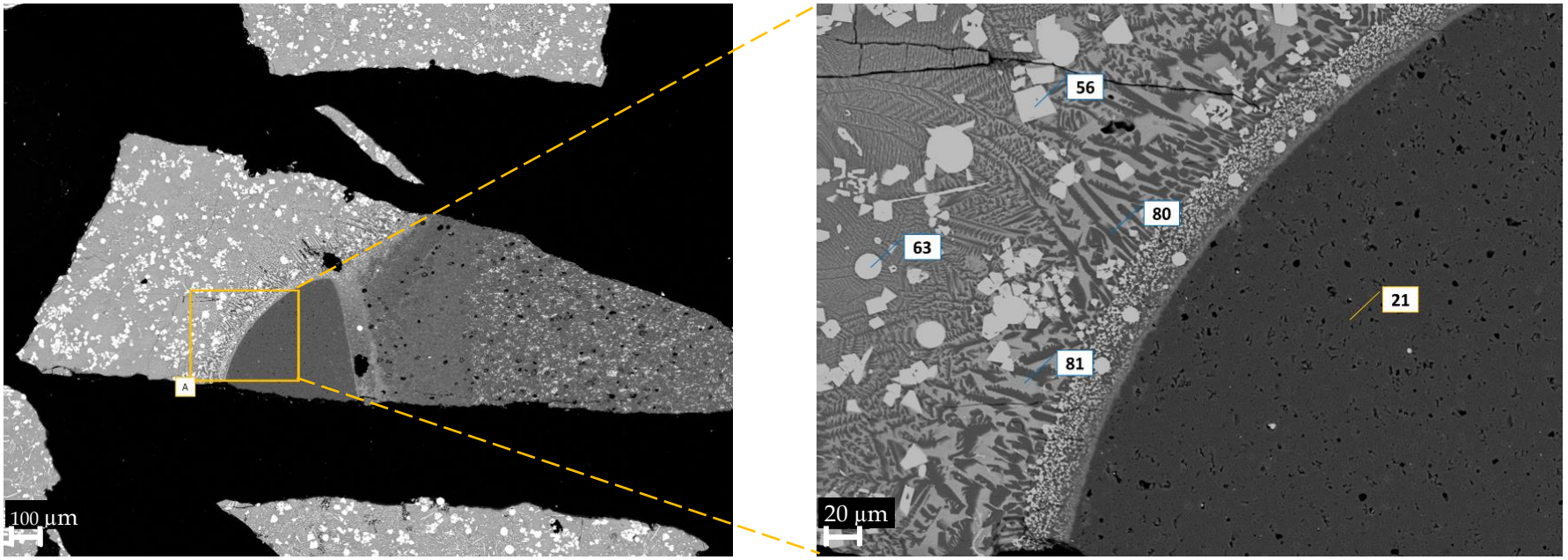

Figure 65. SEM BSE micrographs of slag from PCB smelting Test 32, with scale bar indicating 100 µm (left image) and 20 µm (right image)

Table 49. SEM EDS point analysis of slag from PCB smelting Test 32, mass in wt%

Point	O	Na	Al	Si	K	Ca	Fe	Cu	Sn	Ba	Total	Phase
21	52.5	-	46.4	1.1	-	-	-	-	-	-	100	Al_2O_3
56	18.1	-	1.9	-	-	-	65.3	-	9.7	-	95	FeSnO
63	-	-	-	-	-	-	-	100	-	-	100	Cu Metal
80	45.6	9.2	14.2	19.9	6.9	-	4.4	-	-	-	100	Al_2SiO_5
81	41.5	6.6	1.2	19.2	4.2	9.5	13.4	-	-	3.1	98	Fe_2SiO_4

4.2 CRTs smelting tests

Material masses, elemental mass balance, and chemical compositions of products from the CRTs smelting tests are presented in this section. The results presented are only from tests that achieved Pb recoveries above 60 wt% to the metal. The complete set of results can be found in APPENDIX K.

4.2.1 Product masses

The feed and product masses from the selected tests are presented in Table 50. The recipe additions of the tests presented were similar except that Test 34 evaluated the highest addition of recycled PCB fume and highest total mass of fume addition. Since fume is a source of PbO, it not surprising that Test 34 produced the most metal at 3.46 kg and the most total mass recovered.

Table 50. Feed and product masses of CRTs smelting tests that obtained Pb recoveries above 60 wt%

FEED MASSES							
Test No.	**CRTs glass, kg**	**CRT fume, kg**	**PCB fume, kg**	**Anthracite, kg**	**Na_2CO_3, kg**	**$CaCO_3$, kg**	**Total mass fed, kg**
14	20	0.5	1.0	3	8	2	34.5
17	20	0.5	1.0	3	8	2	34.5
34	20	1.0	2.0	3	8	2	36.0
35	20	1.0	0.5	3	8	2	34.5

PRODUCT MASSES							
Test No.	**Changing Variable**	**Reduction Time, h**	**CRT Metal, kg**	**CRT Slag, kg**	**Cartridge Fumes, kg**	**-**	**Total mass recovered, kg**
14	Temperature	1.0	2.74	22.0	0.54	-	26.3
17	Temperature	1.0	2.88	21.0	0.74	-	25.6
34	Fume ratio	1.0	3.46	25.0	0.95	-	30.4
35	Fume ratio	1.0	2.99	22.0	0.80	-	26.8

The overall material mass balance of the CRTs smelting campaign is presented Table 51. A total of 710 kg CRTs along with a reductant addition of 105 kg anthracite, and flux additions of 238 kg Na_2CO_3 and 73 kg $CaCO_3$ were processed. About 81 kg Pb alloy (metal) and 755 kg CRT slag was produced, and a total of 73 kg fumes was collected. The product mass accounts for 78% of the total feed mass. The unaccounted 22% can be largely attributed to unmeasured gaseous product species of C (such as CO and CO_2) and devolatilisation of volatile components from the Na_2CO_3, $CaCO_3$ and anthracite streams. The CO and CO_2 gases account for the mass of C and O atoms

reduced from the metal oxides in the feed materials (such as PbO, ZnO, SnO_2, Fe_2O_3, CuO and NiO).

Table 51. Overall material mass balance of the CRTs smelting campaign

Feed	**Mass, kg**	**Products**	**Mass, kg**
CRT funnel glass	710	Metal	81
CRT fumes	19.5	Slag	755
PCB fumes	27	Cartridge fumes	28
Anthracite	105	Extraction hood fumes	9
Na_2CO_3	238	Baghouse fumes	36
$CaCO_3$	73		
Total IN	**1172**	**Total OUT**	**909**
Overall material mass accountability, mass %			**78%**

Similarly in this campaign, only 38 wt% of the fume was captured in the cartridge filters. This amount is still too low, meaning a small amount of fume was available for recycle since only fume collected in the cartridge filters was investigated during the test work (except in Test 36 were extraction hood fumes were smelted).

4.2.2 Elemental mass balance

The overall elemental accountability of CRTs smelting tests is presented in Table 52. Similar to the PCBs campaign, good accountabilities were obtained in this campaign for many of the elements in the system including Ca, Mg, Si, Sn, K, Na, Ba and Sr. This implies that the quality of the test work, in respect of mass measurements, sampling procedure and analytical measurements, was adequate and satisfactory to assess the results with high confidence.

The refractory material installed in the furnace of this test work also comprised 93 wt% Al_2O_3. Thus, the over accountability of Al (117 wt%) can be attributed to dissolution of Al_2O_3 from the furnace refractory into the slag. An over accountability of 130 wt% Al was calculated from the PCBs smelting tests. A lower over accountability of Al from the CRTs smelting tests makes sense because lower operating temperatures (1100–1250°C) were applied during the smelting tests.

The elements Cu, Fe and Ni were present in the system in low concentrations. The under accountability of these elements can be attributed primarily to sampling and analytical errors.

Table 52. Overall elemental accountability of CRTs smelting tests

Element	Mass IN, kg	Mass OUT, kg	Accountability, wt%
Al	13.9	16.2	117
Ca	43.4	42.5	98
Cu	1.06	0.78	73
Fe	5.4	4.4	82
Mg	9.72	9.81	101
Ni	0.04	0.04	81
Pb	144	127	88
Si	184	187	101
Zn	13.0	11.4	88
Sn	3.06	2.91	95
K	24.5	23.7	97
Na	128	122	95
Ba	12.9	13.2	102
Sr	11.3	10.6	94
Total	683	572	84

The under accountability of Pb (88 wt%) and Zn (88 wt%) can be attributed to the material mass that is lost through or in the off-gas handling system since a fair amount of Pb distributed to the off-gas stream and Zn predominantly reported to the off-gas stream during the test work. A similar explanation to that provided for the PCBs smelting tests, with regards to mass loss through the off-gas handling system, applies for the CRTs smelting tests.

Take note that the accountabilities of the precious metals Ag, Au, Pd and Pt were not calculated owing to the extremely low concentrations (except for Ag) in the feed material containing the precious metals (*i.e,* PCB fume). Elements present in trace amounts are highly sensitive to sampling and analytical errors leading to inconsistent accountabilities. As a result, the mass balance of the precious metals will be described with the distribution formulation.

The elemental recoveries of selected elements to the product streams are given in Table 53. It is apparent that none of these tests achieved a Pb recovery above 90 wt% to the metal. The highest Pb recovery to the metal was obtained in Test 34 at 70 wt%. Tin was recovered to all three product streams at different recoveries in each test. In Test 35, the highest recovery of Sn (64 wt%) was to the fume stream, but in Test 34, the highest recovery of Sn (45 wt%) was to the metal stream. The recovery of Zn seem to indicate that Zn was mainly recovered to the slag stream. This impression is skewed by the

inherent loss of fume in the off-gas handling system. Since a lower mass of fume was recovered, the recovery calculation will indicate a lower mass of Zn in the fume than in the slag. Even if the concentration of Zn in the slag is low, the mass of Zn in the slag will appear more because slag was produced in large quantities in these tests.

Table 53. Elemental recovery of selected elements to the product streams from CRTs smelting tests that achieved a Pb recovery of more than 60 wt%, mass in wt %

	Test 14			Test 17			Test 35			Test 34		
	Metal	Slag	Fume	Metal	Slag	Fume	Metal	Slag	Fume	Metal	Slag	Fume
Pb	64	3	26	68	2	29	68	0	28	70	0	26
Sn	35	33	50	32	26	55	35	23	64	45	24	39
Zn	-	34	19	-	40	21	-	46	29	-	29	12

The distribution formulation allows for a better analysis of the preferential partitioning of elements to the respective product streams. The distributions of elements to the product streams are presented in Table 54. The distribution patterns of all the elements are generally the same in all tests. Aluminium, Ca, Fe, Si, K and Na preferentially distributed to the slag stream. Elements such as Pb, Cu and the precious metals (Au, Pd, Pt and Ag) preferentially distributed to the metal stream. The element Zn preferentially distributed to the fume while Sn distributed to all three product streams with no clear pattern in the stream of preference.

Table 54. Elemental distribution to the product streams from CRTs smelting tests that achieved a Pb recovery of more than 60 wt%, mass in wt %

	Test 14			Test 17			Test 35			Test 34		
	Metal	Slag	Fume	Metal	Slag	Fume	Metal	Slag	Fume	Metal	Slag	Fume
Al	0	96	4	0	96	4	0	96	4	0	97	3
Ca	0	98	2	0	98	2	0	98	2	0	99	1
Cu	68	0	32	71	0	29	64	0	36	80	0	20
Fe	0	77	23	0	85	15	0	90	10	0	89	11
Pb	69	3	28	69	1	30	71	0	29	72	0	28
Si	0	99	1	0	99	1	0	99	1	0	99	1
Zn	0	40	60	0	32	68	0	27	73	0	38	62
Sn	40	38	22	34	43	23	31	42	27	52	34	14
K	0	95	5	0	95	5	0	92	8	0	93	7
Na	0	100	0	0	100	0	0	100	0	0	100	0
Au	89	0	11	93	0	7	12	0	88	12	0	88
Pd	95	0	5	95	0	5	95	0	5	95	0	5
Pt	99	0	1	98	0	2	99	0	1	99	0	1
Ag	56	6	38	56	9	35	53	4	43	80	2	18

4.2.3 Chemical composition

The chemical composition of metals is presented in Table 55. All four tests obtained metals with Pb grade higher than 95 wt%. In the CRTs test work, the recovery of Sn to the metal was important. Test 34 achieved the highest recovery of Sn (45 wt%) to the metal and consequently giving the metal the highest Sn grade of 3.17 wt%. The metal from Test 34 also featured the highest content of Ag at 370 ppm and Pt at 20.9 wt%. In addition to the highest Pb recovery to the metal of 70 wt%, Test 34 achieved the best results in terms of recovery and grade of Pb, Sn, Pt and Ag in the metal.

Table 55. Chemical composition of metals from CRTs smelting tests that achieved a Pb recovery of more than 60 wt%, mass in wt %

								Mass, ppm				
Test	**Cu**	**Fe**	**Ni**	**Pb**	**Si**	**Zn**	**Sn**	**Au**	**Pd**	**Pt**	**Ag**	**Total**
14	0.48	<0.05	<0.05	98.0	<0.05	<0.05	1.49	1.63	2.69	12.2	164	100
17	0.50	<0.05	<0.05	98.2	<0.05	<0.05	1.33	2.37	2.52	7.08	181	100
35	0.32	<0.05	<0.05	98.8	<0.05	<0.05	0.84	<0.02	1.98	19.8	114	100
34	0.69	<0.05	<0.05	96.1	<0.05	<0.05	3.17	<0.02	2.00	20.9	370	100

The chemical composition of slags and fumes is presented Table 56 and Table 57, respectively. The slag compositions of all four tests were very similar. The major slag components of Test 34 was 48.6 wt% SiO_2, 24.8 wt% Na_2O and 9.93 wt% CaO. The test obtained minor losses of precious metal to the slag at <0.02 ppm (Au+Pd+Pt) and 1.32 ppm Ag. The fumes from the CRT tests predominantly contained PbO (62–79.8 wt%). ZnO was present as a major component with SnO_2, C, K_2O and Na_2O present as minor constituents. The fume collected from Test 34 had a composition of 62 wt% PbO, 29.9 wt% ZnO, 1.87% SnO_2 and 21.6 ppm Ag.

The elemental map of Pb and EDS spectrum showing peaks of Pb for metal from Test 34 is shown in Figure 66 and Figure 67, respectively. The elemental map shows that Pb is present in high concentration and is uniformly distributed throughout the metal. The EDS spectrum detected peaks of Pb and Cu in the metal, confirming the absence of other impurities. The peaks for Sn were detected but there was an issue with how they were displayed on the EDS spectrum (see Figure 102 in APPENDIX K).

A BSE image and EDS point analysis of slag from Test 34 is shown in Figure 68 and Table 58, respectively. The slag was generally homogenous in composition and predominantly comprised a Na silicate glass matrix (confirming the analytical results) with little to no metal entrainment observed.

Table 56. Chemical composition of slags from CRTs smelting tests that achieved a Pb recovery of more than 60 wt%, mass in wt %

															Mass, ppm				
Test	**Al_2O_3**	**CaO**	**CuO**	**FeO**	**MgO**	**NiO**	**PbO**	**SiO_2**	**ZnO**	**SnO_2**	**C**	**K_2O**	**Na_2O**	**BaO**	**SrO**	**Au**	**Pd**	**Pt**	**Ag**	**Total**
14	3.69	7.02	<0.05	0.36	2.06	<0.05	0.57	48.2	0.82	0.23	<0.05	2.74	21.3	1.97	1.65	<0.02	<0.02	<0.02	1.83	90.5
17	4.01	7.53	<0.05	0.64	2.17	<0.05	0.38	53.5	0.70	0.29	<0.05	3.80	23.2	1.84	1.64	<0.02	<0.02	<0.02	3.93	100
35	4.04	6.91	<0.05	0.96	2.14	<0.05	<0.05	49.2	0.50	0.19	<0.05	2.65	24.4	1.93	1.63	<0.02	<0.02	<0.02	1.29	94.6
34	3.84	9.93	<0.05	0.78	2.06	<0.05	<0.05	48.6	1.12	0.37	<0.05	2.65	24.8	1.80	1.53	<0.02	<0.02	<0.02	1.32	97.5

Table 57. Chemical composition of fumes from CRTs smelting tests that achieved a Pb recovery of more than 60 wt%, mass in wt %

															Mass, ppm				
Test	**Al_2O_3**	**CaO**	**CuO**	**FeO**	**MgO**	**NiO**	**PbO**	**SiO_2**	**ZnO**	**SnO_2**	**C**	**K_2O**	**Na_2O**	**BaO**	**SrO**	**Au**	**Pd**	**Pt**	**Ag**	**Total**
14	0.25	1.16	0.22	0.15	0.18	<0.05	79.4	1.96	16.6	1.80	1.64	1.37	0.86	<0.05	<0.05	0.37	0.11	0.07	61.1	106
17	0.14	0.98	0.11	0.15	0.14	<0.05	79.8	1.22	17.2	1.65	1.42	1.82	1.07	<0.05	<0.05	0.23	0.09	<0.02	66.0	106
35	<0.05	0.32	<0.05	0.10	<0.05	<0.05	70.9	<0.05	14.8	0.94	0.98	2.83	1.40	<0.05	<0.05	0.09	0.05	0.12	5.09	92.3
34	<0.05	0.43	0.07	0.17	<0.05	<0.05	62.0	<0.05	29.9	1.87	0.89	2.32	0.90	<0.05	<0.05	0.13	0.03	<0.02	21.6	98.6

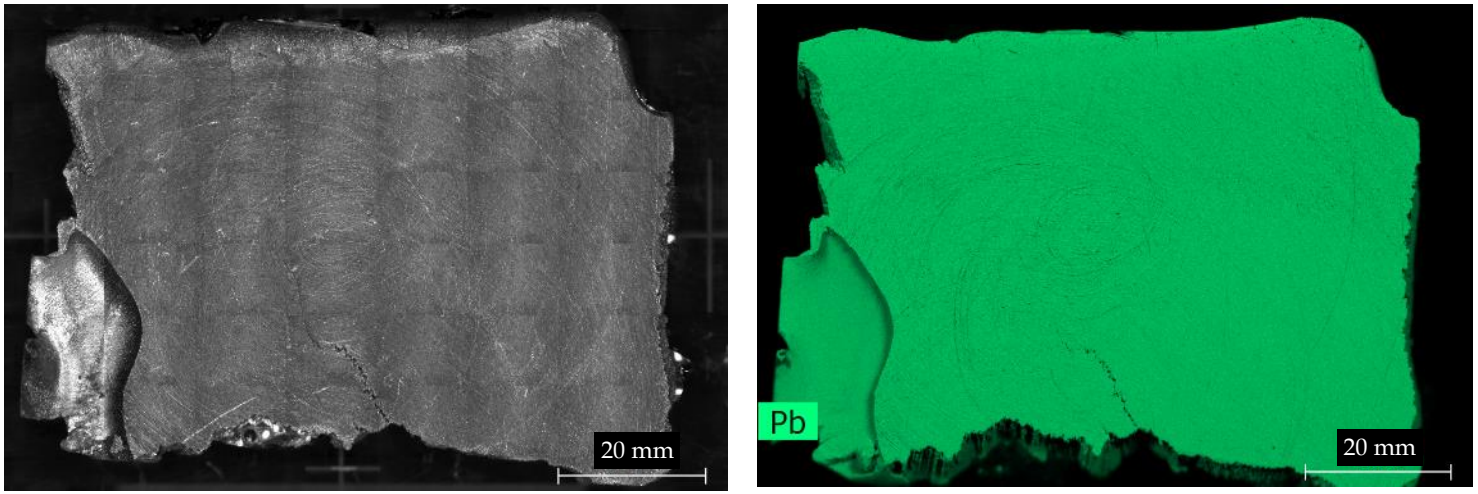

Figure 66. Elemental map of Pb generated by micro-XRF analysis of metal from CRTs smelting Test 34, with scale bar indicating 20 mm

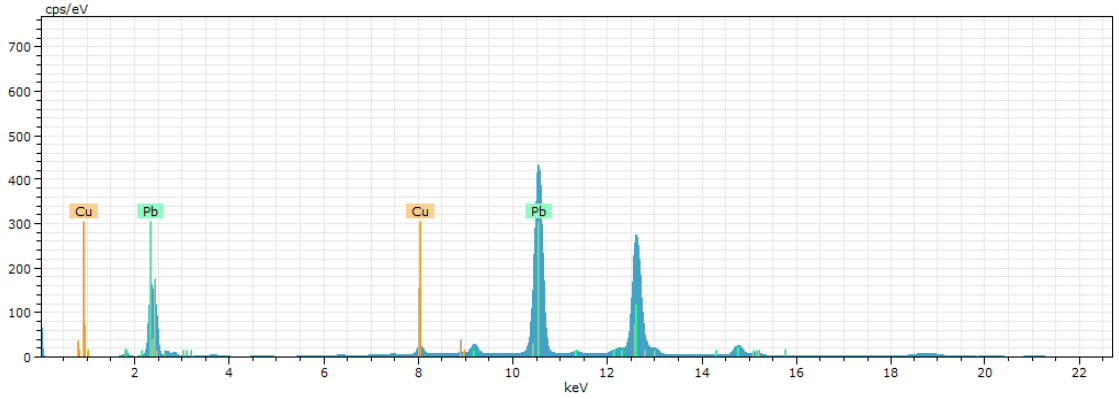

Figure 67. EDS spectrum indicating the peaks of Pb and Cu detected by micro-XRF analysis of metal from CRTs smelting Test 34

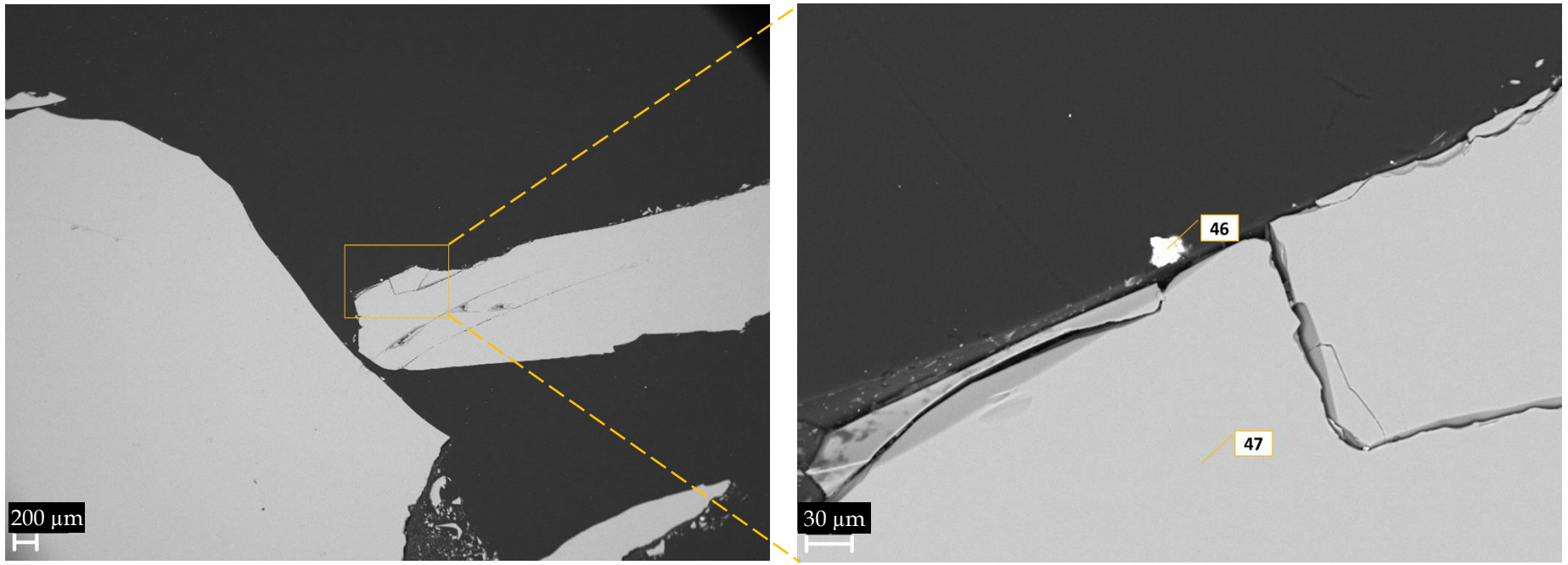

Figure 68. SEM BSE micrograph of slag from CRTs smelting Test 34, with scale bar indicating 200 µm (left image) and 30 µm (right image)

Table 58. SEM EDS point analysis of slag from CRTs smelting Test 34, mass in wt%

Point	O	Na	Mg	Al	Si	K	Ca	Fe	As	Zr	Ru	Sb	Te	Total	Phase
46	21.1	3.9	-	-	-	-	-	6.8	10.7	2.6	11.0	20.2	23.7	100	SbTeAs Alloy
47	46.4	13.1	0.7	1.7	24.2	8.0	6.0	-	-	-	-	-	-	100	Na_2SiO_3 glass

5 DISCUSSION

This chapter addresses the research questions within the context of the literature. The research question for the PCBs smelting process is discussed first, followed by the question for the CRTs smelting process. The chapter is concluded by addressing the primary question of this study.

5.1 PCBs smelting tests

Can oxidative smelting of PCB concentrate and CRT slag produce a crude Cu alloy with a grade of more than 95 wt% Cu?

Yes, the test work demonstrated that a Cu alloy with a grade higher than 95 wt% Cu can be achieved by oxidative smelting of PCB concentrate with recycled CRT slag. The best experimental results obtained a Cu recovery of 94 wt% in comparison to 69 wt% Cu recovery predicted by the theoretical calculations (see Table 59).

Table 59. Comparison of theoretical and experimental results of PCBs smelting tests

Recovery/grade	**Theoretical results**	**Experimental results**
Recovery to metal		
Cu, wt%	69	94
Alloy grade		
Cu, wt%	97	95.1
Sn, wt%	3.3	3.9
Pb, wt%	0.05	0.65
Process conditions	**Theoretical results**	**Experimental results**
Flame stoich. mol% O_2	100	100
Oxidation temp, °C	1350	1350
Amount of burner gas, kg	200	16.1
Flux addition(per kg PCBs)		
CRT slag, wt%	45	45
Fe_2O_3, wt%	27	27

The theoretical result predicted a lower Cu recovery owing to requirement of significant amount of burner gas (200 kg) to oxidise the impurity metals sufficiently enough to obtain an alloy with the required Cu grade. This is because with a flame stoichiometry of 100 mol% O_2, the theoretical calculation assumes almost complete reaction of C_3H_8 with O_2 thus leaving only a very small amount of free O_2 available for oxidation of the impurity metals. As a result, a significant amount of burner gas was required to deliver enough free O_2 to oxidise the impurity metals. According to the

theoretical result, such a large quantity of burner gas resulted in excessive oxidation of Cu. Hence, a lower Cu recover to the metal was predicted.

In reality, a flame stoichiometry of 100 mol% O_2 did not achieve complete reaction of C_3H_8 with O_2, which implied that the amount of free O_2 that was available for oxidation of the impurity metals was much higher than the amount estimated by the theoretical calculation. This provides a reason why the experimental work was able to obtain an alloy at the required Cu grade with a much smaller amount of burner gas (i.e., 16.1 kg) at a flame stoichiometry of 100 mol% O_2.

The main metallic impurities in the PCB concentrate were Sn (13.9 wt%), Zn (9.17 wt%), Pb (6.74 wt%), Al (2.25 wt%) and Fe (1.33 wt%). According to Seetharaman (2014), these impurities can be removed either to the gas or slag phase. At any given temperature, elements with high vapour pressure are easy to remove in the gas phase. The volatilisation of the PCB concentrate was carried out at 1300-1350°C. At these temperatures, almost all the Zn (and some of the Pb) was removed to the gas phase because Zn and Pb have higher vapour pressures than Cu and the other impurities in the alloy (see Figure 10). The removal of Zn and Pb to the gas phase is supported by the trend of high distribution to the gas stream shown in Table 45, and the high concentration of ZnO and PbO in the fumes reported in Table 48.

The other impurities can be removed to the slag phase. The relative ease at which an element can be removed to the slag depends on the O_2 partial pressure in equilibrium with the pure element and the corresponding oxide at any temperature (Seetharaman *et al*., 2014). Elements that are oxidized at relatively low O_2 partial pressures tend to be easily oxidized and removed to the slag (Seetharaman *et al*., 2014). Impurity metals such as Al and Fe, as well as trace amounts of Si and Mn, were readily oxidised from the alloy to below 0.05 wt% as shown in Table 46. This implies that these elements had much lower O_2 partial pressures than Cu at 1350°C.

Pb and Sn proved challenging to remove from the Cu alloy. The alloys that did not meet the required Cu grade, e.g., Test 8 metal (see Table 46), still had significant amount of Sn (8.1 wt%). According to Zhukov *et al*. (2016), in the fire-refining process Cu is oxidised first to Cu_2O and in turn Cu_2O oxidises metals with higher O_2 affinity than Cu. Azakami and Yazawa (1976) found that there is a group of impurity metals that is difficult to remove from Cu during fire refining. These elements all had *K* values between 10^{-2} and 10^{3}. The *K* values of Pb and Sn based on reaction [22] and [23],

respectively, lie between 10^{-2} and 10^{3} as shown in Table 60. This explains the difficulties in removing Pb and Sn from Cu. The *K* values of reaction [22] and [23] are not considerably large, meaning the equilibrium does not predominantly favour the forward reaction. Thus, making it difficult to completely remove Pb and Sn from the Cu alloy to the slag.

Table 60. Equilibrium constant values of oxidation reactions of Pb and Sn with Cu_2O (adapted from Kamberovic (2018))

Reaction	Equilibrium constant, *K*	Reaction no.
$Pb + Cu_2O = PbO + 2Cu$	1.06×10^{-1}	[22]
$Sn + Cu_2O = SnO + 2Cu$	3.69×10^{2}	[23]

The studies by Marin (2006) and Wastawino (2005) showed that there is a linear relationship in the rate of oxidation of impurity metals and O_2 partial pressure. This is true at low O_2 partial pressures as illustrated in Figure 13. Figure 69 shows that at high O_2 partial pressures, Cu is also excessively oxidised resulting in low recoveries of Cu to the metal.

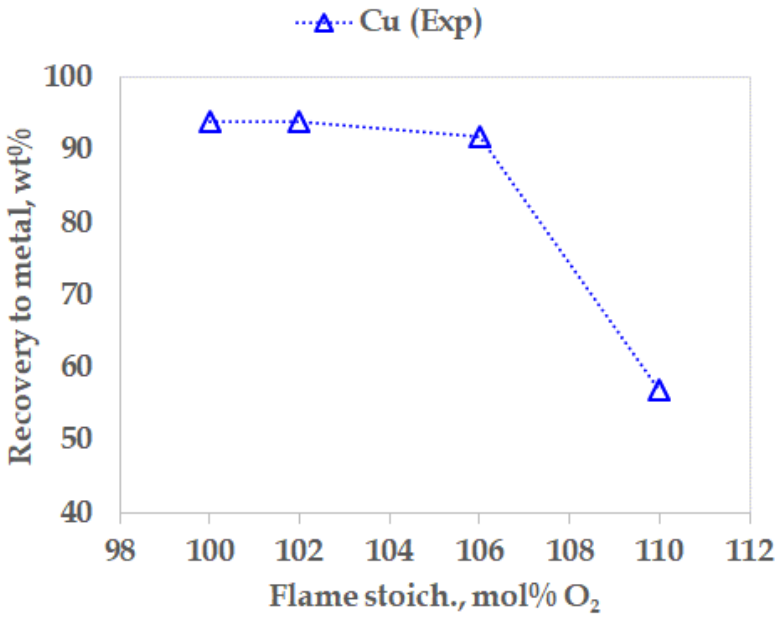

Figure 69. Plot showing experimentally determined relationship of Cu recovery vs. flame stoichiometry at 1350°C

A higher flame stoichiometry increases the partial pressure of O_2 in the furnace. Marin and Utigard (2005) reported that the higher the O_2 partial pressure, the higher the rate of O_2 absorption as Cu. Since Cu is present in high concentration, not all the Cu that

was oxidised to Cu_2O gets to collide and react with impurity metals, for a particular oxidation time. Those Cu atoms will remain oxidised as Cu_2O and lost to the slag.

The test work also confirmed the relationship between elemental recovery and oxidation time (see Figure 70). The longer the oxidation time, the lower the residual impurities in the Cu metal. An extended oxidation time allows for more O_2 to be introduced to the surface of the liquid Cu bath for absorption (Marin and Utigard, 2005) and diffusion of Cu_2O molecules to collide and react with residual impurities resulting in lower concentration of impurities in the Cu metal.

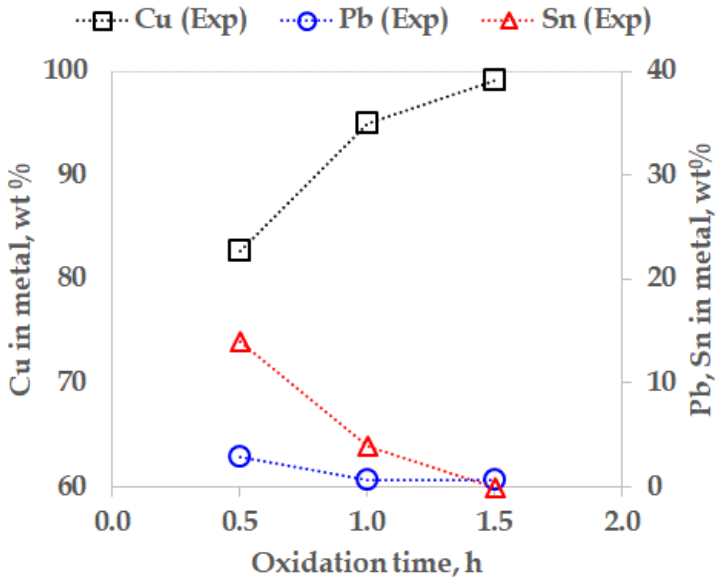

Figure 70. Plot showing experimentally determined relationship of Cu in metal vs. oxidation time, with a flame stoichiometry of 100 mol% O_2 and burner gas flow rate of 15.5 kg/h at 1350°C

The extended oxidation time was also associated with higher Cu losses to the slag (see in Figure 71). As more O_2 is absorbed into the Cu metal more Cu atoms are oxidised to Cu_2O. Given the excessive loss of Cu to slag under extended oxidation time, it implies that the rate of Cu oxidation to Cu_2O is higher than the rate of Cu_2O reduction to Cu by impurity metals. This is because the concentration of impurity metals decreases with time.

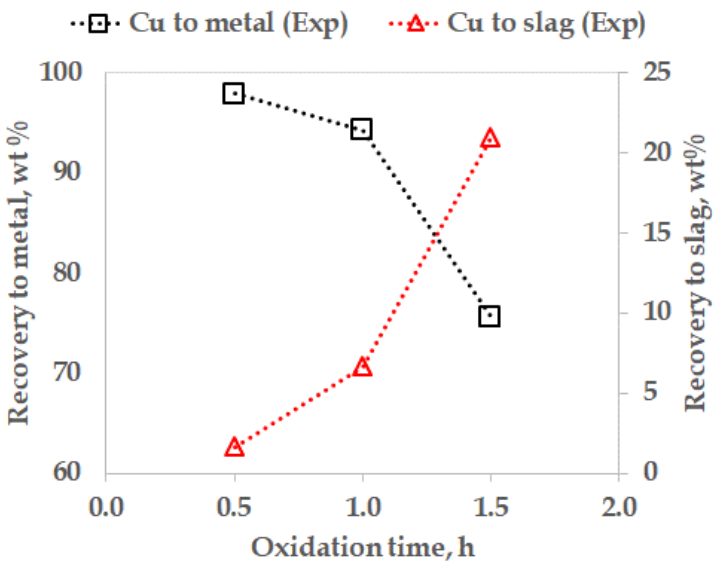

Figure 71. Plot showing experimentally determined relationship Cu recovery vs. oxidation time, with a flame stoichiometry of 100 mol% O_2 and burner gas flow rate of 15.5 kg/h at 1350°C

Higher temperatures are necessary for volatilisation of some impurities (*e.g.* Zn and Pb) and to lower the effective viscosity of the prevailing slag. The slag from the ideal test condition had a chemical composition with a low viscosity at the oxidation temperature. Flux additions of 45 wt% CRT slag and 27 wt% Fe_2O_3 were sufficient to effect a slag viscosity of 1.78 Pa.s, as shown in Figure 62.

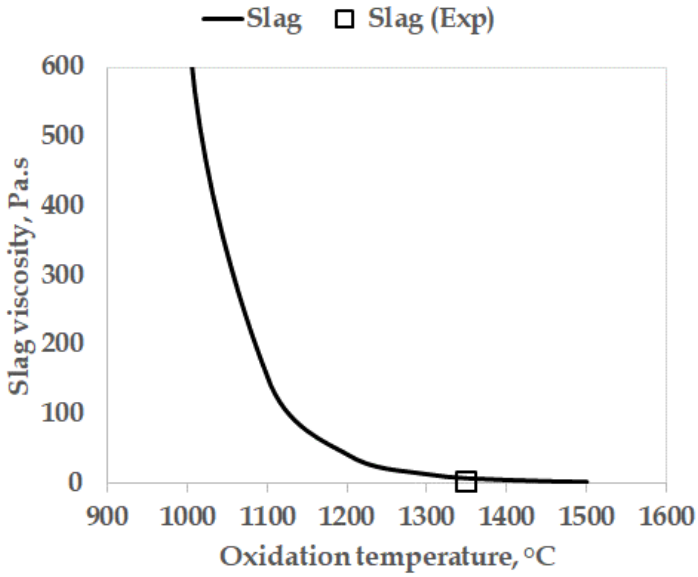

Figure 72. Plot showing relationship of slag viscosity vs. oxidation temperature with a flame stoichiometry of 100 mol% O_2. Viscosity of experimentally produced slag from the best test is superimposed on the graph

5.2 CRTs smelting tests

Can reductive smelting of CRT funnel glass and PCB fume produce a crude Pb alloy with a grade of more than 95 wt% Pb?

Yes, the test work demonstrated that a Pb alloy with a grade higher than 95 wt% Pb can be achieved by reductive smelting of CRT funnel glass with recycled PCB fume. Although the test with the best experimental results obtained a lower Pb recovery of 70 wt% than that predicted by the theoretical calculation, it was able to deliver an alloy with a similar grade (96.1 wt% Pb and 3.17 wt% Sn) to that predicted by the calculations (see Table 61). However, to achieve this grade, the test work had to be carried out under different process conditions from those predicted by the calculations.

The test with the best results was carried out at 1200°C with addition of 5 wt% CRT fume and 10 wt% PCB fume as compared to half those additions in the theoretical calculations. Theoretical estimates typically predict higher recoveries as they do not take into account process inefficiencies associated with actual test work.

Table 61. Comparison of theoretical and experimental results of CRTs smelting tests

Recovery/grade	**Theoretical results**	**Experimental results**
Recovery to metal		
Pb, wt%	78	70
Sn, wt%	85	45
Alloy grade		
Pb, wt%	96	96.1
Sn, wt%	3.44	3.17
Process conditions	**Theoretical results**	**Experimental results**
Flame stoich. mol% O_2	95	95
Reduction temp, °C	1100	1200
Reduction time, h	1	2
C addition (per kg CRTs)		
C, wt%	12.5	12.5
Fume addition (per kg CRTs)		
CRT fume, wt%	2.5	5
PCB fume, wt%	5	10
Flux addition (per kg CRTs)		
Na_2CO_3, wt%	40	40
$CaCO_3$, wt%	10	10

The test work also confirmed the relationships between Pb recovery and process parameters such as reduction temperature and time (see Figure 73 and Figure 74, respectively). The trends indicate that the higher the reduction temperature, the lower the Pb recovery to the metal, and the longer the reduction time, the lower the Pb recovery to the metal. These results correspond well with trends published in literature by Lu *et al*. (2018b).

Lu *et al*. (2018b) argued that the recovery of Pb to metal decreases with increasing temperature owing to oxidation of Pb to PbO and its re-introduction into the slag. This was the case because their tests were carried out in air. The current tests were carried out under a mildly reducing furnace atmosphere; as such oxidation of Pb to PbO is not expected. The PbO concentration in the slag from Test 34 was <0.05 wt% signifying that the Pb did not partition to the slag phase at higher temperatures. Pb is a low melting point metal (~328°C) and it has a characteristic high vapour pressure at high temperatures (Seetharaman *et al*., 2014). Higher reduction temperatures promote higher recovery of Pb to the gas stream, resulting in lower Pb recovery to the metal.

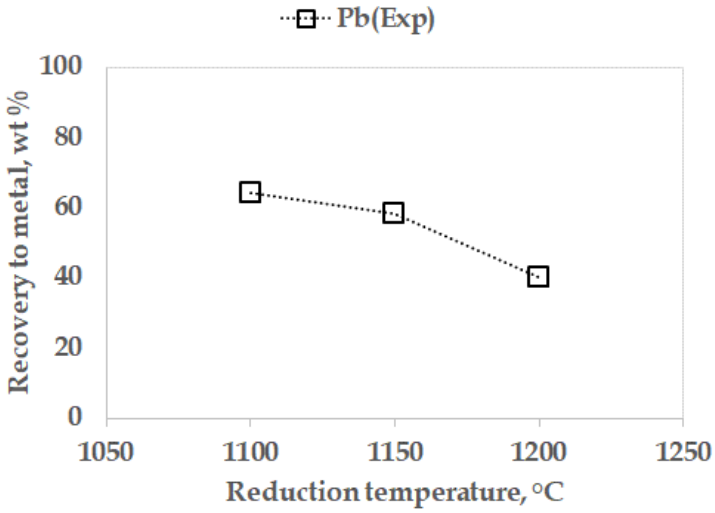

Figure 73. Plot showing experimentally determined relationship of Pb recovery to metal vs reduction temperature, with flame stoichiometry of 95 mol% O_2 and burner gas flow rate of 13.1 kg/h

A similar effect was observed with extended reduction time. The longer the reduction time (see Figure 74) the lower the recovery of Pb to the metal. Test 11 and 24 had a reduction time of 3 h and the PbO concentration of their slags was 0.34 and 0.49 wt%, respectively. This implies that the Pb was not recovered to the slag phase but instead it was recovered to the gas phase. The longer the system is maintained at a high temperature, an increasing amount of Pb atoms in the liquid metal absorb sufficient

energy to escape to the gas phase. This finding implies that having a liquid slag phase floating on top of the liquid Pb metal during the smelting process does not stop the volatilisation of Pb to the gas phase, under the conditions evaluated. This aspect should be investigated further to validate this finding.

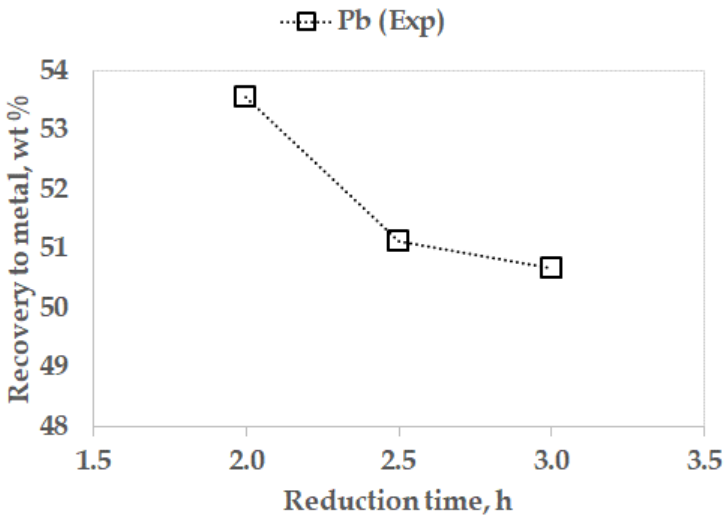

Figure 74. Plot showing experimentally determined relationship of Pb recovery vs. reduction time, with flame stoichiometry of 95 mol% O_2 and burner gas flow rate of 13.1 kg/h at 1200°C

Another trend that was established with the results from Lu *et al*. (2018b) is that Pb recovery initially increases with increasing C addition to a particular point beyond which the recovery of Pb to the metal decreases. For the work reported by Lu *et al*. (2018b) this turning point was established at a C addition of 20 wt%. This C addition is significantly higher than that predicted by the theoretical calculations, which was estimated around 4–5 wt% (see Figure 45) for the current system. The test results indicate that C additions higher than 5 wt% result in lower recovery of Pb to the metal (see Figure 75), for a given temperature and fume addition.

The reason why increasing C additions result in lower Pb recovery to the metal (after the turning point) was not adequately addressed in the work by Lu *et al*. (2018b). It is also not clear from the current work why this phenomenon occurred, and thus, warrants further investigation. It is suspected, however, that the turning point was reached at a lower C addition in the current study because of the mildly reducing furnace atmosphere and the presence of 1–2 wt% C in recycled CRT fume. The reducing furnace atmosphere minimises C burn off and the C recycled with the CRT fume lowers the C requirement of the process.

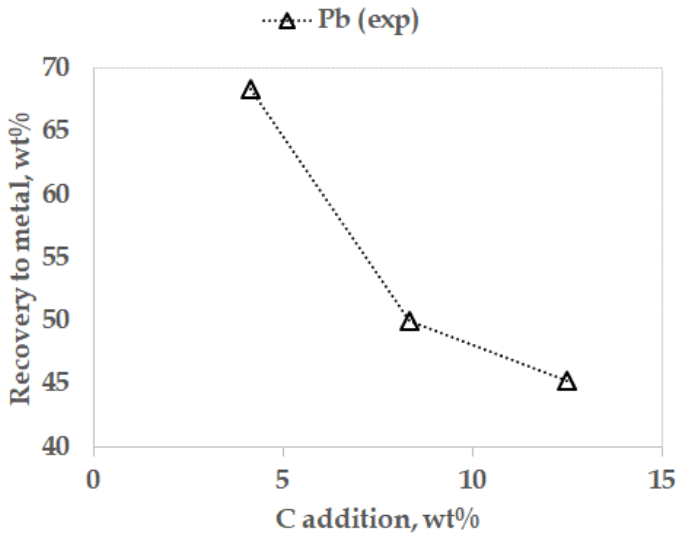

Figure 75. Plot showing experimentally determined relationship of Pb recovery to metal vs. C addition, with flame stoichiometry of 95 mol% O_2 and burner gas flow rate of 13.1 kg/h at 1200°C

According to Shamsuddin (2016), reduction of a metal oxide by C is actually effected via reduction by CO gas, as per reaction [24].

$$(PbO)_{slag/solid} + \{CO\}_{gas} = [Pb]_{metal} + \{CO_2\}_{gas} \quad [24]$$

The equilibrium constant of reaction [24] is dependent on the ratio of the partial pressure of CO to CO_2 as shown by equation [25]:

$$K_{react\,[24]} = \frac{P_{CO2} \times a_{Pb}}{P_{CO} \times a_{PbO}} = \left(\frac{P_{CO2}}{P_{CO}}\right) \quad [25]$$

At equilibrium, the change in Gibbs free energy for equation [25] can be calculated from equation [26]:

$$\Delta G^{o}_{react\,[25]} = -RTln(K) = -RTln\left(\frac{P_{CO2}}{P_{CO}}\right) = 4.606RTlog\left(\frac{P_{CO}}{P_{CO2}}\right) \quad [26]$$

In order to favour the forward reaction of reaction [24], in other words, to promote reduction of PbO to Pb, the ratio of the partial pressures of CO to CO_2 must be higher than the ratio at equilibrium. Most of the reduction tests readily achieved the reduction of PbO to Pb, as evidenced by the low residual PbO in the slags (see Table 56). This signifies that the applied flame stoichiometry of 95 mol% O_2 and the C additions were adequate to provide a ratio of the partial pressure of CO to CO_2 that was higher than the ratio at equilibrium.

The test work has shown that increasing additions of recycled CRT and PCB fume has an effect of increasing the recovery of Pb to the metal (see Figure 76). This is because CRT and PCB fume are rich sources of PbO. CRT fume also contains up to 2 wt% C which contributes to the supply of the reductant required in the system. Increased addition of recycled fume make more PbO available in the system to be reduced to Pb metal. The more metallic Pb particles there are in the slag, the easier it is for the particles to collide and coalescence, and collect at the bottom of the reactor (Okada and Yonezawa, 2013).

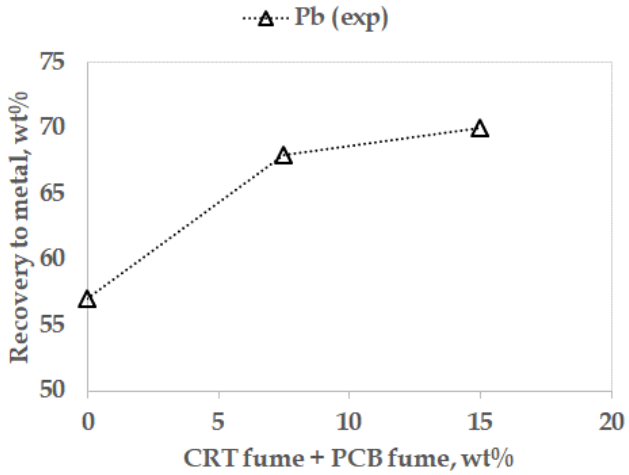

Figure 76. Plot showing experimentally determined relationship of Pb recovery vs. CRT and PCB fume addition, with flame stoichiometry of 95 mol% O_2 and burner gas flow rate of 13.1 kg/h at 1200°C

The slag from the best experimental results had a chemical composition with a low viscosity at the reduction temperature. Flux additions of 40 wt% Na_2CO_3 and 10 wt% $CaCO_3$ were sufficient to effect a slag viscosity of 6.4 Pa.s at a reduction temperature of 1200°C, as shown in Figure 77. This low slag viscosity commensurate with the low degree of metal entrainment observed in the slag depicted in Figure 68. The viscosity of the slag decreases with increasing temperature, resulting in increased percolation of metallic Pb particles through the slag and collection into the metal phase (Okada and Yonezawa, 2013).

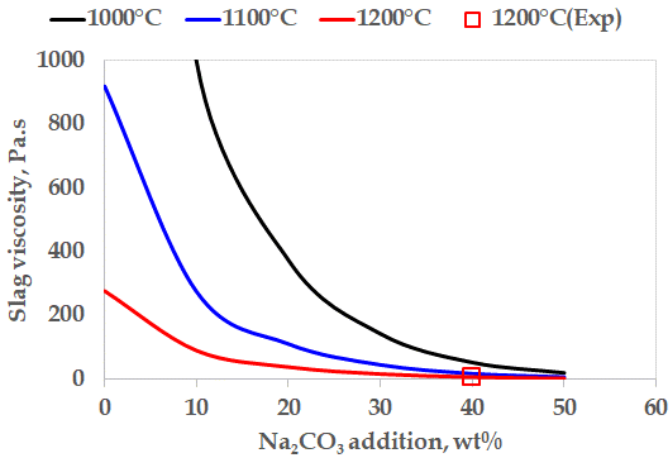

Figure 77. Plot showing relationship of slag viscosity vs. Na_2CO_3 addition. Viscosity of experimentally produced slag from the best test is super imposed on the graph

5.3 Integrated flowsheet

Is it technically feasible to integrate the smelting of waste CRT funnel glass into the same flow sheet as the smelting of waste PCB concentrate?

Yes, it is technically feasible to integrate the smelting of waste CRT funnel glass into the same flow sheet as the smelting of waste PCB concentrate. A simplified integrated flow sheet is illustrated in Figure 78. The flow sheet shows the operating conditions for each process, and summarized compositions of the feed and product streams. The integration of the two processes is achieved by flow of material from one process to other. That is, CRT slag is recycled to the PCB smelting furnace and PCB fume is recycled to the CRT smelting furnace, as depicted in Figure 78.

CRT slag is recycled to the PCB furnace to act as a fluxing agent. The estimated viscosity of the PCB slag from the best test was 1.78 Pa.s. This signifies that the CRT slag contributed positively to improving the properties of the PCB slag. PCB fume was recycled to the CRT furnace as a source of PbO. The best test achieved the required alloy grade specification at the highest Pb recovery to the metal with higher additions of recycled PCB fume (10 wt%). The benefit of increased additions of recycled PCB fume to the CRT smelting process was illustrated in Figure 76.

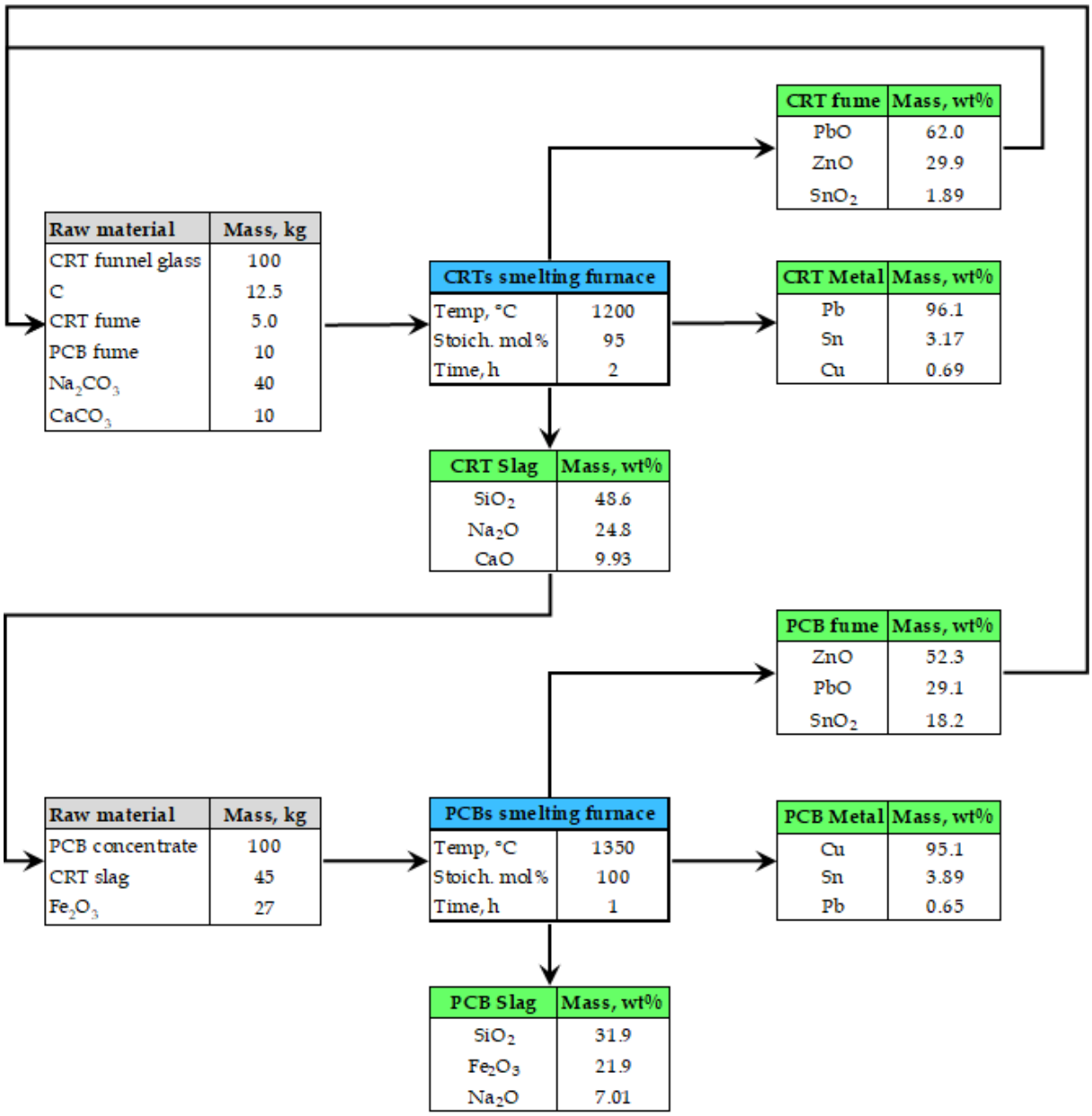

Figure 78. Simplified integrated flowsheet showing summarized smelting conditions, feed and product compositions obtained from the test work

6 CONCLUSIONS

A study was undertaken on a pilot-scale TBRC facility to investigate the development of an integrated flowsheet for the processing of PCBs and CRTs. The flowsheet involved two processes, namely, the smelting PCBs and CRTs. The two processes were integrated via flow of material from one process to the other. PCBs smelting tests were conducted to demonstrate that oxidative smelting of PCB concentrate and recycled CRT slag can produce a crude Cu alloy with a grade of more than 95 wt% Cu. CRTs smelting tests were also conducted to demonstrate that reductive smelting of CRT funnel glass and recycled PCB fume can produce a crude Pb alloy with a grade of more than 95 wt% Pb.

The PCBs smelting condition that achieved the required alloy grade was an average oxidation temperature of 1350°C, flame stoichiometry of 100 mol% O_2, oxidation time of 1 h, and flux addition of 27 wt% Fe_2O_3, per unit mass of PCB concentrate. The amount of material recycled to integrate to the PCBs process was 45 wt% CRT slag to the PCBs smelting furnace. The grade of the Cu alloy obtained was 95.1 wt% Cu, 3.89 wt% Sn, and 0.7 wt% Pb, at a recovery of 94 wt% Cu to the metal.

The CRTs smelting condition that achieved the required alloy grade was an average reduction temperature of 1200°C, flame stoichiometry of 95 mol% O_2, reduction time of 2 h, and reductant addition of 12.5 wt% C per unit mass of CRT funnel glass as well as flux additions of 40 and 10 wt% Na_2CO_3 and $CaCO_3$, respectively. About 5 wt% recycled CRT fume was added. The amount of material recycled to integrate to the CRTs process was 10 wt% PCB fume to the CRTs smelting furnace. The grade of the Pb alloy obtained was 96.1 wt% Pb and 3.17 wt% Sn, at a recovery of 70 wt% Pb to the metal.

The test work provided experimental evidence that the integrated process can produce crude alloys of Cu and Pb at the required grade specification. Therefore, the study has demonstrated that it is technically feasible to integrate the smelting of waste CRT funnel glass into the same flowsheet as the smelting of waste PCB concentrate. This process flowsheet can be optimised and developed into a technology that can provide technical capacity to process low-grade PCBs and CRTs locally for metal recovery.

7 RECOMMENDATIONS

In order to support further development of the process into a viable technology, the following activities are recommended:

1. Further studies should be carried out to improve the fundamental understanding of the reaction rate and mechanism of the reduction of PbO and SnO from CRT funnel glass, as well as the distribution of Pb and Sn to the gas and metal phase. It was observed that Pb and Sn have conflicting behaviour with increasing reductant addition. Understanding why or how such a significant amount of Pb partitions to the off-gas under reducing conditions will inform and improve the design of commercial-scale furnaces to minimize deportment of Pb to the off-gas and promote its recovery to the metal phase. This design will minimize the amount of fume generated and reduce the filtration capacity requirement of the process and capital investment in the off-gas treatment facility.
2. A study should also investigate whether a liquid slag phase floating on top of a liquid Pb metal has any effect on the extent of volatilization of Pb to the gas phase at high operating temperatures (*i.e.*, 1200–1250°C). And if it has an effect, what mechanisms are in operation?
3. Fundamental studies should be undertaken to better understand the role of Fe_2O_3 as a solid oxidant and source of FeO during oxidative smelting of PCBs. The study should quantify and optimize its (a) contribution to the oxidation of impurity metals in the Cu alloy, and (b) effect on slag properties such as liquidus temperature and viscosity.
4. Optimization studies should be undertaken to improve the removal of residual impurities of Pb and Sn to below 0.05 wt% without excessive oxidation of Cu to the slag. This study could possibly investigate a two-step process involving oxidation followed by reduction similar to the fire-refining process.
5. The primary off-gas filtration stage captured only 27–34% of fumes carried by the off-gas. It is recommended that the capacity of the cartridge filters be reviewed with the objective of increasing the filtration capacity to more than 90%. If more fumes can be captured and recycled to the CRTs smelting furnace on a batch-to-batch basis, the recovery of lead to the metal phase, and thus, the metal yield, will increase considerably.

6. Further pilot test work should be undertaken to demonstrate the integrated flow sheet by operating the two processes simultaneously in two TBRC furnaces in the same plant. The test work should run the two furnaces continuously for a minimum period of two weeks under ideal process conditions established in the current study. The process information that will be generated from such a study will confirm the predictions of the process simulation with respect to, among other process objectives, achieving Pb recoveries of up to 98 wt% and increasing the confidence in the technical feasibility of the integrated flow sheet.
7. Operating each furnace continuously under the same process conditions will provide an opportunity to evaluate other process efficiencies such as product quality, reagent consumption, and recoveries of precious metals. In addition to generating products of consistent composition in large quantities to provide sufficient sample for downstream assessment, the process information and operating data will provide valuable information to a techno-economic assessment of the integrated flow sheet.
8. An accurate and reliable technique (including sampling and preparation) should be investigated for analysing PCBs concentrates, especially measurements of precious metals Au, Ag, Pd and Pt. The metal accounting of these elements needs to be accurate as these precious metals drive the economics of the technology.

8 BIBLIOGRAPHY

Alvear Flores, G., Nikolic, S., Mackey, P., 2014. ISASMELT for the recycling of e-scrap and copper in the U.S. Case study example of a new compact recycling plant. *JOM* **66**, 823–832.

Andreola, F., Barbieri, L., Corradi, A., Lancellotti, I., Falcone, R., Hreglich, S., 2005. Glass-ceramics obtained by teh recycling of end of life cathode ray tubes glass. *Waste Management* **25**, 183–189.

Arshadi, M., Mousavi, S., Rasoulnia, P., 2016. Enhancement of simultaneous gold and copper recovery from discarded mobile phone PCBs using bacillus megaterium: RSM based optimization of effective factors and evaluation of their interactions. *Waste Management* **57**, 158–167.

Awasthi, A., Zlamparet, G., Zeng, X., Li, J., 2017. Evaluating waste printed circuit boards recycling: opportunities and challenges, a mini review. *Waste Management* **35**, 346–356.

Azakami, T., Yazawa, A., 1976. Activity measurement of liquid copper binary alloys. *Canadian Metallurgical Quarterly* **15**, 111–122.

Balde, C.P., Forti, V., Gray, V., Kuehr, R., Stegmann, P., 2017. *The global e-waste monitor 2017*. United Nations University (UNU), International Telecommunication Union (ITU), International Solid Waste Association (ISWA), Bonn/Geneva/Vienna.

Bale, C.W., Belisle, E., Chartrand, P., Decterov, S.A., Eriksson, G., Gheribi, A.E., Hack, K., Jung, I.-H., Kang, Y.-B., Melancon, J., Pelton., Arthur.D., Petersen, S., Robelin, C., Sangster, J., Spenser, P., Van Ende, M.-A., 2016. FactSage thermochemical software and database, 2010-2016. *CALPHAD* **54**, 35–53.

Bale, C.W., Belisle, E., Chartrand, P., Decterov, S.A., Eriksson, G., Hack, K., Jung, I.-H., Kang, Y.-B., Melancon, J., Pelton., Arthur.D., Robelin, C., Petersen, S., 2009. FactSage thermochemical software and databases - recent developments. *CALPHAD* **33**, 295–311.

Bernardes, A., Bohlinger, I., Rodriguez, D., Milbrandt, H., Wuth, W., 1997. Recycling of printed circuit boards by melting with oxidising/reducing top blowing process. *The Minerals, Metals & Materials Society Annual Meeting* **126**, 363–375.

Bernardo, E., Scarini, G., Hreglich, S., 2003. Mechanical properties of metal-particulate lead-silicate glass matrix composites obtained by means of powder technology. *Journal of European Ceramics Society* **23**, 1819–1827.

Bizzo, W.A., Figueiredo, R.A., de Andrade, V.F., 2014. Characterisation of printed circuit boards for metal and energy recovery after milling and mechanical separation. *Materials* **7**, 4555–4566.

Brandl, H., Bosshard, R., Wegmann, M., 2001. Computer-munching microbes: metal leaching from electronic scrap by bacteria and fungi. *Hydrometallurgy* **59**, 319–326.

Byung, K., Yang, D.H., Rhee, K.-I., Lee, J.C., Jeong, J.K., Shin, D., 2013. Method for concentrating and recovering noble metals from printed circuit boards of discarded mobile phones and catalysts of discarded cars using discarded nonferrous slag. Patent WO/2013/162118.

Calgaro, C., Schlemmer, D., Silva, M., Maziero, E., Tanabe, E., Bertuol, D., 2015. Fast copper extraction from printed circuit boards using supercritical carbon dioxide. *Waste Management* **45**, 289–297.

Chen, M., Avarmaa, K., Taskinen, P., Klemettinen, L., Michallik, R., O'Brien, H., Jokilaakso, A., 2021. Handling trace elements in WEEE recycling through copper smelting-an experimental and thermodynamic study. *Minerals Engineering* **173**.

Chi, T.D., Lee, J., Pandey, B., Yoo, Y., Jeong, J.K., 2011. Bioleaching of gold and copper from waste mobile phone PCBs by using cyanogenic bacterium. *Mineral Engineering* **24**, 1219–1222.

Chi, X., Streicher-Porte, M., Wang, M., Reuter, M.A., 2011. Informal electronic waste recycling: a sector review with special focus on China. *Waste Management* **31**, 731–742.

Cui, J., Zhang, L., 2008. Metallurgical recovery of metals from electronic waste: A review. *Journal of Hazardous Materials* **158**, 228–256.

DEA, 2018. South Africa state of waste: A report on the state of waste (No. Final draft report). Department of Environmental Affairs (DEA), Pretoria, South Africa.

DEA, 2013. National norms and standards for disposal of waste to landfill, National Environmental Management: Waste Act No. 59 of 2008, Department of Environmental Affairs (DEA).

ERA, 2018. South African e-waste industry waste management plan (V.1) 2019-2024. E-waste Recycling Authority (ERA).

Finlay, A., Liechti, D., 2008. E-waste assessment South Africa. E-waste Association of South Africa (eWASA).

Gosh, B., Gosh, M.K., Parhi, P., Mukherjee, P.S., Mishra, B.K., 2015. Waste printed circuit boards recycling: An extensive assessment of current status. *Journal of Cleaner Production* **94**, 5–19.

Gu, F., Summers, P., Hall, P., 2019. Recovering materials from waste mobile phones: recent technological developments. *Journal of Cleaner Production* **237**, 1–10.

Guo, J., Guo, J., Xu, Z., 2009. Recycling of non-metallic fractions from waste printed circuit boards: a review. *Journal of Hazardous Materials* **168**, 567–590.

Gurung, M., Adhikari, B., Kawakita, H., Ohto, K., Inoue, K., Alam, S., 2013. Recovery of gold and silver from spent mobile phones by means of acidothiourea leaching followed by adsorption using biosorbent prepared from persimmon tannin. *Hydrometallurgy* **133**, 84–93.

Ha, V.H., Lee, J., Jeong, J.K., Hai, H.T., Jha, M., 2010. Thiosulphate leaching of gold from waste mobile phones. *Journal of Hazardous Materials* **178**, 1115–1119.

Hadi, P., Xu, M., Lin, C., Hui, C., McKay, G., 2015. Waste printed circuit board recycling technologies and product utilization. *Journal of Hazardous Materials* **283**, 234–243.

Hageluken, C., 2006. Recycling of electronic scrap at Umicore's integrated metals smelter and refinery. *World of Metallurgy - Erzmetall* **59**, 152–161.

Hedemalm, P., Carlson, P., Palm, V., 1995. Waste from electrical and electronic products: a survey of the content of material and hazardous substances, in: Electric and Electronic Products. Presented at the TemaNord, Nordic Council of Ministries, Copenhagen, Denmark.

Herat, S., 2008. Recycling of cathode ray tubes in electronic waste. Clean **36**, 19–24.

Hilson, G., Monhemius, A., 2006. Alternatives to cyanide in the gold mining industry: what prospects for the future? *Journal of Cleaner Production* **14**, 1158–1167.

Horeh, N., Mousavi, S., Shojaosadati, S., 2016. Bioleaching of valuable metals from spent lithium-ion mobile phone batteries using Aspergillus niger. *Journal of Power Sources* **32**, 257–266.

Hu, B., Hui, W., 2017. Lead recovery from waste CRT funnel glass by high-temperature melting process. *Journal of Hazardous Materials* **343**, 220–226.

Hubau, A., Chagnes, A., Minier, M., Touze, S., Chapron, S., Guezennec, A., 2019. Recycling-oriented methodology to sample and characterize teh metal composition of waste printed circuit boards. *Waste Management* **91**, 62–71.

ICER, 2004. Materials recovery from waste cathode ray tubes (CRTs) (No. Report No. GLA15-006). Industry council for electronic equipment recycling, Banbury, England.

Iji, M., Yokoyama, S., 1997. Recycling of printed wiring boards with mounted electronic components. *Circuit World* **23**, 10–15.

Inano, H., Tomita, K., Tada, T., Hiroyoshi, N., 2019. Metal recovery from printed circuit boards using CRT glass by reduction melting. *Technologies and Eco-innovation towards sustainability* II 185–197.

Kamberovic, Z., Ranitovic, M., Korac, M., Jovanovic, N., Tomovic, B., Gajic, N., 2018. Pyro-refining of mechanically treated waste printed circuit boards in a DC arc-furnace. *Journal of Sustainable Metallurgy*.

Kasper, A., Berselli, G., Freitas, B., Tenorio, J.A.S., Bernardes, A., Veit, H.M., 2011. Printed wiring boards for mobile phones: characterization and recycling of copper. *Waste Management* **31**, 2536–2545.

Kasper, A., Veit, H.M., 2018. Gold recovery from printed circuit boards of mobile phones scraps using a leaching solution alternative to cyanide. *Brazilian Journal of Chemical Engineering* **35**, 931–942.

Kaya, M., 2019. Waste printed circuit baord (WPCB) recycling: Conventional and emerging technology approach. *Encyclopedia of Renewable and Sustainable Materials*.

Kaya, M., 2016. Recovery of metals and non-metals from electronic waste by physical and chemical recycling processes. *Waste Management* **57**, 64–90.

Khaliq, A., Rhamdhani, M.A., Brooks, G.A., Masood, S., 2014. Metal extraction processes for electronic waste and existing industrial routes: A review and Australian perspective. *Resources* **3**, 152–179.

Kim, B., Lee, J., Seo, S., Park, Y., Sohn, H., 2004. A process for extracting precious metals from spent printed circuit boards and automobile catalysts. *JOM* **56**, 55–58.

Kim, E., Kim, M., Lee, J., Pandey, B., 2011. Selective recovery of gold from waste mobile phone PCBs by hydrometallurgical process. *Journal of Hazardous Materials* **198**, 206–215.

Kogan, V., 2006. Process for the recovery of precious metals scrap by means of hydrometallurgical techniques. WO 6006/013568 A3.

Korf, N., Lovik, A.N., Figi, R., Schreiner, C., Kuntz, C., Mahlitz, P., Rosslein, M., Wager, P., Rotter, V., 2019. Multi-element chemical analysis of printed circuit boards - challenges and pitfalls. *Waste Management* **92**, 124–136.

La Brooy, S., Linge, H., Walker, G., 1994. Review of gold extraction from ores. *Mineral Engineering* **7**, 1213–1241.

Ladou, J., 2006. Printed circuit board industry. *International Journal of Hygiene and Environmental Health* **209**, 211–219.

Laubertova, M., Malindzakova, M., Trpcevska, J., Gajic, N., 2019. Assessment of sampling and chemical analysis of waste printed circuit boards from WEEE: Gold content determination. *Metallurgical and Materials Engineering* **25**, 171–182.

Lee, C.H., Chang, C.T., Fan, K.S., Chang, T.C., 2004. An overview of recycling and treatment of scrap computers. *Journal of Hazardous Materials* **114**, 93–100.

Lee, C.H., Chang, S.L., Wang, K.M., Wen, L.C., 2000. Mangement of scrap computer recycling in Taiwan. *Journal of Hazardous Materials* **73**, 209–220.

Legarth, J.B., Alting, L., Danzer, B., Tartler, D., Brodersen, K., Scheller, H., Feldmann, K., 1995. A new strategy in teh recycling of printed circuit boards. *Circuit World* **21**, 10–15.

Li, J., Shrivastava, P., Gao, Z., Zhang, H.-C., 2004. Printed circuit board recycling: A state-of-the-art survey. *IEEE Transactions on electronics packaging manufacturing* **27**, 33–42.

Li, J., Xu, X., Liu, W., 2012. Thiourea leaching gold and silver from printed circuit boards of waste mobile phones. *Waste Management* **32**, 1209–1212.

Liu, X.B., Tanaka, M., Matsui, Y., 2006. Electrical and electronic waste managment in China. *Waste Management and Research* **24**, 92–101.

Lu, H., Li, J., Guo, J., Xu, Z., 2008. Movement behaviour in electrostatic separation: recycling of metal materials from waste printed circuit board. *Journal of Material Processing Technologies* **197**, 101–108.

Lu, X., Jiani, Y., Yuxi, L., Xing'an, N., Yujie, W., Wei, H., Jian, S., 2018a. A method of extracting lead from leaded waste electronic rubbish cathode-ray tube glass. Patent CN108486381.

Lu, X., Ning, X., Chen, D., Chuang, K., Shih, K., Wang, F., 2018b. Lead extraction from cathode ray tube (CRT) funnel glass: Reaction mechanisms in thermal reduction with addtion of carbon (C). *Waste Management* **76**, 671–678.

Lu, X., Shih, K., Liu, C., Wang, F., 2013. Extraction of metallic lead from cathode ray tube (CRT) funnel glass by thermal reduction with metallic iron. *Environmental Science and Technology* **47**, 9972–9978.

Lv, J., Yang, H., Jin, Z., Ma, Z., Song, Y., 2016. Feasibility of lead extraction from waste cathode ray tubes (CRT) funnel glass through a lead smelting process. *Waste Management* **57**, 198–206.

Lydall, M., Nyanjowa, W., James, Y., 2017. Mapping South Africa's waste electrical and electronic equipment (WEEE) dismantling, pre-processing and processing technology landscape (No. Report No. 7574). MINTEK, Randburg, South Africa.

Marin, T., 2006. Factors affecting the rates of oxidation and reduction of liquid copper during fire refining (PhD Thesis). University of Toronto, Canada.

Marin, T., Utigard, T., 2005. The kinetic and mechanism of molten copper oxidation by top blowing of oxygen. *JOM* 58–62.

MCC, 1994. Electronics industry environmental roadmap. United States.

Mear, F.O., Yot, P.G., Cambon, M., Ribes, M., 2006. The characterization of waste cathode-ray tube glass. *Waste Management* **26**, 1468–1476.

Meek, T., 1993. Inside the CRT: monitor technology explained. PC Novice 40–43.

Menad, N., 1999. Cathode-ray tube recycling. *Resources, Conservation and Recycling* **26**, 143–154.

Meng, W., Wang, X., Yuan, W., Wang, J., Song, G., 2016. The recycling of leaded glass in cathode ray tube (CRT), in: *Procedia Environmental Sciences*. Presented at the

Tenth International Conference on Waste Management and Technology, Mianyang, China, pp. 954–960.

Miyoshi, H., Chen, D., Akai, T., 2004. A novel process utilizing subcritical water to remove lead from wasted lead silicate glass. *The Chemical Society of Japan* **33**.

Murugan, R.V., Bharat, S., Deshpande, A.P., Varughese, S., Haridoss, P., 2008. Milling and separation of the multi-component printed circuit board materials and the analysis of elutriation based on a single particle model. *Powder Technology* **183**, 169–176.

Musson, E., Yong-Chul, J., Tonwsend, T.G., Il-Hyun, C., 2000. Characterization of lead leachability from cathode-ray tubes using the toxicity characteristics leaching procedure. *Environmental Science and Technology* **34**, 4376–4381.

Nair, A., 2021. E-waste management market. Allied Market Research. URL https://www.alliedmarketresearch.com/e-waste-management-market (accessed 1.3.22).

Nakajima, K., Takeda, O., Miki, T., Matsubae, K., Nagasaka, T., 2011. Thermodynamic analysis for the controllability of elements in the recycling process of metals. *Environmental Science and Technology* **45**, 4929–4936.

Ogunniyi, I.O., Vermaak, M.K.G., Groot, D.R., 2009. Chemical composition and liberation characterisation of printed circuit board comminution fines for beneficiation investigation. *Waste Management* **29**, 2140–2146.

Okada, T., Yonezawa, S., 2013. Energy-efficient modification of reduction-melting for lead recovery from cathode ray tube glass. *Waste Management* **33**, 1758–1763.

Pruksathorn, K., Damronglerd, S., 2005. Lead recovery from waste frit glass residue of electronic plant by chemical-electrochemical methods. *Korean Journal of Chemical Engineering* **22**, 873–876.

Quinet, P., Proost, J., van Lierde, A., 2005. Recovery of precious metals from electronic scrap by hydrometallurgical processing routes. *Minerals and Metal Processing* **22**, 17–22.

Reuter, M., 2014. Outotec Ausmelt top submerged lance (TSL) lead (& zinc/copper) smelitng opportunities & infrastructure, in: Metallurgy a Key Enabler of the Circular Economy. Presented at the GDMB Lead Committee Meeting.

Robinson, B.H., 2009. E-waste: An assessment of global production and environmental impacts. *Science of the Total Environment* **408**, 183–191.

Rosenqvist, T., 1974. *Principles of extractive metallurgy*. McGraw-Hill, New York.

Ruan, J., Zhu, X., Qian, Y., Hu, J., 2014. A new strain for recovering precious metals from waste printed circuit boards. *Waste Management* **34**, 901–907.

Sarvar, M., Salarirad, M., Shabani, M., 2015. Characterization of mechanical separation of metals from computer printed circuit boards (PCBs) based on mineral processing methods. *Waste Management* **45**, 246–257.

Sasai, R., Kubo, H., Kamiya, M., Itoh, H., 2008. Development of an eco-friendly material recycling process for spent lead glasll using a mechanochemical process and Na(2)EDTA reagent. *Environmental Science and Technology* **42**, 4159–4164.

Saterlay, A.J., Wilkins, S.J., Compton, R.G., 2001. Towards greener disposal of waste cathode ray tubes via ultrasonically enhanced lead leaching. *Green Chemistry* **3**, 149–155.

Seetharaman, S., McLean, A., Guthrie, R., Sridhar, S., 2014. Treatise on process metallurgy, 14th ed, Process fundamentals. Elsevier, Oxford.

Shah, M., Tipre, D., Dave, S., 2014. Chemical and biological processes for multimetal extraction from waste printed circuit boards of computers and mobile phones. *Waste Management and Research* **32**, 1134–1141.

Shamsuddin, M., 2016. Physical chemistry of metallurgical processes, 1st ed. John Wiley & Sons, Inc., New Jersey.

Shaw, 2013. An analysis of the demand for CRT glass processing in the U.S. Shaw Environmental Inc., United States.

Shuey, S.A., Vildal, E.E., Taylor, P., 2006. Pyrometallurgical processing of electronic waste. SME Annual Meeting Preprint 06-37.

Siegmund, A., 2001. Secondary lead smelting at the beginning of the 21st century, in: *Proceedings of EMC 2001*. Presented at the European Metallurgical Conference (EMC), Zurich, Switzerland, pp. 1–17.

Silvas, F., Correa, M., Caldes, M., Moraes, V., Espinosa, D.C.R., Tenorio, J.A.S., 2015. Printed circuit board recycling: physical processing and copper extraction by selective leaching. *Waste Management* **46**, 503–510.

SMS group, 2018. Urbangold - complete solution for electronic scrap recycling. SMS-group magazine. URL https://www.sms-group.com/de/sms-group-magazine/uebersicht/urbangold-complete-solution-for-electric-scrap-recycling/ (accessed 6.22.19).

SMS group, 2017. Aurus, Russia, places order with SMS Group to supply Urbangold compact plant for electronic scrap recycling. URL https://www.sms-group.com/press-media/press-releases/press-detail/aurus-russia-places-order-with-sms-group-to-supply-urbangold-compact-plant-for-electronic-scrap-recycling-792/ (accessed 4.23.19).

Sukhomlinov, D., Avarmaa, K., Taskinen, P., Jokilaakso, A., 2020. Slag-copper equilibria of selected trace elements in black-copper smelting. Part II. Trace element distributions. *Mineral Processing and Extractive Metallurgy Review* **41**, 171–177.

Sukhomlinov, D., Klemettinen, L., Avarmaa, K., O'Brien, H., Taskinen, P., Jokilaakso, A., 2019. Distribution of Ni, Co, precious and platinum group metals in copper making process. *Metallurgical and Materials Transactions B* **50**, 1752–1765.

Szalatkiewics, J., 2013. Metals recovery from waste printed circuit boards processed in plasmatron plasma reactor, in: *IFAC Proceedings Volumes*. Presented at the 16th IFAC Symposium on Control Optimization and Automation in Mining, Minerals and Metal Processing, San Diego, USA, pp. 478–483.

Tesfaye, F., Lindberg, D., Hamuyuni, J., Taskinen, P., Hupa, L., 2017. Valuable metals and energy recovery from electronic waste streams, in: 146th Annual Meeting and Exhibition. Presented at the TMS2017, San Diego, USA.

Tetronics, 2019. Plasma treatment: How it works. URL https://tetronics.com/our-technology/how-it-works/ (accessed 11.18.19).

Tsydenova, O., Bengtsson, M., 2011. Chemcial hazards associated with treatment of waste electrical and electronic equipment. *Waste Management* **31**, 45–58.

UNEP, 2013. UNEP annual report 2013 (No. DCP/1792/NA). United Nations Environment Programme (UNEP), Nairobi, Kenya.

Valache, M., Lafranchi, B., Weber, F., Guy, C., 1997. End of life electronics goods reycycling: towards industrial solutions for cathode ray tubes, in: *Recovery, Recycling and Re-Integration*. Presented at the R'97 International Congress, Geneva, Switzerland, pp. 321–327.

Veit, H.M., de Oliveira, E., Richter, G., 2015. Thermal processes for lead removal from the funnel glass of CRT monitors. *Revista Escola de Minas* **68**, 287–294.

Wang, Y., Zhu, J., 2012. Preparation of lead oxide nanoparticles from cathode-ray tube funnel glass by self-propagating method. *Journal of Hazardous Materials* 215–216, 90–97.

Wastawino, H., 2005. Factors determining the rate of copper oxidation (Master Thesis). University of Chile, Chile.

William, J.H., Williams, P.T., 2007. Separation and recovery of materials from scrap printed circuit boards. *Resources, Conservation and Recycling* **51**, 691–709.

Wood, J., Creedy, S., Matusewicz, R., Reuter, M., 2011. Secondary copper processing using Outotec Ausmelt TSL technology, in: MetPlant 2011 Plant Design & Operating Strategies - World's Best Practice. Presented at the AusIMM, Perth, Australia.

Xiu, F., Qi, Y., Zhang, F., 2015. Leaching of Au, Ag, and Pd from waste printed circuit boards of mobile phone by iodide lixiviant after supercritical water pre-treatment. *Waste Management* **41**, 134–141.

Xiu, F., Qi, Y., Zhang, F., 2013. Recovery of metals from waste printed circuit boards by supercritical water pre-treatment combined with acid leaching process. *Waste Management* **33**, 1251–1257.

Xu, Q., Li, G., He, W., Huang, J., Shi, X., 2012. Cathode ray tube (CRT) recycling: Current capabilities in China and research progress. *Waste Management* **32**, 1566–1574.

Yamane, L.H., de Moraes, V.T., Espinosa, D.C.R., Tenorio, J.A.S., 2011. Recyling of WEEE: Characterization of spent printed circuit boards from mobile phones and computers. *Waste Management* **31**, 2553–2558.

Yan, L., Shi, K., Liu, Y.Z., 2008. Assessment and selection of panel-funnel separation techniques of end-of-life CRT glass. *Journal of Anyang Institute of Technology* 19–23.

Yin, F., Wang, H., Liu, Z., 2008. The reycling technology of waste CRT display units. *Environmental Engineering* **26**, 44–46.

Yot, P.G., Mear, F.O., 2009. Lead extraction from waste funnel cathode-ray tubes glasses by reaction with silicon carbide and titanium nitride. *Journal of Hazardous Materials* **172**, 117–123.

Zhang, C., Wang, J., Bai, J., Guan, J., Wu, W., Guo, C., 2013. Recovering lead from cathode ray tube funnel glass by mechano-chemical extraction in alkaline solution. *Waste Management and Research* **31**, 759–763.

Zhang, S., Forssberg, E., 1997. Mechanical separation-orientated characterization of electronic scrap. *Resources, Conservation and Recycling* **21**, 247–269.

Zhao, Y., Wen, X., Li, B., Tao, D., 2004. Recovery of copper from printed circuit boards. *Minerals and Metal Processing* **21**, 99–102.

Zhukov, V., Skopov, G., Holod, S., 2016. Pyrometallurgy of copper. UO RAN, Ekateringburg.

APPENDIX A: SUPPORTING FIGURES AND TABLES

Table 62. Typical chemical compositions of PCBs as reported in literature (wt%)

Material	Species	(a)	(b)	(c)	(d)^	(e)	(f)	(g)	(h)
Metals	Cu	20	26.8	10	15.6	22	17.9	23.5	6.9
(max. 40%)	Al	2	4.7	7	-	-	4.78	1.33	14.2
	Pb	2	-	1.2	1.35	1.55	4.19	0.99	6.3
	Zn	1	1.5	1.6	0.16	-	2.17	1.51	2.2
	Ni	2	0.47	0.85	0.28	0.32	1.63	2.35	0.85
	Fe	8	5.3	-	1.4	3.6	2	1.22	20.5
	Sn	4	1	-	3.24	2.6	5.28	1.54	1.0
	Hg (ppm)	-	-	-	-	-	-	-	22
	Cd (ppm)	-	-	-	-	-	-	-	94
	Sb (ppm)	0.4	0.06	-	-	-	-	-	94
	As (ppm)	-	-	-	-	-	-	-	13
	Ga (ppm)	-	-	-	-	-	-	-	13
	Ge (ppm)	-	-	-	-	-	-	-	16
	Se (ppm)	-	-	-	-	-	-	-	16
	In (ppm)	-	-	-	-	-	-	-	16
	Bi (ppm)	-	-	-	-	-	-	-	63
	Be (ppm)	-	-	-	-	-	-	-	157
	Ta (ppm)	-	-	-	-	-	-	-	157
	Au (ppm)	1000	80	280	420	350	350	570	16
	Ag (ppm)	2000	3300	110	1240	-	1300	3301	189
	Pd (ppm)	50	-	-	10	-	250	294	3
	Pt (ppm)	-	-	-	-	-	4.6	30	-
Ceramics	SiO_2	15	15	-	-		-	-	
(max. 30%)	Al_2O_3	6	-	-	-	30#	-	-	24.9#
	(CaO+MgO)	6	-	-	-		-	-	
	(Titanates+mica)	3	-	-	-		-	-	
Plastics	PE	9.9	-	-	-				
(max. 30%)	PPE	4.8	-	-	-		-	-	
	Polyesters	4.8	-	-	-		-	-	
	Epoxy	4.8	-	-	-	16$	-	-	23$
	PVC	2.4	-	-	-		-	-	
	PTFE	2.4	-	-	-		-	-	
	Nylon	0.9	-	-	-		-	-	

(a) Shuey *et al*. (2006), (b) Zhao *et al*. (2004), (c) Zhang and Forssberg (1997), (d) Kim *et al*. (2004) ^ PCBs incinerated, (e) Iji and Yokoyama (1997), (f) Kogan (2006), (g) Ogunnyi *et al*. (2009), (h) MCC (1994), #Total ceramics, $Total plastics

The heterogeneous mixture of metals in PCBs is attributed to the many electronic components attached to the board. The components are described in Table 63 (adapted from Li *et al.* (2004)).

Table 63. Description of electronic components found in PCBs

Component	**Description**	**Metals used**
Capacitors	Devices that store electrical energy in an electrical field	Pd, Pt, Ta, Ti and Al
Chips or integrated circuits (ICs)	Set of electronic circuits on one small flat pieces of semi-conductor material used mainly as a timer, logic gate, computer memory, microcontroller or microprocessor	Ga, Ge, Ta, Te, As, Sb, Si, In and Se
Connectors	Pins, rods or plates used to make quick and reliable electrical contacts on a circuit board	Cu, Au, Ag or Fe
Relays	Electrically operated switch used to control circuits with an independent low-power signal	Cu or Fe
Resistor	Devices that implement electrical resistance used to reduce current flow, adjust signal level or divide voltage	Ta, Ni or Bi
Solder	Low melting point fusible alloy used to create permanent bonds between metals for electrical connections on a circuit board	Sn, Pb, Cu, Zn and Sb
Switches	Electrical devices used to manually cut off or reconnect power from an electrical supply	Hg, Cd or Be
Transistors	Semiconductor devices used to amplify or switch electrical signals or power	Si or Ge

The metals present in PCBs can be summarized into the following groups:

- Base metals (Cu, Al, Zn, Ni, Fe & Sn),
- Precious metals (Au, Ag, Pd & Pt),
- Toxic metals (Pb, Cd, As, Sb, Hg, Cr, Mn, In, Bi & Be), and
- Scarce metals (Ga, Ge, Ta, Te & Se).

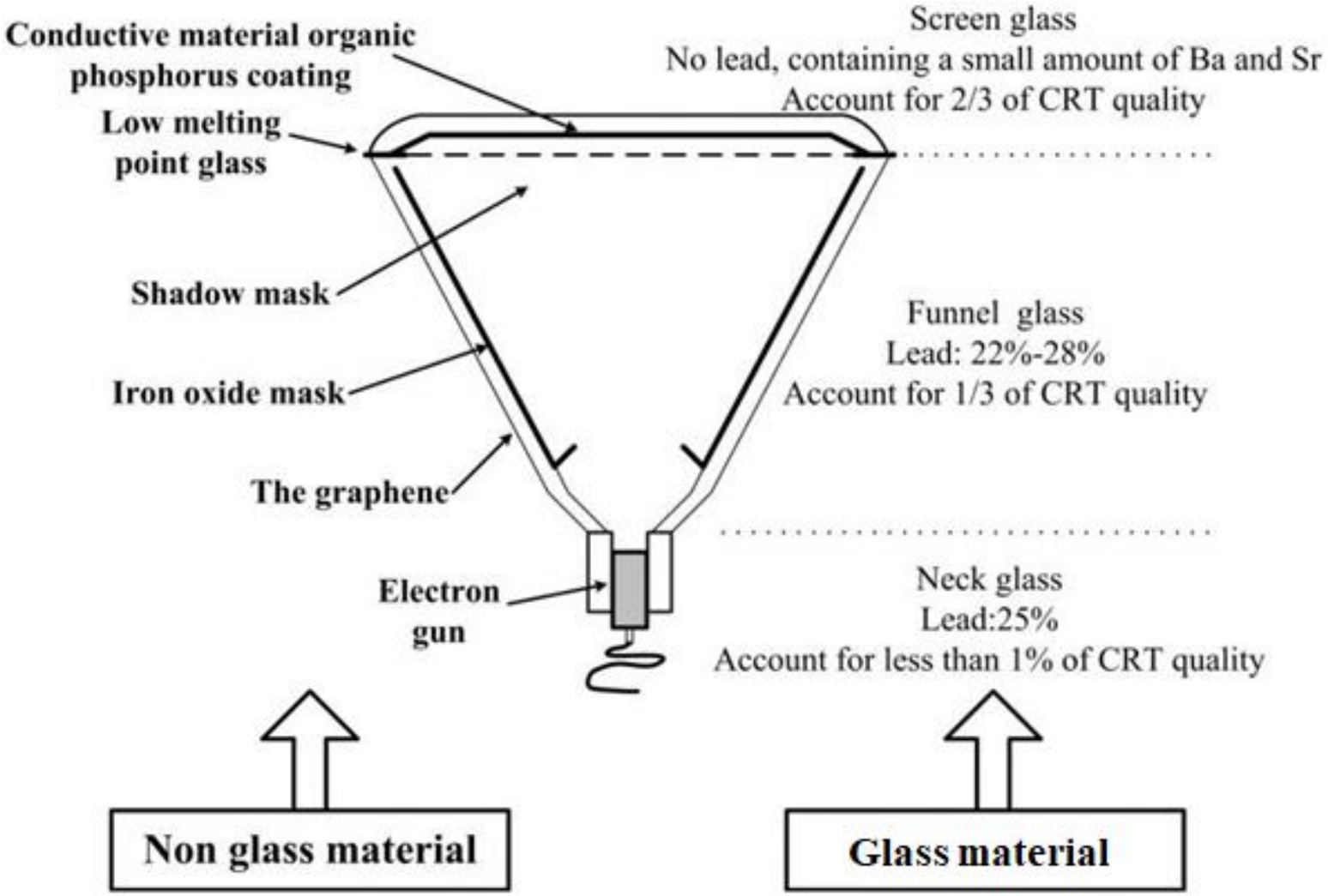

Figure 79. A schematic of a typical CRT showing glass and non-glass materials (source: Meng et al. [2016])

Table 64. Chemical composition of CRT glass from different manufacturers compared against values published in literature, wt%. Values from literature were averaged and presented in Table 64 as "Standard conc."(source: Mear et al. [2006])

Oxide	SiO_2	PbO	K_2O	Na_2O	Al_2O_3	CaO	MgO	BaO	SrO	Sb_2O_3	Fe_2O_3	TiO_2	As_2O_3	ZnO	ZrO_2	Others
Color panel																
Min. conc.	60.00	0.00	6.00	7.80	2.00	0.00	0.00	9.00	6.00	0.25	0.07	0.40	0.00	0.00	0.00	8.48
Max. conc.	63.00	3.00	7.50	9.00	3.50	2.00	1.00	11.00	10.00	0.50	0.12	0.60	0.20	0.60	2.50	0.00
Standard conc.	62.00	0.00	7.50	8.00	2.20	0.50	0.20	10.00	8.50	0.35	0.08	0.50	0.02	0.30	1.50	0.00
HITASHI	58.86	0.00	7.33	7.57	2.21	1.10	0.21	9.30	8.19	0.61	0.04	0.36	0.00	0.01	2.47	1.73
MATSUSHITA	59.74	0.00	7.57	7.16	2.06	0.07	0.00	10.06	8.68	0.65	0.07	0.37	0.01	0.52	1.58	1.48
SAMSUNG	59.51	0.04	7.57	7.19	2.10	0.31	0.06	9.57	8.75	0.59	0.06	0.37	0.01	0.39	1.80	1.68
SONY	59.21	0.01	7.64	7.14	2.07	0.07	0.01	9.93	8.81	0.57	0.07	0.36	0.01	0.51	1.57	2.02
TOSHIBA	60.21	0.00	7.71	6.89	2.05	0.01	0.01	8.99	9.31	0.53	0.07	0.39	0.00	0.52	1.56	1.74
Average values	59.51	0.01	7.56	7.19	2.10	0.31	0.06	9.57	8.70	0.59	0.10	0.37	0.01	0.39	1.80	1.73
Color funnel																
Min. conc.	52.00	19.00	7.50	6.00	3.50	2.00	1.20	0.00	0.00	0.10	0.05	0.00	0.00	0.00	0.00	8.65
Max. conc.	56.00	23.00	8.50	8.00	5.00	4.00	2.00	2.00	1.00	0.30	0.07	0.10	0.10	0.10	0.00	0.00
Standard conc.	52.00	22.00	7.80	6.80	4.00	3.80	1.80	1.00	0.50	0.25	0.06	0.05	0.01	0.00	0.00	0.00
HITASHI	43.37	21.32	6.72	5.08	3.95	2.99	1.58	0.09	0.36	0.88	0.06	0.03	0.00	0.00	0.04	13.53
MATSUSHITA	50.19	23.32	7.30	5.71	3.62	3.78	1.67	0.53	0.69	0.55	0.07	0.05	0.00	0.04	0.09	2.39
SAMSUNG	52.94	23.39	7.74	5.67	2.10	3.53	2.40	0.10	0.47	0.40	0.08	0.03	0.00	0.03	0.04	1.07
SONY	50.51	22.51	7.32	5.64	3.38	3.80	1.83	1.03	1.04	0.53	0.12	0.09	0.00	0.06	0.19	1.96
TOSHIBA	51.85	24.12	7.46	5.54	3.35	3.70	1.77	0.04	0.39	0.48	0.07	0.05	0.00	0.01	0.06	1.09
Average values	49.77	22.90	7.31	5.53	3.28	3.56	1.85	0.36	0.60	0.57	0.10	0.05	0.00	0.03	0.08	4.01
Black & white (panel and funnel)																
Min. conc.	64.00	2.80	6.00	6.50	3.00	0.00	0.00	9.00	0.00	0.30	0.05	0.10	0.00	0.00	0.00	8.25
Max. conc.	66.00	4.40	7.50	8.00	5.00	1.00	0.00	12.00	2.00	0.60	0.20	0.20	0.30	0.10	0.50	0.00
Standard conc.	65.00	4.00	7.00	7.00	3.00	0.50	0.00	11.00	1.00	0.45	0.12	0.15	0.01	0.05	0.25	0.47
Funnel CLINTON Corp.	63.55	3.47	6.24	6.90	3.08	0.03	0.01	12.74	1.15	0.75	0.06	0.00	0.01	0.01	0.01	2.00
Panel CLINTON Corp.	63.88	3.42	6.28	7.00	3.10	0.02	0.01	12.85	1.15	0.74	0.06	0.01	0.00	0.00	0.03	1.46

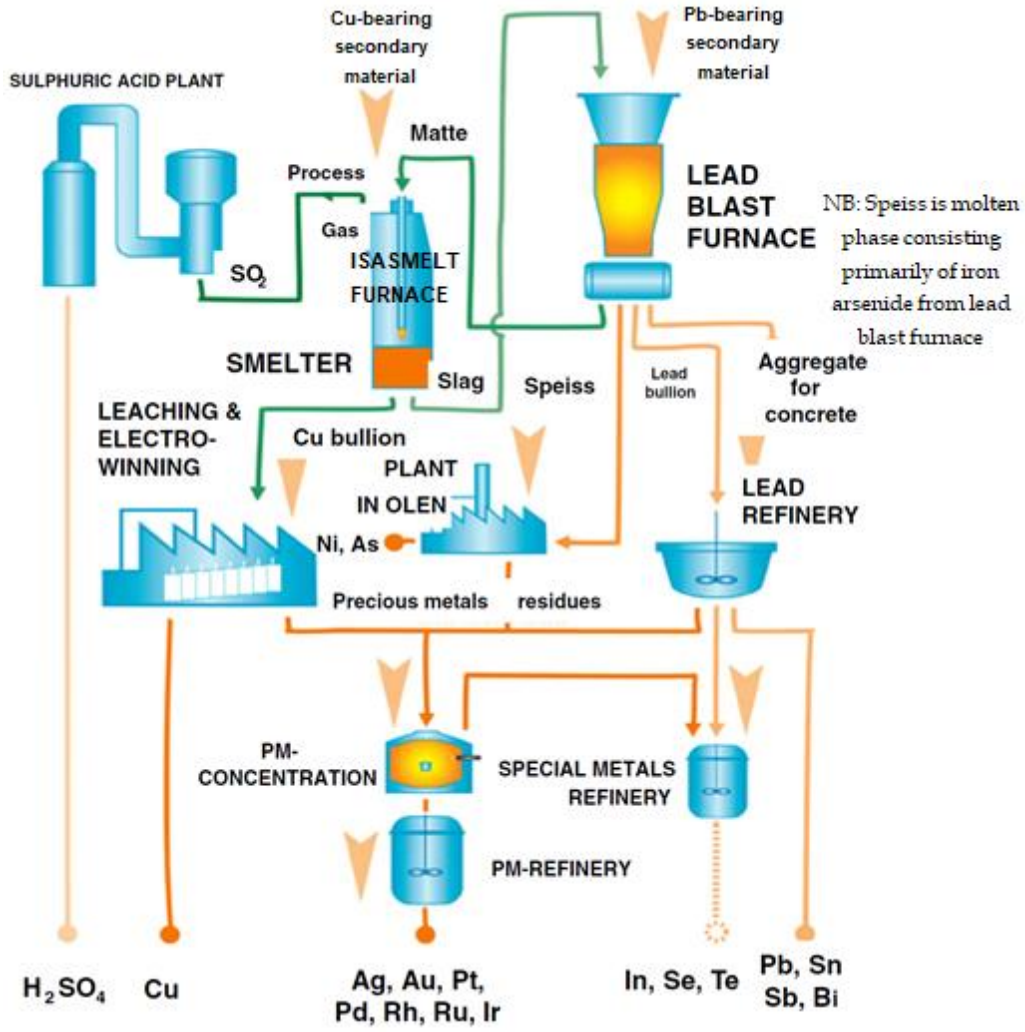

Figure 80. Process flow sheet of Umicore ISASMELT plant (adapted from Hageluken [2006])

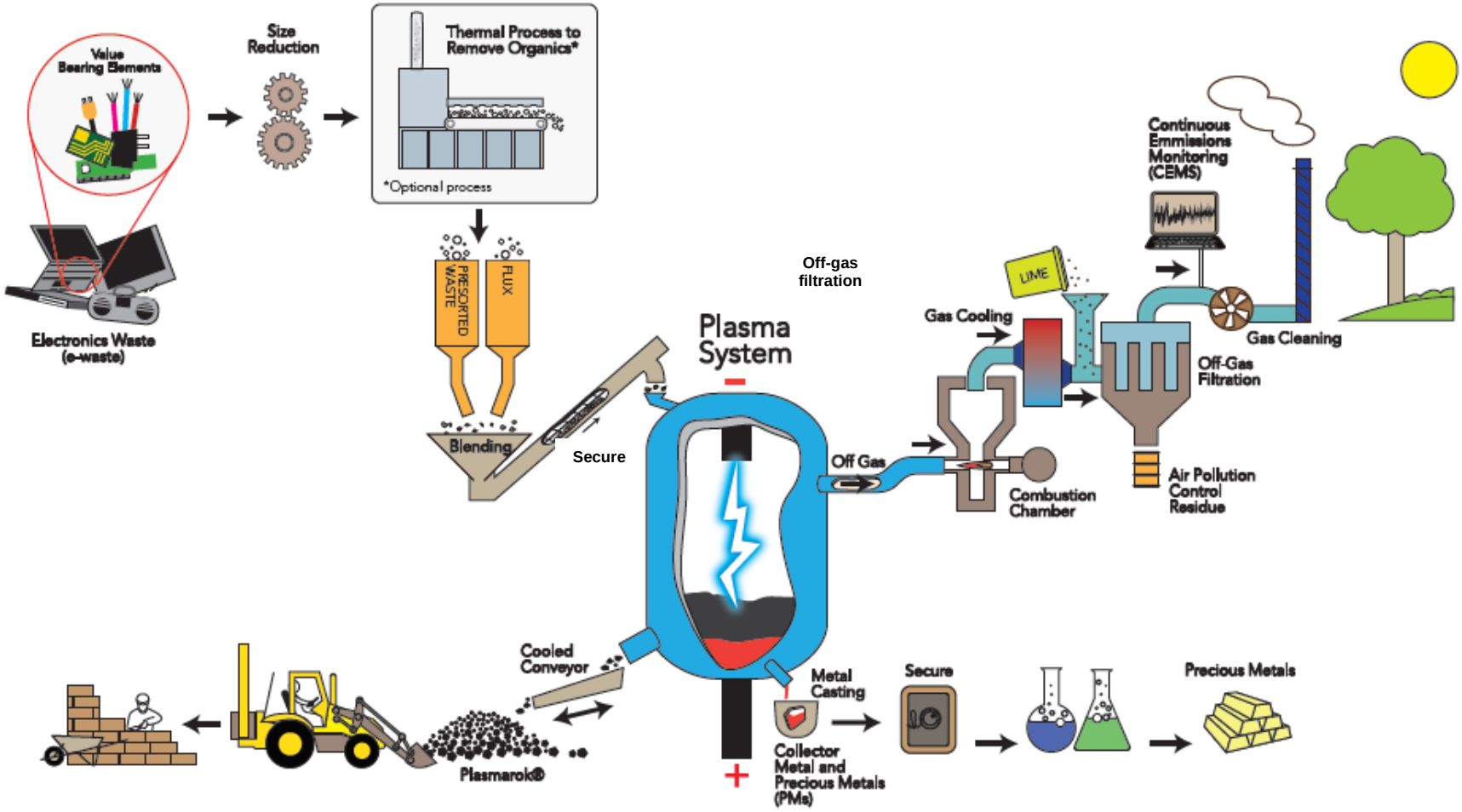

Figure 81. Process flow sheet of Tetronics electronics waste treatment process through a plasma arc furnace (adapted from Tetronics [2019])

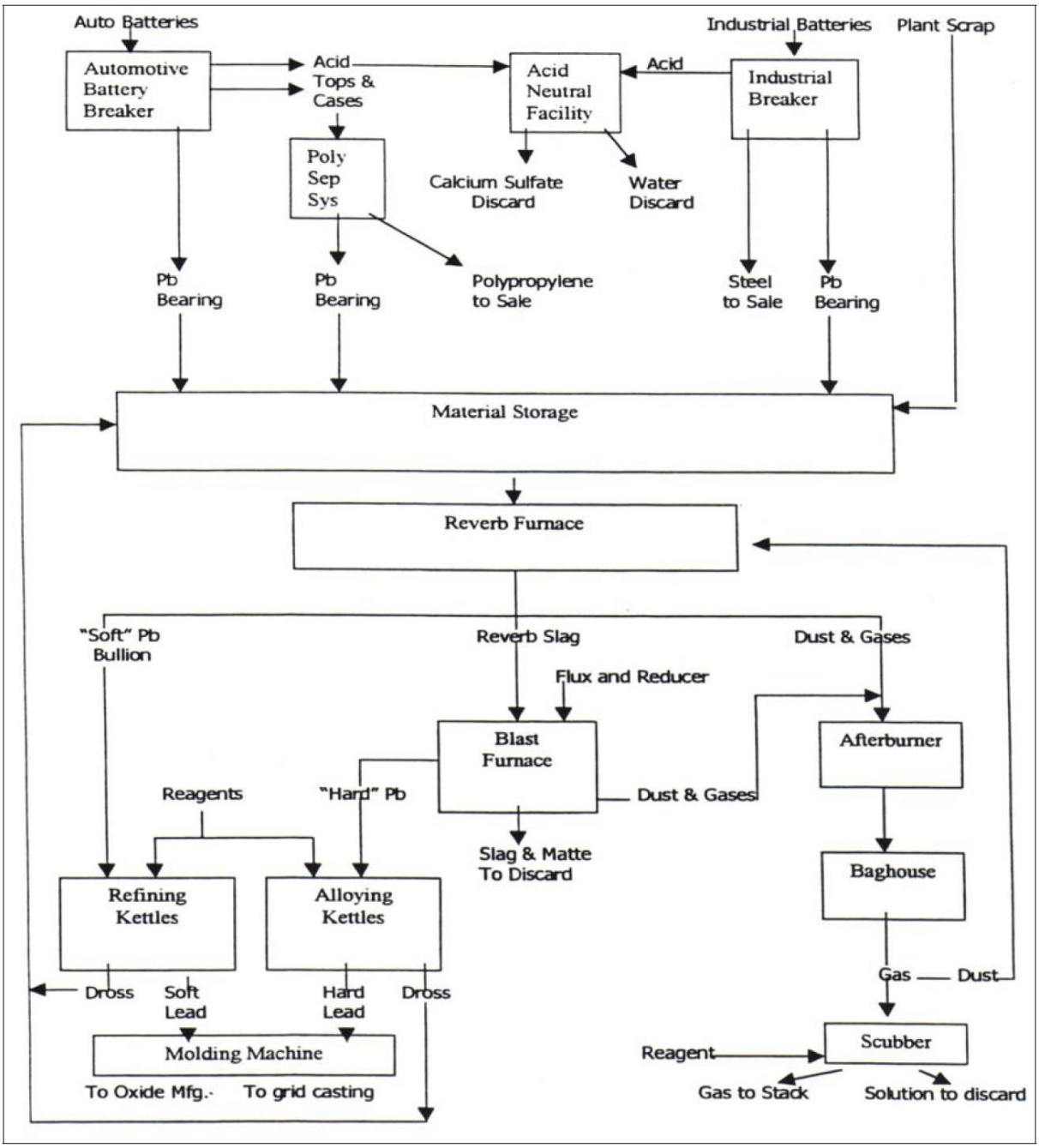

Figure 82. Flow sheet of a typical secondary Pb smelter in North America (source: Siegmund [2001])

APPENDIX B: PCBs PRE-PROCESSING TECHNIQUES

PCBs undergo mechanical, physical and chemical processes to separate metallic components from the non-metallic components (see Figure 83). The details of each process are briefly discussed in this section.

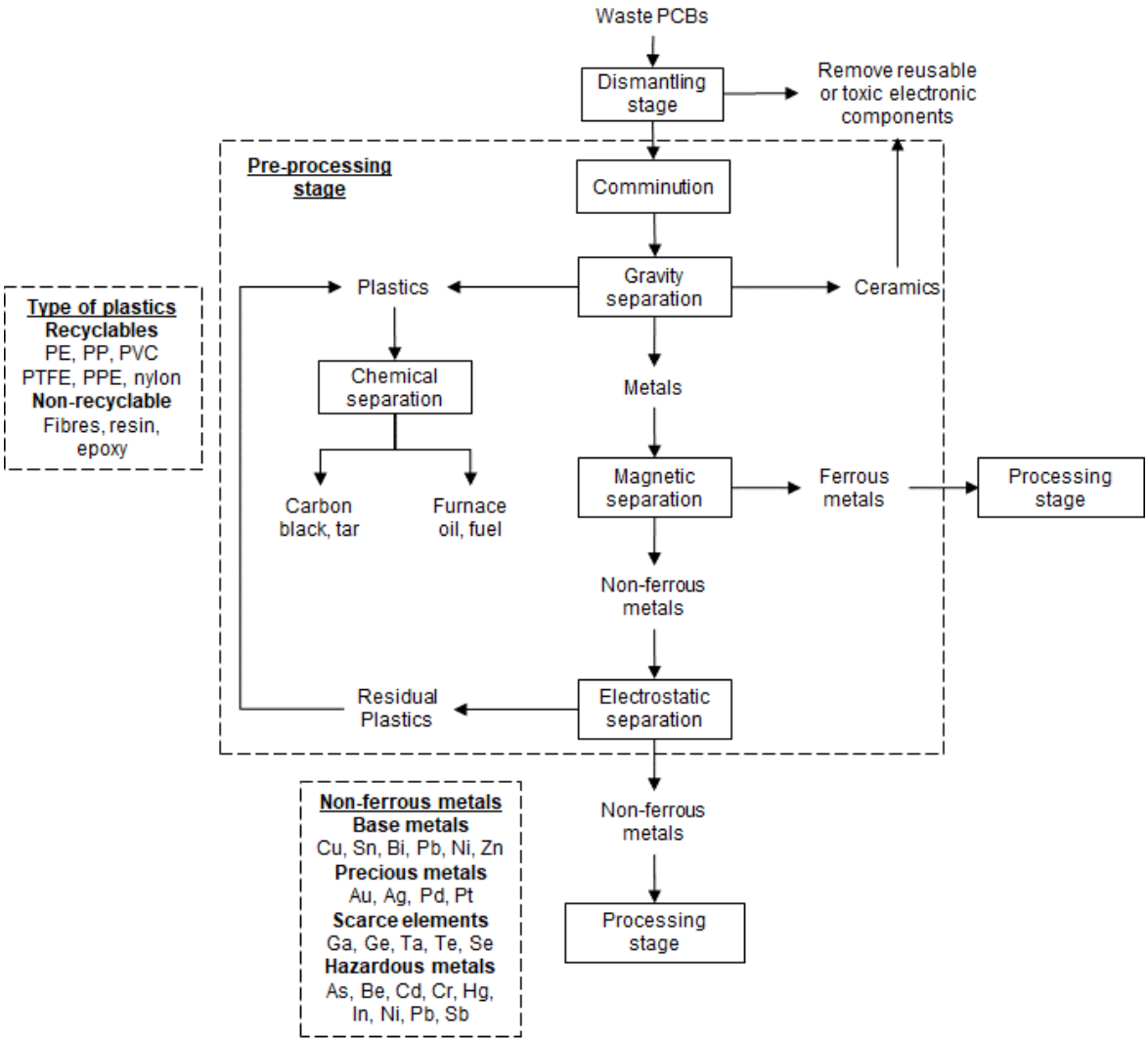

Figure 83. Flow sheet showing the pre-processing stage of PCBs (adopted from Kaya [2016])

Mechanical processes

The stripped boards then go through comminution, which serves the purpose of liberating metallics from the non-metallics fractions by size reduction. Various types of hammer crushers, rotary crushers, shredders and cutter equipment are used. Low speed high torque shear shredders are ideal for primary crushing, while a number of ball mills are used for finer grinding (Zhang and Forssberg, 1997). The comminution

equipment is operated in line with a sieve to classify the different-sized particles. Screening has not only been utilized to prepare a uniform-sized feed to a certain process but also to upgrade the metals content (Zhang and Forssberg, 1997). After primary shredding and screening, secondary stage crushing with dry air cyclone classification are used with dust collection systems.

Sampling of PCBs for chemical analysis normally occurs after the comminution step. A typical flowsheet depicting the steps involved in the pre-processing stage of PCBs is illustrated in Figure 83.

Physical processes

The next step after comminution is gravity separation. Gravity concentration methods separate materials of different specific gravity by their relative movement in response to gravity as well as other factors such as particle size and forces exerted by viscous liquids (Zhang and Forssberg, 1997). Shaking tables, water or airflow tables, heavy media separation and sifting are common gravity separators used in PCBs recycling to achieve separation of metals from plastics and ceramic components (Savar *et al*., 2015).

The metals concentrate from the gravity separation step is further upgraded in a magnetic separator to separate magnetic metallic particles (ferrous) from non-magnetics particles (non-ferrous). Yamane *et al*. (2011) reported that magnetic separators, in particular, low-intensity drum separators, are widely used for recovery of ferromagnetic metals, which includes Fe, Ni and steel, and non-magnetic fractions, which includes Cu, Pb and Zn. The non-magnetic fraction flows to the next physical process step while the ferrous fraction is recycled to Fe and steel recycling industry for processing.

Residual plastics and other fine non-metallics are separated from the non-ferrous fraction by an electrostatic separator. The Corona-electrostatic method is the most effective separation technology for metallic and non-metallics at present (Hadi et al., 2015). Materials are separated by their difference in electrical conductivity, specifically difference in polarity and amount of charge acquired by particles to be separated (Lu *et al*., 2008). The product streams are sent to the next respective steps.

Chemical processes

The residual plastics removed from the electrostatic separation step is recycled and combined with plastic fractions removed at the gravity separation step. A number of chemical processes are applied to treat this fraction depending on the type of plastic. Pyrolysis, gasification, depolymerization and hydrogenolytic degradation are some of the processes that are applied to decompose the polymers to low molecular weight products such as carbon black, tars or oils which can be used as fuel (Guo *et al.*, 2009).

APPENDIX C: CRTs PRE-PROCESSING TECHNIQUES

Pre-processing of CRTs is mainly focussed around separating the Pb-rich funnel glass from the Pb-free panel glass (see Figure 84). The three main pre-processing techniques of CRTs are briefly discussed in this section.

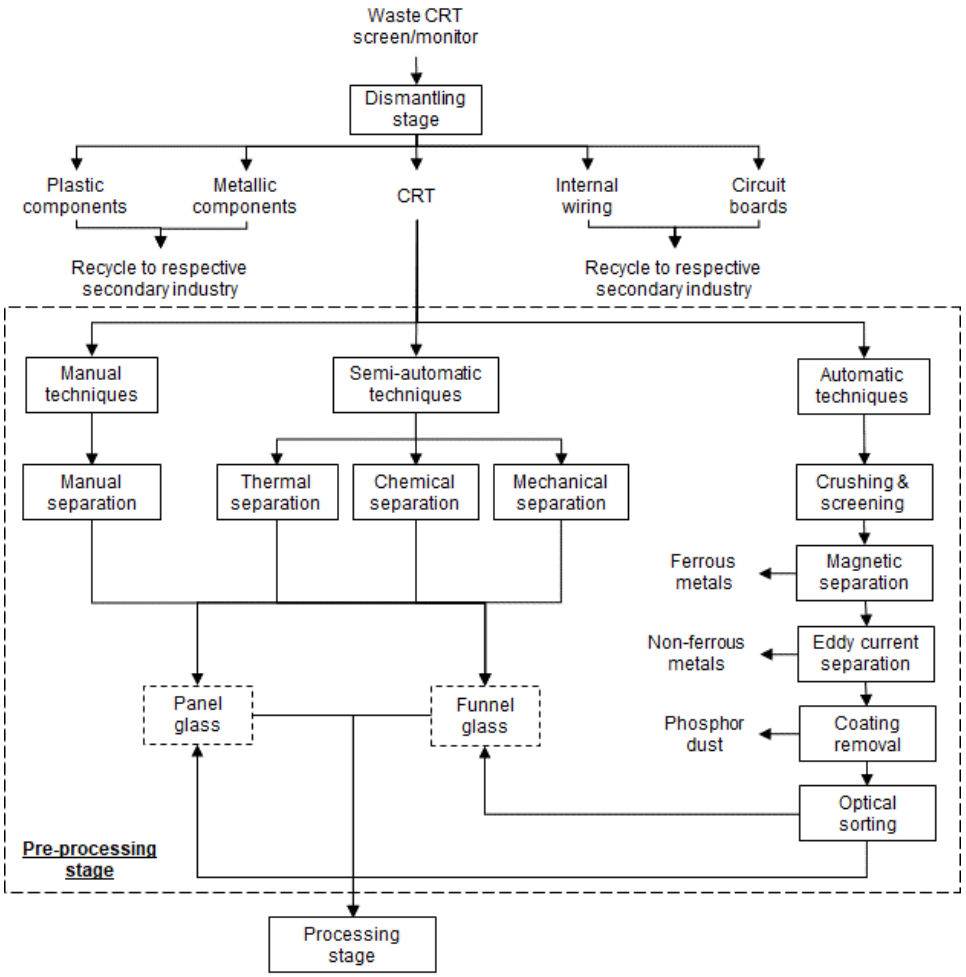

Figure 84. Flow sheet showing the pre-processing stage of CRTs (adapted from Xu et al. *[2012])*

Manual separation

Manual separation techniques are prevalent in the informal sector of developing countries. Primitive methods such as physical dismantling by using tools such as hammer, chisel, and screw driver are adopted to separate the panel and funnel glass as well as to extract other recyclable components within the tube such as electron gun, deflection metals, shadow mask and implosion protection band (Liu *et al*., 2006).

A hammer is used to break off the neck glass, which also releases the vacuum, followed by gently breaking the funnel glass while the panel glass is intact. A vacuum cleaner is used to collect the phosphor dust from the inside surface of the panel glass. The clean panel and funnel glasses are broken into smaller pieces and stored in different bulk bags (Liu *et al*., 2006).

Manual techniques are considered to be cost-efficient due to use of unskilled manual labour but commonly have poor standards in terms of protection of the environment and health of the workers, and they are not suitable to handle high volumes of CRTs (*Xu et al., 2012*).

Chemical separation

This is one of the three semi-automatic techniques used in the e-waste industry, with the other two being thermal and mechanical separation. Chemical separation involves the use of a hot HNO_3 bath to leach the frit solder in the panel-funnel interface (Yan *et al*., 2008). This requires the CRT to be soaked into the bath for a particular period of time.

The hot acid bath method is relatively simple and cheap. However, this method cannot achieve a clean separation between the panel and funnel glass. Furthermore, treatment of wastewater incurs additional costs (Yan *et al*., 2008),

Thermal separation

Thermal separation can be achieved by use of a laser cutter or electrically-heated wire. In the electric wire heating method, a nickel-chrome wire is wound along the panel-funnel interface and heated for a short period (Lee *et al*., 2004). The heated area is then suddenly cooled by blowing cold air to thermally shock and create a crack in the interface that allows the panel glass to be separated from the funnel glass. The laser cutting method applies the same principle except that the heating is effected via a laser beam.

The limitation with the electric wire heating method is that it cannot be used for all sizes of CRTs. It is most appropriate for dismantling CRTs with 14- to 25-inch screens. In addition, the noise and dust emissions can have adverse effects on the health and safety of the workers (Hu *et al*., 2007).

In contrast, the laser cutting method is very efficient and can be used for all CRT sizes (Yin *et al*., 2008). This method can cut up to two CRTs per minute, depending on the size. The disadvantage with this method is that laser cutting is energy intensive, thus it is associated with high operating costs and significant capital investment (Xu *et al*., 2012).

Mechanical separation

Mechanical separation is achieved with a spinning diamond saw. The CRT monitor is placed on a rotating handle and contacted with a spinning diamond saw disc at the panel-funnel interface under dry or wet conditions (Herat, 2008). This method is efficient and no additional treatment is necessary but the process is slow and the resulting dust (under dry conditions) Pbs to difficulties and unsafe working conditions (Herat, 2008).

Automatic techniques

The separation of panel from funnel glass can be achieved by using sensor guided automatic sorting (Xu *et al*., 2012). The stripped CRTs are first crushed, sieved, and partly separated into coarse and fine glass cullet. Ferrous metals are separated from the glass by magnetic separation while non-ferrous metals are removed by eddy currents.

The phosphor coating on the panel glass as well as the Fe oxide coating on the funnel glass is removed by washing the cullet in a tumbling mill. After washing off the dust, the cullet is dried using electric oven. The dried cullet is then separated into panel and funnel glass pieces by optical sorting (Xu *et al*., 2012).

The advantage of crushing and sorting techniques is that they eliminate the need to separate the whole panel and funnel glass, but rather these are crushed together and then sorted. The drawback is that state-of-the-art equipment have significant capital requirements. Furthermore, the use of X-ray equipment in a plant requires appropriate shielding and must follow strict rules to protect workers from exposure (Yan *et al*., 2008).

APPENDIX D: ALTERNATIVE PROCESSING OF PCBs AND CRTs

Alternative processing of PCBs

Thiosulfate and thiourea are used as leachates primarily aimed at dissolving Au from PCBs, with thiosulfate considered a nontoxic and low-price alternative to highly oxidising and corrosive acids (Ha *et al*., 2010; Li *et al*., 2012). Thiosulfate leaching generally takes place in an alkaline environment and optimal leaching rates can be achieved under ambient temperatures (<40°C) (Kasper and Veit, 2018). The highest leaching rates of Au (90% from PCBs) were reported by Ha *et al*. (2010) from a mixed lixiviant of thiosulfate, ammonia and tetra-ammine cuprate (II) ions. In thiosulfate leaching processes, large quantities of reagents are consumed resulting in higher operating costs that are not financially feasible for commercial application (Gu *et al*., 2019).

Leaching with thiourea takes places under acidic conditions (Li *et al*., 2012). Ferric ions are usually added as an oxidising agent to reduce the dissolution time (Gurung *et al*., 2013). Besides Au, thiourea is able to leach out other precious metals such as Ag and Pd. The highest leaching rates of Au (95%), Ag (93%) and Pd (99%) were achieved at a pH of 1 and temperature of 70°C (Quinet *et al*., 2005). Gurung *et al*. (2013) reported that Au leaching rates with thiourea are generally higher than those of thiosulfate, and leaching times are shorter with thiourea leaching.

Halide leaching was studied by Xiu *et al*. (2015) whereby an iodide-iodide halide leaching method was applied to extract Au, Ag and Pd. This method was considered uneconomical for large-scale practice as iodide is consumed in large volumes and the reagent is expensive (Awasthi *et al*., 2017).

Bacteria-assisted leaching reactions employed in biometallurgy have been regarded by Cui and Zhang (2008) as a potential major technological breakthrough. Several studies have been undertaken to investigate the bioleaching of PCBs, and acidophilic bacteria are the most frequently used micro-organisms in bioleaching processes (Arshadi *et al*., 2016; Horeh *et al*., 2016). A study by Chi *et al*. (2011) used a cyanide-generating bacterium to leach Au and Cu from PCBs. This method was considered uneconomically viable due to low leaching rates (10.8% Au and 11.4% Cu) and long processing duration (8 days).

Ruan *et al*. (2014) also obtained low leaching rates of 8.2% Au, 12.1% Ag, and 52.3% Cu after leaching with pseudomonas chlororaphis bacterium for a period of 3 days. However, the work of Shah *et al*. (2014) discovered that the oxidation of Fe^{2+} to Fe^{3+} medium promotes the leaching efficiency of bioleaching processes. This discovery helped increase leaching rates of Cu, Ni and Zn to 99%, 84%, and 99%, respectively, after a duration of 6–8 days. Despite the high leaching efficiencies, the extended leaching durations make these processes challenging to industrialize (Arshadi *et al*., 2016).

Alternative processing of CRTs

The study by Pruksathorn and Damronglerd (2005) found that HNO_3 and acetic acid were better solutions for the dissolution of PbO compared with NaOH, HCl, and H_2SO_4. They reported that more than 95% of the Pb was leached by 0.1 mol/kg HNO_3 or 0.5 mol/kg acetic acid. Miyoshi *et al*. (2004) studied a subcritical hydrothermal process at 355°C and 24 MPa followed by HNO_3 leaching at 100°C to remove 93% Pb from the silicate glass.

Other studies such as the work of Saterlay *et al*. (2001) reported the use of power ultrasound to enhance the removal of Pb via an accelerated leaching protocol. Sasai *et al*. (2008) studied the use of a chelate reagent sodium ethylenediamine tetra-acetate dehydrate during a wet ball-milling process at room temperature.

APPENDIX E: RATE OF OXYGEN ABSORPTION

Marin and Utigard (2005) investigated the effect of O_2 partial pressure, flow rate of O_2 gas mixture, and lance tip distance from surface of liquid Cu, on the rate of O_2 absorption into liquid Cu. All tests were carried out at 1200°C and O_2 gas mixture was blown on the surface of liquid Cu held in an Al_2O_3 crucible.

Figure 85 shows O_2 partial pressures as a function of time for different starting partial pressures of nitrogen. The test with 0 kPa partial pressure of nitrogen showed a lower O_2 partial pressure (in (a)) and a faster drop in O_2 partial pressure (in (b)) compared to tests with nitrogen added to the gas mixture. This signifies that the presence of other gaseous species in the gas mixture interferes and lowers the rate of O_2 absorption.

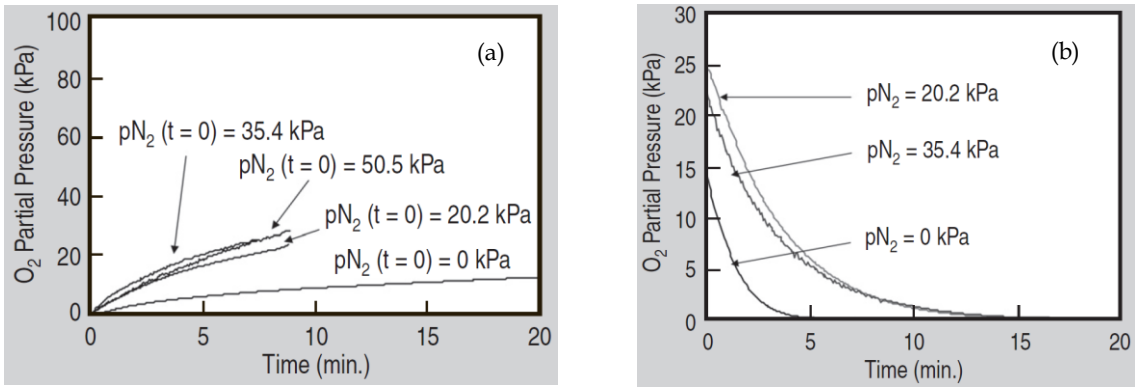

Figure 85. Graphs showing partial pressure of O_2 as a function of time for different starting partial pressures of nitrogen with (a) O_2 flow into the system, (b) without O_2 flow into system (valves closed) (source: Marin and Utigard [2005])

Figure 86(a) clearly depicts the relation between O_2 absorption rate and O_2 partial pressure. The higher the O_2 partial pressure, the higher the rate of O_2 absorption. Furthermore, a higher flow rate of O_2 gas mixture resulted in even higher rate of O_2 absorption relative to a lower flow rate. Figure 86(b) illustrates that the shorter the distance between the tip of the lance and the liquid Cu surface, the higher the rate of O_2 absorption.

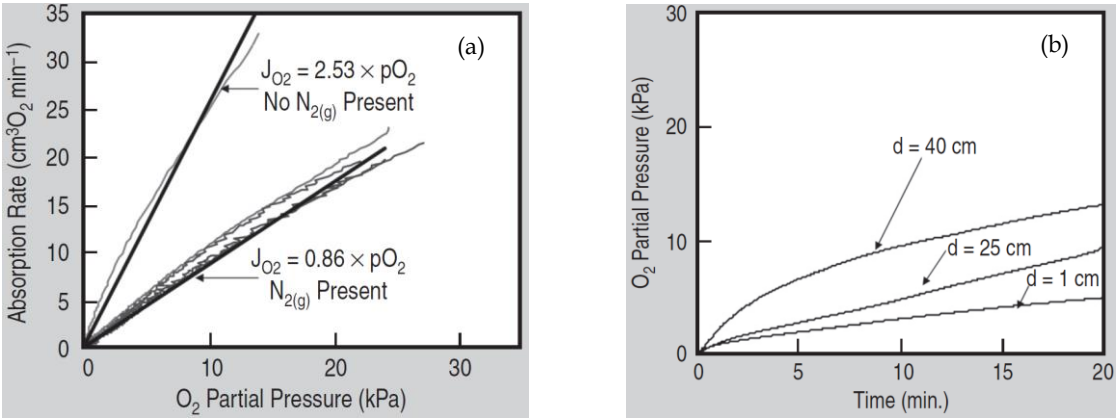

Figure 86. Graphs showing (a) absorption of rate of O_2 as a function of O_2 partial pressure, (b) O_2 partial pressure as a function of time for different lance tip distances from surface of liquid Cu (source: Marin and Utigard [2005])

APPENDIX F: MANUAL SEPARATION OF CRTs

Manually separating the components of a CRT presents health and safety risks. The risks associated with a Pb-bearing glassy material necessitates the use of personal protective equipment (PPE) and tools listed in Table 65. A step-wise procedure to safely dismantle the CRT and manually separate out the metallic, plastic and rubber components as well as separating panel glass from funnel glass is presented in a flow chart in Figure 87.

Table 65: PPE and tools required for manual separation and smashing of CRTs

Item	PPE requirements	Item	Tools and equipment requirements
1	Hard hat	1	Chisel
2	Face shield	2	Hammer
3	Clear safety goggles	3	Spatula
4	Dust mask	4	Brush
5	Ear plugs	5	Vacuum cleaner
6	Coveralls	6	Ladle
7	Long sleeve leather gloves	7	Bulk bags
8	Safety boots	8	Forklift

Pictures showing the typical physical appearance of the metallic, plastic and rubber components manually separated from the CRTs are shown in Figure 88 and Figure 89.

Figure 87: Process flowsheet illustrating the step-wise procedure for the manual separation of CRTs

(a) (b) (c)

Figure 88. Components manually separated from CRTs include (a) shadow mask, (b) metal bands, and (c) plastic casings

(d) (e) (f)

Figure 89. Components manually separated from CRTs include (d) electron gun, (e) rubber inserts, and (c) phosphor dust

APPENDIX G: OTHER RAW MATERIALS

Pictures depicting the typical physical appearance of other raw materials used in the test work are given in Figure 90 and Figure 91.

(a) (b) (c) (d)

Figure 90. Picture of other raw materials including (a) anthracite, (b) Na_2CO_3, (c) $CaCO_3$, and (d) hematite

(a) (b) (c)

Figure 91. Typical physical appearance of recycled materials including (a) CRT slag, (b) CRT fume, and (c) PCB fume

APPENDIX H: DETAILED ANALYTICAL RESULTS OF PCBs

Bulk chemical composition of PCBs

The chemical composition of PCB concentrate as analysed by Mintek's ACD is presented in Table 66. The composition of the metallics component of the PCBs was reconstituted from masses and volumes given in Table 67 and solution concentrations given in Table 73. The final PCB concentrate composition was calculated from the contribution of metallics and ceramics components applying the mass distribution given in Table 69.

Table 68 presents the chemical composition of PCB concentrate as analysed by Scrooby's. A field image map and phases detected by QEMSCAN are shown in Figure 92 and Table 70, respectively. The bulk modal composition of the PCB size fractions and the reconciled composition of the PCB concentrate as analysed by Mintek's MNL is given in Table 71 and Table 72, respectively.

Table 66. Chemical composition of PCB concentrate as analysed by Mintek's ACD, mass %

														Mass, ppm				
Sample	**Al**	**Ca**	**Cr**	**Cu**	**Fe**	**Mg**	**Mn**	**Ni**	**Pb**	**Si**	**Ti**	**Zn**	**Sn**	**Au**	**Pd**	**Pt**	**Ag**	**Total**
Cu	<0.05	<0.05	<0.05	93.2	0.06	<0.05	<0.05	0.10	0.28	0.01	<0.05	0.10	0.40	<0.1	431	18	989	**94.1**
Brass	0.15	<0.05	0.75	66.0	4.09	<0.05	0.07	0.71	1.83	0.03	<0.05	21.1	5.24	<0.1	246	20	1256	**100**
Solder	10.2	<0.05	0.03	21.7	1.48	<0.05	0.01	1.47	6.12	0.02	0.01	10.9	43.6	<0.1	85	<0.1	1536	**95.4**
Mixed fines	0.57	<0.05	<0.05	66.7	1.33	<0.05	0.02	0.15	2.70	0.01	<0.05	2.66	22.8	<0.1	261	<0.1	1474	**96.9**
Metallics	**1.40**	**<0.05**	**0.25**	**67.1**	**1.98**	**<0.05**	**0.03**	**0.47**	**2.28**	**0.02**	**<0.05**	**9.09**	**14.5**	**<0.1**	**273**	**11**	**1304**	**97.2**

Sample	**Al_2O_3**	**CaO**	**Cr_2O_3**	**CuO**	**FeO**	**MgO**	**MnO**	**NiO**	**PbO**	**SiO_2**	**TiO_2**	**ZnO**	**SnO**	**K_2O**	**Na_2O**	**BaO**	**SrO**	**Total**
Ceramics	27.3	0.80	0.22	17.2	2.88	1.59	0.65	0.22	7.27	19.8	0.37	5.79	-	-	-	-	-	**84.1**

														Mass, ppm				
Sample	**Al**	**Ca**	**Cr**	**Cu**	**Fe**	**Mg**	**Mn**	**Ni**	**Pb**	**Si**	**Ti**	**Zn**	**Sn**	**Au**	**Pd**	**Pt**	**Ag**	**Total**
PCB conc	1.90	0.02	0.24	64.3	1.96	0.04	0.05	0.46	2.44	0.38	0.01	8.82	13.8	<0.1	260	10.0	1239	**98.1**

Table 67. Mass and volume of PCB fractions dissolved in Aqua Regia by Mintek's ACD

	Hand sorting		**Dissolution**				**Wash water**
Sample	**Mass (g)**	**Mass fraction**	**Start mass (g)**	**Mass dissolved (g)**	**Vol of filtrate solution (L)**	**Residue (g)**	**Vol of wash water (L)**
Brass	77.9	30%	38.1	37.5	0.133	0.60	0.11
Cu	51.2	20%	24.9	24.7	0.075	0.20	0.10
Solder	30.7	12%	14.9	12.9	0.073	2.00	0.19
Mixed fines	87.8	34%	44.9	39.1	0.126	5.80	0.20
Non-metallics	11.0	4%					
Total	**259**	**100%**	123	114		8.60	

Table 68. Chemical composition of PCB concentrate as analysed by Scrooby's, mass %

														Mass, ppm				
Sample	**Al**	**Ca**	**Cr**	**Cu**	**Fe**	**Mg**	**Mn**	**Ni**	**Pb**	**Si**	**Ti**	**Zn**	**Sn**	**Au**	**Pd**	**Pt**	**Ag**	**Total**
Metallics1	1.29	<0.05	<0.05	62.4	0.93	<0.05	0.08	0.28	8.45	<0.05	<0.05	6.74	17.9	6.00	<0.1	<0.1	854	**98.1**
Metallics2	1.61	<0.05	<0.05	65.2	1.45	<0.05	0.06	0.24	5.56	<0.05	<0.05	10.1	14.6	10.0	<0.1	<0.1	558	**98.8**
Metallics3	2.24	<0.05	<0.05	65.7	0.50	<0.05	0.03	0.25	6.95	<0.05	<0.05	8.73	12.5	22.0	<0.1	<0.1	634	**96.9**
AVERAGE	**1.71**	**<0.05**	**<0.05**	**64.4**	**0.96**	**<0.05**	**0.05**	**0.26**	**6.99**	**<0.05**	**<0.05**	**8.52**	**15.0**	**12.7**	**<0.1**	**<0.1**	**682**	**97.9**
Sample	**Al_2O_3**	**CaO**	**Cr_2O_3**	**CuO**	**FeO**	**MgO**	**MnO**	**NiO**	**PbO**	**SiO_2**	**TiO_2**	**ZnO**	**SnO**	**K_2O**	**Na_2O**	**BaO**	**SrO**	**Total**
Ceramics1	64.1	2.37	0.16	<0.05	0.52	3.64	0.28	0.04	1.27	21.1	0.60	<0.05	<0.05	0.64	<0.05	1.03	0.06	**95.8**
Ceramics2^	12.8	1.00	<0.05	0.10	0.10	<0.05	<0.05	0.2	72.7	10.8	0.30	<0.05	<0.05	0.30	<0.05	0.20	<0.05	**98.5**
Ceramics3	50.7	2.54	0.33	0.3	0.72	4.92	0.12	0.82	<0.05	34.4	0.57	<0.05	<0.05	0.72	<0.05	0.72	<0.05	**96.9**
AVERAGE	**57.4**	**2.46**	**0.25**	**0.30**	**0.62**	**4.28**	**0.20**	**0.43**	**1.30**	**27.8**	**0.59**	**<0.05**	**<0.05**	**0.68**	**<0.05**	**0.88**	**0.06**	**97.1**
^ - values not included in calculation of average composition for ceramics due to significant anomaly with results of this sample																		
														Mass, ppm				
Sample	**Al**	**Ca**	**Cr**	**Cu**	**Fe**	**Mg**	**Mn**	**Ni**	**Pb**	**Si**	**Ti**	**Zn**	**Sn**	**Au**	**Pd**	**Pt**	**Ag**	**Total**
PCB conc	2.84	0.07	0.01	61.22	0.93	0.10	0.06	0.26	6.68	0.52	0.01	8.10	14.3	12	<0.1	<0.1	648	**95.1**

Table 69. Distribution of metallics, ceramics and plastics from PCB concentrate analysed by Scrooby's, mass %

Sample	Metallics	Ceramics	Plastics	Total
PCB conc1	96.0	3.2	0.79	**100**
PCB conc2	95.3	4.6	0.09	**100**
PCB conc3	94.1	4.07	1.82	**100**
AVERAGE	**95.1**	**4.0**	**0.9**	**100**

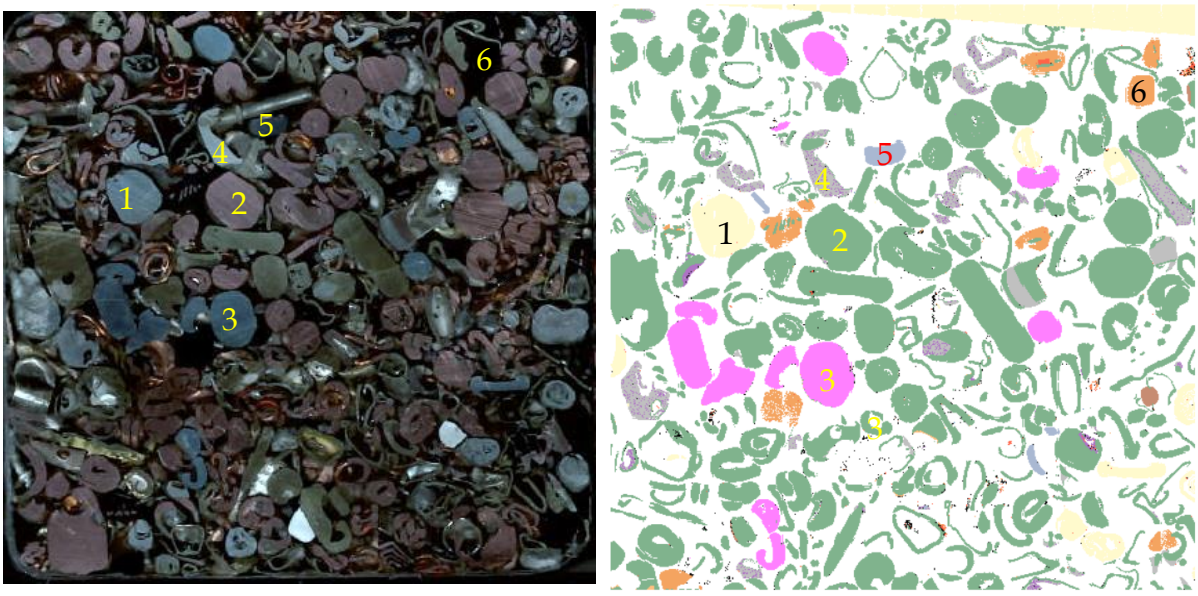

(a) (b)

Figure 92. Image of (a) polished slab of PCB concentrate, and (b) false colour field image map generated by QEMSCAN. Particles numbered are 1=Al, 2=Cu, 3=Zn, 4=SnPb, 5=Fe, 6=ceramic

Table 70. List of metals, alloys and oxides detected with the QEMSCAN by Mintek's MNL

Grouping	Metal/alloy	Grouping	Metal/alloy/oxide
Cu	Cu	Ag	Ag
	CuZn (brass)		AgNi
	CuZnNi	Nickel	Ni
	CuNi		NiSn
	CuSn		NiP
	CuMn	Silicon	Si
Zn	Zn	Titanium	Ti
	ZnSn		TiV
Al	Al		TiMn
	AlAg	Manganese	MnNi
Pb	Pb	Ceramics	SiO_2
	PbTi		MnO
	PbSn (solder)		SiMgAlCaO
	PbSi		AlSiO
Sn	Sn		AlCaO
	SnPb		CuZnSnFeSiO
	SnCu		AgPdCaAlSiO
Iron	Fe	Other	Plastics
	FeCr		
	FeCrNi		
	FeCrMn		
	FeNi		
	FeNiCo		

Table 71. Bulk modal composition of PCB concentrate fractions as analysed with QEMSCAN by Mintek's MNL

Phase Grouping	Abundance (mass %)				
	+3.35mm	+2.36mm	+1.7mm	-1.7mm	Total
Cu	26.6	18.4	16	9.4	70.3
Zn	2.4	0.5	0.1	0.2	3.2
Al	0.6	0.6	0.6	0.2	2
Pb	0.4	1.6	1.2	1.5	4.8
Sn	1.9	4.1	4.9	5	15.9
Fe	0.3	0.4	0.4	0.2	1.3
Ag	0.1	<0.1	<0.1	<0.1	0.2
Ni	<0.1	<0.1	<0.1	<0.1	0.1
Si	<0.1	<0.1	<0.1	<0.1	0.1
Ti	<0.1	<0.1	0.1	<0.1	0.1
Mn	0.5	0.2	0.1	<0.1	0.8
Ceramics	0.1	0.3	0.4	0.3	1.1

Table 72. Reconciled chemical composition of PCB concentrate as analysed by Mintek's MNL, mass %

Sample	Al	Ag	Cu	Fe	Mg	Mn	Ni	Pb	Si	Sn	Zn	Total
PCB conc	2	0.2	62.2	1.1	0.01	0.1	0.3	6.8	0.3	13.5	10.6	**97.1**

Table 73. Concentration of base metals in filtrate (FF) and wash water (WW) solutions collected after dissolution of PCB fractions in Aqua Regia, mass in ppm

Sample	Al	Cr	Cu	Fe	Mg	Mn	Ni	Pb	Si	Ti	Zn
Mixed fines FF	1685	7.93	193.5^	3935	<2	65.6	450	5645	18.8	8.27	7845
Mixed fines WW	59.3	<2	8340	126	<2	2.39	15.4	1710	4.60	<2	257
Brass FF	431	2080	184^	11.4^	4.26	206	1980	4630	72.3	3.59	58.8^
Brass WW	7.54	29.9	2810	169	<2	3.53	30.1	684	6.51	<2	915
Cu FF	11.8	<2	295^	187	12.7	4.38	317	879	8.92	<2	313
Cu WW	<2	<2	8925	7.10	<2	<2	9.51	31.3	6.36	<2	10.2
Solder FF	16.9^	47.7	35.7^	2510	7.96	15.6	2440	2930	17.4	14.6	18^
Solder WW	402	<2	967	39.4	<2	<2	62	2970	5.52	<2	456

^ - *mass reported in g/L*

Table 74. Concentration of precious metals in filtrate (FF) and wash water (WW) solutions collected after dissolution of PCB fractions in Aqua Regia, mass in ppm

Sample	Ag	Au	Ir	Os	Pd	Pt	Rh	Ru
Mixed fines FF	454	<5	<5	13.3	81.1	<5	<5	17.5
Mixed fines WW	2.20	<5	<5	<5	<5	<5	<5	<5
Brass FF	354	<5	<5	41.1	69.4	5.59	<5	46
Brass WW	0.63	<5	<5	<5	<5	<5	<5	<5
Cu FF	325	<5	<5	<5	142	6.08	<5	<5
Cu WW	1.66	<5	<5	<5	<5	<5	<5	<5
Solder FF	269	<5	<5	<5	15.1	<5	<5	11
Solder WW	1.10	<5	<5	<5	<5	<5	<5	<5

Phase-chemical composition of PCB concentrate

The Cu-rich fraction (see Figure 93) predominantly contained Cu metal varying in shapes from rounded to elongated and angular particles. Some of these Cu particles had rims of Sn-Pb alloy. The Cu-Zn-rich fraction (see Figure 94) comprised mostly Cu and Cu-Zn alloy. Minor presence of Sn-Pb alloy and Sn metal were also detected. Traces of Fe and Al metal were also detected in this sample. The mixed-fines fraction (see Figure 95) was composed of Cu and Sn metal, and alloys of Cu-Sn, and Sn-Pb.

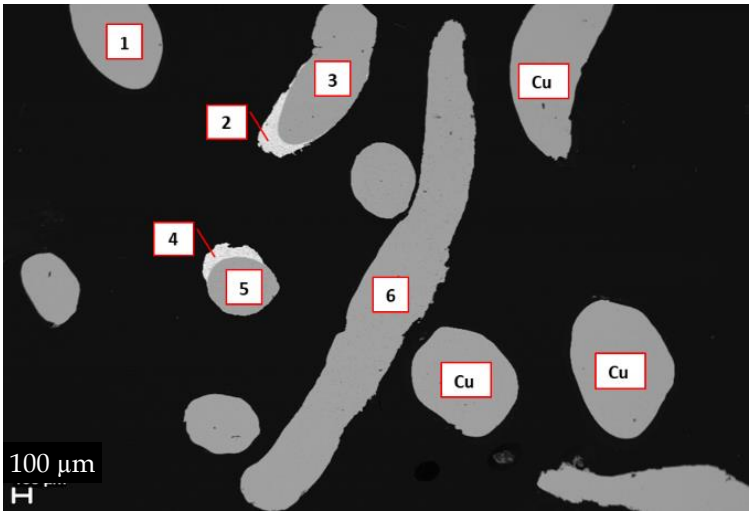

(a)

No.	Cu	Sn	Pb	Phase
1	100			Cu metal
3	100			Cu metal
5	100			Cu metal
6	100			Cu metal
2		100		Sn metal
4		10.4	89.6	PbSn alloy

(b)

Figure 93. (a) SEM BSE micrograph of Cu-rich fraction of PCB concentrate, with scale bar indicating 100 µm, and (b) EDS point analysis

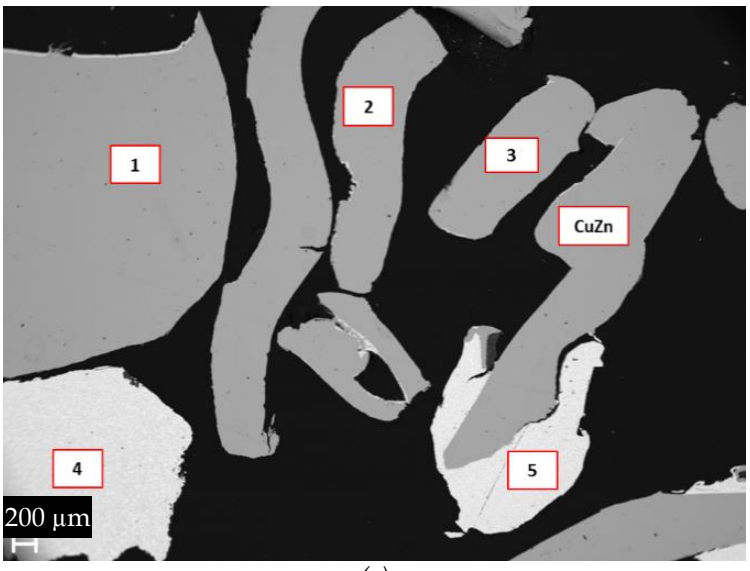

(a)

No.	Cu	Zn	Sn	Pb	Phase
1	67.5	32.5			CuZn
2	64.2	35.8			CuZn
3	66.0	34.0			CuZn
4			77.9	22.1	SnPb
5			77.7	22.3	SnPb

(b)

Figure 94. (a) SEM BSE micrograph of CuZn-rich fraction of PCB concentrate, with scale bar indicating 200 µm, and (b) EDS point analysis

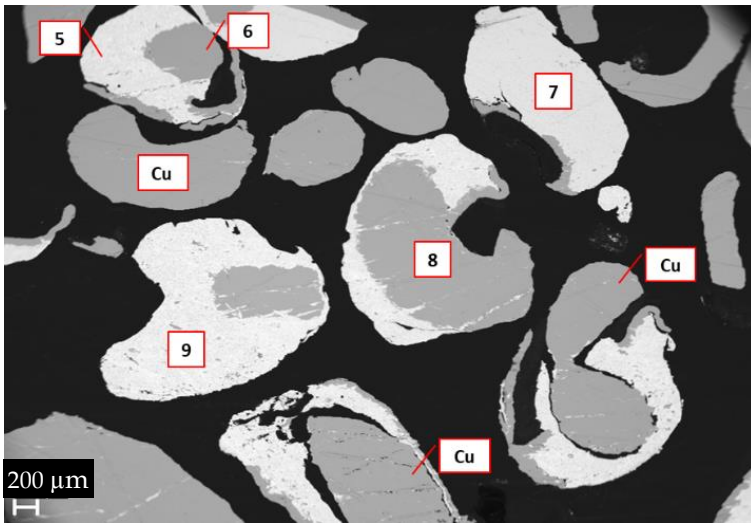

(a)

No.	Cu	Sn	Pb	Phase
5		90.9	9.1	SnPb alloy
6	90.1	9.9		CuSn alloy
7		88.2	11.8	SnPb alloy
8	100.0			Cu metal
9		100.0		Sn metal

(b)

Figure 95. (a) SEM BSE micrograph of mixed fraction of PCB concentrate, with scale bar indicating 200 µm, and (b) EDS point analysis

APPENDIX I: TEMPERATURE VERIFICATION PROFILES

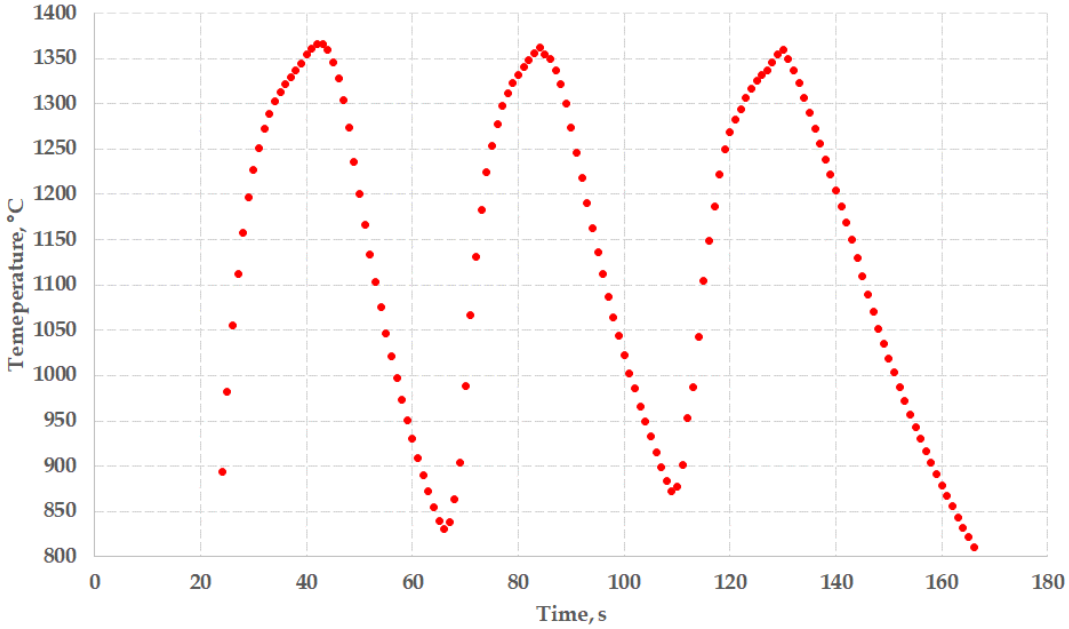

Figure 96. Temperature verification of metal bath from PCBs smelting Test 32 during Stage 2

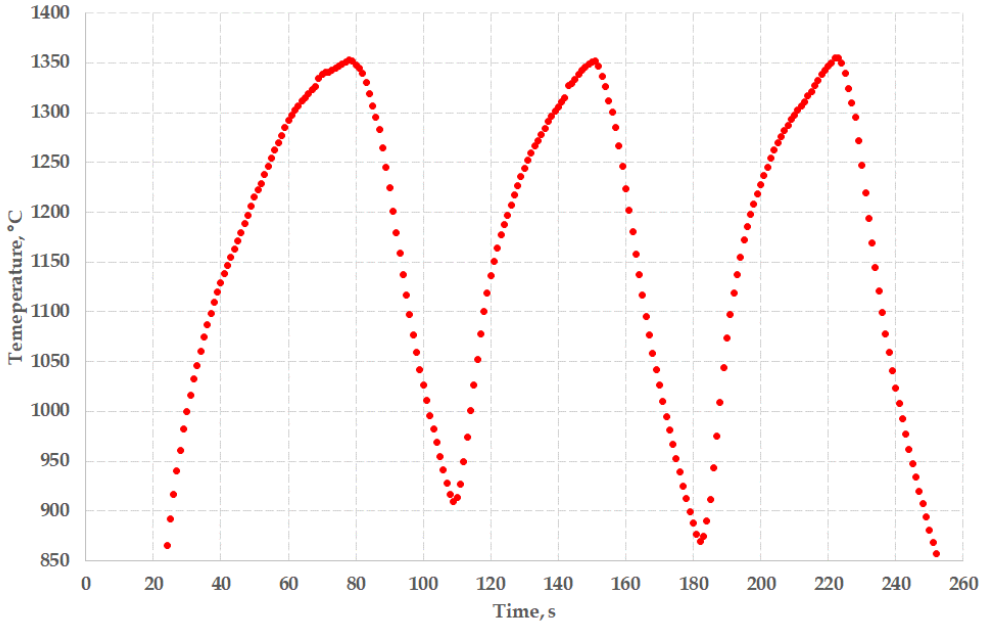

Figure 97. Temperature verification of slag bath from PCBs smelting Test 32 during Stage 3

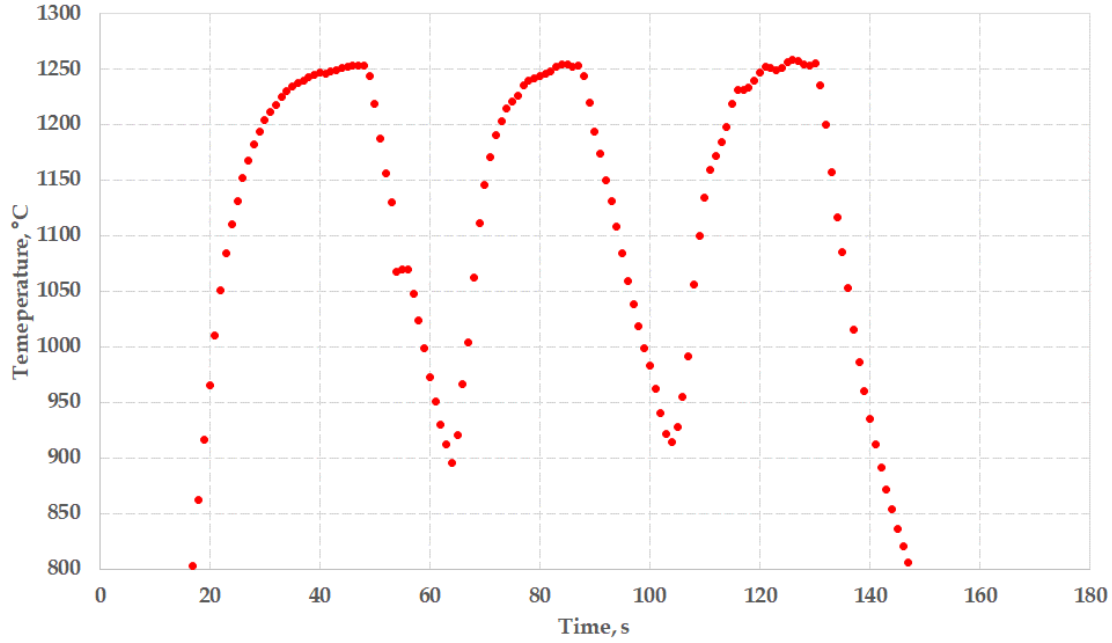

Figure 98. Temperature verification of slag bath from CRTs smelting Test 9 during the 2nd 30 min in Stage 3

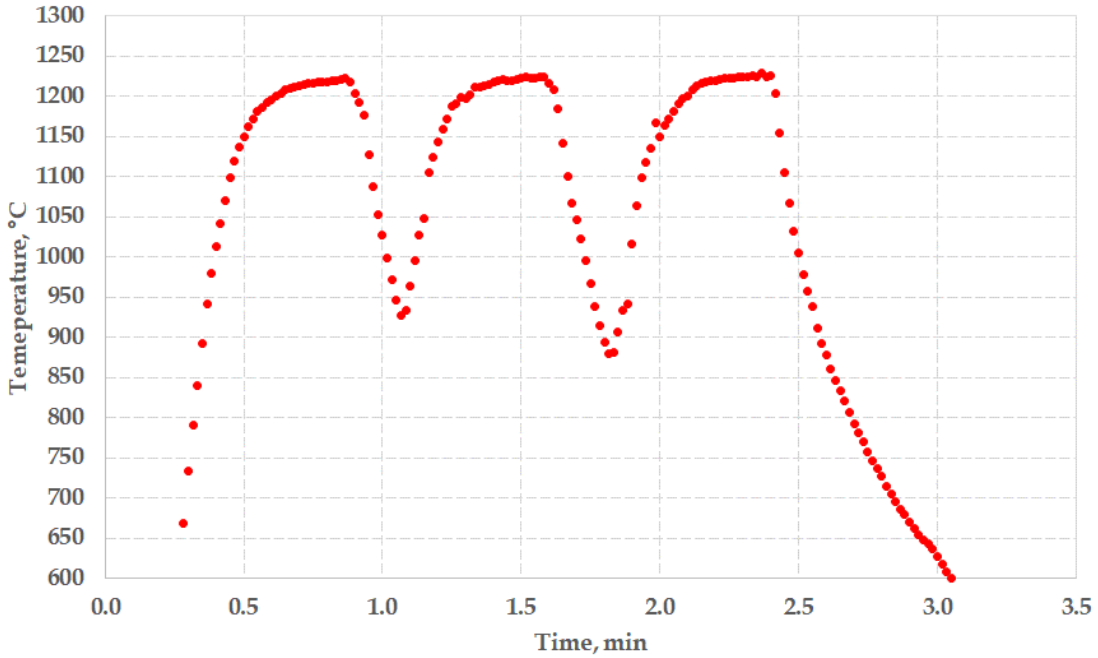

Figure 99. Temperature verification of slag bath from CRTs smelting Test 9 during the 3rd 30 min in Stage 3

APPENDIX J: COMPLETE SET OF RESULTS OF PCBs SMELTING TESTS

Table 75. Complete list of product masses and tapping temperatures of PCBs smelting tests

Test No.	Test Repeat	Changing Variable	Test Time, h	Metal, kg	Slag, kg	Cartridge Fumes, kg	Extraction Fumes, kg	Tapping Temp, °C
1	-	Oxidation time	2.3	5.09	1.45	0.26	-	1357
2	-	Oxidation time	3.0	5.37	-	0.95	-	1359
3	-	Oxidation time	5.0	3.92	2.24	0.80	-	1341
4	-	Oxidation time	2.5	6.11	7.34	0.39	-	1379
5	-	Oxidation time	3.2	7.36	4.58	0.12	-	1339
6	-	Oxidation time	3.7	7.17	4.43	0.67	0.20	1349
7	-	Oxidation time	2.6	7.39	7.24	0.56	-	1334
8	-	Oxidation time	3.4	6.50	8.50	0.67	-	1350
9	-	Oxidation time	3.8	2.52	10.4	1.15	0.51	1404
10	-	Flame stoich.	3.3	7.52	8.78	0.80	-	1340
11	-	Flame stoich.	2.6	6.05	9.12	0.68	-	1369
12	-	Flame stoich.	2.7	4.04	10.5	0.32	0.53	1362
13	-	Fluxing agent	3.1	7.41	4.85	0.17	-	1333
14	-	Fluxing agent	3.1	8.43	8.49	0.77	-	1360
15	-	Fluxing agent	3.1	8.46	7.90	1.21	0.97	1317
16	1R	Oxidation time	2.7	7.00	3.01	0.49	-	1327
17	2R	Oxidation time	3.2	5.37	-	0.80	-	1383
18	3R	Oxidation time	3.7	7.57	-	1.05	0.29	1339
19	4R	Oxidation time	2.6	7.03	6.25	0.56	-	1342
20	5R	Oxidation time	3.1	7.61	5.42	0.32	-	1356
21	6R	Oxidation time	3.6	7.38	5.11	0.95	1.02	1328
22	10R	Flame stoich.	2.6	7.30	7.79	0.86	-	1321
23	11R	Flame stoich.	2.5	7.65	8.39	0.98	-	1368
24	12R	Flame stoich.	2.7	7.25	8.28	0.71	0.80	1342
25	13R	Fluxing agent	3.3	7.56	4.88	0.95	-	1279
26	14R	Fluxing agent	3.1	8.10	7.95	0.75	-	1341
27	15R	Fluxing agent	3.1	8.00	7.65	0.47	-	1323
28	7R	Oxidation time	2.6	7.40	8.00	0.39	-	1339
29	8R	Oxidation time	3.1	7.01	8.68	0.36	-	1332
30	9R	Oxidation time	3.6	7.04	7.99	0.47	1.22	1370
31	-	Oxidation time	2.6	7.41	8.01	0.82	-	1353
32	-	Oxidation time	3.2	6.21	8.77	0.57	-	1363
33	-	Oxidation time	3.6	4.78	8.92	1.10	-	1370
34	-	Flux ratio	3.1	7.26	6.91	0.85	-	1369
35	-	Flux ratio	3.1	7.11	10.2	0.50	-	1334
36	-	Flux ratio	3.0	7.18	2.64	0.41	1.16	1352
Total	**-**	**-**	**111**	**243**	**231**	**24**	**6.7**	**-**

Table 76. Chemical composition of metals from PCBs smelting tests, wt%

									Mass, ppm			
Test	**Cu**	**Fe**	**Mn**	**Ni**	**Pb**	**Si**	**Zn**	**Sn**	**Au**	**Pd**	**Pt**	**Ag**	**Total**
1	86.5	<0.05	<0.05	0.32	1.77	<0.05	<0.05	11.3	62.1	173	<2	1533	100
2	94.1	<0.05	<0.05	0.29	0.47	<0.05	<0.05	4.93	62.8	188	<2	1700	100
3	99.7	<0.05	<0.05	0.08	0.05	<0.05	<0.05	0.04	98.7	200	15.6	558	100
4	93.6	<0.05	<0.05	0.39	1.02	<0.05	<0.05	4.83	47.1	187	<2	1500	100
5	81.2	<0.05	<0.05	0.46	1.93	<0.05	<0.05	16.3	33.0	174	15.5	849	100
6	83.4	<0.05	<0.05	0.47	2.11	<0.05	<0.05	13.9	41.7	165	<2	740	100
7	81.2	<0.05	<0.05	0.42	3.11	<0.05	<0.05	15.1	39.8	161	<2	1400	100
8	90.3	<0.05	<0.05	0.33	1.16	<0.05	<0.05	8.08	54.8	54.8	54.8	1400	100
9	99.7	<0.05	<0.05	0.05	0.09	<0.05	<0.05	0.01	58.1	189	<2	1100	100
10	99.3	<0.05	<0.05	0.42	0.13	<0.05	<0.05	0.01	53.4	174	<2	980	100
11	95.5	<0.05	<0.05	0.21	0.77	<0.05	<0.05	3.31	72.6	197	<2	1700	100
12	88.1	<0.05	<0.05	0.10	0.14	<0.05	<0.05	11.5	85.7	205	<2	1100	100
13	81.3	<0.05	<0.05	0.42	3.46	<0.05	<0.05	14.7	46.7	156	15.8	1450	100
14	80.2	<0.05	<0.05	0.46	4.74	<0.05	<0.05	14.4	36.4	151	17.6	1200	100
15	80.9	<0.05	<0.05	0.44	5.07	<0.05	<0.05	13.4	47.3	155	29.9	1700	100
16	87.6	<0.05	<0.05	0.39	1.73	<0.05	<0.05	10.2	48.6	176	3.84	1400	100
17	92.6	<0.05	<0.05	0.35	0.29	<0.05	<0.05	6.61	45.8	177	8.17	1000	100
18	99.7	<0.05	<0.05	0.11	0.08	<0.05	<0.05	0.01	76.2	183	6.99	920	100
19	87.5	<0.05	<0.05	0.48	0.93	<0.05	<0.05	10.9	43.8	170	12.2	980	100
20	85.6	<0.05	<0.05	0.40	1.43	<0.05	<0.05	12.4	44.7	173	835	940	100
21	85.8	<0.05	<0.05	0.40	1.25	<0.05	<0.05	12.4	49.3	169	18.3	1200	100
22	84.0	<0.05	<0.05	0.41	2.40	<0.05	<0.05	13.1	45.4	163	35	1200	100
23	82.4	<0.05	<0.05	0.41	2.73	<0.05	<0.05	14.4	45.6	158	28.0	730	100
24	87.4	<0.05	<0.05	0.43	1.60	<0.05	<0.05	10.4	46.8	167	22.4	860	100
25	83.9	<0.05	<0.05	0.37	2.88	<0.05	<0.05	12.8	49.4	165	7.7	530	100
26	82.1	<0.05	<0.05	0.39	4.26	<0.05	<0.05	13.2	44.2	163	180	640	100
27	84.4	<0.05	<0.05	0.37	3.40	<0.05	<0.05	11.7	41.5	166	16.2	890	100
28	84.5	<0.05	<0.05	0.37	1.93	<0.05	<0.05	13.1	46.4	165	16.4	955	100
29	87.9	<0.05	<0.05	0.35	1.78	<0.05	<0.05	9.84	51.0	170	8.18	1200	100
30	87.8	<0.05	<0.05	0.34	1.22	<0.05	<0.05	10.5	48.5	165	8.82	820	100
31	82.7	<0.05	<0.05	0.37	2.89	<0.05	<0.05	13.9	40.2	159	<2	830	100
32	95.1	<0.05	<0.05	0.27	0.65	<0.05	<0.05	3.89	53.9	178	38.5	1100	100
33	99.1	<0.05	<0.05	0.09	0.62	<0.05	<0.05	0.01	23.7	211	30.9	1410	100
34	83.6	<0.05	<0.05	0.46	2.80	<0.05	<0.05	13.1	50.6	186	19.4	501	100
35	86.4	<0.05	<0.05	0.45	1.96	<0.05	<0.05	11.2	37.3	181	0.85	447	100
36	85.3	<0.05	<0.05	0.44	1.42	<0.05	<0.05	12.7	35.6	172	31.0	1240	100

Table 77. Chemical composition of slags from PCBs smelting tests, wt%

																Mass, ppm			
Test	**Al_2O_3**	**CaO**	**CuO**	**FeO**	**MgO**	**MnO**	**NiO**	**PbO**	**SiO_2**	**ZnO**	**SnO_2**	**K_2O**	**Na_2O**	**BaO**	**SrO**	**Au**	**Pd**	**Pt**	**Ag**	**Total**
1	16.3	0.87	4.0	48.6	0.47	2.62	<0.05	0.17	21.3	0.34	1.35	0.81	1.24	0.83	0.24	0.84	0.18	<0.02	128	99.1
2	-	-	-	-	-	-	-	-	-	-	-	-	-	-	-	-	-	-	-	-
3	8.88	1.04	60.8	8.65	0.36	0.40	0.51	0.86	8.3	1.70	7.54	0.53	1.17	0.34	0.23	8.38	1.60	0.05	930	101
4	18.2	3.43	10.6	17.2	0.95	0.83	0.28	0.86	22.0	1.75	8.24	2.81	5.59	1.21	0.69	1.05	0.29	0.06	147	94.7
5	17.6	4.07	2.45	22.5	1.18	1.08	0.07	0.13	28.0	0.58	2.98	2.81	9.12	1.54	0.75	0.40	0.10	0.04	38.2	94.9
6	17.3	4.07	4.92	23.0	1.16	0.93	<0.05	0.22	27.0	0.70	2.64	3.00	7.90	1.47	0.82	1.48	0.31	0.03	124	95.2
7	11.8	4.51	1.51	24.7	1.21	1.16	<0.05	0.10	30.4	0.24	2.17	3.96	9.88	1.73	1.13	0.35	0.09	0.03	20.4	94.4
8	14.2	4.08	4.16	20.1	1.12	0.99	0.08	0.44	32.9	0.63	5.22	2.83	7.37	1.60	0.98	0.66	0.16	0.03	44.8	96.7
9	10.3	2.98	32.05	13.4	0.80	0.72	0.22	0.86	20.0	1.00	5.90	2.43	5.81	1.08	0.68	2.70	0.52	0.04	420	98.2
10	14.2	4.17	2.97	22.4	1.16	1.08	<0.05	0.24	28.2	0.71	3.48	3.36	6.76	1.48	0.96	0.52	0.10	0.05	28.0	91.2
11	9.07	3.85	10.1	20.7	0.99	0.76	0.20	1.99	24.2	1.23	9.79	3.20	6.17	1.29	0.90	0.55	0.12	0.02	56.4	94.5
12	10.5	3.44	19.0	17.6	0.95	0.84	0.25	1.14	22.9	1.22	6.87	2.35	6.72	1.24	0.80	0.36	0.08	0.03	120	95.9
13	14.1	5.89	3.27	6.51	1.61	0.34	0.07	0.07	39.2	0.45	1.16	3.71	15.5	1.77	1.35	0.63	0.17	0.52	36.1	94.9
14	12.5	25.7	1.04	3.92	1.62	0.26	<0.05	0.06	30.7	0.41	0.68	3.38	11.0	1.30	1.03	0.21	0.06	0.04	13.6	93.6
15	13.8	6.90	1.19	3.73	1.26	0.25	<0.05	0.05	32.1	0.63	1.57	2.45	30.1	1.29	1.04	0.35	0.09	0.02	17.5	96.3
16	27.0	3.86	5.81	10.8	0.96	0.61	0.11	0.60	24.6	1.51	6.46	1.80	11.7	0.98	0.44	0.82	0.17	0.03	112	97.2
17	-	-	-	-	-	-	-	-	-	-	-	-	-	-	-	-	-	-	-	-
18	-	-	-	-	-	-	-	-	-	-	-	-	-	-	-	-	-	-	-	-
19	12.3	4.17	2.30	22.5	1.23	1.12	<0.05	0.16	31.7	0.50	2.07	3.50	10.1	1.50	1.04	0.89	0.19	0.02	33.7	94.2
20	19.1	3.69	3.86	19.7	1.19	1.10	0.07	0.41	30.2	1.67	2.92	2.60	6.39	1.24	0.66	1.80	0.42	0.07	63.5	94.7
21	17.5	3.82	2.92	20.5	1.20	1.14	<0.05	0.19	30.3	0.58	2.93	2.75	7.11	1.37	0.85	0.70	0.16	<0.02	43.2	93.1
22	17.9	3.46	6.11	18.8	1.13	1.02	0.17	0.33	27.6	1.29	5.29	2.65	6.71	1.18	0.71	0.87	0.18	<0.02	81.5	94.3
23	11.9	4.23	2.12	22.5	1.24	1.11	<0.05	0.17	35.3	0.49	2.04	3.00	8.14	1.44	1.07	0.80	0.16	<0.02	55.4	94.8
24	13.4	4.17	2.52	21.5	1.18	1.12	<0.05	0.15	33.6	0.35	2.27	3.29	8.61	1.46	1.04	0.51	0.07	<0.02	20.0	94.6
25	14.6	5.92	1.73	6.54	1.59	0.41	<0.05	0.12	42.6	0.55	0.03	3.53	10.9	1.65	1.34	0.64	0.13	<0.02	59.1	91.4
26	13.2	25.5	0.67	3.70	1.53	0.27	<0.05	0.11	36.7	0.25	0.55	2.41	9.73	1.28	1.06	0.06	0.03	<0.02	11.4	96.9
27	12.9	7.33	1.41	3.38	1.14	0.25	<0.05	0.13	32.3	0.55	2.37	2.32	25.8	1.25	1.04	0.12	0.04	<0.02	11.9	92.1
28	14.1	4.65	1.98	21.7	1.11	1.12	<0.05	0.23	35.5	0.32	1.65	2.45	9.56	1.43	1.05	0.42	0.10	<0.02	23.6	96.9

29	13.7	3.92	3.61	22.5	0.98	1.12	0.06	1.18	31.7	0.30	4.67	1.97	9.18	1.31	0.95	0.66	0.10	<0.02	26.4	97.1
30	12.6	3.98	4.13	22.8	1.04	1.16	0.06	0.69	32.9	0.27	5.25	2.02	8.64	1.37	1.00	1.58	0.29	<0.02	61.0	97.9
31	11.2	4.38	1.65	25.5	1.11	1.30	<0.05	0.20	36.0	0.40	1.02	2.22	7.98	1.46	1.14	0.48	0.12	<0.02	32.5	95.5
32	11.2	3.88	5.96	21.9	0.98	1.11	0.17	1.08	31.9	0.75	6.22	2.03	7.01	1.29	0.93	0.56	0.12	0.18	46.3	96.4
33	7.22	3.44	18.4	18.9	0.83	0.93	0.24	2.43	27.4	0.87	5.57	1.55	5.54	1.12	0.87	1.72	0.34	<0.02	26.3	95.3
34	14.7	4.52	3.42	16.3	1.18	0.85	<0.05	0.56	36.4	1.99	2.46	2.15	8.37	1.45	1.08	1.29	0.24	<0.02	74.4	95.5
35	12.8	3.54	2.43	28.3	0.98	1.45	<0.05	0.51	34.0	0.49	2.77	1.69	5.87	1.33	0.91	0.43	0.10	0.03	164	97.0
36	21.9	5.34	10.4	17.2	0.91	0.79	0.31	0.86	26.3	2.39	7.26	1.67	3.66	1.05	0.60	2.37	0.41	0.07	444	101

Table 78. Chemical composition of fumes from PCBs smelting tests, wt%

																Mass, ppm				
Test	**Al_2O_3**	**CaO**	**CuO**	**FeO**	**MgO**	**MnO**	**NiO**	**PbO**	**SiO_2**	**ZnO**	**SnO_2**	**K_2O**	**Na_2O**	**BaO**	**SrO**	**Au**	**Pd**	**Pt**	**Ag**	**Total**
1	1.03	2.05	1.20	2.41	0.40	0.08	0.17	23.3	0.87	50.2	14.4	0.59	0.36	<0.05	<0.05	0.62	0.23	0.30	877	97.1
2	0.34	0.28	2.29	0.41	<0.05	<0.05	<0.05	25.6	<0.05	47.9	21.3	0.34	0.14	<0.05	<0.05	1.98	0.25	1.99	1500	98.7
3	0.28	0.46	2.13	0.60	0.22	<0.05	0.09	26.2	<0.05	48.3	21.8	0.44	0.22	<0.05	<0.05	1.70	0.25	0.16	1100	101
4	0.15	0.36	1.46	0.40	0.22	<0.05	0.07	25.0	<0.05	46.8	24.4	0.43	0.22	<0.05	<0.05	1.16	0.19	0.15	750	99.6
5	<0.05	0.28	1.85	0.64	0.13	<0.05	<0.05	22.3	<0.05	46.8	21.3	0.42	0.20	<0.05	<0.05	0.27	0.06	<0.02	1100	94.0
6	<0.05	<0.05	2.60	0.41	0.12	<0.05	<0.05	25.5	<0.05	49.2	14.1	0.43	0.27	<0.05	<0.05	0.91	0.21	0.09	1233	92.8
7	<0.05	0.14	2.10	0.14	<0.05	<0.05	<0.05	27.6	<0.05	55.9	13.6	0.48	0.30	<0.05	<0.05	0.89	0.18	0.08	1100	100
8	<0.05	0.11	1.70	0.15	0.10	<0.05	<0.05	29.7	<0.05	52.4	15.9	0.40	0.20	<0.05	<0.05	1.20	0.19	0.03	1400	101
9	<0.05	<0.05	1.89	0.18	<0.05	<0.05	<0.05	29.2	<0.05	52.5	16.1	0.44	0.28	<0.05	<0.05	2.03	0.24	0.09	2800	101
10	0.13	0.11	1.75	0.13	0.13	<0.05	<0.05	29.8	<0.05	51.8	18.3	0.54	0.20	<0.05	<0.05	1.10	0.16	<0.02	1600	103
11	0.20	<0.05	1.48	0.09	<0.05	<0.05	<0.05	30.1	<0.05	44.7	21.5	0.38	0.16	<0.05	<0.05	1.53	0.12	0.03	3050	98.8
12	0.25	<0.05	1.82	0.10	<0.05	<0.05	<0.05	29.7	<0.05	50.4	17.9	0.49	0.31	<0.05	<0.05	1.92	0.17	<0.02	2300	101
13	0.38	<0.05	2.35	0.08	<0.05	<0.05	<0.05	28.3	<0.05	51.5	12.1	0.59	0.51	<0.05	<0.05	1.19	0.15	<0.02	4000	96.3
14	0.23	0.07	1.70	0.09	0.08	<0.05	<0.05	27.3	<0.05	57.0	11.3	0.76	0.59	<0.05	<0.05	1.34	0.18	<0.02	6300	99.7
15	0.13	<0.05	1.66	0.10	<0.05	<0.05	<0.05	25.0	<0.05	53.6	8.56	1.51	1.92	<0.05	<0.05	1.07	0.14	<0.02	4900	93.0
16	0.24	<0.05	1.10	0.08	<0.05	<0.05	<0.05	23.9	<0.05	55.1	13.2	1.24	1.66	<0.05	<0.05	1.09	0.13	<0.02	2500	96.7

17	0.21	0.18	1.58	0.07	0.09	<0.05	<0.05	29.8	<0.05	41.6	23.5	0.55	0.74	<0.05	<0.05	2.05	0.19	<0.02	3500	98.7
18	0.53	<0.05	1.85	0.07	<0.05	<0.05	<0.05	26.8	<0.05	41.4	27.9	0.37	0.47	<0.05	<0.05	1.34	0.15	<0.02	4800	100
19	0.18	<0.05	1.95	<0.05	<0.05	<0.05	<0.05	25.4	<0.05	48.4	22.1	0.30	0.23	<0.05	<0.05	0.87	0.12	<0.02	2300	98.8
20	0.15	<0.05	1.55	0.08	<0.05	<0.05	<0.05	25.2	<0.05	51.8	14.3	0.36	0.31	<0.05	<0.05	0.80	0.13	0.02	838	93.9
21	0.10	<0.05	2.18	0.20	<0.05	<0.05	<0.05	27.6	<0.05	41.2	21.7	0.38	0.36	<0.05	<0.05	0.91	0.14	<0.02	3200	94.1
22	0.11	<0.05	1.48	0.13	<0.05	<0.05	<0.05	27.1	<0.05	51.4	10.89	0.41	0.32	<0.05	<0.05	0.68	0.12	<0.02	4400	92.3
23	0.10	<0.05	1.44	0.10	<0.05	<0.05	<0.05	26.9	<0.05	51.6	10.84	0.44	0.34	<0.05	<0.05	0.71	0.12	0.03	3900	92.2
24	0.10	<0.05	1.10	0.24	<0.05	<0.05	<0.05	25.7	<0.05	49.6	14.9	0.54	0.36	<0.05	<0.05	1.06	0.13	<0.02	2900	92.9
25	<0.05	<0.05	1.41	<0.05	<0.05	<0.05	<0.05	28.3	<0.05	46.5	16.3	0.70	0.58	<0.05	<0.05	0.86	0.13	<0.02	3700	94.2
26	0.10	<0.05	1.33	0.13	<0.05	<0.05	<0.05	25.4	<0.05	54.1	8.24	0.91	0.80	<0.05	<0.05	0.73	0.12	<0.02	2950	91.2
27	<0.05	<0.05	1.79	<0.05	<0.05	<0.05	<0.05	23.4	<0.05	58.0	6.32	1.28	3.08	<0.05	<0.05	0.82	0.13	<0.02	3900	94.2
28	<0.05	<0.05	1.55	<0.05	<0.05	<0.05	<0.05	26.8	<0.05	53.6	6.61	0.94	1.04	<0.05	<0.05	0.66	0.10	<0.02	4800	91.1
29	<0.05	<0.05	1.88	<0.05	<0.05	<0.05	<0.05	29.6	<0.05	50.8	8.52	0.82	0.99	<0.05	<0.05	0.91	0.14	<0.02	3500	92.9
30	0.09	<0.05	2.97	<0.05	<0.05	<0.05	<0.05	36.5	<0.05	50.3	11.8	0.77	0.81	<0.05	<0.05	1.13	0.18	<0.02	2500	103
31	<0.05	<0.05	1.29	<0.05	<0.05	<0.05	<0.05	30.4	<0.05	60.9	5.66	0.68	0.66	<0.05	<0.05	0.70	0.16	<0.02	3800	99.9
32	<0.05	<0.05	1.34	<0.05	<0.05	<0.05	<0.05	29.1	<0.05	52.3	18.2	0.56	0.43	<0.05	<0.05	1.16	0.17	<0.02	5000	103
33	<0.05	<0.05	1.50	<0.05	<0.05	<0.05	<0.05	28.2	<0.05	47.2	23.7	0.64	0.47	<0.05	<0.05	2.39	0.25	0.03	3000	102
34	<0.05	<0.05	1.90	<0.05	<0.05	<0.05	<0.05	28.9	<0.05	55.4	16.0	0.53	0.42	<0.05	<0.05	1.04	0.17	<0.02	6300	104
35	<0.05	<0.05	1.50	<0.05	<0.05	<0.05	<0.05	29.6	<0.05	54.7	13.1	0.70	0.61	<0.05	<0.05	1.00	0.15	0.02	3600	101
36	<0.05	<0.05	2.27	<0.05	<0.05	<0.05	<0.05	29.9	<0.05	59.7	11.03	0.43	0.32	<0.05	<0.05	1.13	0.18	<0.02	3300	104
B1-36	<0.05	<0.05	1.7	<0.05	<0.05	<0.05	<0.05	27.5	<0.05	53.9	15.5	0.72	0.78	<0.05	<0.05	1.24	0.16	0.08	3400	100
EHF	2.17	0.43	13.8	1.45	<0.05	<0.05	0.08	25.7	1.26	37.3	8.86	0.56	0.96	<0.05	<0.05	8.27	2.71	2.19	5100	93.1
BHF	7.82	1.41	1.70	5.92	1.41	0.76	<0.05	21.5	6.51	36.5	9.90	0.71	0.65	<0.05	<0.05	0.92	409	200	2200	95.0

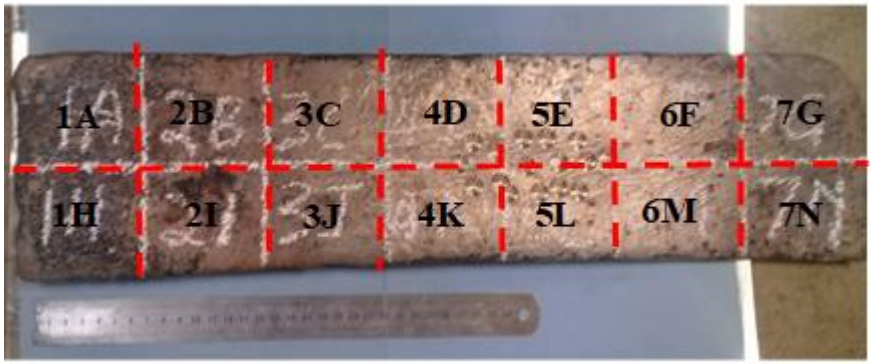

Figure 100. Image of metal slab from PCBs smelting Test 12 showing the 14 sections analysed to assess compositional variation

Table 79. Chemical composition of the 14 sections of metal slab from PCBs smelting Test 12 to assess composition variation, mass in wt%

Sample ID	Pb	Sn	P	S	Fe	Ni	As	Sb	Bi	Mg	Zn	Mn	Si	Al	Cu
1_A Spark 1	2.21	11.66	0.0048	0.021	0.082	0.428	0.0069	0.097	0.0045	0.0001	<0.002	<0.0005	<0.001	<0.0002	85.5
1_A Spark 2	2.13	11.60	0.0050	0.021	0.089	0.431	0.0072	0.099	0.0045	0.0001	<0.002	<0.0005	<0.001	<0.0002	85.6
1_A Spark 3	2.14	11.64	0.0049	0.022	0.080	0.432	0.0072	0.100	0.0046	0.0001	<0.002	<0.0005	<0.001	<0.0002	85.6
1_A Average	2.16	11.63	0.0049	0.022	0.084	0.431	0.0071	0.099	0.0045	0.0001	<0.002	<0.0005	<0.001	<0.0002	85.6
1_H Spark 1	1.99	11.53	0.0048	0.022	0.115	0.429	0.0071	0.097	0.0043	0.0001	<0.002	<0.0005	0.0042	<0.0002	85.8
1_H Spark 2	1.89	11.55	0.0047	0.020	0.126	0.428	0.0071	0.097	0.0043	0.0001	<0.002	<0.0005	0.0042	<0.0002	85.9
1_H Spark 3	2.10	11.59	0.0048	0.022	0.091	0.433	0.0071	0.097	0.0043	0.0001	<0.002	<0.0005	<0.001	0.021	85.6
Average	1.99	11.56	0.0048	0.021	0.111	0.430	0.0071	0.097	0.0043	0.0001	<0.002	<0.0005	0.0021	0.0057	85.8
2_B Spark 1	2.18	11.39	0.0019	0.030	0.287	0.413	0.0077	0.091	0.0055	0.0002	0.010	0.0035	0.033	0.010	85.6
2_B Spark 2	1.91	11.31	0.0044	0.022	0.145	0.437	0.0070	0.091	0.0042	0.0002	<0.002	<0.0005	0.0046	<0.0002	86.1
2_B Spark 3	2.04	11.57	0.0047	0.021	0.094	0.431	0.0073	0.099	0.0041	0.0002	<0.002	<0.0005	0.0001	<0.0002	85.7
Average	2.04	11.42	0.0037	0.021	0.176	0.427	0.0073	0.094	0.0046	0.0002	<0.002	<0.0005	0.0130	0.0023	85.8
2_I Spark 1	2.12	11.65	0.0044	0.022	0.080	0.421	0.0072	0.098	0.0045	0.0001	<0.002	<0.0005	<0.001	<0.0002	85.6
2_I Spark 2	2.12	11.58	0.0041	0.024	0.097	0.418	0.0070	0.097	0.0048	0.0002	<0.002	<0.0005	0.0043	<0.0002	85.6
2_I Spark 3	1.92	11.13	0.0044	0.017	0.073	0.421	0.0073	0.067	0.0042	0.0001	<0.002	<0.0005	<0.001	<0.0002	86.3

Sample ID	Pb	Sn	P	S	Fe	Ni	As	Sb	Bi	Mg	Zn	Mn	Si	Al	Cu
Average	2.05	11.45	0.0043	0.021	0.083	0.420	0.0070	0.0970	0.0045	0.0001	<0.002	<0.0005	<0.001	<0.0002	85.9
Sample ID	Pb	Sn	P	S	Fe	Ni	As	Sb	Bi	Mg	Zn	Mn	Si	Al	Cu
3_C Spark 1	2.15	11.81	0.0050	0.020	0.066	0.421	0.0070	0.098	0.0046	0.0001	<0.002	<0.0005	<0.001	<0.0002	85.4
3_C Spark 2	2.15	11.44	0.0048	0.022	0.089	0.423	0.0068	0.096	0.0049	0.0001	<0.002	<0.0005	<0.001	<0.0002	85.8
3_C Spark 3	2.11	11.43	0.0050	0.023	0.065	0.416	0.0070	0.096	0.0044	0.0001	<0.002	<0.0005	<0.001	<0.0002	85.8
Average	2.14	11.56	0.0050	0.022	0.073	0.420	0.0069	0.097	0.0046	0.0001	<0.002	<0.0005	<0.001	<0.0002	85.7
3_J Spark 1	2.05	11.57	0.0049	0.023	0.079	0.424	0.0070	0.096	0.0044	0.0001	<0.002	<0.0005	<0.001	<0.0002	85.7
3_J Spark 2	1.87	10.82	0.0039	0.020	0.152	0.395	0.0057	0.076	0.0035	0.0003	<0.002	<0.0005	<0.001	<0.0002	86.6
3_J Spark 3	2.02	11.09	0.0048	0.020	0.075	0.415	0.0067	0.091	0.0044	0.0001	<0.002	<0.0005	0.0046	<0.0002	86.3
Average	1.98	11.16	0.0045	0.021	0.102	0.411	0.0065	0.088	0.0041	0.0002	<0.002	<0.0005	<0.001	<0.0002	86.2
4_D Spark 1	2.08	11.73	0.0050	0.021	0.079	0.422	0.0071	0.099	0.0046	0.0001	<0.002	<0.0001	<0.001	<0.0002	85.6
4_D Spark 2	2.09	11.63	0.0051	0.021	0.082	0.414	0.0072	0.098	0.0047	0.0001	<0.002	<0.0001	<0.001	<0.0002	85.6
4_D Spark 3	2.06	11.57	0.0052	0.024	0.084	0.417	0.0072	0.097	0.0046	0.0001	<0.002	<0.0001	<0.001	<0.0002	85.7
Average	2.08	11.64	0.0051	0.022	0.081	0.418	0.0071	0.098	0.0046	0.0001	<0.002	<0.0001	<0.001	<0.0002	85.6
4_K Spark 1	2.10	11.66	0.0051	0.024	0.077	0.421	0.0072	0.098	0.0044	0.0001	<0.002	<0.0005	<0.001	<0.0002	85.6
4_K Spark 2	2.05	11.57	0.0048	0.020	0.086	0.422	0.0068	0.095	0.0044	0.0003	<0.002	<0.0005	<0.001	<0.0002	85.7
4_K Spark 3	2.03	11.68	0.0049	0.021	0.092	0.415	0.0068	0.093	0.0042	0.0001	<0.002	<0.0005	<0.001	<0.0002	85.7
Average	2.06	11.64	0.0049	0.021	0.085	0.419	0.0069	0.095	0.0043	0.0002	<0.002	<0.0005	<0.001	<0.0002	85.7
5_E Spark 1	2.11	11.55	0.0047	0.021	0.080	0.424	0.0066	0.096	0.0046	0.0001	<0.002	<0.0005	<0.001	<0.0002	85.7
5_E Spark 2	2.10	11.72	0.0048	0.021	0.084	0.429	0.0067	0.095	0.0043	0.0001	<0.002	<0.0005	<0.001	<0.0002	85.5
5_E Spark 3	2.03	11.56	0.0047	0.022	0.103	0.423	0.0067	0.096	0.0043	0.0001	<0.002	<0.0005	<0.001	<0.0002	85.7
Average	2.08	11.61	0.0047	0.021	0.089	0.425	0.0067	0.096	0.0044	0.0001	<0.002	<0.0005	<0.001	<0.0002	85.7
5_L Spark 1	2.05	11.44	0.0050	0.021	0.087	0.427	0.0068	0.093	0.0045	0.0001	<0.002	<0.0005	<0.001	<0.0002	85.9
5_L Spark 2	2.12	11.67	0.0044	0.021	0.092	0.429	0.0063	0.091	0.0042	0.0001	<0.002	<0.0005	<0.001	<0.0002	85.6
5_L Spark 3	2.32	11.93	0.0050	0.023	0.078	0.402	0.0072	0.101	0.0047	0.0001	0.0040	<0.0005	<0.001	<0.0002	85.1
Average	2.16	11.68	0.0048	0.022	0.086	0.419	0.0067	0.095	0.0045	0.0001	<0.002	<0.0005	<0.001	<0.0002	85.5
6_F Spark 1	1.95	10.98	0.0046	0.017	0.082	0.420	0.0066	0.087	0.0041	0.0001	<0.002	<0.0005	<0.001	<0.0002	86.5
6_F Spark 2	2.13	11.62	0.0049	0.022	0.082	0.425	0.0071	0.100	0.0046	0.0001	<0.002	<0.0005	<0.001	<0.0002	85.6
6_F Spark 3	2.03	11.37	0.0048	0.020	0.097	0.422	0.0069	0.091	0.0041	0.0001	<0.002	<0.0005	<0.001	<0.0002	85.9
Average	2.04	11.32	0.0048	0.020	0.087	0.422	0.0069	0.093	0.0043	0.0001	<0.002	<0.0005	<0.001	<0.0002	86.0

Sample ID	Pb	Sn	P	S	Fe	Ni	As	Sb	Bi	Mg	Zn	Mn	Si	Al	Cu
6_M Spark 1	2.14	11.77	0.0049	0.023	0.080	0.435	0.0072	0.101	0.0046	0.0002	<0.002	<0.0005	<0.001	<0.0002	85.4
6_M Spark 2	2.00	11.39	0.0047	0.019	0.090	0.433	0.0071	0.095	0.0041	0.0001	<0.002	<0.0005	0.0026	<0.0002	86.0
6_M Spark 3	2.17	11.66	0.0046	0.021	0.091	0.432	0.0073	0.101	0.0045	0.0001	<0.002	<0.0005	<0.001	<0.0002	85.5
Average	2.10	11.61	0.0047	0.021	0.087	0.433	0.0072	0.099	0.0044	0.0001	<0.002	<0.0005	<0.001	<0.0002	85.6
Sample ID	**Pb**	**Sn**	**P**	**S**	**Fe**	**Ni**	**As**	**Sb**	**Bi**	**Mg**	**Zn**	**Mn**	**Si**	**Al**	**Cu**
7_G Spark 1	2.14	11.49	0.0046	0.021	0.104	0.427	0.0072	0.099	0.0044	0.0001	<0.002	<0.0005	0.0040	<0.0002	85.7
7_G Spark 2	2.02	11.56	0.0046	0.020	0.093	0.430	0.0068	0.097	0.0046	0.0001	<0.002	<0.0005	<0.001	<0.0002	85.8
7_G Spark 3	2.14	11.60	0.0046	0.022	0.092	0.434	0.0070	0.098	0.0045	0.0001	<0.002	<0.0005	<0.001	<0.0002	85.6
Average	2.10	11.55	0.0046	0.021	0.097	0.430	0.0070	0.098	0.0045	0.0001	<0.002	<0.0005	<0.001	<0.0002	85.7
7_N Spark 1	2.03	11.69	0.0048	0.022	0.083	0.435	0.0073	0.100	0.0045	0.0001	<0.002	<0.0005	<0.001	<0.0002	85.6
7_N Spark 2	2.26	11.65	0.0048	0.024	0.099	0.428	0.0070	0.097	0.0044	0.0001	<0.002	<0.0005	0.0039	<0.0002	85.4
7_N Spark 3	2.15	11.63	0.0045	0.024	0.070	0.433	0.0062	0.096	0.0048	0.0001	<0.002	<0.0005	<0.001	<0.0002	85.6
Average	2.15	11.68	0.0047	0.0021	0.084	0.432	0.0069	0.098	0.0046	0.0001	<0.002	<0.0005	<0.001	<0.0002	85.5

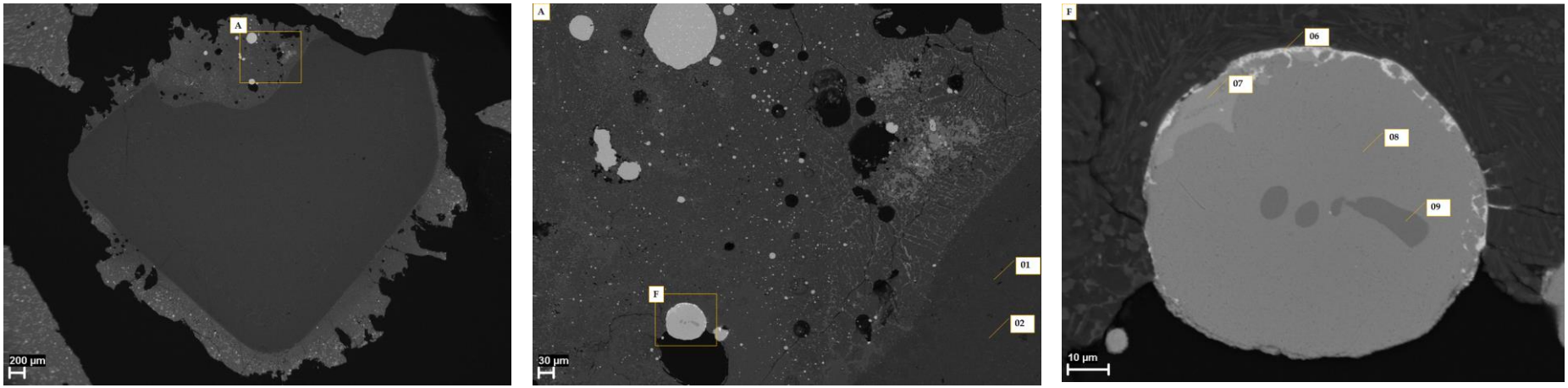

Figure 101. SEM BSE micrographs of slag from PCBs smelting Test 32

Table 80. SEM EDS point analysis of slag from PCBs smelting Test 32, mass in wt%

Point	O	Na	Al	Si	K	Fe	Cu	Sn	Pb	Total	Phase
1	46.8	1.6	45.6	4.7	1.3	-	-	-	-	100	Al_2O_3
2	46.9	1.4	46.7	4.1	0.9	-	-	-	-	100	Al_2O_3
6	-	-	-	-	-	-	5.70	-	94.3	100	CuPb alloy
7	-	-	-	-	-	-	69.0	31.0	-	100	CuSn alloy
8	-	-	-	-	-	2.60	84.5	13.0	-	100	CuSn alloy
9	-	-	-	-	-	91.3	8.70	-	-	100	FeCu alloy

APPENDIX K: COMPLETE SET OF RESULTS OF CRTs SMELTING TESTS

Table 81. Complete list of product masses and tapping temperatures of CRTs smelting tests

Test No.	Test Repeat	Changing Variable	Test Time, h	Metal, kg	Slag, kg	Cartridge Fumes, kg	Extraction Fumes, kg	Tapping Temp, °C
1	-	Reductant	3.6	2.39	18.7	0.36	-	1188
2	-	Reductant	3.0	1.75	20.1	0.66	-	1289
3	-	Reductant	3.1	1.58	19.4	0.66	0.68	1279
4	-	Flux	3.1	1.37	20.0	1.00	-	1257
5	-	Flux	3.1	2.31	23.0	0.87	-	1275
6	-	Flux	3.1	1.67	20.0	0.74	-	1273
7	-	Flux	3.2	1.76	22.2	0.50	0.22	1271
8	-	Flux	3.1	2.49	19.0	0.65	-	1250
9	-	Reaction time	3.0	2.27	21.0	1.09	0.52	1263
10	-	Reaction time	3.7	2.17	20.0	1.08	-	1261
11	-	Reaction time	4.2	2.19	20.0	1.20	-	1252
12	-	Temperature	3.1	2.04	20.0	0.90	-	1141
13	-	Temperature	3.1	2.42	21.0	0.95	0.67	1169
14	-	Temperature	3.1	2.74	22.0	0.54	-	1128
15	-	Temperature	3.1	2.45	23.0	0.66	-	1182
16	-	Temperature	3.2	1.69	22.0	0.66	1.11	1228
17	16R	Temperature	3.2	2.88	21.0	0.74	-	1230
18	15R	Temperature	3.0	1.90	22.0	0.94	0.70	1189
19	13R	Temperature	3.1	2.30	21.0	0.90	-	1165
20	14R	Temperature	3.1	2.53	21.1	0.75	-	1159
21	12R	Temperature	3.1	2.06	19.0	0.65	0.63	1143
22	9R	Reaction time	3.1	2.49	21.0	0.92	-	1220
23	10R	Reaction time	4.0	1.79	21.0	0.85	-	1252
24	11R	Reaction time	4.1	1.87	19.5	0.97	1.79	1224
25	1R	Reductant	3.0	1.64	22.0	0.59	-	1238
26	2R	Reductant	3.0	2.12	22.0	0.75	-	1240
27	3R	Reductant	3.1	1.96	20.0	0.65	0.35	1202
28	4R	Flux	3.1	1.57	19.0	0.80	-	1245
29	5R	Flux	3.1	1.99	22.0	0.36	-	1249
30	6R	Flux	2.5	1.94	19.8	0.63	0.44	1214
31	7R	Flux	3.7	1.65	22.7	0.66	-	1232
32	-	Fume ratio	3.0	3.35	22.8	0.79	-	1239
33	-	Fume ratio	3.0	2.34	23.0	0.68	1.42	1230
34	32R	Fume ratio	3.1	3.46	25.0	0.95	-	1238
35	33R	Fume ratio	3.1	2.99	22.0	0.80	-	1248
36		Fume ratio	3.4	5.33	18.0	0.80	0.92	1243
Total	**-**	**-**	**116**	**81**	**755**	**28**	**9**	**-**

Table 82. Chemical composition of metals from CRTs smelting tests

									Mass, ppm			
Test	**Cu**	**Fe**	**Ni**	**Pb**	**Si**	**Zn**	**Sn**	**C**	**Au**	**Pd**	**Pt**	**Ag**	**Total**
1	0.41	<0.05	0.05	99.5	<0.05	<0.05	<0.05	<0.05	<0.02	<0.02	<0.02	<0.02	100
2	0.32	<0.05	<0.05	99.7	<0.05	<0.05	<0.05	<0.05	<0.02	<0.02	<0.02	<0.02	100
3	0.13	<0.05	<0.05	99.9	<0.05	<0.05	<0.05	<0.05	<0.02	<0.02	<0.02	<0.02	100
4	0.36	<0.05	<0.05	99.6	<0.05	<0.05	<0.05	<0.05	<0.02	<0.02	<0.02	<0.02	100
5	0.21	<0.05	<0.05	99.8	<0.05	<0.05	<0.05	<0.05	<0.02	<0.02	<0.02	<0.02	100
6	0.08	<0.05	0.11	99.8	<0.05	<0.05	<0.05	<0.05	<0.02	<0.02	<0.02	<0.02	100
7	0.07	<0.05	0.07	99.9	<0.05	<0.05	<0.05	<0.05	<0.02	<0.02	<0.02	<0.02	100
8	0.15	<0.05	0.07	99.8	<0.05	<0.05	<0.05	<0.05	<0.02	<0.02	<0.02	<0.02	100
9	0.06	<0.05	<0.05	98.5	<0.05	<0.05	1.39	<0.05	1.17	1.98	11.7	285	100
10	0.05	<0.05	<0.05	98.4	<0.05	<0.05	1.53	<0.05	1.91	1.35	14.6	333	100
11	0.95	<0.05	0.12	96.9	<0.05	<0.05	2.08	<0.05	2.88	9.95	17.4	311	100
12	0.63	<0.05	<0.05	97.2	<0.05	<0.05	2.21	<0.05	6.72	7.12	0.02	405	100
13	1.00	<0.05	0.21	96.4	<0.05	<0.05	2.41	<0.05	1.51	1.26	14.7	320	100
14	0.48	<0.05	<0.05	98.0	<0.05	<0.05	1.49	<0.05	1.63	2.69	12.2	164	100
15	0.11	<0.05	<0.05	98.9	<0.05	<0.05	1.01	<0.05	1.21	2.53	15.9	209	100
16	<0.05	<0.05	<0.05	98.5	<0.05	<0.05	1.48	<0.05	0.67	1.62	7.84	205	100
17	0.50	<0.05	<0.05	98.2	<0.05	<0.05	1.33	<0.05	2.37	2.52	7.08	181	100
18	0.26	<0.05	<0.05	98.6	<0.05	<0.05	1.15	<0.05	1.27	2.98	0.02	303	100
19	0.71	<0.05	0.09	97.8	<0.05	<0.05	1.45	<0.05	0.37	0.45	2.31	316	100
20	1.59	<0.05	0.06	96.5	<0.05	<0.05	1.89	<0.05	0.02	3.87	10.0	369	100
21	0.21	<0.05	<0.05	99.2	<0.05	<0.05	0.56	<0.05	1.22	2.60	0.02	388	100
22	1.18	<0.05	0.16	96.2	<0.05	<0.05	2.43	<0.05	2.56	1.67	9.80	233	100
23	0.76	<0.05	<0.05	97.8	<0.05	<0.05	1.49	<0.05	1.95	2.68	11.9	377	100
24	0.92	<0.05	0.15	97.7	<0.05	<0.05	1.24	<0.05	1.73	2.56	12.9	339	100
25	0.06	<0.05	<0.05	99.9	<0.05	<0.05	<0.05	<0.05	<0.02	<0.02	<0.02	<0.02	100
26	0.06	<0.05	0.25	99.7	<0.05	<0.05	<0.05	<0.05	<0.02	<0.02	<0.02	<0.02	100
27	0.05	<0.05	<0.05	99.9	<0.05	<0.05	<0.05	<0.05	<0.02	<0.02	<0.02	<0.02	100
28	0.24	<0.05	<0.05	99.8	<0.05	<0.05	<0.05	<0.05	<0.02	<0.02	<0.02	<0.02	100
29	0.05	<0.05	<0.05	99.9	<0.05	<0.05	<0.05	<0.05	<0.02	<0.02	<0.02	<0.02	100
30	0.05	<0.05	0.12	99.8	<0.05	<0.05	<0.05	<0.05	<0.02	<0.02	<0.02	<0.02	100
31	0.06	<0.05	<0.05	99.9	<0.05	<0.05	<0.05	<0.05	<0.02	<0.02	<0.02	<0.02	100
32	0.83	<0.05	0.06	95.8	<0.05	<0.05	3.29	<0.05	<0.02	2.19	39.1	92.1	100
33	0.52	<0.05	0.12	98.4	<0.05	<0.05	0.97	<0.05	<0.02	2.80	28.9	110	100
34	0.69	<0.05	<0.05	96.1	<0.05	<0.05	3.17	<0.05	<0.02	2.00	20.9	370	100
35	0.32	<0.05	<0.05	98.8	<0.05	<0.05	0.84	<0.05	<0.02	1.98	19.8	114	100
36	4.52	<0.05	<0.05	91.6	<0.05	<0.05	3.88	<0.05	<0.02	12.1	46.2	276	100

Table 83. Chemical composition of slags from CRTs smelting tests

															Mass, ppm				
Test	**Al_2O_3**	**CaO**	**CuO**	**FeO**	**MgO**	**NiO**	**PbO**	**SiO_2**	**ZnO**	**SnO_2**	**C**	**K_2O**	**Na_2O**	**BaO**	**SrO**	**Au**	**Pd**	**Pt**	**Ag**	**Total**
1	4.39	7.13	<0.05	0.44	2.01	<0.05	0.71	51.6	0.13	<0.05	<0.05	4.28	20.4	2.06	1.72	<0.02	<0.02	<0.02	<0.02	94.9
2	3.76	7.16	<0.05	0.36	2.07	<0.05	0.67	51.8	0.07	<0.05	<0.05	4.56	20.9	2.08	1.74	<0.02	<0.02	<0.02	<0.02	95.2
3	3.76	7.18	<0.05	0.37	2.02	<0.05	0.50	52.6	<0.05	<0.05	<0.05	3.17	21.6	2.06	1.72	<0.02	<0.02	<0.02	<0.02	95.0
4	3.80	7.42	<0.05	0.40	2.12	<0.05	0.83	54.1	<0.05	<0.05	<0.05	3.38	17.3	2.12	1.77	<0.02	<0.02	<0.02	<0.02	93.3
5	3.67	6.74	<0.05	0.37	1.99	<0.05	0.60	48.2	<0.05	<0.05	<0.05	2.89	26.1	1.91	1.65	<0.02	<0.02	<0.02	<0.02	94.1
6	3.83	5.39	<0.05	0.36	2.06	<0.05	0.82	53.7	<0.05	<0.05	<0.05	4.34	21.6	2.00	1.69	<0.02	<0.02	<0.02	<0.02	95.8
7	3.72	8.66	<0.05	0.42	2.06	<0.05	0.46	53.9	<0.05	<0.05	<0.05	4.46	21.35	1.92	1.65	<0.02	<0.02	<0.02	<0.02	98.6
8	3.74	7.22	<0.05	0.40	2.04	<0.05	1.00	49.9	<0.05	<0.05	<0.05	5.39	20.4	1.92	1.74	<0.02	<0.02	<0.02	<0.02	93.7
9	4.00	7.74	<0.05	0.35	2.11	<0.05	0.40	54.4	0.56	0.23	<0.05	4.66	20.6	2.04	1.73	<0.02	<0.02	<0.02	1.56	98.7
10	4.25	7.85	<0.05	0.37	2.16	<0.05	0.38	55.4	0.61	0.32	<0.05	3.74	21.3	1.75	1.68	<0.02	<0.02	<0.02	2.46	100
11	4.23	7.47	<0.05	0.36	2.07	<0.05	0.34	51.1	0.49	0.33	<0.05	3.78	19.2	1.92	1.70	<0.02	<0.02	<0.02	1.96	93.0
12	4.14	7.86	<0.05	0.46	2.21	<0.05	0.52	55.9	0.70	0.29	<0.05	3.92	22.8	2.01	1.69	<0.02	<0.02	<0.02	2.63	102
13	4.06	8.16	<0.05	0.41	2.29	<0.05	0.75	58.0	0.78	0.27	<0.05	5.20	18.1	1.95	1.67	<0.02	<0.02	<0.02	1.97	102
14	3.69	7.02	<0.05	0.36	2.06	<0.05	0.57	48.2	0.82	0.23	<0.05	2.74	21.3	1.97	1.65	<0.02	<0.02	<0.02	1.83	90.5
15	3.38	6.95	<0.05	0.35	1.84	<0.05	0.43	65.1	0.72	0.30	<0.05	3.65	23.2	1.84	1.64	<0.02	<0.02	<0.02	3.49	109
16	4.16	11.0	<0.05	0.42	2.17	<0.05	0.47	53.3	0.73	0.25	<0.05	3.56	21.2	1.73	1.63	<0.02	<0.02	<0.02	1.50	101
17	4.01	7.53	<0.05	0.64	2.17	<0.05	0.38	53.5	0.70	0.29	<0.05	3.80	23.2	1.84	1.64	<0.02	<0.02	<0.02	3.93	100
18	3.84	7.32	<0.05	0.45	1.99	<0.05	0.26	51.8	0.82	0.34	<0.05	3.82	23.9	1.77	1.64	<0.02	<0.02	<0.02	1.75	97.9
19	3.54	7.98	<0.05	0.73	2.09	<0.05	0.43	52.4	0.73	0.32	<0.05	3.14	21.3	2.01	1.70	<0.02	<0.02	<0.02	1.31	96.4
20	3.36	7.89	<0.05	0.69	2.02	<0.05	0.34	48.8	0.83	0.42	<0.05	2.33	20.9	1.95	1.60	<0.02	<0.02	<0.02	1.11	91.2
21	2.99	7.99	<0.05	0.78	2.07	<0.05	0.79	50.9	1.00	0.52	<0.05	3.13	19.0	2.04	1.70	<0.02	<0.02	<0.02	11.6	93.0
22	3.55	8.06	<0.05	0.81	2.09	<0.05	0.76	50.5	0.71	0.29	<0.05	2.66	19.8	2.01	1.68	<0.02	<0.02	<0.02	2.57	93.0
23	3.72	7.88	<0.05	0.76	2.09	<0.05	0.26	52.2	0.53	0.29	<0.05	2.88	22.1	2.03	1.71	<0.02	<0.02	<0.02	0.99	96.5
24	3.82	7.93	<0.05	0.74	2.07	<0.05	0.49	52.4	0.53	0.36	<0.05	3.60	19.4	2.06	1.69	<0.02	<0.02	<0.02	1.91	95.1
25	3.99	8.12	<0.05	0.62	2.12	<0.05	0.73	55.0	0.25	<0.05	<0.05	3.40	20.7	2.17	1.71	<0.02	<0.02	<0.02	<0.02	98.8
26	3.97	8.06	<0.05	0.54	2.17	<0.05	0.52	52.8	0.11	<0.05	<0.05	4.33	21.5	1.96	1.68	<0.02	<0.02	<0.02	<0.02	97.6
27	3.99	8.07	<0.05	0.69	2.14	<0.05	0.56	53.9	0.07	<0.05	<0.05	3.67	20.8	1.99	1.68	<0.02	<0.02	<0.02	<0.02	97.6
28	4.14	8.34	<0.05	0.80	2.26	<0.05	0.74	57.6	<0.05	<0.05	<0.05	4.13	17.3	2.11	1.77	<0.02	<0.02	<0.02	<0.02	99.1

29	3.87	7.74	<0.05	0.89	2.11	<0.05	0.34	50.7	<0.05	<0.05	<0.05	3.71	21.3	1.93	1.62	<0.02	<0.02	<0.02	<0.02	94.2
30	4.16	5.93	<0.05	1.16	2.27	<0.05	0.85	53.9	<0.05	<0.05	<0.05	2.96	23.2	2.15	1.73	<0.02	<0.02	<0.02	<0.02	98.3
31	4.06	9.50	<0.05	0.99	2.21	<0.05	0.53	54.6	<0.05	<0.05	<0.05	4.43	20.6	2.04	1.66	<0.02	<0.02	<0.02	<0.02	100.6
32	4.08	7.28	<0.05	0.75	2.20	<0.05	<0.05	54.0	1.21	0.34	<0.05	2.44	23.8	1.95	1.63	<0.02	<0.02	<0.02	7.04	99.7
33	3.99	6.98	<0.05	0.68	2.14	<0.05	<0.05	52.4	0.46	0.19	<0.05	3.54	24.8	1.92	1.63	<0.02	<0.02	<0.02	0.98	98.8
34	3.84	9.93	<0.05	0.78	2.06	<0.05	<0.05	48.6	1.12	0.37	<0.05	2.65	24.8	1.80	1.53	<0.02	<0.02	<0.02	1.32	97.5
35	4.04	6.91	<0.05	0.96	2.14	<0.05	<0.05	49.2	0.50	0.19	<0.05	2.65	24.4	1.93	1.63	<0.02	<0.02	<0.02	1.29	94.6
36	5.31	8.34	<0.05	2.42	1.79	<0.05	<0.05	40.7	4.39	0.76	<0.05	1.97	29.7	1.46	1.26	<0.02	<0.02	<0.02	1.89	98.1

Table 84. Chemical composition of fumes from CRTs smelting tests

														Mass, ppm				
Test	**Al_2O_3**	**CaO**	**CuO**	**FeO**	**MgO**	**PbO**	**SiO_2**	**ZnO**	**SnO_2**	**C**	**K_2O**	**Na_2O**	**BaO**	**SrO**	**Au**	**Pd**	**Pt**	**Ag**	**Total**
1	<0.05	<0.05	<0.05	0.15	<0.05	85.7	<0.05	3.30	<0.05	1.39	1.92	1.19	<0.05	<0.05	<0.02	<0.02	<0.02	<0.02	93.6
2	<0.05	<0.05	<0.05	0.08	<0.05	89.7	<0.05	2.53	<0.05	0.88	3.94	1.17	<0.05	<0.05	<0.02	<0.02	<0.02	<0.02	98.3
3	<0.05	<0.05	<0.05	0.10	<0.05	89.2	<0.05	2.21	<0.05	0.95	2.23	1.34	<0.05	<0.05	<0.02	<0.02	<0.02	<0.02	96.0
4	<0.05	<0.05	<0.05	0.08	<0.05	89.5	<0.05	1.93	<0.05	0.69	1.45	0.97	<0.05	<0.05	<0.02	<0.02	<0.02	<0.02	94.6
5	<0.05	<0.05	<0.05	0.13	<0.05	90.9	<0.05	2.25	<0.05	1.04	2.33	1.49	<0.05	<0.05	<0.02	<0.02	<0.02	<0.02	98.2
6	<0.05	<0.05	<0.05	0.09	<0.05	89.2	<0.05	2.01	<0.05	0.76	1.80	1.19	<0.05	<0.05	<0.02	<0.02	<0.02	<0.02	95.0
7	<0.05	<0.05	<0.05	0.08	<0.05	88.2	<0.05	2.11	<0.05	1.04	1.61	1.00	<0.05	<0.05	<0.02	<0.02	<0.02	<0.02	94.1
8	<0.05	<0.05	<0.05	0.13	<0.05	88.5	<0.05	2.67	<0.05	0.95	1.80	1.42	<0.05	<0.05	<0.02	<0.02	<0.02	<0.02	95.5
9	<0.05	0.22	0.09	0.10	0.11	91.6	0.36	10.3	0.95	0.92	1.50	0.58	<0.05	<0.05	0.13	0.07	0.21	33.4	107
10	<0.05	0.32	0.10	0.09	0.10	86.0	0.62	12.0	1.23	1.11	1.94	1.28	<0.05	<0.05	0.21	0.08	0.09	50.0	105
11	0.49	1.53	0.56	0.39	0.20	76.4	2.70	18.3	2.67	1.95	1.62	0.84	<0.05	<0.05	0.77	0.18	0.03	107	108
12	0.21	0.95	0.23	0.10	0.13	81.5	1.82	14.7	1.71	1.16	1.27	0.41	<0.05	<0.05	0.29	0.08	0.09	56.8	104
13	0.15	0.62	0.18	0.15	0.11	82.6	1.07	14.2	1.46	1.01	1.18	0.39	<0.05	<0.05	0.25	0.07	0.02	48.7	103
14	0.25	1.16	0.22	0.15	0.18	79.4	1.96	16.6	1.80	1.64	1.37	0.86	<0.05	<0.05	0.37	0.11	0.07	61.1	106
15	0.15	0.66	0.14	0.14	0.13	80.7	0.98	16.3	1.63	1.25	1.2	0.4	<0.05	<0.05	0.31	0.15	0.12	55.3	104
16	0.11	0.53	0.11	0.12	0.12	82.2	0.86	16.5	1.50	1.24	1.73	0.95	<0.05	<0.05	0.22	0.09	<0.02	55.9	106
17	0.14	0.98	0.11	0.15	0.14	79.8	1.22	17.2	1.65	1.42	1.82	1.07	<0.05	<0.05	0.23	0.09	<0.02	66.0	106

18	0.26	1.55	0.23	0.13	0.18	71.4	2.42	17.0	1.94	1.79	1.88	1.32	<0.05	<0.05	0.32	0.09	0.05	68.2	100
19	0.11	0.74	0.10	0.14	0.20	68.7	1.48	17.9	1.36	1.22	0.82	0.50	<0.05	<0.05	0.18	0.06	<0.02	138	93.3
20	0.20	0.45	0.08	0.08	<0.05	70.9	0.65	15.7	1.79	1.11	2.20	1.46	<0.05	<0.05	0.17	0.07	<0.02	143	94.6
21	<0.05	0.52	0.07	0.07	0.11	64.5	0.68	19.5	1.38	1.03	1.28	1.22	<0.05	<0.05	0.14	0.05	<0.02	146	90.4
22	<0.05	0.32	0.06	0.09	0.08	64.8	0.45	20.3	1.37	0.96	1.70	1.15	<0.05	<0.05	0.11	0.05	<0.02	129	91.3
23	<0.05	0.27	<0.05	0.10	<0.05	72.6	0.18	17.3	1.19	0.69	1.36	0.95	<0.05	<0.05	0.10	0.05	<0.02	130	94.6
24	<0.05	0.21	<0.05	0.07	0.10	67.9	0.20	17.0	1.16	0.89	1.79	1.86	<0.05	<0.05	0.13	0.06	<0.02	141	91.2
25	<0.05	0.49	<0.05	<0.05	<0.05	79.6	0.49	6.59	<0.05	0.85	2.29	1.52	<0.05	<0.05	<0.02	<0.02	<0.02	<0.02	91.8
26	<0.05	0.52	<0.05	0.06	<0.05	86.3	0.45	2.90	<0.05	0.78	2.28	1.46	<0.05	<0.05	<0.02	<0.02	<0.02	<0.02	94.7
27	<0.05	0.34	<0.05	0.07	0.11	87.6	0.43	2.82	<0.05	0.86	2.54	1.54	<0.05	<0.05	<0.02	<0.02	<0.02	<0.02	96.3
28	<0.05	0.27	<0.05	0.11	<0.05	90.3	0.39	3.96	<0.05	0.54	1.86	0.88	<0.05	<0.05	<0.02	<0.02	<0.02	<0.02	98.3
29	<0.05	0.21	<0.05	<0.05	<0.05	83.8	0.43	2.91	<0.05	1.07	0.86	3.15	<0.05	<0.05	<0.02	<0.02	<0.02	<0.02	92.4
30	<0.05	0.15	<0.05	0.09	0.10	83.7	0.41	2.39	<0.05	0.82	2.57	1.99	<0.05	<0.05	<0.02	<0.02	<0.02	<0.02	92.2
31	<0.05	0.35	<0.05	0.08	0.10	86.1	0.47	2.72	<0.05	0.81	3.13	2.09	<0.05	<0.05	<0.02	<0.02	<0.02	<0.02	95.8
32	<0.05	0.33	<0.05	0.10	<0.05	68.4	<0.05	29.4	1.65	1.07	2.19	0.74	<0.05	<0.05	0.14	0.08	0.07	19.1	103.8
33	<0.05	0.43	<0.05	<0.05	<0.05	78.7	<0.05	11.3	0.86	1.05	2.80	1.31	<0.05	<0.05	0.09	0.04	<0.02	4.50	96.5
34	<0.05	0.43	0.07	0.17	<0.05	62.0	<0.05	29.9	1.87	0.89	2.32	0.90	<0.05	<0.05	0.13	0.03	<0.02	21.6	98.6
35	<0.05	0.32	<0.05	0.10	<0.05	70.9	<0.05	14.8	0.94	0.98	2.83	1.40	<0.05	<0.05	0.09	0.05	0.12	5.09	92.3
36	<0.05	0.24	0.06	0.12	<0.05	29.8	<0.05	59.1	0.88	0.94	1.64	1.40	<0.05	<0.05	0.17	0.09	0.02	11.6	94.2

Table 85. Chemical composition of blended fumes from CRTs smelting tests

															Mass, ppm				
Test	**Al_2O_3**	**CaO**	**CuO**	**FeO**	**MgO**	**PbO**	**SiO_2**	**ZnO**	**SnO_2**	**C**	**K_2O**	**Na_2O**	**BaO**	**SrO**	**Au**	**Pd**	**Pt**	**Ag**	**Total**
1-6	<0.05	<0.05	<0.05	0.08	<0.05	95.1	<0.05	2.40	0.19	1.17	1.78	1.22	<0.05	<0.05	0.10	0.05	<0.02	33.1	102
7-9	<0.05	0.20	<0.05	0.07	<0.05	90.3	<0.05	6.67	0.53	1.02	1.85	1.38	<0.05	<0.05	0.11	0.04	<0.02	44.1	102
10-12	<0.05	0.60	0.15	0.12	<0.05	82.9	0.66	14.8	1.57	1.28	1.56	1.54	<0.05	<0.05	0.28	0.08	<0.02	77.5	105
13-15	<0.05	0.71	0.15	0.26	0.09	81.9	0.88	16.0	1.57	1.24	1.49	1.40	<0.05	<0.05	0.28	0.09	<0.02	99.3	106
16-18	<0.05	0.83	0.12	0.19	0.09	79.1	0.90	17.9	1.71	1.58	1.81	1.98	<0.05	<0.05	0.24	0.08	<0.02	93.1	106
19-21	<0.05	0.49	0.11	0.09	<0.05	74.3	0.51	18.1	1.51	1.27	1.51	1.22	<0.05	<0.05	0.16	0.06	<0.02	83.2	99.1

22-24	<0.05	0.38	<0.05	0.93	<0.05	82.3	0.32	17.7	1.40	0.88	1.48	1.38	<0.05	<0.05	0.11	0.03	<0.02	80.5	107
25-27	<0.05	0.10	<0.05	0.44	<0.05	98.7	<0.05	4.07	0.23	0.88	1.81	1.40	<0.05	<0.05	0.06	0.04	<0.02	28.5	108
28-30	<0.05	<0.05	<0.05	0.10	<0.05	92.3	<0.05	2.56	0.10	0.82	1.99	1.74	<0.05	<0.05	0.04	0.03	<0.02	24.0	99.6
31-33	<0.05	0.21	<0.05	0.19	<0.05	84.3	<0.05	13.3	0.81	1.06	2.45	2.20	<0.05	<0.05	0.08	0.04	<0.02	51.2	105
EHF	2.53	3.22	1.66	1.36	0.63	49.2	13.1	12.6	1.74	1.68	2.60	3.97	<0.05	<0.05	1.34	1.14	1.53	330	94.2
BHF	2.67	1.30	0.23	1.93	1.00	59.9	3.06	14.6	1.46	2.33	1.78	0.21	<0.05	<0.05	0.36	116	72.8	186	90.5

Note: EHF-extraction hood fume; BHF-baghouse fume

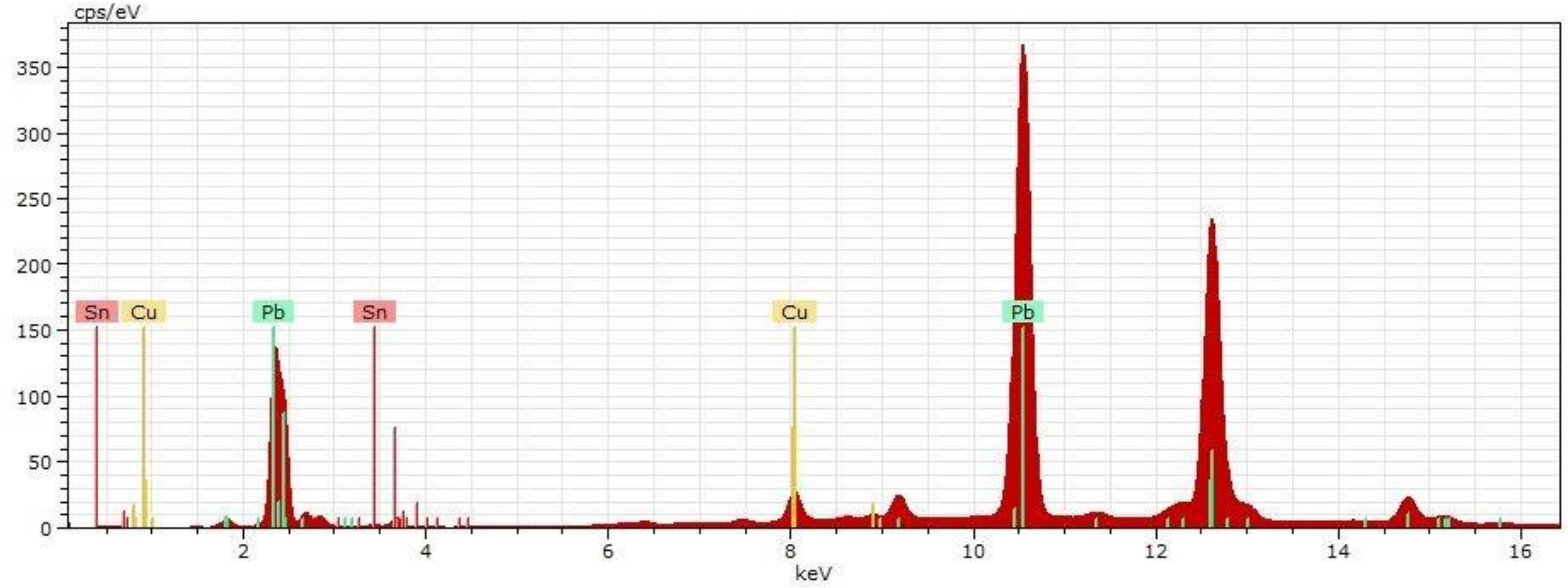

Figure 102. EDS spectrum indicating the peaks of Pb, Sn and Cu detected by micro-XRF analysis of metal from CRTs smelting Test 34

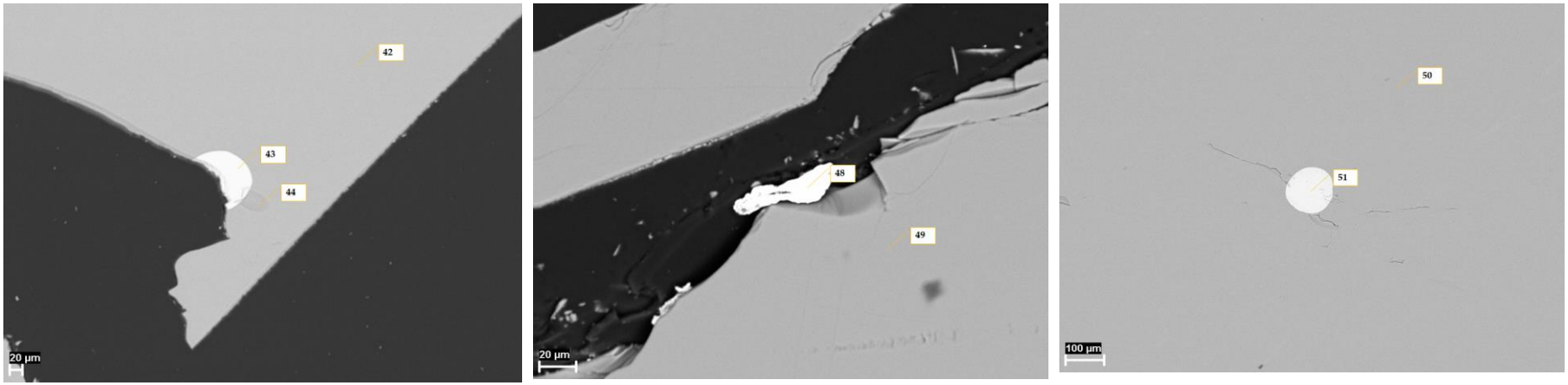

Figure 103. SEM BSE micrographs of slag from CRTs smelting Test 34

Table 86. SEM EDS point analysis of slag from CRTs smelting Test 34, mass in wt%

Point	O	Na	Mg	Al	Si	S	K	Ca	Cr	Fe	Ni	Total	Phase
42	46.3	13.6	0.7	1.7	24.3	-	7.7	5.8	-	-	-	100	Na_2SiO_3 glass
43	33.7	-	5.1	7.9	-	-	-	-	33.2	20.2	-	100	$FeCr_2O_4$
44	47.0	13.6	0.8	1.6	23.4	-	7.8	5.9	-	-	-	100	Na_2SiO_3 glass
48	-	-	-	-	-	0.8	-	-	-	40.0	59.1	100	NiFe alloy
49	-	-	-	-	-	8.2	-	-	-	66.8	25.0	100	Na_2SiO_3 glass
50	-	-	-	-	-	7.9	-	-	-	56.8	35.3	100	Na_2SiO_3 glass
51	34.0	-	5.1	8.8	-	-	-	-	34.9	16.3	-	100	$FeCr_2O_4$